Title: Advanced Cuttings Transport Study

Type of Report: Annual
Reporting Period Start Date: July14, 1999
Reporting Period End Date: July 13, 2000

Principal Authors:
Ergun Kuru, Principal Investigator
Stefan Miska, Co-Principal Investigator
Nicholas Takach, Co-Principal Investigator
Kaveh Ashenayi, Co-Principal Investigator
Gerald Kane
Mark Pickell
Len Volk
Mike Volk
Barkim Demirdal
Affonso Lourenco
Evren Ozbayoglu
Paco Vieira
Neelima Godugu

Date of Issue: July 30, 2000
DOE Award Number: DE-FG26-99BC15178

The University of Tulsa
600 South College Avenue
Tulsa, Oklahoma 74104

DISCLAIMER

ABSTRACT

ACTS flow loop is now operational under elevated pressure and temperature. Currently, experiments with synthetic based drilling fluids under pressure and temperature are being conducted.

Based on the analysis of Fann 70 data, empirical correlations defining the shear stress as a function of temperature, pressure and the shear rate have been developed for Petrobras synthetic drilling fluids. PVT equipment has been modified for testing Synthetic oil base drilling fluids. PVT tests with Petrobras Synthetic base mud have been conducted and results are being analyzed

Foam flow experiments have been conducted and the analysis of the data has been carried out to characterize the rheology of the foam. Comparison of pressure loss prediction from the available foam hydraulic models and the test results has been made

Cuttings transport experiments in horizontal annulus section have been conducted using air, water and cuttings. Currently, cuttings transport tests in inclined test section are being conducted.

Foam PVT analysis tests have been conducted. Foam stability experiments have also been conducted. Effects of salt and oil concentration on the foam stability have been investigated. Design of ACTS flow loop modification for foam and aerated mud flow has been completed. A flow loop operation procedure for conducting foam flow experiments under EPET conditions has been prepared

Design of the lab-scale flow loop for dynamic foam characterization and cuttings monitoring instrumentation tests has been completed. The construction of the test loop is underway.

As part of the technology transport efforts, Advisory Board Meeting with ACTS-JIP industry members has been organized on May 13, 2000.

TABLE OF CONTENTS

LIST OF TABLES

STUDY OF FLOW OF SYNTHETIC DRILLING FLUIDS UNDER ELEVATED PRESSURE AND TEMPERATURE CONDITIONS

STUDY OF CUTTINGS TRANSPORT WITH AERATED MUDS UNDER LPAT CONDITIONS

STUDY OF FOAM FLOW BEHAVIOR UNDER ELEVATED PRESSURE AND ELEVATED TEMPERATURE CONDITIONS

LIST OF FIGURES

ACTF DESIGN AND CONSTRUCTION ACCOMPLISHMENTS

STUDY OF FLOW OF SYNTHETIC DRILLING FLUIDS UNDER ELEVATED PRESSURE AND TEMPERATURE CONDITIONS

STUDY OF CUTTINGS TRANSPORT WITH FOAM UNDER LOW PRESSURE AND AMBIENT TEMPERATURE CONDITIONS

STUDY OF CUTTINGS TRANSPORT WITH AERATED MUDS UNDER LOW PRESSURE AND AMBIENT TEMPERATURE CONDITIONS

STUDY OF FOAM FLOW BEHAVIOR UNDER ELEVATED PRESSURE AND ELEVATED TEMPERATURE CONDITIONS

DEVELOPMENT OF CUTTINGS MONITORING METHODOLOGY

DEVELOPMENT OF A METHOD FOR CHARACTERIZING BUBBLES IN ENERGIZED FLUIDS

1. INTRODUCTION

This annual report includes a review of the progress made in ACTS Flow Loop development and research during the period of time between July 14, 1999 and July 13, 2000.

The report presents information on the following specific subjects;

a-) Progress in Advanced Cuttings Transport Facility design and development (Tasks 1 and 2),

b-) Progress report on the research project (Task 8) "Study of Flow of Synthetic Drilling Fluids Under Elevated Pressure and Temperature Conditions",

c-) Progress report on the research project (Task 6) " Study of Cuttings Transport with Foam Under LPAT Conditions (Joint Project with TUDRP)",

d-) Progress report on the research project (Task 7) " Study of Cuttings Transport with Aerated Muds Under LPAT Conditions (Joint Project with TUDRP)",

e-) Progress report on the research project (Task 9) " Study of Foam Flow Behavior Under EPET Conditions",

f-) Progress report on the instrumentation tasks (Tasks 11 and 12)

g-) Activities towards technology transfer and developing contacts with oil and service company members.

2. EXECUTIVE SUMMARY

The Year 1 construction plans (Task 1) have been successfully completed. The ACTS flow loop is now operational under elevated pressure and temperature. Calibration tests with water under elevated pressure and temperature have been conducted. Currently, synthetic base drilling fluid tests are being conducted under elevated pressure and temperature.

Analysis of Fann 70 data for Petrobras synthetic base drilling fluid has been completed. Empirical correlations of shear stress as a function of temperature, pressure and shear rate for Petrobras data have been developed. PVT (Pressure volume temperature) equipment has been modified for testing synthetic drilling fluids. The equipment was calibrated by measuring PVT properties of water. The base oil of the Petrobras synthetic drilling fluid and the drilling fluid itself have been tested. Analysis of the base oil PVT data has been completed and presented in this report. Currently, PVT data of Petrobras mud is being analyzed. Results have shown that the base oil compressibility is two to five times higher than water compressibility under the same temperature and pressure conditions.

Experiments with foam flow in pipes and annulus have been conducted. Analysis of the data for rheological characterization of foam has been completed. Preliminary results have shown that the wall slip effect is not negligible and should be included in the calculation of actual wall shear rates. The results have also shown that the yield power law is not applicable for the foam under consideration. Power law model shows better fit to experimental data for 70% and 80 % quality foams, where as the Bingham Plastic model simulates better the behavior of the 90 % quality foam. Comparison of the pressure losses predicted from the available foam hydraulic models with the experimental results have shown that there is no “best model” which predicts frictional pressure losses for foam flow in pipes under all conditions. The model predictions differed by 5% to 250% from the experimental results depending on the pipe geometry , foam quality and foam flow rate.

Cuttings transport experiments have been conducted by using air, water and solid mixtures. Preliminary results have shown that it may not be possible to avoid cuttings bed deposition in horizontal wells under any practical combination of air and water flow rates. Results have also shown that for the given borehole geometry and the total flow rate, the cuttings bed height in horizontal wells is increased by increasing gas flow rate. A reduction in the average pressure drop was also observed as the gas flow rate is increased. Currently, experiments in the inclined annulus are being conducted

Design concepts for ACTS flow-loop modification for aerated mud and foam flow (Task #2, Year II) have been discussed with members of ACTS-JIP. Some possible modification of the initial design concepts have been identified based

on the discussion with industry members. The design concept is now finalized and the preparations for the purchase of the required equipment is underway. The three-phase Moyno pump has been ordered and expected to be in by the end of August 2000.

Experiments have been conducted to investigate the influence of salt and mineral oil addition on the foam stability. The foam stability was measured by using two different parameters: half life time and drainage rate. Results indicate that stability is not considerably affected by the salt presence up to 20% w/v. The oil presence, however, enhanced the foam stability. PVT analysis of foam has been conducted. Foam density values predicted as a function of pressure and temperature by using theoretical models seem to be significantly different than the measured values.

A software for controlling the data sampling and data storage during cuttings monitoring process have been developed.

Design of the lab-scale flow loop for dynamic foam characterization and cuttings monitoring instrumentation tests has been completed. The construction of the test loop is underway.

Continuous efforts have been spent to facilitate effective technology transfer. Two advisory board meetings with ACTS-JIP industry members have been organized (November 16, 1999 and May 23, 2000) Currently there are 9 members of the ACTS-JIP including, BP-Amoco, Chevron, Dowell Schlumberger, Halliburton, Intevep, JNOC, Petrobras, Statoil, and The U.S. D.O.E.

3. ACTF DESIGN AND CONSTRUCTION ACCOMPLISHMENTS

3.1 Construction since July 15, 1999

The primary construction objective for this past year has been the capability to heat the drilling mud. This has been completed. We now have the capability to heat the drilling mud in the test loop to 200 °F and return it (cool it) to some temperature slightly lower than ambient. We have also added:

- A second 100 Bbl. mud storage tank;
- Components to mix and transfer mud;
- New piping to connect the new mud and mix tanks;
- Insulation covering all of flow loop piping and the two 100 Bbl. tanks
- Additional instrumentation;
- A canopy covering over the boiler end of the test loop;
- Additional electrical power.

Specific components included are:

1. A 2,000,000 btu, indirect fired, natural gas boiler. The unit was manufactured by Heatec, Inc. in Chattanooga, Tennessee. It includes computerized controls which control the gas flame, a surge tank, and a number of safety devices;
2. A new gas regulator and supply line from the gas supply line to the test loop;
3. An Alfa-Laval plate heat exchanger for transferring boiler heat to the drilling mud being tested;
4. A 1,500,000 btu air/water cooling tower. The unit was manufactured by Baltimore Aircoil Company in Madera, California. It includes a water circulation pump, electronic control cabinet, and controls;
5. An Alfa-Laval plate heat exchanger for transferring the drilling mud heat to the cooling tower;
6. An additional 100 Bbl. fiberglass mud storage tank;
7. A 5 Bbl fiberglass mud mixing tank;
8. A small mud transfer pump;
9. A high volume, low head, centrifugal jockey pump;
10. A large tank mixer for one of the 100 Bbl. mud storage tanks;
11. A small tank mixer for the mud mixing tank;
12. Piping insulation for all of the flow loop piping;
13. Insulation blankets for all of the flow loop valves, flanges, chokes, and heating heat exchanger;
14. Tank insulation for each of the 100 Bbl. mud storage tanks;
15. Temperature sensors installed throughout the loop
16. A new Micro-Motion flow meter replacing the one we had borrowed last year;

17. A high range Differential Pressure Transmitter for the 2-inch rheology line;
18. Additional electrical power transformers for the boiler, cooling tower pump and fan, tank mixers, booster and transfer pumps, and for the future Moyno pump;
19. Additional electrical switch and fuse cabinets;
20. Electrical conduits installed between the electrical transformer location and the equipment location;
21. A canopy cover constructed over one end of the test loop covering the boiler, boiler controls, cooling tower controls, the mixing tank, and both mud storage tanks.

Construction efforts for "Year 1" have been completed except for the addition of the Moyno pump. Pictures showing the current status of the ACTS flow loop are given in Figs. 3.1-3.6. Figure 3.7 shows a floor plan of the current ACTS test loop with recent additions. Some future additions are also indicated in dashed lines.

The Moyno pump has been placed on order and is anticipated on site by the end of August, 2000. The Moyno has unique capabilities which will make it a valuable tool in our research effort. These include:

a. A near pulsation free flow;
b. Flow rate control with the variable frequency drive system;
c. The ability to "pump" solids;
d. The ability to compress gas as a single phase or in two or three phase flow.

The Tri-Phaze® is still a relatively new piece of equipment to the industry. The concept of pumping liquids, solids, and gas all in the same pump; at the same time, is unduplicated. The pump we have selected is called an 11,000 BPD pump. In reality, according to Moyno and the pump curve they have given us, it has a maximum volumetric flow rate of approximately 15,000 BPD (435 gpm). Maximum differential pressure is approximately 500 psi. Figure 3.8 shows a copy of the pump curve.

Figure 3.1 - ACTS Flow Loop-General Overview

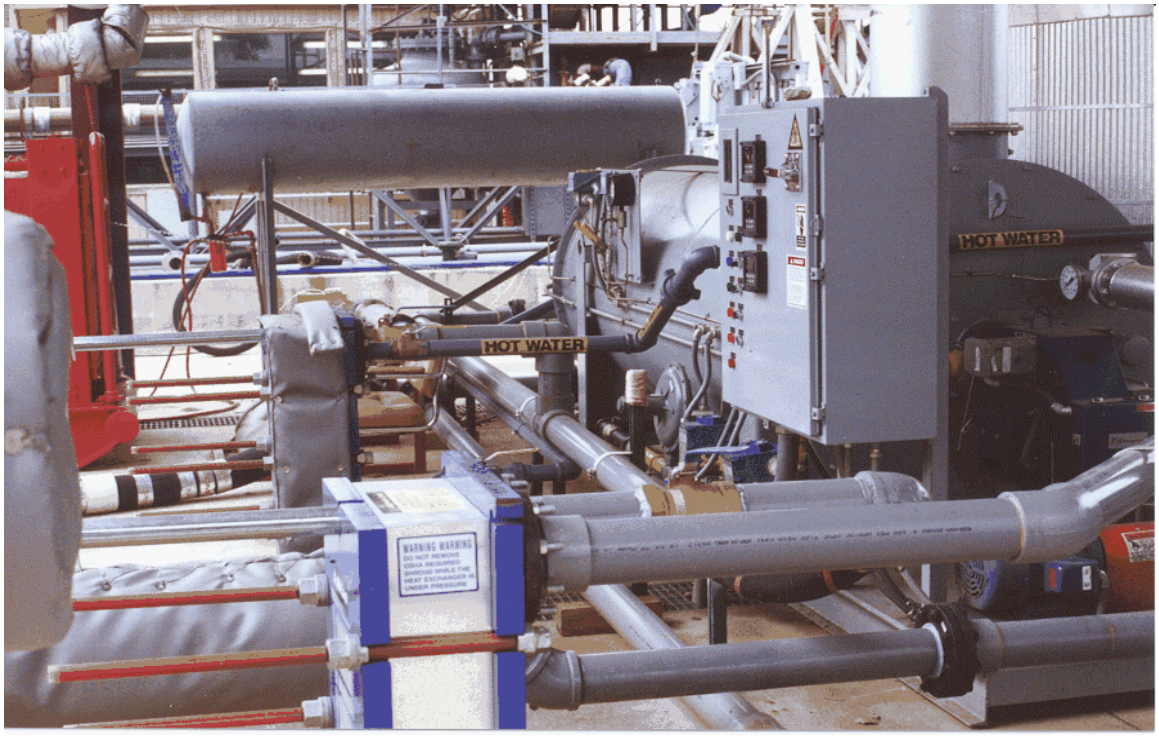

Figure 3.2 - Boiler and Heat Exchangers

Figure 3.3 - Cooling Tower

Figure 3.4 – Liquid Mass Flow Meter

Figure 3.5- Suction Piping

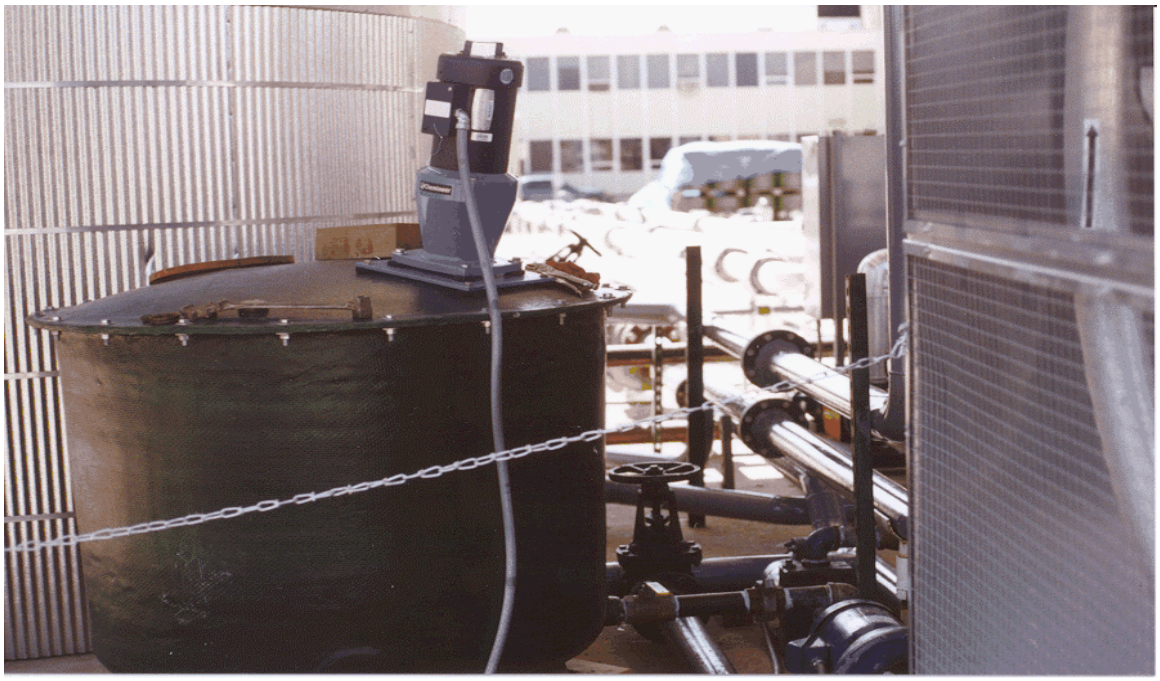

Figure 3.6 - Mud Mixing Tank

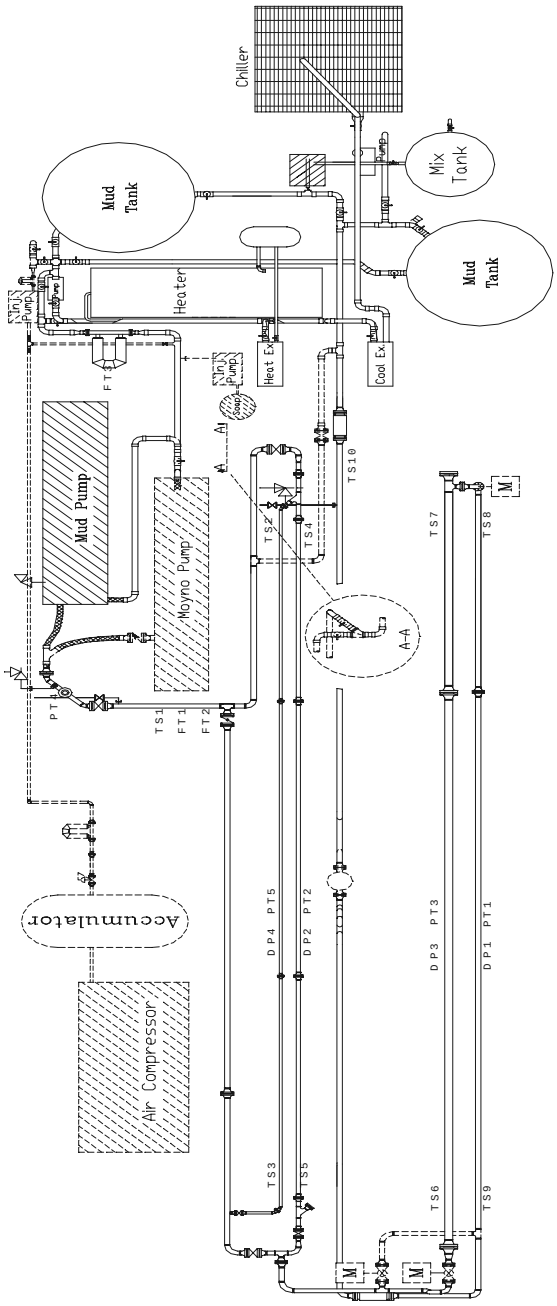

Figure 3.7 - Piping Plan and Layout

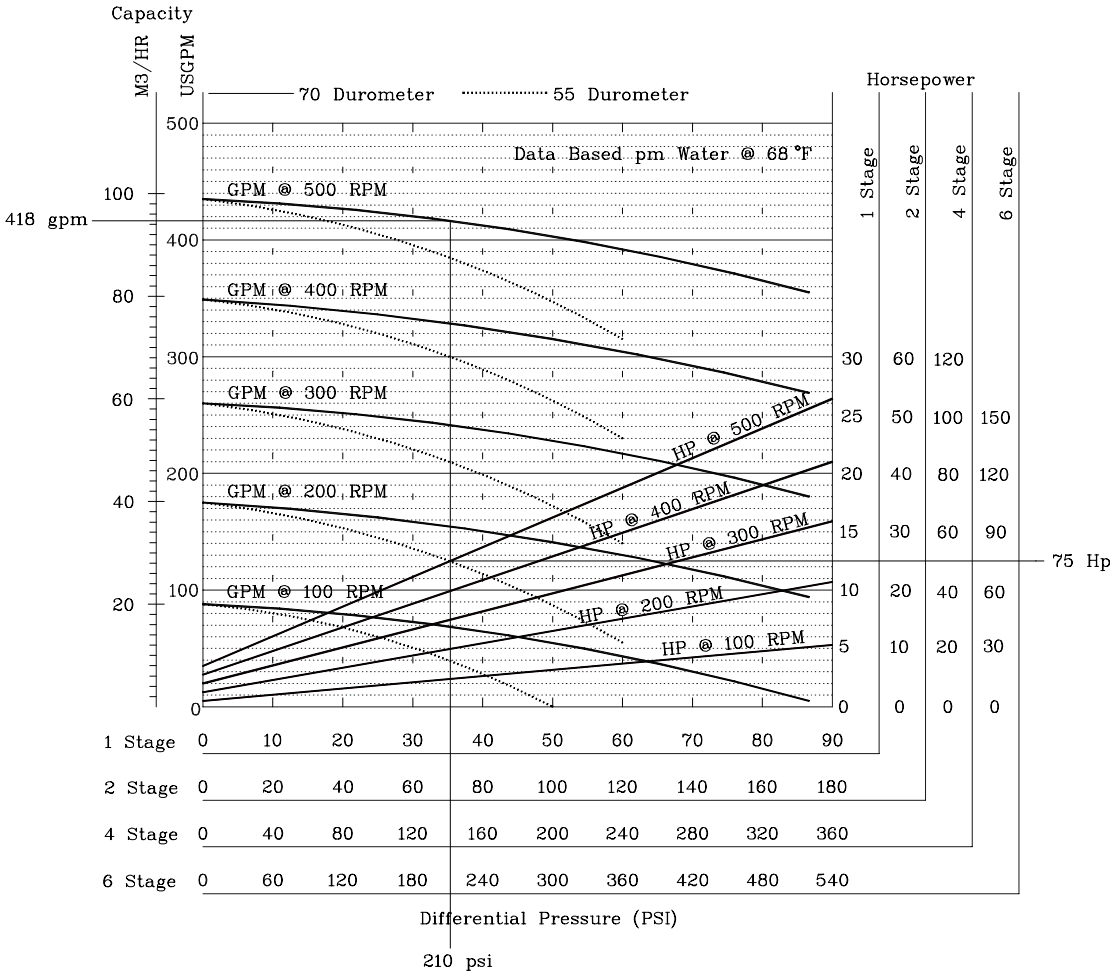

Figure 3.8 - Moyno Pump Curve

3.2. Planned Construction

The feature piece of equipment for the coming year will be an air compressor for the purpose of making foam and for two phase flow. Several scenarios have been proposed. In essence, these scenarios may be classified in two groups. Low pressure compressors which introduce air upstream of the liquid pump and high pressure compressors which introduce air downstream of the liquid pump. The primary difference in these two types is one of cost.

Figure 3.9 shows the scenario of the low pressure compressor introducing air upstream of the liquid pump:

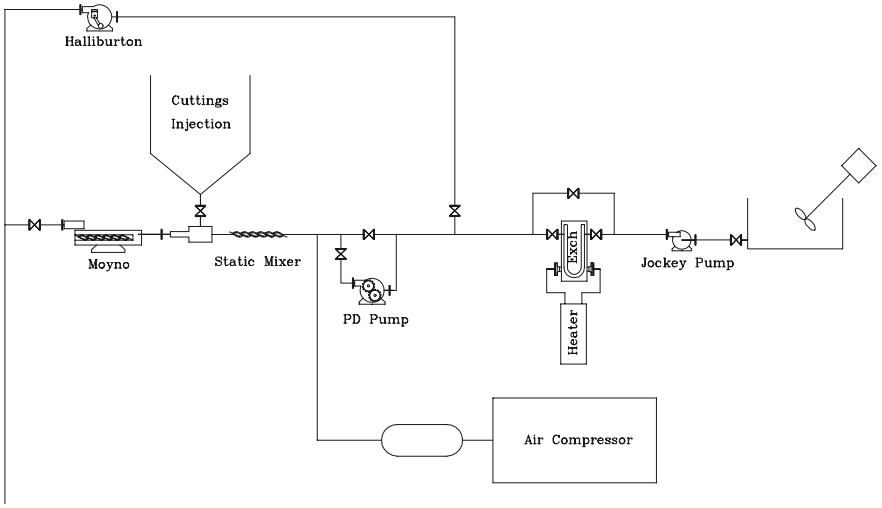

Figure 3.9 - Low Pressure Compressor Scenario

Figure 3.10 shows the scenario of a high pressure compressor introducing air downstream of the liquid pump.

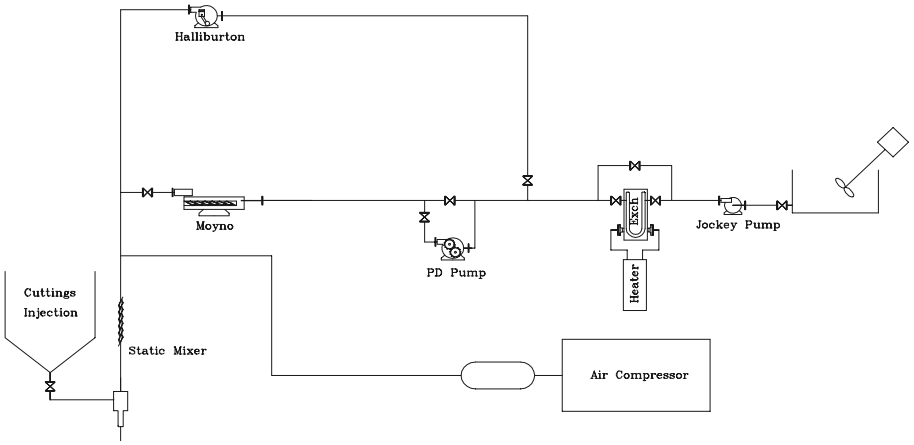

Figure 3.10 - High Pressure Compressor Scenario

In the scenario of a low pressure compressor which would introduce air upstream of the liquid pump, a compressor capable of producing 400 SCFM at 200 psig has been quoted to us for $31,150. After compression by the Moyno this would result in a pressure up to 700 psig. By comparison, a 400 SCFM compressor capable of producing 700 psig would cost approximately $70,000. In addition to the increased cost of a high pressure compressor, in this scenario, the cuttings injection tank would have to be located on the high pressure side in order to have

sufficient flow to move the cuttings in the pipe and this would also be an increase in cost.

It is anticipated that we will get a low pressure compressor based on the rational above, however as we approach our time to purchase the air compressor we will look at used equipment as well as new equipment. It is possible that we could purchase a good used high pressure compressor. We will evaluate the used equipment market and our options at the time.

Since an air phase is being introduced into the test loop, the air must be removed. As a part of the cuttings transport portion of the project, a cuttings removal tower which includes air removal has been planned as shown in Fig. 3.11

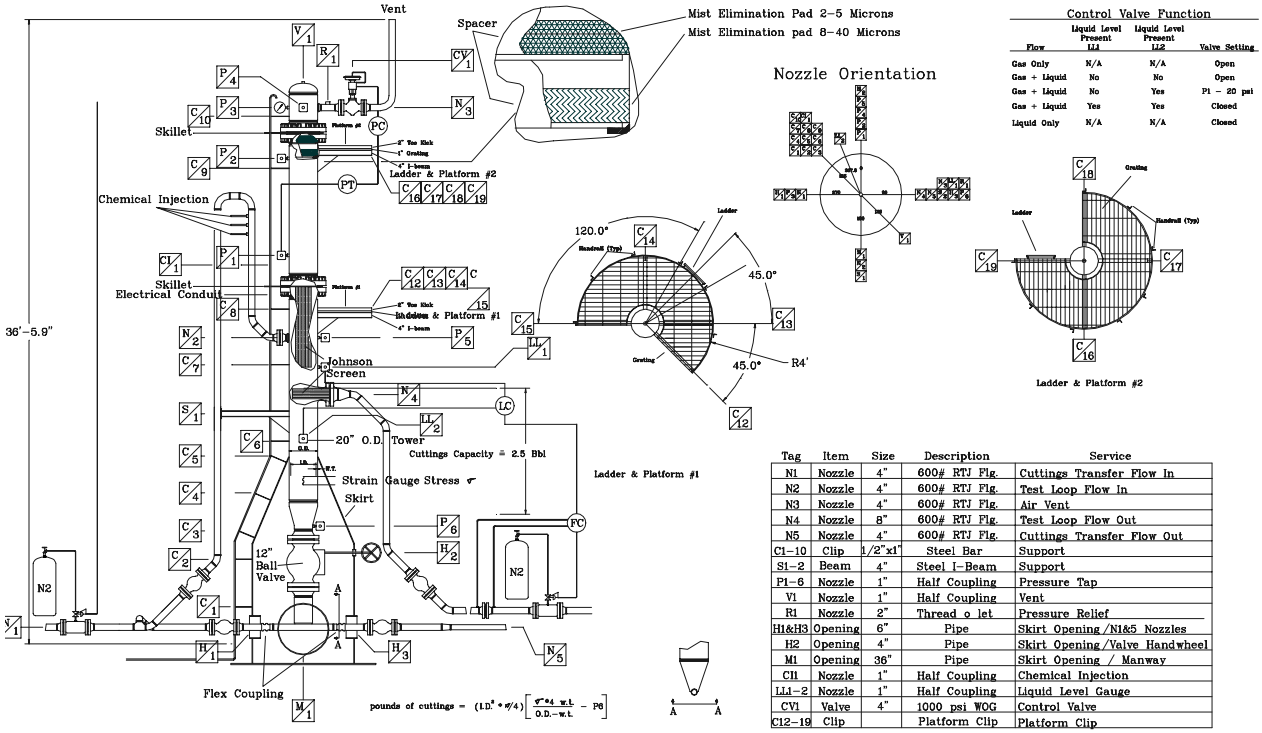

Tag	Item	Size	Description	Service
N1	Nozzle	4"	600# RTJ Flg.	Cuttings Transfer Flow In
N2	Nozzle	4"	600# RTJ Flg.	Test Loop Flow In
N3	Nozzle	4"	600# RTJ Flg.	Air Vent
N4	Nozzle	8"	600# RTJ Flg.	Test Loop Flow Out
N5	Nozzle	4"	600# RTJ Flg.	Cuttings Transfer Flow Out
C1-10	Clip	1/2"x1"	Steel Bar	Support
S1-2	Beam	4"	Steel I-Beam	Support
P1-6	Nozzle	1"	Half Coupling	Pressure Tap
V1	Nozzle	1"	Half Coupling	Vent
R1	Nozzle	2"	Thread o let	Pressure Relief
H1&H3	Opening	6"	Pipe	Skirt Opening /N1&5 Nozzles
H2	Opening	4"	Pipe	Skirt Opening /Valve Handwheel
M1	Opening	36"	Pipe	Skirt Opening / Manway
CI1	Nozzle	1"	Half Coupling	Chemical Injection
LL1-2	Nozzle	1"	Half Coupling	Liquid Level Gauge
CV1	Valve	4"	1000 psi WOG	Control Valve
C12-19	Clip		Platform Clip	Platform Clip

Figure 3.11 - Cuttings Removal Tower

The complete tower, however, is not for this coming year but for the 2001 construction season. Therefore, only the air removal section (Fig. 3.12) will be built this year.

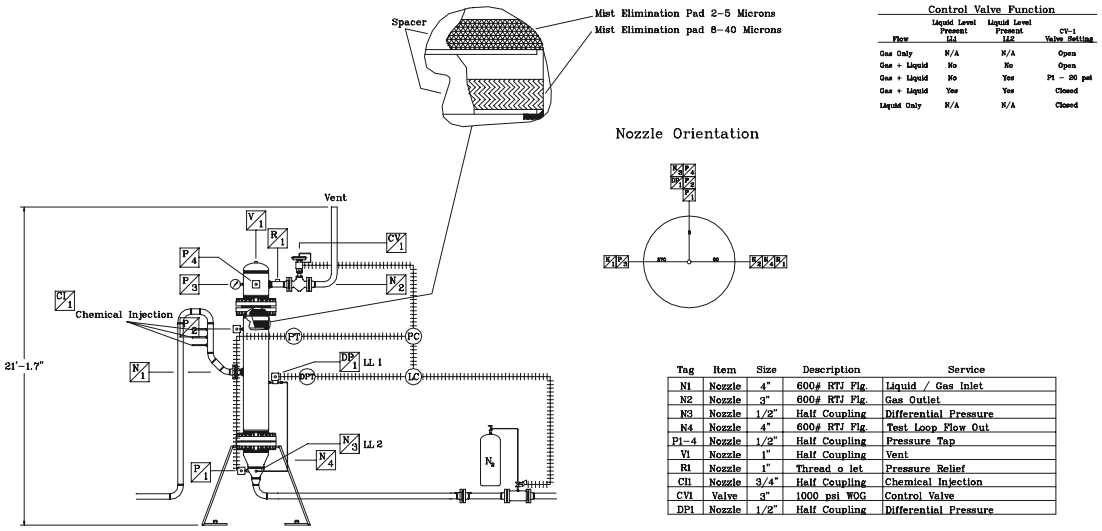

Figure 3.12 - Air Removal Section

This air removal system will provide for injection of foam breaker chemical to break the foam, vent the air back to atmosphere through a choke valve, and allow the liquid to go to one of the storage tanks. It is anticipated that the liquid to make the foam will come from one of the 100 Bbl. storage tanks and after use will be placed in the other 100 Bbl storage tank. The reason for this is to maintain a consistent water source for making the foam that has not previously been contaminated with surfactant or foam breaker.

Other components planned for this coming years construction include:

a. An air accumulator tank to be used in conjunction with the air compressor. This will minimize "cycling" of the air compressor and help maintain an more constant pressure and flow rate;
b. A surfactant injection system for injecting surfactant into the test loop at precise rates;
c. A static mixer to mix the water, surfactant, and air to make foam;
d. A back-pressure automation system which will enable us to more precisely and more efficiently control the test pressure;
e. An additional Micro-Motion flow meter to measure the small liquid volumes required for foam tests;
f. A small liquid pump for foam test requirements;
g. A Micro-Motion flow meter for the air;
h. Clear Drilling Sections to allow give us a visual check on what is inside the pipes;
i. Liquid Hold-up valves and actuators so we can measure the liquid hold-up in two phase flow.

4. STUDY OF FLOW OF SYNTHETIC DRILLING FLUIDS UNDER ELEVATED PRESSURE AND TEMPERATURE CONDITIONS

Investigator: Barkim Demirdal

4.1 Objectives

- To determine the effect of down-hole conditions (temperature and pressure) on rheological behavior of synthetic based drilling fluids both using rotational viscometer and pipe viscometer
- To develop a correlation, which is based on Fann 70 HPHT rotational viscometer analysis, to determine dial readings of a particular fluid at any pressure, temperature and shear rate and to investigate the applicability of the correlation for weighted synthetic based drilling fluids
- To investigate the change in wall parameters (n' and K') with change in fluid density, flow regime and cross section and to modify wall parameters as a function of fluid density, down hole conditions, geometry and flow regime. To investigate the effect of pressure and temperature on equivalent diameter in order to determine behavior of fluid flowing in a concentric annuli
- To determine the relation between wall parameters (n' and K') and rheological parameters (n, K and τ_Y) under down-hole conditions at different flow geometries using the experimental data and analytical relations
- To compare the effect of temperature and pressure on the densities of both synthetic base oil and synthetic based drilling fluid. To determine whether these fluids are compressible than water based and oil based drilling fluids or not
- To compare the experimental results obtained under laminar flow with analytical solutions determined for Yield Power Law fluids and to modify the analytical solutions by introducing the effect of pressure and temperature to rheological parameters and density
- To compare the experimental results obtained under transient and turbulent conditions with empirical correlations and to modify these equations by introducing temperature and pressure corrections in density and rheological parameters
- To introduce pressure and temperature effect to pressure loss calculation methods and improve the accuracy these methods' estimating actual frictional pressure losses

4.2 Introduction

In last 20-25 years, two important trends have been observed in drilling industry. These are, increase in the number of offshore operations and increase in depth of wells. These two major trends force the industry to conduct more research on flow and rheology of drilling fluids.

As the number of offshore drilling operations increase, discharge of cuttings contaminated with drilling fluids becomes a very important challenge to overcome. It is desirable to use a drilling fluid that would not only fulfill the

operational advantages of the conventional drilling fluids but also provide environmental safety issues. Although, oil based drilling fluids were preferred due to operational advantages such as better shale inhibition, well bore stabilization and lubrication when compared to water based drilling fluids, they may have some environmental restrictions. This disadvantage was a major reason to come up with a new drilling fluid type, known as synthetic based drilling fluids (SBDF).

The second important trend, increase in deep and ultra deep drilling operations, resulted in high flow rates of drilling fluid circulation, to maximize the energy transfer to the bit for higher rate of penetration. To be able to achieve this aim, the drilling fluid specifications should be done correctly to determine parasitic pressure losses precisely. It was also observed that synthetic based drilling fluids help to overcome the challenges in deep and ultra-deep drilling compared to water based fluids. Synthetic based drilling fluids avoid gas hydrate formation in blowout preventers and reduce hole-cleaning problems in large diameter riser sections.

Despite the advantages of synthetic based drilling fluids in offshore and deep and ultra deep well operations, it is difficult to predict their rheological behavior under down-hole temperature and pressure conditions. In most cases, non-Newtonian fluid models determined at surface conditions have been used to determine frictional pressure losses. Calculated frictional pressure losses do not match with the ones measured in the field. This discrepancy between calculated and measured pressure losses is even higher for synthetic base drilling fluids since their rheological properties and densities are severely affected with changes in down-hole conditions.

Synthetic based drilling fluid rheology changes with down-hole conditions severely due to thinning and thickening effect of temperatures and compressibility effect of pressure and temperature on the oil phase of the drilling fluid. As it is known, parasitic pressure loss determination has vital importance in selecting suitable mud pumps and estimating ECD (Equivalent Circulating Densities). Therefore, predicting the fluid rheology under well bore conditions is an important problem to overcome, in order to design suitable hydraulic programs.

In order to reduce the gap between calculated and measured frictional pressure losses, the effect of pressure and temperature on fluid rheology and density should be analyzed carefully. Only after that, appropriate corrections on pressure loss equations can be made and measured pressure losses can be estimated with higher accuracies.

The aim of this study is to determine the rheological behavior of synthetic based drilling fluids under down-hole conditions and to determine the expected pressure losses in both laminar and turbulent flow conditions during pipe flow and annular flow. We will attempt to relate surface rheological properties to down hole rheological models by using correlation between pipe viscometer and rotational viscometer data. In this manner, it would be possible to investigate if laminar flow properties can be used to define turbulent flow characteristics and rheological models under turbulent flow of water-in-oil emulsions.

In this research, firstly shear stress-shear rate relation of the synthetic based drilling fluid is determined. High pressure-high temperature (HPHT) Fann 70 rotational viscometer data are used to determine the behavior of the drilling fluid. As a result of the analysis, fluid's shear stress-shear rate relation is determined as Yield Power Law (Herschel-Buckley) model at every temperature and pressure that it is tested.

After that, the effect of temperature, pressure and shear rate on shear stress is determined again using Fann 70 HPHT rotational viscometer results. In the process of rheological characterization, it was aimed to find out a single relation that will relate dial readings with shear rate, temperature and pressure. Once such a relation is known, then fluids' shear stress could be determined under any down-hole conditions at any flow rate. In order to determine such a function, non-linear and linear regression analysis techniques were used. Most of the non-linear regression analysis is conducted using a statistical software package called "STATISTICA". This report covers the detailed summary of rheological modeling and rheological characterization processes.

As indicated above, by using Fann HPHT 70 data, shear stress' relation to flow rate, temperature and pressure is determined. However, it should be remembered that the model is based on rotational laminar flow data. In order to determine the applicability of this model to pipe and annular flow (in laminar, transition and turbulent flow regimes), ACTS flow loop will be used. This report covers the last modifications in the ACTS flow loop and calibration experiments results that are obtained by circulating water at elevated pressure and elevated temperature conditions.

As it is mentioned above, not only the rheology but also the densities of drilling fluids are affected from changes down-hole conditions. In order to determine the effect of pressure and temperature on density of fluid, mercury free PVT equipment was used. As a first phase of PVT experiments, calibration of the apparatus with water is completed. The results of these calibration experiments and the detailed explanation of experimental procedure and properties of PVT equipment are given in this report. After calibration experiments were completed and experimental procedure is developed, Petrobras synthetic based oil was tested in order to determine the effect of pressure and temperature on base oil density. Experimental results and detailed analysis of these results were summarized in this report as well. In addition to that, density behavior of base oil is compared with other drilling fluids.

4.3 Literature Review

Considerable effort has been devoted to understanding the flow of non-Newtonian fluids, particularly in pipes. Since laminar flow mechanisms are easier to understand compared to turbulent flow, basic laminar flow equations that are valid for non-Newtonian systems were reviewed first.

Analysis of non-Newtonian fluid flow in turbulent flow is much more complex. Very little is known about the rheological properties of fluids under turbulent flow conditions. For that reason, correlation between turbulent frictional losses and laminar fluid properties are determined to define realistic

approximations of fluid properties in turbulent flow. To do that, a great effort has been spent to find the answer of the question “How can these laminar relations be used to define turbulent flow of non-Newtonian systems?”.

4.3.1.Studies on Non-Newtonian Fluid Flow In Pipes and Annuli:

A general relationship for steady, stabilized, laminar flow of time-independent purely viscous fluid in a pipe, was developed by Rabinowitsch [1] and Mooney [2] as;

$$Q = \pi \int_0^{\tau_w} \frac{R^3 \tau^2}{\tau_w^3} f(\tau) d\tau \quad \text{.....(4.1)}$$

where

$$\tau_w = -\frac{D}{4}\frac{dP}{dL} \quad \text{.....(4.1a)}$$

Equation (4.1) can be arranged and differentiated with respect to $D\Delta P/4L$, resulting in

$$f(\tau_w) = -\left(\frac{du}{dr}\right)_w = 3\frac{8V}{D} + \frac{D\Delta P}{4L}\frac{d(8V/D)}{d(D\Delta P/4L)} \quad \text{.....(4.2)}$$

This is a general relationship showing the shear rate at the wall when a time independent fluid is flowing through a pipe under laminar flow conditions.
Defining a wall parameter *n'* that is equal to

$$n' = \frac{d\, ln(D\Delta P/4L)}{d\, ln(8V/D)} \quad \text{.....(4.3)}$$

equation (3.1.2) becomes

$$-\left(\frac{du}{dr}\right)_w = \frac{8V}{D}\left[\frac{1+3n'}{4n'}\right] \quad \text{.....(4.4)}$$

Equations (4.1) and (4.4) are known as the “Rabinowitsch-Mooney Relations”. One should be aware that this form of the equation is general and independent of a fluid’s rheological model. To solve this equation, various methods have been used. These methods can be divided into two basic categories. Some investigators assume a functional relationship between shear rate and shear stress. This approach indicates that the, rheological model of the fluid will be constant throughout the flow and independent of pressure and temperature. On the other hand, some investigators have adopted a generalized correlation to solve the integral.

By using the second approach Metzner and Reed [3] developed a generalized approach that may be applied to laminar pipe flow of time-independent fluids. They carry the Rabinowitsch-Mooney approach further by defining the equation;

$$\frac{D\Delta P}{4L} = K'\left(\frac{8V}{D}\right)^{n'} \quad \text{.....(4.5)}$$

In this way, the shear stress-shear rate relation of the fluid is evaluated using wall parameters. Next, they used the “Fanning Friction Factor” equation and defined the friction factor, *f* as

$$f = \frac{g_c D \Delta P}{2 \rho V^2 L} \quad \text{.....(4.6)}$$

and defined a generalized Reynolds number, $N_{Re,MR}$, under laminar flow conditions as

$$f = 16 / N_{Re,MR} \quad \text{.....(4.7)}$$

Combining equations (4.6) and (4.7) and using the definition of $D\Delta P/4L$ in equation (4.5), the "*Generalized Reynolds Number*" can be shown as,

$$N_{Re,MR} = \frac{D^{n'} V^{2-n'} \rho}{g_c K' 8^{n'-1}} \quad \text{.....(4.8)}$$

Savins, Burdyn and Wallick [4] also tried to solve the "Rabinowitsch-Mooney Relationship" with relations derived from functional relationships between observed kinematic and dynamic parameters in simple shearing flows. Using this relation, they represented the laminar flow data by a single curve in which $f(\tau_w)$ is plotted as a function of τ_w. This representation is independent of the rheological model of the fluid. After a $f(\tau_w)$ *vs.* τ_w diagram is prepared, using the values of $f(\tau_w)$ and τ_w taken from the smoothed curve, flow rate and pressure drop can be determined from the following relations;

$$Q = D^3 f(\tau_w) k_1 \quad \text{.....(4.9)}$$

and

$$\Delta P / L = \tau_w k_2 / D \quad \text{.....(4.10)}$$

In their pipe-flow scale-up example, the main aim is to find the appropriate values of $f(\tau_w)$ and τ_w for given design flow rates and tube diameter. Based on this approach, they developed a computer program in which laminar parameters $f(\tau)$ and τ are given to define wall characteristics (*n'* and *K'*) of the fluid. Then, for given conditions of flow rate and diameter, the program determines shear rate at the wall ($f(\tau_w)$) and shear stress at the wall (τ_w) by searching an interpolation table that is constructed beforehand. They also proposed a way to determine the pressure losses of inelastic fluids under turbulent flow conditions, using the characteristic rheological parameters of the fluid that were evaluated at existing wall stress under laminar flow. They used the f-N_{Re} relation found by Dodge & Metzner [5] as follows (derivation of this equation can be found in the May 99 ACTS-ABM Report [6],

$$\frac{1}{\sqrt{f}} = \frac{4.0}{n'^{0.75}} \log\left[N_{Re,MR} f^{(1-n'/2)}\right] - \frac{0.40}{n'^{1.2}} \quad \text{.....(4.11)}$$

An iterative method is used to determine the existing wall shear stress under turbulent flow conditions for rheologically complex drilling fluids. Basically, they determined the wall shear stress at laminar flow conditions and assumed that this value should be higher in turbulent flow conditions. Shear stress at the wall is increased until the iteration matches with the shear stress obtained using the Fanning pressure loss equation;

$$\tau_w = \frac{f\rho V^2}{2g_c} \quad \text{.....(4.12)}$$

Their study agreed well with Dodge's experimental data, both in turbulent and laminar flow conditions.

Zamora and Lord (1974) [7], proposed a new numerical and graphical technique to determine the pressure losses of non-Newtonian fluids in pipes and annuli. Their model was developed from the theoretical analysis of power law fluids and extended to a general model to approximate Bingham plastics and Herschel Buckley (Yield power law) fluids. The general shear stress shear rate relation of a fluid can be written as;

$$\tau = \tau_o + K\gamma^n \quad \text{.....(4.13)}$$

or in terms of rotational viscometer readings, this can be represented as;

$$\theta = \theta_o + KR^n \quad \text{.....(4.14)}$$

They overcome the difficulty of defining the shear rate in measuring surfaces by proposing a geometry factor (G) that is based on the analytical work of Fredrickson and Bird [8]. This geometry factor accurately relates viscometer rotation to shear rate as follows;

$$R = 0.939\frac{GV}{D} \quad \text{.....(4.15)}$$

As it is known, another difficulty is to define the viscosity term in the Reynolds number for non-Newtonian fluids. They have used the nominal viscosity term that is proposed by Annis [9] and defined the viscosity at any shear rate shear stress condition as follows

$$\mu = 300\frac{\theta}{R} \quad \text{.....(4.16)}$$

Substituting this definition into the classical Reynolds number, and using definition of R from equation (4.15), a generalized N_{Re} can be computed as;

$$N_{Re} = \frac{G\rho V^2}{20.66\theta} \quad \text{.....(4.17)}$$

Dividing by the geometry factor (G), a modified Reynolds number, N_{Re}' is obtained as;

$$N'_{Re} = \frac{\rho V^2}{20.66\theta} \quad \text{.....(4.18)}$$

This equation is equivalent to the generalized Reynolds number derived by Metzner and Reed [3]. The only difference is that, Zamora and Lord's value is in terms of rotational viscometer readings instead of pipe flow wall parameters.

They also tried to improve the above relations to calculate pressure losses in the turbulent flow as well. Approximations proposed by Schuh [10] were used to calculate Reynolds number as a function of *n* in laminar-transition and transition-turbulent region as follows

$$N_{Re,Lam-Tr} = 3470 - 1370n \quad \text{.....(4.19)}$$

and

$$N_{Re,Tr-Tur} = 4270 - 1370n \quad \text{.....(4.20)}$$

It is assumed that fluid rheology can be described using power law model in turbulent flow. As a result, the fluid rheology in turbulent flow is shown as;

$$\theta = k'' R^s \quad \text{.....(4.21)}$$

where *s* is defined from the Blasius constants as a function of laminar *n*.

The study of Zamora and Lord improved determination of a geometry factor that allows defining flow in pipes, annuli and parallel plates. Correction for down hole conditions and better turbulent flow correlations are needed to improve this simple technique

Randall and Anderson [11] also tried to develop friction factors and empirical corrections from current theories to model flow of non-Newtonian fluids. They pumped water based drilling fluids through drill pipes and annuli to determine pressure losses. They developed log-log charts of shear stress vs. velocity and determined laminar and turbulent *n'* values. They found that *n* in turbulent conditions is higher than *n'* in laminar flow. They also compared rheological parameters obtained from pipe viscometer results with those obtained from a Fann viscometer.

They found an empirical fit to the data by using rotational viscometer readings as

$$f = \left(\frac{N_{Re,MR}}{10000} \right)^A 0.01016 - 0.0014 \left(\frac{2.9 + \sqrt{2\theta_3 - \theta_6}}{1 + \log(\theta_6 - \theta_3)} \right) \quad \text{.....(4.22)}$$

where

$$A = -0.01 \frac{\theta_6}{\theta_3} - 1 + 0.1 \log(\theta_6 - \theta_3) 10 + [5 \log(\theta_6 - \theta_3)]^{1.4} \quad \text{.....(4.23)}$$

They assumed that fluid behaves as Bingham plastic while flowing through the annulus. Since fluid do not exactly follow the power law fluid model, it was decided that using Metzner and Reed [3] $N_{Re,MR}$ would not be realistic. For that reason, to determine the transition between laminar and turbulent regimes, pressure losses were calculated for both of them and actual correct regime is chosen as the one that gives higher pressure loss. It was found that Bingham plastic equation for laminar flow

$$\Delta P = \frac{\tau_{YP} L}{225(d_o - d_i)} + \frac{\mu_P L V}{1500(d_o^2 - d_i^2)} \quad \text{.....(4.24)}$$

predicted high pressure losses for drilling fluids with high yield stresses. To obtain more precise results, equation (4.24) is modified to;

$$\Delta P = \left(\frac{\mu_p}{\mu_p + \tau_{YP}} \right) \frac{\tau_{YP} L}{225(d_o - d_i)} + \frac{\mu_P L V}{1500(d_o^2 - d_i^2)} \quad \text{.....(4.25)}$$

They also found that pressure losses in the annulus could be determined more accurately using the modified Fanning equation for the annular flow derived by Vaughn et al. [12]

$$\Delta P = \frac{2 f_a L \rho V^2}{g((d_{ao} - d_{ai})(d_{ai} - d_{ao})^{4-2n'}} \quad \text{.....(4.26)}$$

where the friction factor is defined as

$$f_a = 16n'/N_{Re} \quad \text{.....(4.27)}$$

for laminar flow and

$$f = \left(\frac{N_{Re,MR}}{10000} \right)^{A/2} 0.01016 - 0.0014 \left(\frac{2.9 + \sqrt{2\theta_3 - \theta_6}}{1 + \log(\theta_6 - \theta_3)} \right) \quad \text{.....(4.28)}$$

for turbulent flow.

As a result of this study, rotational viscometer results were correlated to determine frictional pressure losses in both laminar and turbulent flows. It also helps to define a correlation for the annular section. However, while determining the *f vs.* N_{Re} relation, they do not account for the change in fluid properties under down-hole conditions.

As mentioned, annular flow of non-Newtonian fluids is important in drilling applications while determining cutting transport efficiency and predicting annular pressure losses. The major difficulty in predicting the pressure losses in the annulus is in defining the annular geometry effectively. Several equivalent diameter concepts have been proposed. However applicability of those theorems has not been verified with experimental results yet. Not so much work has been done on annular flow and the work done has been mostly on small scale experimental set up that does not represent actual drilling situations.

Work done by Langlinais, Bourgoyne and Holden [13] is important in this manner. They obtained experimental results from two wells by using water based drilling fluids. They compared the applicability of three widely used “equivalent diameter concepts” (Hydraulic Radius, Crittendon Criteria, and Slot Approximation), together with power law and Bingham plastic fluid approximations, to experimental results.

They modified the Reynolds number to annular flow by replacing diameter with equivalent diameter and viscosity with apparent viscosity. Their modified Reynolds number expression is;

$$N_{Re} = \frac{928 \rho V d_e}{\mu_a} \quad \text{.....(4.29)}$$

where apparent viscosity is,

$$\mu_a = \mu_P \quad \text{.....(4.30)}$$

for Bingham plastic fluids and

$$\mu_a = K \frac{(d_o - d_i)^{(1-n)}}{144V^{(1-n)}} \left[\frac{2 + 1/n}{0.0208} \right]^n \quad \text{.....(4.31)}$$

for power law fluids.

Pressure loss equations shown by Bourgoyne et al.[14], were used in this study to determine theoretical pressure losses.

Langlinais et al. found that, pressure losses in annulus is more sensitive to “d_e” rather than to the rheological model. They have determined that the Crittendon criteria together with Bingham plastic model approximated the experimental data with high accuracy.

Guillot and Denis [15] worked on the flow of cement slurries in pipes and concentric annuli. Their work is similar to the objective of that research in such a way that, they have tried to extend coaxial cylinder viscometer measurements to

laminar and/or turbulent flow of cement slurries in pipes and annuli. They have developed a small scale pipe viscometer and tested bentonite mud and several cement formulations. They have used coaxial cylinder viscometer for rheological characterization purposes.

Experimental results show that, Bingham plastic model leads to over prediction of frictional pressure losses in all regimes and samples. In case of power law fluid assumption, quality of the fit depends on the "non-Newtonian" character of fluid. When fluid becomes more Newtonian, accuracy of theoretical results is increasing. The reason for such a discrepancy is due to the fact that, shear rate data obtained from coaxial cylinder is far less than that of fluid experienced in pipes and annuli. In order to get rid of that discrepancy, they propose using pipe data and coaxial cylinder data together. They have proposed a new model that is applicable to fluids under investigation above $20s^{-1}$.

$$\tau = \psi\gamma^{m} + \mu_{\infty}\gamma \quad \text{.....(4.32)}$$

They have determined "*m*" and "ψ" using power law fit of the data. Then μ_{∞} is identified using both pipe and coaxial cylinder data. It is found out that, frictional pressure loss prediction of the data is much better than those that use other rheological parameters.

They have also observed that, annular slot flow equation is more accurate to predict frictional pressure losses compared to pipe flow equations with "hydraulic diameter".

It is stated at the end of this study that, more studies should be done in order to understand the transition regime mechanism of non-Newtonian fluids in both pipes and annuli.

Jensen and Sharma [16] did an extensive work on friction factor and equivalent diameter correlations for annular non-Newtonian flow. They have investigated different *f*-d_{eq} correlations for use in determining the frictional pressure losses in annuli.

They have used actual well results as experimental part of their work. They have tried 64 different combinations of four different equivalent diameters and 16 different friction factor correlations that are proposed by previous investigators, to estimate the frictional pressure losses in annuli. They have determined that, the best combination of equivalent diameter and friction factor correlation for Bingham plastic fluids is hydraulic diameter and Chen's correlation [17] respectively. On the other hand, for power law fluids none of the combinations gave approximate results with experimental values.

In order to increase the accuracy of Bingham plastic fluid annular pressure loss estimations and improve power law fluid annular pressure loss estimations, they have proposed the following correlations that based on experimental results taken from actual wells;

<u>For Bingham Plastic Fluids:</u>

*Equivalent Diameter: $d_e = d_o - d_i$ .....(4.33)

*Friction Factor Correlation: $f = \left[-2\log\left(\frac{\varepsilon}{0.31 d_e} + \frac{3.7}{N_{\mathrm{Re}}} \right) \right]^{-2}$ .....(4.34)

For Power Law Fluids;

*Equivalent Diameter: $d_e = d_o - d_i$ ……..(4.33)

*Friction factor Correlation: $f = \frac{y}{N_{\mathrm{Re}}^{z}}$ ……..(4.35)

where;

$z = \frac{1.75 - \log(n)}{7}$ ……..(4.35a)

and

$y = \frac{[\log(n) + 3.93]}{[(100 - 27d_e)(246 - 236n)]}$ ……(4.35b)

The accuracy of the proposed correlations is better than the ones proposed before. However, it should be noted that, during theoretical pressure loss estimations, authors did not correct rheological parameters for down-hole conditions and assume that the reason of discrepancy between actual and calculated pressure losses is due to different definitions of friction factor and equivalent diameter correlations.

4.3.2.Studies on Rheological Characterization Of Oil Based & Synthetic Based Drilling Fluids Under HPHT Conditions:

The rheology of invert emulsions varies with temperature and pressure. Several methods have been proposed to model the rheological parameters or at least the viscosity under different temperature and pressure conditions. Some of these methods were reviewed in the ABM May 99 [6] report. Other contributions by previous investigators on the rheology of invert emulsions, summarized below.

Minton and Bern [18] study the rheological behavior of low toxicity oil based drilling fluids. They derive correction factors to correlate rheological parameters measured in down-hole conditions. They compared the annular and pipe frictional pressure losses obtained from actual wells using Measurement While Drilling (MWD) tools to theoretical pressure losses calculated using corrected and uncorrected rheological parameters.

As a starting point in analyzing the effect of temperature and pressure on rheological parameters of the fluid, they used assumption of Stiff [19] to relate temperature and viscosity. The relation between viscosity and temperature can be shown as,

$\mu = C_1 e^{-(\alpha T)}$ ……(4.36)

Using a similar assumption, relation between pressure and viscosity can be shown as, (Johnston [20])

$\mu = C_2 e^{(\beta P)}$ ……(4.37)

Combining these two equations and relating to reference conditions results in

$\mu(T, P) = \mu_o e^{[\alpha(T - T_o) + \beta(P - P_o)]}$ ……..(4.38)

They concluded that for the same shear rate, the shear stress at the desired conditions of temperature and pressure is related to the shear stress at reference conditions as follows;

$$\tau(T,P,\gamma)=\tau_o(\gamma)e^{[\alpha(T-T_o)+\beta(P-P_o)]} \quad \text{.....(4.39)}$$

Comparing theoretical results with actual pressure losses they found that the Bingham plastic model is able to predict the flow of low toxicity invert emulsion fluids under the conditions analyzed. Furthermore, rheological parameters that are corrected for down-hole conditions are more accurate below depths of 2000 ft.

They have stated that, improved rheological models are still needed for down-hole fluid behavior estimations and these models should also include density correction factor.

Hemphill [21] predicted the rheological behavior of ester based drilling fluids under down-hole conditions. Rather than using a specific rheological model, he correlated the changes in dial readings with temperature and pressure. This model was investigated by Hemphill et. al. [22] while working on the rheological characterization of ester-based invert emulsions used in Norway. By this method, use of certain rheological models, thus defining fluid with a certain model, is avoided. He related all the results to a relative parameter measured at 120^{o}F and 0 psig. Using this parameter, Relative Dial Readings is defined as;

$$RDR=\tau/\tau_{120^oF,0\,psi} \quad \text{.....(4.40)}$$

Pressures applied during the tests were 0, 2000, 4000, 6000 and 8000 psi. Temperature applied during tests range between 50-240^{o}F. At each pressure/temperature combination, the rheological behavior of the fluid was measured at eight specific shear rates; 600, 300, 200, 100, 60, 30, 6 and 3 rpm using a Fann 70 HPHT rotational viscometer.

As a result of that study, it was observed that both water content and solid content of ester based drilling fluids affect the density behavior under down-hole conditions. It was also mentioned that using single pressure and temperature coefficients to predict down-hole rheology over a wide range of shear rate may cause problems in defining the rheological model of the fluid. It was shown that each individual shear rate requires its own set of coefficients derived from curve fitting techniques. Under these circumstances, it was found that ester based fluid behavior becomes increasingly non linear as temperature is higher than 75-80^{o}F. Moreover, RDR values decrease with shear rate at constant pressure values.

This approach might be useful in research we are conducting. Since it does not assume any rheological model, it would be easier to define the rheological properties of the fluid under given conditions accurately.

A recent study on effect of pressure and temperature on rheology of drilling fluids have been published by Davison et al. [23]. They have studied the rheological characterization of 18 different drilling fluids using Fann 70 HPHT rotational viscometer. Since low temperature, high pressure conditions are likely to happen in deep and ultra deep drilling conditions (especially around riser), they have tested the fluids in the range of -1^{o}C to 90^{o}C and 1bar to 344.7 bar.

They have conducted Fann 70 experiments in two different sets. In one set, they have increased the temperature (occurs in pipe flow) and determine the

rheological parameters of drilling fluids while in the other set they have lowered the temperature (occurs in annular flow) and determine rheological parameters.

They have found out that, best model to describe shear stress-shear rate relation for any fluid at different oil/synthetic:water ratios and different densities, is yield power law model. When the rheological parameters of fluids were investigated, they have found out that there is hysteresis in viscosity of drilling fluids. The shear stresses measured while cooling down are higher then shear stresses measured while heating the samples.

Experimental results also show that, effect of base oil type and oil/synthetic:water ratio to shear stresses is important especially at low temperatures. For that reason, fluid selection should be done carefully for offshore applications.

In addition to these, ECD calculations with and without pressure and temperature corrected rheological parameters show that careful modeling of fluid hydraulics and well temperature profile is necessary for accurate frictional pressure loss predictions.

4.4 Fann 70 HPHT Rotational Viscometer Experiments

Fann 70 HPHT Rotational viscometer tests were conducted to determine changes in rheological properties of fluids under elevated pressure and temperature conditions. Since fluids in rotational viscometers were subject to lower shear rates, they flow under laminar conditions. For that reason the rheological parameters were obtained under laminar flow conditions.

Temperature and pressure test ranges of Fann 70 HPHT rotational viscometer is higher than that of pipe viscometer (ACTS). Thus, it would be necessary to extrapolate the pipe viscometer readings to higher pressure and temperature conditions in order to compare them with Fann 70 HPHT rotational viscometer results. Fluids were tested with HPHT Fann 70 rotational viscometer in temperature range of 40^{o}F-280^{o}F and pressure range of 500psig-12000 psig (Table 4.1).

Rheological characterization of Petrobras synthetic based drilling fluid has carried out with two different approaches. First approach aimed to show shear stress-shear rate relation of Petrobras drilling fluid using well defined models in all different pressure and temperature conditions. By doing so, it would be understood whether, the shear rate-shear stress relation of the fluid could be defined with one single model in all different down-hole conditions or not. The second approach aimed to determine how shear stress is changing with temperature, pressure and shear rate. The advantage of second relation is that, user did not need to fit the drilling fluid shear stress-shear rate relation to any kind of rheological model which might be valid for experimental ranges while they might be void in other conditions.

4.4.1 Rheological Model Analysis of Petrobras Synthetic Based Drilling Fluid:

First of all, drilling fluid's rheological model under surface conditions is determined using Chan 35 rotational viscometer readings. In addition to that, Fann 70 rotational viscometer tests have been used in order to determine the

rheological behavior of Petrobras synthetic based drilling fluid under different pressure and temperature conditions. The “RHEO” subprogram in the YPL TUDRP software is used to determine a rheological model that best fits Fann 70 and Chan 35 viscometer test results of Petrobras synthetic based drilling fluid. At the end of the analysis, it is concluded that the Yield Power Law model predicts the shear stress-shear rate relation of the fluid at surface conditions with an error of 1.03 % while Power Law model predicts it with an error of 22.8% and Bingham Plastic with an error of 10.8%. It is also observed that in other test temperature and pressures Yield Power Law predicts the actual shear stress-shear rate relation of the Petrobras synthetic based drilling fluid with high accuracy compared to Power Law and Bingham Plastic model approximations (Table 4.2).

In order to check the validity of the results obtained by RHEO.for, two other software packages (Rheological Modeling Wizard (RMW) and (Klotz-Brigham (KLOTZ)), which are also used to determine rheological parameters using rotational viscometer readings, have been used. These programs also agreed that best approximation to the shear stress-shear rate behavior of Petrobras synthetic based drilling fluid is Yield Power Law model for all tested ranges of pressures and temperatures.

In this approach, effect of pressure and temperature on rheological parameters that are designated for a particular rheological model, (yield power law model parameters in this case) are determined.

As it can be seen from Figures 4.1 – 4.3, *Flow Behavior Index (n)*, *Consistency Index (K)* and *Yield Point (τ_Y)* are affected by both pressure and temperature. Effect of pressure and temperature on flow behavior index (n) is hard to explain. However, still there is a trend that can be seen at all different pressure conditions. As the temperature is increased, flow behavior index started to increase until certain temperature (around 150 ^oF). That means, fluid approaches to a Newtonian behavior when temperature is increased from 40^oF to 150^oF, regardless of the pressure applied on it. However as temperature is increased further more, it is found out that Petrobras synthetic based drilling fluid again becomes more non-Newtonian (pseudoplastic in particular) since flow behavior index started to decrease. Effect of pressure becomes important at this point because at higher pressures (8000 and 12000 psig) rate of decrease in flow behavior index with increasing temperature is slower than rate in lower pressures. Lower than 8000 psig, the rate of decrease in flow behavior index is almost same for other pressure conditions.

On the other hand, yield stress of Petrobras synthetic based drilling fluid is strongly affected by temperature while almost not affected by pressure. The yield stress at lower temperatures are 15-16 times higher than yield stresses at high temperatures in all pressure conditions. For that reason, behavior of yield stress for synthetic based drilling fluids should be determined carefully before they are used in deep and ultra deep offshore operations where drilling fluids are subjected to low temperature conditions.

Temperature is more effective in consistency index as well. As temperature is increased, consistency index decreases under isobaric conditions. The consistency index at low temperature conditions is 5-10 times higher than

consistency index at higher temperatures. Since consistency index is changing with temperature, detailed rheological analysis of the fluid should be done for high pressure and high temperature conditions. Another interesting observation is that, at high temperature conditions (> 200^{o}F), further increase in temperature resulted in slight increase in consistency index as well. This interesting effect of temperature can be observed much better at low pressure conditions. Pressure also effects consistency index of synthetic based drilling fluids. As pressure is increased, consistency is increased under isothermal conditions. At low temperature conditions, increase in pressure resulted in increase in consistency index. Due to such a nature of synthetic based drilling fluids, careful study of behavior of consistency index under low temperature, high pressure conditions should be carried out for deep and ultra deep offshore operations where fluids are subjected to low temperature, high pressure conditions while flowing through riser.

4.4.2 Rheological Characterization of Petrobras Synthetic Based Drilling Fluid Under HPHT Conditions

Second approach aimed to determine shear stress of a particular fluid at different temperature, pressure and shear rate conditions. By doing so, it would be unnecessary to try to fit the actual shear stress-shear rate data to rheological models. It was decided to use Hemphill's [21] "Relative Dial Readings (RDR)" approach for rheological characterization. This approach is independent of any assumption of rheological model. RDR is defined as the ratio of the dial reading determined for any pressure and temperature (using Fann 70 HPHT Rotational Viscometer) to dial reading determined under surface conditions (14.7 psia and 70 ^{o}F).

$$RDR = \frac{\theta_{T,P}}{\theta_{14.7\,psi,70^{o}\,F}} \quad \text{.....(4.41)}$$

It is aimed to find out a single relation that will relate RDRs with shear rate, temperature and pressure. Because, once such a relation for a specific fluid is determined, then fluids' shear stress could be determined under any down-hole conditions at any flow rate. In order to determine such a function, non-linear and linear regression analysis techniques are used. Most of the non-linear regression analysis is conducted using a statistical analysis software package called "STATISTICA".

4.4.2.1.Procedure to Develop Model:

1. First of all the effects of temperature and pressure on RDRs at each shear rate are determined using 3D plots (Figures 4.4 – 4.6). It is found out that, the effect of temperature on RDRs is more dominant than the effect of pressure. Analysis also shows that pressure is more effective at lower temperatures and higher shear rates. However, effect of pressure is negligible especially at high temperatures regardless of the shear rate applied to the fluid system. Another interesting property of the fluid is that, dial readings of the fluid are increasing with increasing temperature after 200^{o}F, especially at lower shear rates.
2. The effect of temperature on RDR is determined at each pressure-shear rate condition as a starting point of the rheological characterization

process (Figures 4.7 – 4.11). It is observed that there is an inverse relation between RDR and temperature at all pressure and shear rate conditions. However, it was also seen that dial readings at lower shear rates are increasing with increasing pressure even at high temperatures.

3. Different two parameter models (Freundlich, Reciprocal, Ratkowsky, Bern et. al and Arrhenius models) were fitted to the experimental results using nonlinear regression analysis program called “STATISTICA”. Among these type curves, "Arrhenius Relation" approximated the relation between RDR and temperature with highest accuracy. Arrhenius relation in terms of the parameters under investigation can be shown as follows;

   ARRHENIUS RELATION: $RDR(T) = C_1 \exp(C_2 / T)$ ……(4.42)

4. Once the relation between RDR and temperature was determined, the next step is to determine whether coefficients of the model (C_1 and C_2) are dependent to pressure and shear rate. It has been found out that, both C_1 and C_2 are functions of pressure and shear rate (Table 4.3). Once these coefficients were defined as functions of pressure and shear rate, RDR as a function of temperature, pressure and shear rate can be written as follows;

   $RDR(T, P, \gamma) = C_1(P, \gamma) \exp[(C_2(P, \gamma)/T]$ ……..(4.43)

5. In order to get a general expression, regression analysis was carried out to determine the effect of pressure and/or shear rate on these constants (C_1 and C_2). It is decided to analyze the effect of pressure on C_1 and C_2 under constant shear rate conditions as the second phase of rheological characterization process.

   Third degree polynomial defines the relation between C_1 and pressure as;

   $C_1(P) = C_3 + C_4 * P - C_5 * P^2 + C_6 * P^3$ ……..(4.44)

   The absolute error range of this relation in approximating C_1, ranges from 0.2-12%. The highest errors (10-12%) occurred while determining the C_1 at pressure of 2000 psig. Other than this, average errors are always smaller than 7% (Table 4.4).

   Similar analysis has been carried to determine the effect of pressure on C_2. Again, a third degree polynomial best describes the effect of pressure on coefficient C_2 under constant shear rate conditions.

   $C_2(P) = C_7 - C_8 * P + C_9 * P^2 - C_{10} * P^3$ ……(4.45)

   The absolute error of the above relation in determining coefficient C_2 is ranging between 0.06-12.5%. Again the highest discrepancies between calculated and predicted values are determined at 2000 psig (Table 4.5).

6. In order to determine $C_1(P,\gamma)$ and $C_2(P,\gamma)$ to use in equation (4.43), the effect of shear rate on coefficients shown in equation (4.44) and (4.45) should be determined. Non-linear regression analysis is carried out using either one parameter or two parameter curves. All the analysis was carried using statistical software program "STATISTICA". The relations between coefficients and shear rates are shown in Appendix A-2 (Tables 4.6-4.13).

7. Substituting relations defined in Appendix A-2 (A-2.1 – A-2.4) in to equation (4.44), coefficient C_1 can be written as a function of pressure and shear rate as follows;

$$C_1(P,\gamma) = (0.0371Ln(\gamma) + 0.0039) + \left[4.289\times10^{-5} * \log10(\gamma) - 3.476\times10^{-6}\right] * P - \left[-5.926\times10^{-10} + 8.499\times10^{-9} * \log10(\gamma)\right] * P^2 + \left[-6.636\times10^{-14} + 4.436\times10^{-13} * \log10(\gamma)\right] * P^3$$

……(4.46)

Similarly, substituting relations (A-2.5 – A-2.8) in to equation (4.45), coefficient C_2 can be written as a function of pressure and shear rate as follows;

$$C_2(P,\gamma) = \left[177.307 * (1+\gamma)^{(-0.1009353)}\right] - 0.025 * P + \left[-5.674\times10^{-6} + 7.083\times10^{-7} * \log10(\gamma)\right] * P^2 - \left[2.284\times10^{-10} + 6.616\times10^{-11} * \log10(\gamma)\right] * P^3$$

……..(4.47)

8. These two equations (4.46 and 4.47) can be substituted into equation (4.43). As a result of this, an equation relating RDR to both down hole conditions (pressure and temperature) and shear rate (in other words flow rate or average velocity) can be determined by using one equation with the following form

$$RDR(T,P,\gamma) = \frac{\theta_{P,T}}{\theta_{14.7\,psi,70^oF}} = C_1(P,\gamma)\exp\left[(C_2(P,\gamma)/T)\right] \quad \text{……..(4.48)}$$

Knowing the surface rotational viscometer readings of a particular fluid, shear stresses of fluid at any down hole conditions under any flow rate can be determined using the relation proposed above.

As a next step, the applicability of the proposed model was investigated. Dial readings determined using equation (4.48) were compared with dial readings of Fann 70 HPHT rotational viscometer for each pressure, temperature and shear rate conditions.

4.4.2.2.Comparison of Calculated and Measured Dial Reading Results:

Dial reading results obtained from Fann 70 HPHT rotational viscometer were compared with dial readings calculated from the model (Figures 4.12-4.15). Proposed model does not always accurately predicted the measured shear stresses. In order to determine the accuracy of the model, sensitivity analysis on the results was carried out in four different regions of pressure and shear rate. As a result of that, the applicability of the model is investigated in more detailed way. These four regions can be listed as;

- Low Pressure (< 4000 psig)- High Shear Rate (> 6 RPM)
- Low Pressure (< 4000 psig)- Low Shear Rate (< 6 RPM)
- High Pressure (> 4000 psig)- High Shear Rate (> 6 RPM)
- High Pressure (> 4000 psig)- Low Shear Rate (< 6 RPM)

From the comparison of experimental and calculated dial readings, it was observed that, at pressures less than 4000 psig, model predicts the experimental dial readings with high accuracies for all shear rates as long as temperature is

below 200 ^{o}F. The only exception to this fact is observed for 4000 psig, 6 RPM readings where model over predicted the experimental results with errors as high as 80%.

As a conclusion, at low pressure ranges, model predicted the experimental values with errors lower than 10 %, as long as temperature is lower than 200 ^{o}F. Disagreement between measured and calculated dial reading values was observed much severe in lower shear rate values. The reason for such inconsistency is simple. The chosen function to determine the relationship between RDR and temperature is Arrhenius equation that is monotonously decreasing function. However, closer look at the data proves that, although fluid's dial readings are decreasing with increasing temperature, at lower shear rates dial readings do not change with temperature or even increase as temperature increases hence the model fails.

For high pressures range (> 4000 psig), it is observed that model predicted experimental values with high accuracies at all temperatures as long as high shear rate range is concerned. At lower shear rates (< 6 RPM), model over predicted the experimental values in almost all temperature ranges. The reason of such a failure in the model is again due to behavior of fluid at high pressure-high temperature conditions at low shear rates

4.5 Density Behavior of Synthetic Based Drilling Fluids Under HPHT Conditions

Density of oil based and synthetic based drilling fluids are sensitive to changes in down-hole conditions. For that reason, in order to calculate pressure losses precisely, not only the rheological behavior but also the densities of drilling fluids should be corrected as a function of down-hole conditions.

Mercury free PVT system is used to investigate the effect of pressure and temperature on density and compressibility of Petrobras synthetic based drilling fluid and synthetic based oil. By using this system, volume of the cell at different temperature and pressure conditions can be determined. As a result of that, not only the density variation but also the compressibility of the fluid as a function of pressure and temperature can be determined.

The diagram of the apparatus can be seen in Figure 4.16. PVT cell has an inner diameter of 2.500 inches and outer diameter of 5.500 inches (3.000 inches of steel thickness for high pressure conditions). It is divided in to two by a hydraulic Teflon piston. The piston is connected to a rod that is attached to "Linear Variable Differential Transducer (LVDT)". LVDT is used to measure the position of piston hence the volume of the sample in the cell. When piston is pushed against sample side until it does not move anymore, LVDT should show a value of –3.000 inches. The total length of the piston is 6 inches so LVDT ranges from –3.000 inches to +3.000 inches.

Preliminary calculations showed that the minimum volume that is needed in the cell before sample start pushing the piston is 88 ml. This volume is called "minimum or dead volume". In other words, the total volume in the cell at any temperature and pressure can be defined as;

$$V_{cell} = 88ml + \frac{\pi}{4}(2.5)^2 * (LVDT_{final} - 3.000) \quad \text{.....(4.49)}$$

In order to increase the pressure in the cell, oil is injected to the hydraulic oil side of the piston while all the sample lines are closed in the sample side. In order to increase the temperature of the cell, oven in which the PVT cell is mounted should be used.

The oven is a forced-air oven and temperature is controlled with a microprocessor controller. The maximum working temperature of oven is 500 ^{o}F. However, the temperature limit for the LVDT is 300 ^{o}F. For that reason, it is planned to go as high up to 280 ^{o}F as a maximum temperature. Operating pressure of the cell is 10000 psig. It is planned to go as high up to 5000 psig in these research. Test matrixes for calibration experiments with water and base oil and synthetic based drilling fluid experiments can be seen in Tables 4.14-4.15.

In order to determine the accuracy and sensitivity of temperature sensors, pressure transducers and LVDT, calibration experiments with water at different temperatures and pressures are conducted.

4.5.1 PVT Calibration Experiments

In order to determine the accuracy of the data acquisition system, density of water is determined under different pressure and temperature conditions. Then, experimental data is compared with the published data available in the literature. Examples of such plots are shown in Figures 4.17-4.18. Deionized, distilled water is used as calibration fluid.

First three sets of experiments were carried out without evacuating the cell. In the last set of experiments, PVT cell was evacuated with a vacuum pump and then sample was introduced to the test media. From the density data it can be said that all experiments were in agreement with each other. Comparison with theoretical data shows that, experimental changes in density of water are slightly higher than theoretical ones. The reason for such small deviation is due to not removing all the air from PVT cell (valid for first three experiments) and test water. Although the air quantity in the system is small and does not affect density results, it severely affects the compressibility of water since air is extremely compressible compared to liquids. Example of comparison between theoretical and experimental compressibility with and without evacuation can be seen in Figures 4.19-4.20.

Experimental data obtained using vacuum pump is in better agreement with theoretical results. In order to get more accurate compressibility results, PVT cell and sampling valves are evacuated before sample entry with a vacuum pump. It is evident from this data that, the process of placing sample in to the cell is very important. All the air in the cell and sampling valves should be sucked before introducing sample to the system.

4.5.2 Experimental Procedure

1. Density of the fluid at ambient conditions is measured using volumetric flask and electronic balance.
2. At least 450 ml of fluid sample is placed in the accumulator.

3. Piston should be pushed to the bottom of the cell by injecting sample from the accumulator to the cell
4. Evacuation of the cell and sampling valves through valve # 1 must be done using a vacuum pump.
5. Once the cell and sampling valves are evacuated, valve #1 is closed and sample from accumulator is transferred to PVT cell.
6. During this process, the pressure in the cell increases while fluid is filling the cell. Once all the fluid in the accumulator is injected to the cell, valve #1 is opened and oil is injected to the hydraulic side until 1st droplets of sample is observed at valve #1 exit. This would provide bleeding any air that might be trapped in fittings.
7. Once the line between valve #2 and valve #1 is full of sample, sample in the cell is isolated from sampling lines. By doing so, mass in the system remains constant through out the experiments.
8. LVDT position is recorded as initial position and mass in the cell is determined using $LVDT_{ini}$ and density that is determined at step 1.
9. Next, pressure is increased on the sample by injecting oil to the hydraulic side of the system. Pressure on the hydraulic oil side is controlled using air pump and backpressure valve (valve#7)
10. LVDTs are recorded at different pressure conditions, are used to calculate volume. Then the density of the sample at each pressure condition can be determined
11. Once change in volume or density of sample as a function pressure is determined under isothermal conditions, then isothermal compressibility can be found using either of the equations below.

$$C_o = \frac{1}{\rho}\left(\frac{\partial \rho}{\partial P}\right)_{T=cons\tan t} \quad \text{.....(4.50)}$$

or

$$C_o = -\frac{1}{V}\left(\frac{\partial V}{\partial P}\right)_{T=cons\tan t} \quad \text{.....(4.51)}$$

12. In order to determine the compressibility at different temperatures, oven should be set to the desired temperatures.
13. As temperature increases, the pressure in the cell increases as well due to sample expansion. The pressure in the cell should be maintained constant by using the backpressure valve (valve#7)
14. Once the temperature in the cell is reached the desired temperature, backpressure valve is closed and experiments at various pressures are conducted. Once volume change of sample at different pressures and temperatures is known, density of the sample can be determined since the mass of the sample in the cell is always constant during experimentation period.

4.5.3 Petrobras Synthetic Based Oil Experiments

Initially, it has been decided to determine the effect of pressure and temperature on Petrobras synthetic base oil itself. After that, the Petrobras synthetic based drilling fluid is going to be tested and the effect of additives and

emulsifiers on density and compressibility of Petrobras synthetic based drilling fluid system would be determined. This part of the report summarizes the work done in order to determine the effect of pressure and temperature on density and compressibility of Petrobras synthetic base oil.

A mercury free PVT system is used to for this purpose as well. As it is mentioned above, volume of the cell at different temperature and pressure conditions can be determined by using this system. As a result, both the density variation and the compressibility of the fluid as a function of pressure and temperature are determined. The test matrix for base oil experiments is shown is Table 4.15.

The initial temperature and pressure conditions for each experiment were taken as 80 F and 30 psig respectively. Experiments were conducted in the way it is described in the "Experimental Procedure" section.

4.5.3.1.Observations and Results:

The first observation in base oil experiments is the change in the physical appearance of Petrobras synthetic base oil at high temperatures ($240^oF<T<280^oF$). Although the base oil at the beginning of experiments (@ 80^oF) is colorless and odorless, it has been found out that between temperatures of 240^oF-280^oF, its properties have changed in such a way that, a yellow solution with an unpleasant odor is collected from PVT cell at the end of experiments. New base oil samples were used for each test, except for the last one (Exp. #4) where altered base oil from previous experiments were used in order to check whether, altering in color and odor affects the response of fluid's density to temperature and pressure or not.

Effect of pressure at each test temperature was shown in Figures 4.21 – 4.26. All experiments were shown in these graphs to show the agreement of experiments. One should remember that first three experiments were conducted using clear solution of synthetic base oil whereas fourth experiment is conducted using the altered synthetic base oil. All the experiments were in good agreement so it has been concluded that the alteration in the base oil due to temperature is not affecting the compressibility behavior of the fluid.

In all temperatures, as pressure is increased, the density of the base oil increased. This is expected since increase in pressure decreases to volume while the mass in the system is kept constant. Since density is the ratio of mass per volume, density increases as volume decreases.

The relation between density and pressure under isothermal conditions can be shown as;

$$\rho = b\,exp(a * P) \quad \text{.....(4.52)}$$

for incompressible fluids. It has been found out that the definition that relates density behavior of incompressible fluids with pressure under isothermal conditions, can be used to approximate the behavior of synthetic base oil at different temperatures with high accuracies. The regression fit of that equation to the experimental data is shown in Table B-3 for all different test temperatures

The combined effect of pressure and temperature on Petrobras synthetic base oil can be seen in Figure 4.27and Table 4.16. As it was mentioned above, as a result of increase in pressure at isothermal conditions, the volume of the

fluid is decreased. Hence the density of the fluid is increased if the mass is kept constant. Although the amount of compressibility of fluid at a pressure condition depends on temperature at which the pressure is applied, pressure always tends to decrease the volume of the fluid. On the other hand, as temperature of the fluid is increased, the molecular forces between particles decrease and molecules tend to move freely in the system. As a result of that, increase in temperature, increases the volume and hence the density decreases under isobaric conditions.

The effect of temperature on density of Petrobras synthetic base oil is much more effective in lower pressures since molecules can move freely without an existence of another force that tried to keep them in order. Experimental study show that, once the temperature is increased from 80^{o}F to 280^{o}F (which is typically observed in deep and ultra deep drilling) the density of the base oil decreases in the range of 0.7 ppg (10.69% less than original density) to 0.35 ppg (5.34% less than original density) depending on the pressure conditions (30 psig and 5000 psig respectively). This data shows the importance of introducing the effect of pressure and temperature on density in pressure loss calculations. Since the effect of temperature is more effective and increase in temperature decreases the density of the fluid, without proper relation between density and temperature, well control problems can occur in actual practices, especially at deep and ultra deep drilling operations.

4.5.3.2 .Isothermal Compressibility of Petrobras Synthetic Based Oil:

As it was mentioned above, density of the fluid increases as pressure on the fluid is increased under isothermal conditions. However, the rate of change of density with rate of change of pressure is not constant in all temperature conditions.

Isothermal compressibility can be defined as follows;

$$(C_o)_{T,P} = \left(\frac{1}{\rho}\right)_P \left(\frac{\partial \rho}{\partial P}\right)_{T,P} \quad \text{.....(4.53)}$$

Since the relation between density of the fluid and applied pressure can be obtained by using equation (4.52) and experimental results, the partial derivative of equation (4.52) together with density at specific pressure, will give the isothermal compressibility of the fluid at specified temperature and pressure. Figure 4.28 shows the change in compressibility of Petrobras synthetic base oil with temperature.

Isothermal compressibility of base oil is almost constant for the experimental range of 30 psig to 5000 psig. This is another indication of the fact that, this fluid can be classified as incompressible or slightly compressible fluid. However, as the temperature is increased, the compressibility of the oil is increased except for the data of 120^{o}F. While the temperature is increased from 80^{o}F to 120^{o}F, experimental results show that the compressibility of the oil decreases slightly. However, this might be as a result of error range of the experimental set-up. After that point, increasing the temperature increases the compressibility of the fluid while the rate of change of density per rate of change of pressure is constant for a specific temperature in all conditions. It should be noted that, although Petrobras paraffin base oil can also be classified as

incompressible fluid, the compressibility values are 2-3,5 times higher than that of deionized distilled water in similar conditions.

4.5.3.3. Comparison of Petrobras Synthetic Base Oil to Other Drilling Fluids

Finally, the experimental data obtained for Petrobras synthetic base oil is compared with water based drilling fluid and oil based drilling fluid data available in literature. Data presented by McMordie et al. [24] is used for that comparison. Behavior of different based drilling fluids at different temperature conditions were compared (Figures 4.29-4.30)

At lower temperatures, the change in density of base oil with increasing pressure is higher than that of water. However, the change in density of water based drilling fluid and oil based drilling fluids are higher than both water and base oil. It was observed that, oil based drilling fluid is most sensitive one to pressure at 80^oF with density increase of 0.37 ppg with increase of 5500 psig.

As the temperature is increased, it has been noted that the change in density of Petrobras base oil is higher than that of water and water based drilling fluid. Increasing the temperature from 80^oF to 200^oF reduces the density of Petrobras base oil of about 0.35 ppg. However the reduction in the oil-based drilling fluid is of about 0.5 ppg with increase in temperature. It is found out that, oil based drilling fluid is still the most sensitive one among them to pressure and temperature conditions. Although, Petrobras base oil is an oil, fluctuations in density with pressure and temperature is more close to that of water based drilling fluids than low toxic mineral oil based drilling fluid.

4.5.3.4. Volumetric Characterization of Petrobras Synthetic Based Oil with respect to High Pressure and High Temperature Conditions;

As it was mentioned before, turbulent frictional pressure losses of fluids are not only related to the rheology of the fluid but also related to the density as well. For that reason, in order to determine frictional pressure losses of drilling fluids precisely, effect of pressure and temperature on density of the drilling fluids should be studied carefully.

This part of the study focused on developing empirical correlations to define density as a function of pressure and temperature. Linear and non-linear regression techniques, which were the case of rheological characterization process, were used for this purpose.

As it was mentioned above, by analyzing the relation between density and pressure under isothermal conditions, it is possible to determine whether fluid can be classified as incompressible or not. For that reason, first of all the relation between pressure and density is analyzed and it is found out that Petrobras synthetic base oil can be classified as "incompressible fluid". This relation is shown in equation (5.52)

Once the relation between density and pressure under isothermal conditions is determined, the effect of temperature on coefficients "*a*" and "*b*" was determined. Relation between temperature and coefficient "*a*" can be shown by a second degree polynomial as;

$$a(T) = X * T^2 + Y * T + Z \quad \text{.....(4.54)}$$

where,

$X = -2.779*10^{-06}$

Y = $-2.362*10^{-03}$
Z = 6.604
for the particular fluid under investigation. Estimating coefficient "*a*" with the above equation is giving accurate results (Figure 4.31) and average error between calculated and experimental "*a*" is always lower than 0.04 %.

Similarly, effect of temperature on coefficient "*b*" is also determined using a similar approach. As a result of regression, it is found out that effect of temperature on "*b*" can be shown by second degree polynomial as well.

$$b(T) = P*T^2 + Q*T + S \quad \text{.....(4.55)}$$

where,
P = $1.773*10^{-10}$
Q = $-3.378*10^{-08}$
S= $7.446*10^{-06}$
for Petrobras synthetic base oil. Estimation of experimental "b" using the above equation is also accurate and average error is always less than 3.5 % (Figure 4.32).

By substituting equations (4.55) and (5.54) into equation (5.53), the relation between density and down-hole conditions can be established as follows,

$$\rho(P,T) = \left(x*T^2 + y*T + z\right)\exp\left[\left(p*T^2 + q*T + r\right)*P\right] \quad \text{.....(4.56)}$$

Accuracy of equation in estimating experimental results is good and average error between calculated and measured densities is always lower than 0.3 % in all pressure and temperature conditions (Figure 4.33). This relation would help to correct density as a function of pressure and temperature. By substituting this definition of density in to Fanning frictional pressure loss equation, pressure losses can be estimated with the correction of density with respect to pressure and temperature. Table 4.17 summarizes the results of numerical calculation of the effect of pressure and temperature on the density of Petrobras mud base oil.

4.6. Advanced Cutting Transport Study (ACTS) Flow Loop

4.6.1. Modifications of the ACTS Facility

With the addition of heating and cooling system (Figures 3-1 - 3-6), the flow loop is now fully functional both at elevated pressures and elevated temperatures. The heating/cooling part of the system is designed in such a way that, it would be possible to heat or cool the fluid while circulating in the flow loop or by passing the flow loop. In order to transfer the heat from hot fluid (glycerol) to cold sampling fluid, plate frame heat exchanger is used in the heating process. Another plate frame heat exchanger is used to transfer heat from hot sampling fluid to cold water in the cooling process.

In the case of synthetic based drilling fluid experiments, it is planned to heat the fluid while circulating through the flow loop. By that way not only the fluid but also the system is heated and the temperature is expected to stabilized more easily. Since the system is insulated, heat transfer between the system and surrounding is minimized. As a result of such low heat loss rate, once the desired temperature is reached, heating or cooling mechanism is stopped and

experiments with elevated pressures are conducted at different flow rates. The temperature in the system remains stable during the time of experimentation.

ACTS flow loop consists of three rheology sections with nominal diameters of 2", 3"and 4" and an annular section. The geometrical dimensions of test sections are given in Table 4.18. It should be noted that, five feet of pipes at both the entrance and exit are available for use as a quieting section between the pressure taps and the entrance or exit to the test section. Thus, a separation of at least 55 ft between pressure taps is available for measuring differential pressure losses.

Temperature in the system is observed through 10 thermo couples installed to different locations on the flow loop. Inlet and outlet temperatures of each test sections (2", 3", 4" and annular section) are observed through 8 of these thermo couples. Among other two, one of them is installed to the discharge section of the piston pump in order to determine the temperature of the fluid while entering to the system. Other one is installed to the "0 psig" section of the system in order to determine the effect of choke on temperature of the fluid that is circulating in the system.

In addition to these, another storage tank with capacity of 100 barrels and a mixing tank with capacity of 5 barrels are installed to the system. As a result of these renovations, it is now possible to mix different solutions and add additives to drilling fluids.

Differential pressure transducers, absolute pressure transmitters, temperature sensors and micro motion mass flow meter are connected to a computer. As a result of that, system pressures, differential pressure losses, temperature distribution in the system and flow rates can be measured, data can be sorted and averaging intervals can be controlled using the data acquisition system. The data acquisition system utilizes Lab View software.

4.6.2. Calibration Experiments Under Elevated Temperature and Elevated Pressure Conditions

As it is summarized above, the flow loop consists of many devices and equipment that have to be controlled for successful experimental analysis. In order to determine accuracy of these devices and equipments and reliability of the data acquisition system, preliminary experiments are conducted with regular tap water. The test matrix for the calibration experiments is shown in Table 4.19.

During the experimentation process, first of all the water is circulated through the system and heat exchanger. Centrifugal pump that is installed to the suction side of the triplex pump is used in this process. Once the temperature of the fluid is stabilizes at desired temperature, boiler is turned off. Triplex pump is used to circulate the fluid in the system with the desired flow rate during test period. Pressure in the system is increased using the choke that is installed on the return line. Once all the pressure data at fixed flow rate is obtained, flow rate is increased and procedure is repeated for the same pressures.

A typical experimental procedure can be seen in Figures 4.34-4.35 for different temperatures. Under constant pressure and flow rate conditions, temperature of the system is stable especially at lower flow rates and pressures.

As the flow rate and pressure in the system is increased, the temperature of the fluid circulating in the system also increases. This is an expected behavior since increase in flow rate increases the frictional pressure losses all through the system. As friction in the system increases, heat is generated and temperature of the fluid circulating in the system increases. Increase in the system pressure is even more drastically effect the temperature of the system. There are mainly two reasons for that. First of all, as pressure in the system increases, fluid molecules are forced to compress. Due to this compression, frictional pressure loss, hence the temperature is increased. More important than that is, the considerable amounts of temperature increase after the choke. The temperature difference between the pressurized part of the system and unpressurized part of the system ranges from 2 ^{o}F-4 ^{o}F depending upon the pressure of the system.

As a conclusion, even boiler is not working, fluid is gaining heat because of pressure and flow rate. However, the fluctuation in the temperature is not more than 5^{o}F. Then, it can be assumed that temperature is constant during experimentation process. It should be noted that, temperature fluctuations are more severe while working at lower temperatures such as 60 or 80^{o}F.

Once the experiments are completed, experimental results were compared with theoretical water pressure loss results. In all of the temperature and pressure conditions, flow regime of water is fully turbulent even at lowest flow rate of 50 gpm. Since this is the case, Colebrook's semi-empirical equation developed for Newtonian fluid flow in pipes is used in theoretical calculations.

$$\frac{1}{\sqrt{f}} = 4 * \log 10\left[N_{\mathrm{Re}} * f_{turb}{}^{0.5}\right] - 0.395 \quad \text{.....(4.57)}$$

Experimental frictional pressure loses are slightly higher than calculated values. Since calculations based on smooth pipe assumption, it is normal for experimental results to be slightly higher than calculated results due to roughness of pipes. In other words, experimental frictional pressure losses are in agreement with calculated frictional pressure losses (Figure 4.36 – 4.38) for all pressure and temperature conditions in all rheology sections.

In the case of annular flow, several different friction correlations and equivalent diameter definitions are used. These different methods can be listed as;

- Blasius' Correlation with Hydraulic Diameter
- API 13-D Annular Pressure Loss Correlation
- Meter & Bird's Method [25]
- Gunn & Darling Solution [26]
- Colebrook Correlation with Hydraulic Diameter
- Colebrook Correlation with Jones & Leung [27] Equivalent Diameter

It has been found out that, in all temperatures, pressures and flow rates, except the last one, all of correlations and methods listed above overestimated the experimental frictional pressure losses that occur as a result of turbulent flow of water in concentric annuli. As it can be seen from Figures 4.39 - 4.41, only Colebrook correlation with Jones & Leung equivalent diameter approximated the experimental results with high accuracies. These results show the importance of the further studies on the flow of non-Newtonian fluids through annuli. As it was

mentioned above, while Colebrook correlation with hydraulic radius resulted in over prediction of experimental data with 100 % at high flow rates, with changing the diameter definition in the correlation (Jones & Leung), excellent accuracy between calculated and experimental pressure losses is established. The equivalent diameter they have proposed to use in Colebrook equation can be shown as follows,

$$d_{eq} = \frac{d_L^2}{d_{hy}} \quad \text{.....(4.58)}$$

where;

$$d_L = \left[d_o^2 + d_i^2 - \frac{\left(d_o^2 - d_i^2\right)}{\ln\left(d_o / d_i\right)} \right]^{1/2} \quad \text{.....(4.58a)}$$

and

$$d_{hy} = d_o - d_i \quad \text{.....(4.58b)}$$

Another important observation in calibration experiments is that, effect of pressure on frictional pressure losses of water is almost negligible at a constant temperature. Experimental pressure losses obtained under different system pressures are almost coinciding with each other. These results is also in agreement with the PVT calibration experiments where it is observed that change of density of water is negligible even at higher pressures.

4.7 Conclusions

- Petrobras synthetic based drilling fluid's shear stress-shear rate relation can be depicted by using yield power law model in all pressures and temperatures at which the Fann 70 rotational viscometer experiments were conducted
- Effect of temperature and pressure on rheological parameters is important. Especially effect of temperature on "Consistency Index" and "Yield Point" should be analyzed carefully (i.e. low temperature effects). Effect of pressure on "Flow Behavior Index" and "Consistency Index" should also be analyzed carefully for accurate frictional pressure loss estimations and better hydraulic design computations.
- A single relation can be established amongst rotational viscometer dial readings and pressure, temperature and shear rate. As a result of that, it would be possible to determine frictional pressure losses as a function of pressure, temperature and flow rate without considering the rheological model of the fluid under any down-hole conditions
- PVT Cell which is mostly used to determine bubble and dew point for reservoir engineering purposes can be used to determine the effect of pressure and temperature on density of drilling fluids and drilling fluid compressibilities
- As a result of PVT experiments, relation between Petrobras synthetic base oil density and pressure at isothermal conditions is determined. It is concluded that, Petrobras synthetic base oil can be classified as "incompressible" or "slightly compressible" fluid.

- Density corrections with respect to down-hole conditions are important in order to determine frictional pressure losses accurately. For that reason, an empirical relation is developed to determine density as a function of pressure and temperature.
- It is found out that, Petrobras synthetic based drilling fluid's density is less sensitive to changes in pressure compared to that of oil based drilling fluids, in all temperatures. It is also found out that, temperature is effecting oil based drilling fluid density more than it effects Petrobras synthetic based oil density.
- Effect of pressure on density of Petrobras synthetic based oil is less than the effect of pressure on water density at low temperatures (i.e. 80^oF). However, as the temperature is increased, effect of pressure on Petrobras synthetic based drilling fluid density becomes more dominant compared to that of water.
- ACTS flow loop is fully functional to work under elevated pressure and temperature conditions. Calibration experiments with water showed that data acquisition and instrumentation are in good condition.
- Using hydraulic radius as equivalent diameter resulted in over predicting the experimental pressure losses. Careful study of annular flow of non-Newtonian fluids is needed to obtain correlations that would predict experimental pressure losses with higher accuracies.
- In the case of Newtonian annular turbulent flow, Colebrook equation with Jones & Leung diameter predicts the frictional pressure losses in the annulus precisely.
- Effect of temperature is more dominant than effect of pressure on frictional pressure losses of Newtonian fluids flowing through pipes and annuli.

Nomenclature

C_o	isothermal compressibility
d_{eq}	equivalent diameter
d_i	pipe diameter
d_o	hole diameter
f	Fanning friction factor, dimensionless
f_a	friction factor in the annulus
g_c	conversion factor, 32.174 lbmassft/lbforcesec^2
G	geometry factor
K	fluid consistency index
K’	consistency index at the wall
L	measured depth
m	Guillot and Denis’ rheological model parameter
n	flow behavior index
n’	generalized flow behavior index of Metzner and Reed
ΔP	pressure drop, upstream minus downstream conditions
P	pressure, psig
P_a	pressure drop in annulus

P_n	a dimensionless function of n
Q	volumetric flow rate
r	tube radius
R	rotational viscometer shear rate
R_1 and R_2	inner and outer radii of annulus
u	local linear velocity in the x-direction at *r* or *y*
V	mean linear velocity in the *x*-direction
V_a	average bulk velocity in annulus
α	temperature constant
β	pressure constant
μ_p	plastic viscosity
μ, μ_{eff}, μ_{ea}	viscosity, effective viscosity, effective viscosity in annulus
ρ	density of fluid
ρ_i	density at 80 ^oF, 30 psig
θ	Rotational viscometer readings
γ	shear rate
τ	shear stress
τ_{YP}	yield stress (point)
τ_w	shear stress at the wall of a tube, $D\Delta P/4L$, lbforce/ft^2
τ_y	yield stress
ψ	Guillot and Denis' rheological model parameter
ε	roughness of pipe

References

1. Rabinowitsch, B.Z.; Pyhs. Chem. Series, 145, 1, 1929
2. Mooney, M.J.; Rheology., 2, 210, 1931
3. Metzner, A.B. and Reed, J.C.; "Flow of Non-Newtonian Fluids-Correlation of the Laminar, Transition and Turbulent Flow Regions", AIChE Journal, Vol.1, 434, 1955
4. Savins J.G., Burdyn R.F. and Wallick, G.C.; "Scaling Pumping Requirements-Inelastic Fluids in Turbulent Flow and Inelastic/Elastic Fluids in Laminar Flow", SPE 495, September 1963
5. Dodge, D.W. and Metzner, A.B.; "Turbulent Flow of Non-Newtonian Systems", AIChE Journal, Vol. 5, 189, 1959
6. Demirdal, B.; "Study of Flow of Synthetic Based Drilling Fluids Under Elevated Pressure and Temperature Conditions", ACTS-ABM Report, May, 1999
7. Zamora M. and Lord, D.L.; "Practical Analysis of Drilling Mud Flow in Pipes and Annuli", SPE 4976, October, 1974
8. Fredrickson, A.G. and Bird, R.B.; "Non-Newtonian Flow in Annuli", Ind. and Engr. Chem., 50, No.3, 347, 1958
9. Annis, M.: "Composition and Performance Analysis of Water Base Drilling Fluids", Dresser-Magcobar Publication, August-1969
10. Schuh, F.J.; "Computer Makes Surge Pressure Calculations Useful", Oil and Gas Journal, August-1964

11. Randall, B.V. and Anderson, D.B.; “Flow of Mud During Drilling Operations”, SPE 9444, July-1982
12. Vaughn, R.D.; “Axial Laminar Flow of Non-Newtonian Fluids in Narrow Eccentric Annuli”, Soc. Pet. Engr. J., 277-280, December-1965
13. Langlinais, J.P., Bourgoyne, A.T. and Holden, W.R.; “Frictional Pressure Losses for the Flow of Drilling Mud and Mud/Gas Mixtures”, SPE 11993, October-1983
14. Bourgoyne, A.T., Chenevert, M.E., Milheim, K.K. and Young, F.S.; “Applied Drilling Engineering”, SPE Textbook Series, 1986
15. Guillot, D.J. and Denis, J.H.: "Prediction of Laminar & Turbulent Friction Pressures of Cement Slurries in Pipes and Centered Annuli", SPE Annual Conference, October-1988
16. Jensen, T.B. and Sharma, M.P.: "Study of Friction Factor and Equivalent Diameter Correlations for Annular Flow of Non-Newtonian Drilling Fluids", ASME, February-1986, New Orleans-Louisiana
17. Chen, J.J.J.: "Technical Note 400: A Simple Explicit Formula for the Estimation of Pipe Friction Factor", Proceedings of the Institution of Civil Engineers, Part 2, Vol. 77, March 1984, pp- 63-64
18. Minton, R.C. and Bern, P.A.; “Field Measurement and Analysis of Circulating System Pressure Drops With Low-Toxicity Oil-Based Drilling Fluids”, SPE 17242, March-1988
19. Stiff, H,A.; “Interpolating or Extrapolating Drilling Fluid Viscosities to Reference Temperatures”, J. Pet. Tech., October-1970
20. Johnston, W.G.: “A Method to Calculate the Pressure Viscosity Coefficient from Bulk Properties of Lubricants”, ASLE Transactions, Vol. 24, 1980
21. Hemphill, Terry; “Prediction of Rheological Behavior of Ester-Based Drilling Fluids Under Downhole Conditions”, SPE 35330, March 1996
22. Kenny, P., Hephilll, T. and Bell, G.; “Unique Hole Cleaning Capabilities of Ester Based Drilling Fluid Systems”, SPE 28308, presented at the 69th Annual Technical Conference and Exhibition in New Orleans, September-1994
23. Davison ,M.; Saasen, A.; Clary, S.: "The rheological Characteristics of Certain Drilling Fluids in Long, Cold Risers", Europe Africa Technology Center, Report No.: SC-97-11, November-1997
24. McMordie Jr., W.C.; Bland, R.G. and Hauser, J.M.: "Effect of Temperature and Pressure on Density of Drilling Fluids", SPE 11114, September-1982
25. Meter, D.M. and Bird, R.B. : "Turbulent Newtonian Flow in Annuli", AIChE Journal, Vol. 7, No. 1, March 1961, pg. 41-45
26. Gunn, D.J. and Darling, C.W.W.: "Fluid Flow and Energy Losses in Non-Circular Conduits", Trans. Inst. Chem. Engrs., Vol. 41, 1963, pg. 163-173
27. Jones, O.C. Jr. and Leung, J.C.M. "An Improvement in the Calculation of Turbulent Friction in Smooth Concentric Annuli", ASME Jour. Fluids Engineering, December, 1981

APPENDIX-A

A-1. RHEOLOGICAL MODELING OF 8.6 ppg PETROBRAS SYNTHETIC BASED FLUID USING FANN &) HPHT ROTATIONAL VISCOMETER

Table 4.1. Test Matrix of Petrobras Synthetic Based Drilling Fluid Fann 70 HPHT Rotational Viscometer Experiments

	PRESSURE, psig				
Temperature, F	**500**	**2000**	**4000**	**8000**	**12000**
40	θ600-θ3	θ600-θ3	θ600-θ3	θ600-θ3	θ600-θ3
80	θ600-θ3	θ600-θ3	θ600-θ3	θ600-θ3	θ600-θ3
120	θ600-θ3	θ600-θ3	θ600-θ3	θ600-θ3	θ600-θ3
200	θ600-θ3	θ600-θ3	θ600-θ3	θ600-θ3	θ600-θ3
280	θ600-θ3	θ600-θ3	θ600-θ3	θ600-θ3	θ600-θ3

*****Shear Rates: 600 RPM, 300 RPM, 200 RPM, 100 RPM, 6 RPM, 3 RPM

Table 4.2. HPHT Fann 70 Experiments Rheological Model Analysis

	AVERAGE	**ERROR For EACH**	**MODEL (%)**
Temperature, F	**Yield Power Law**	**Power Law**	**Bingham Plastic**
40	1.3 - 2.1	23.3 - 25.3	8.7 - 11.9
Standard Cond.	1.03	22.8	10.8
80	1.1 - 4.1	19.2 - 22.8	12.9 - 22.3
120	3.4 - 14.0	18.9 - 25.6	5.4 - 22.5
200	5.8 - 10.3	17.3 - 25.5	11.5 - 21.7
280	5.9 - 9.1	18.2 - 28.4	9.4 - 33.9

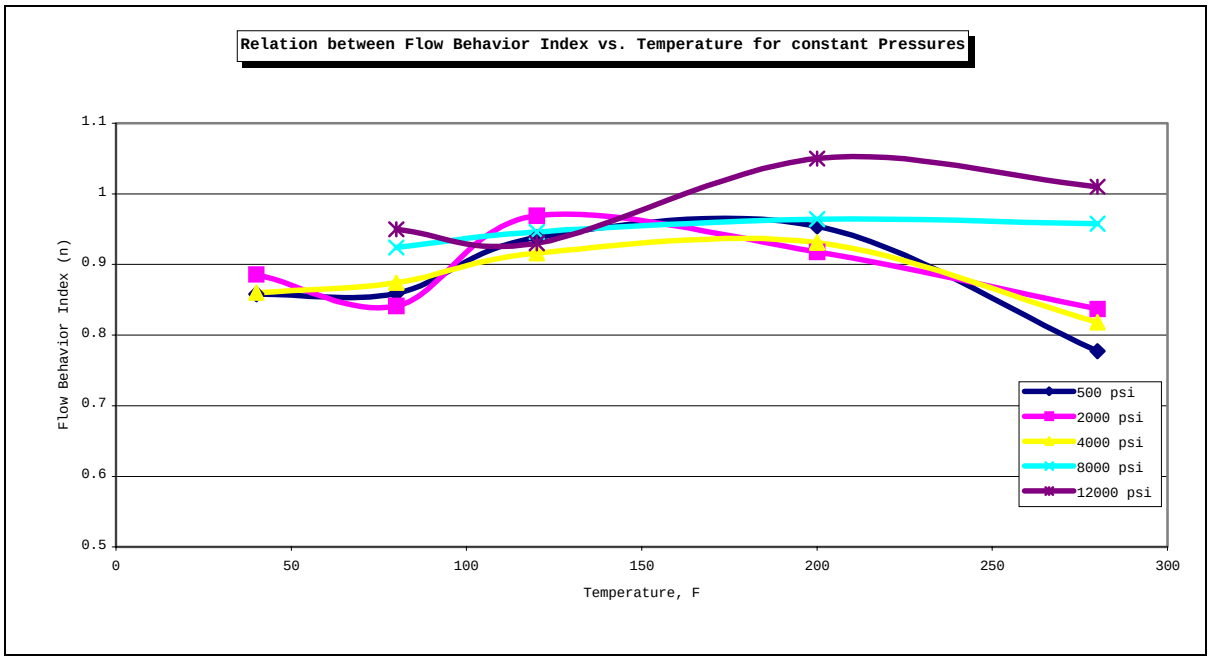

Figure 4.1 Effect of P & T on Yield Power Law Flow Behavior Index of 8.6 ppg Petrobras Synthetic Based Drilling Fluid

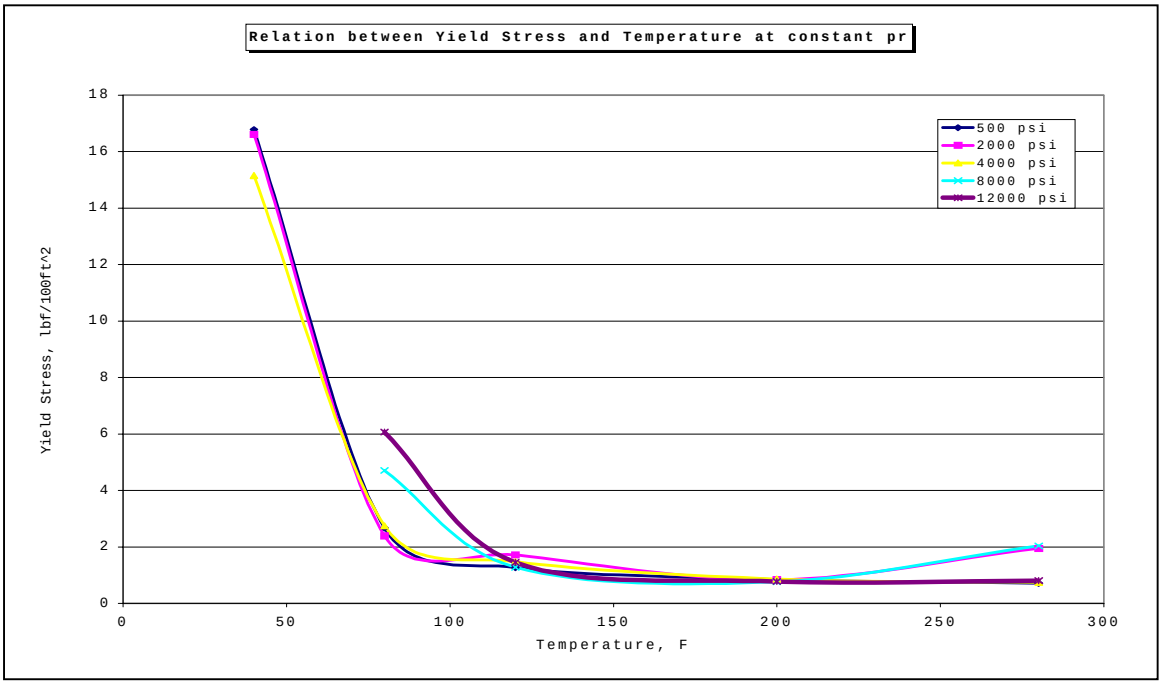

Figure 4.2. Effect of P & T on Yield Power Law Yield Stress of 8.6 ppg Petrobras Synthetic Based Drilling Fluid

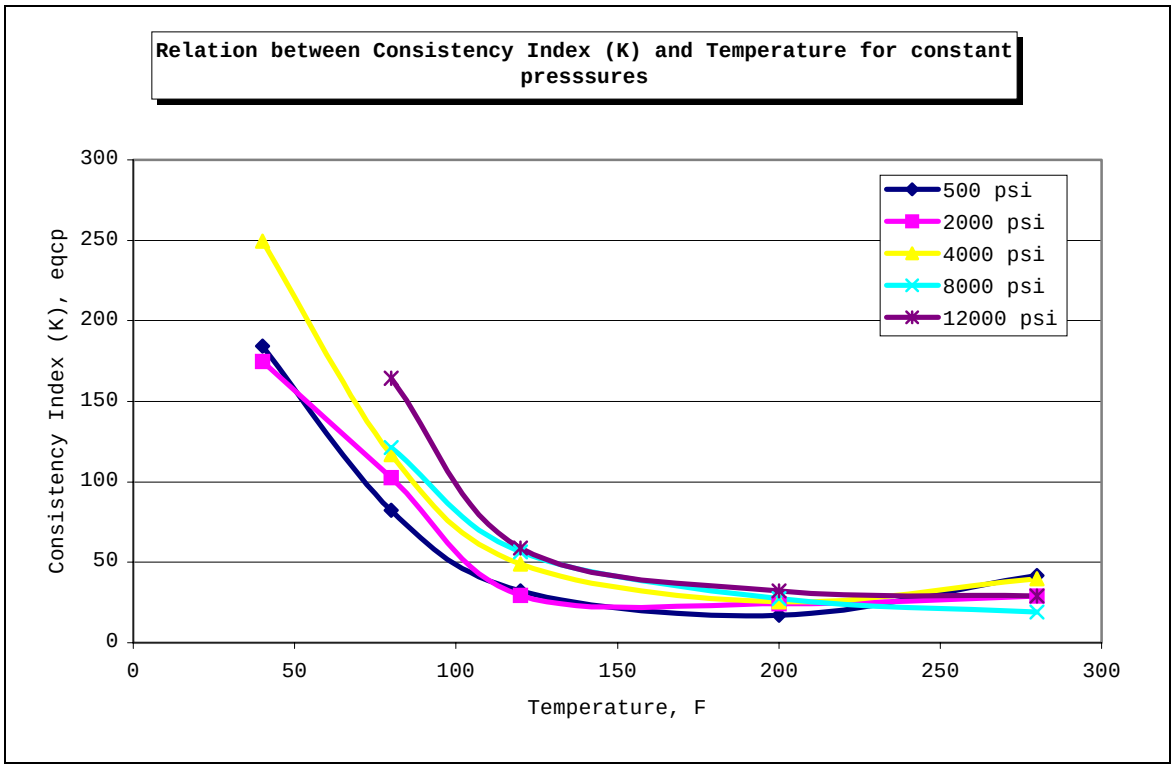

Figure 4.3. Effect of P and T on Yield Power Law Consistency Index of 8.6 ppg Petrobras Synthetic Based Drilling Fluid

A-2. Rheological Characterization of 8.6 ppg Petrobras Synthetic Based Drilling Fluid Using Fann 70 HPHT Data:

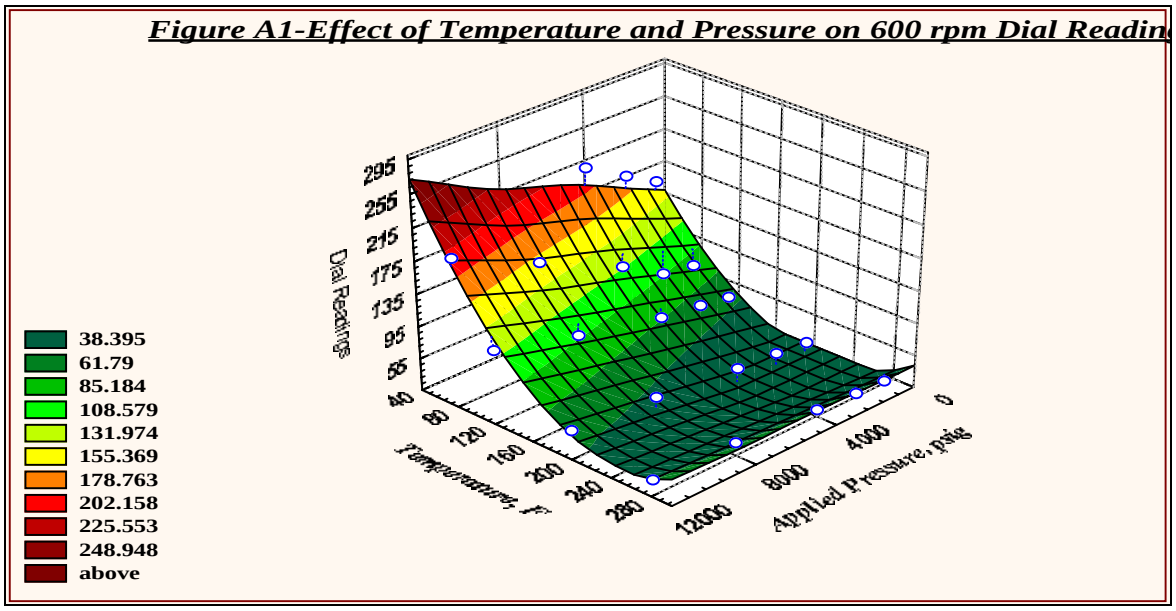

Figure 4.4. Effect of P and T on 600 RPM Dial Reading

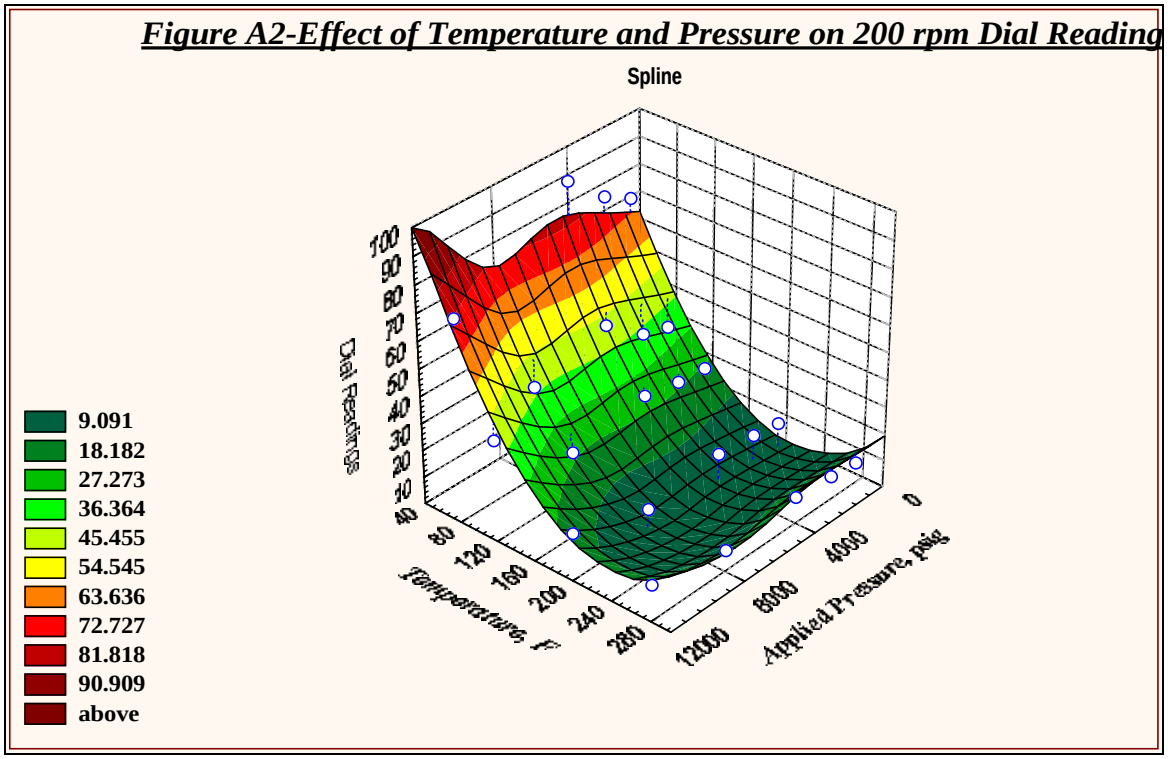

Figure 4.5. Effect of P and T on 200 RPM Dial Reading

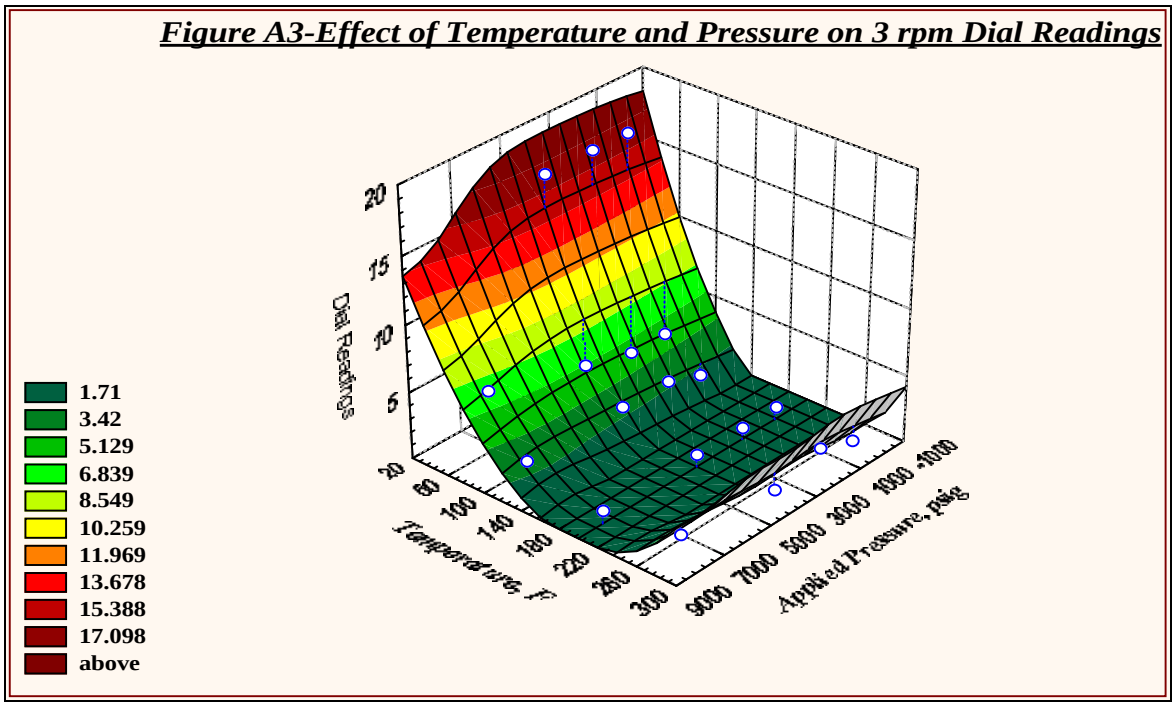

Figure 4.6. Effect of P and T on 3 RPM Dial Reading

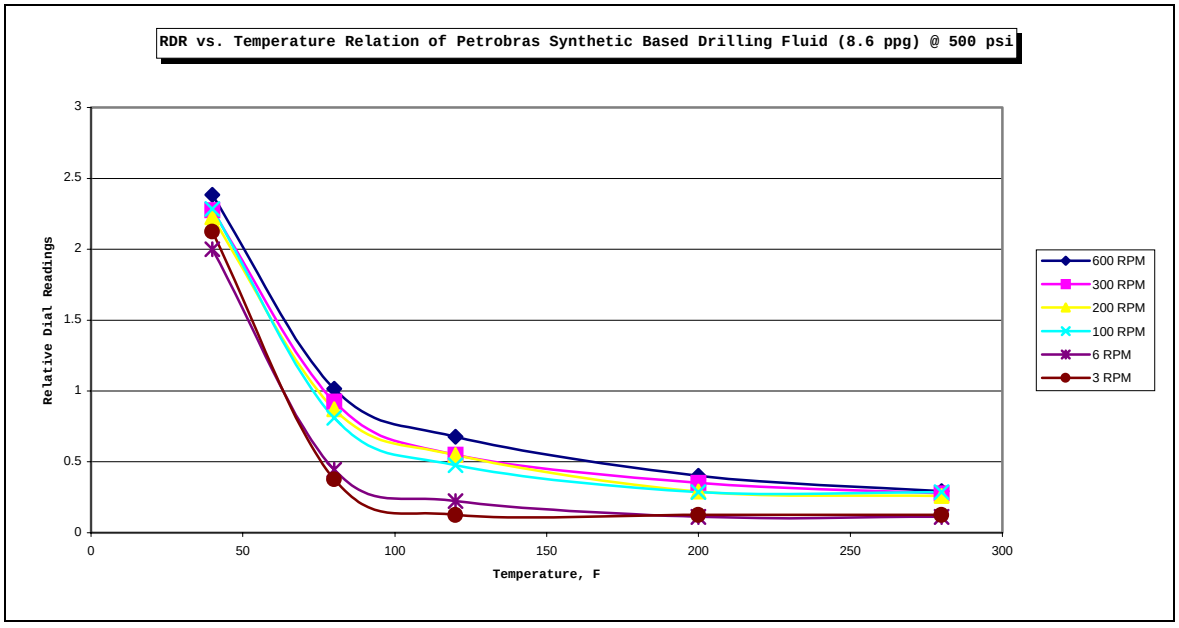

Figure 4.7.Effect of Temperature on Synthetic Based Drilling Fluid RDR Readings @ Different Shear Rates (Pressure = 500 psig)

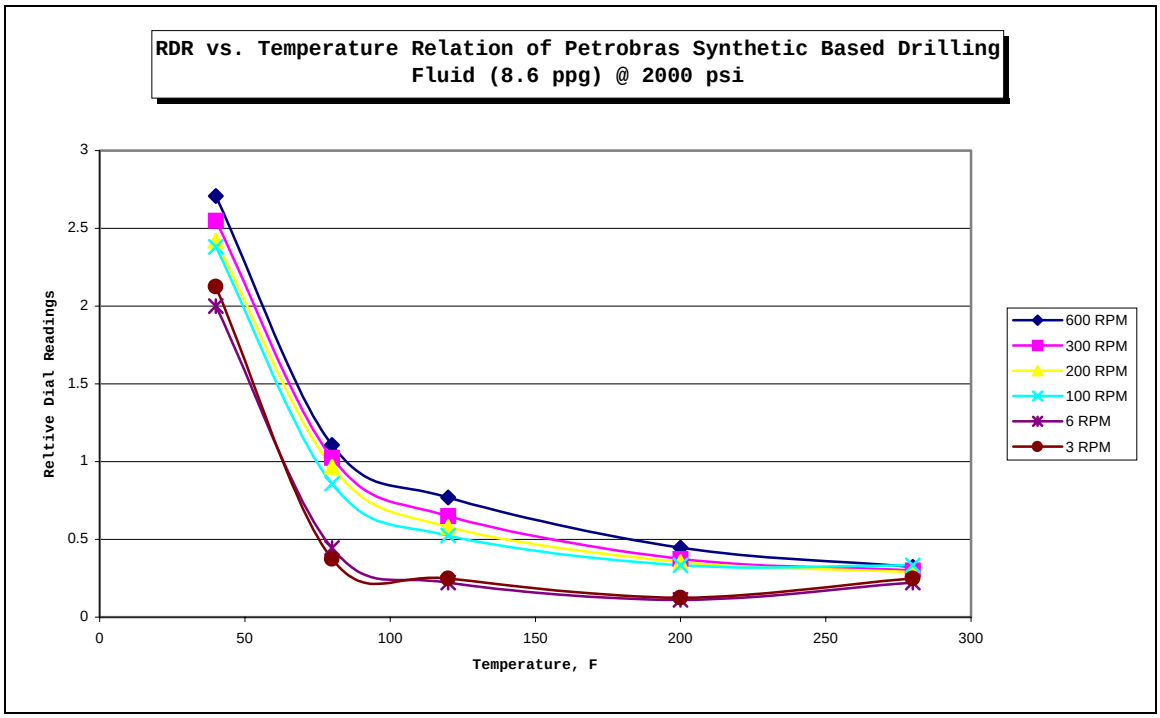

Figure 4.8 Effect of Temperature on Synthetic Based Drilling Fluid RDR Readings @ Different Shear Rates (Pressure = 2000 psig)

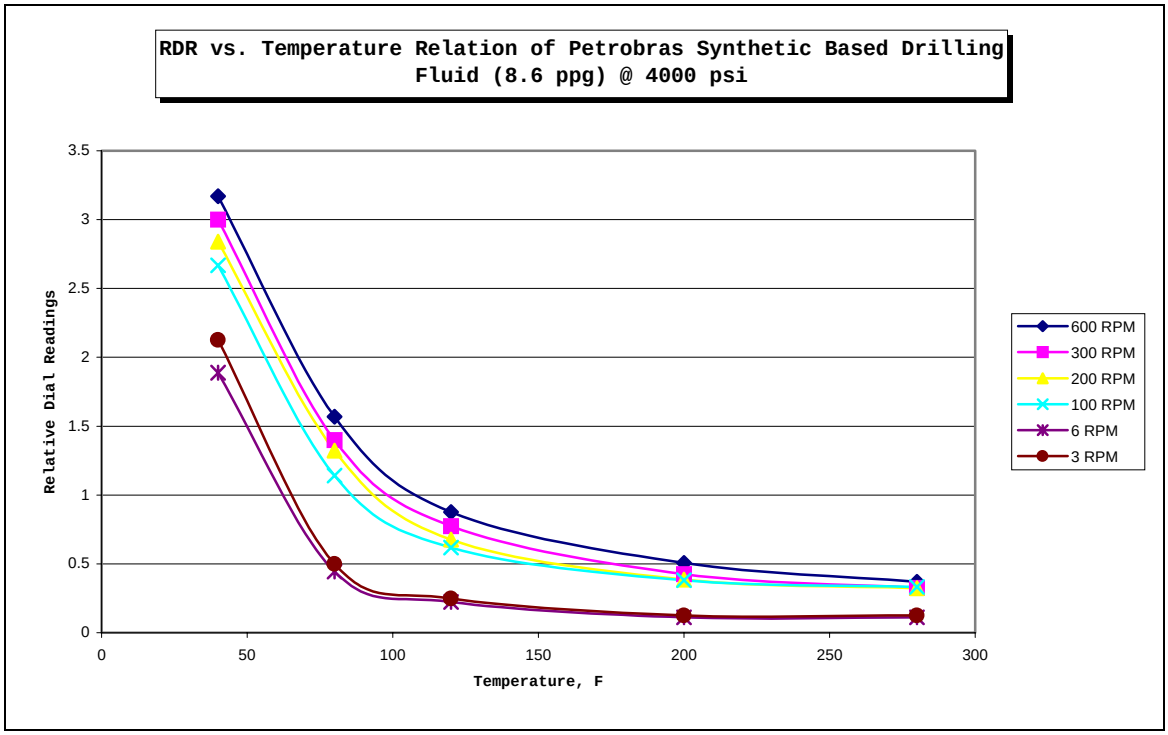

Figure 4.9.Effect of Temperature on Synthetic Based Drilling Fluid RDR Readings @ Different Shear Rates (Pressure = 4000 psig)

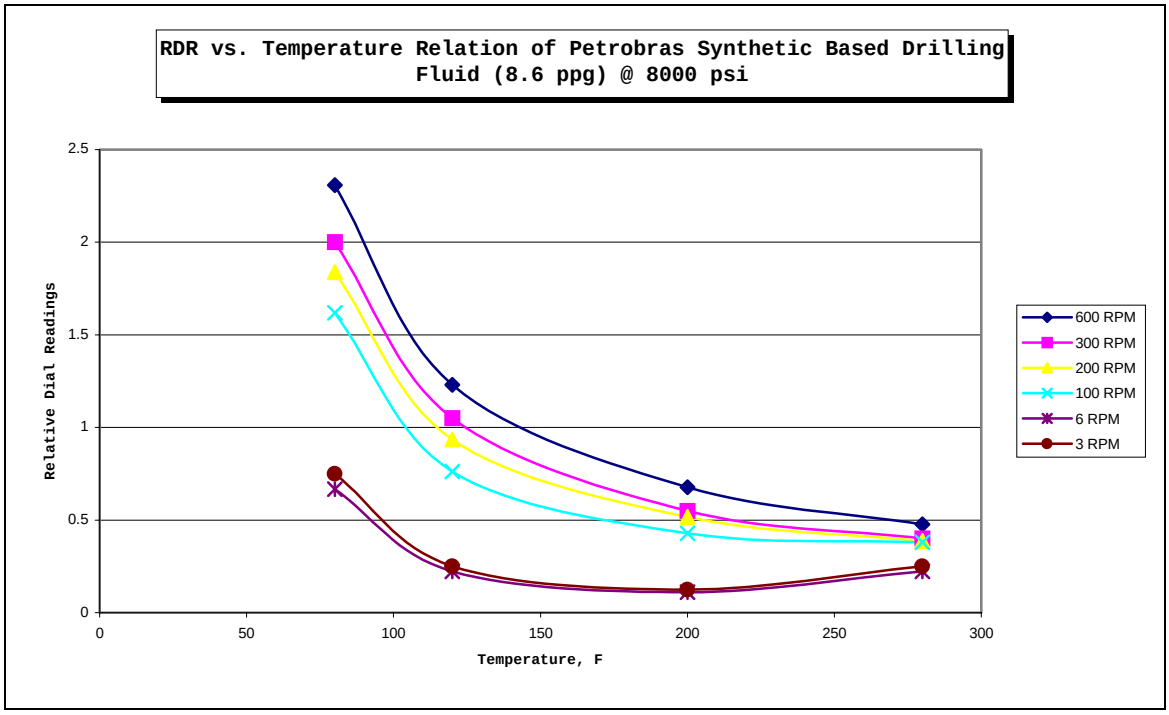

Figure 4.10 Effect of Temperature on Synthetic Based Drilling Fluid RDR Readings @ Different Shear Rates (Pressure = 8000 psig)

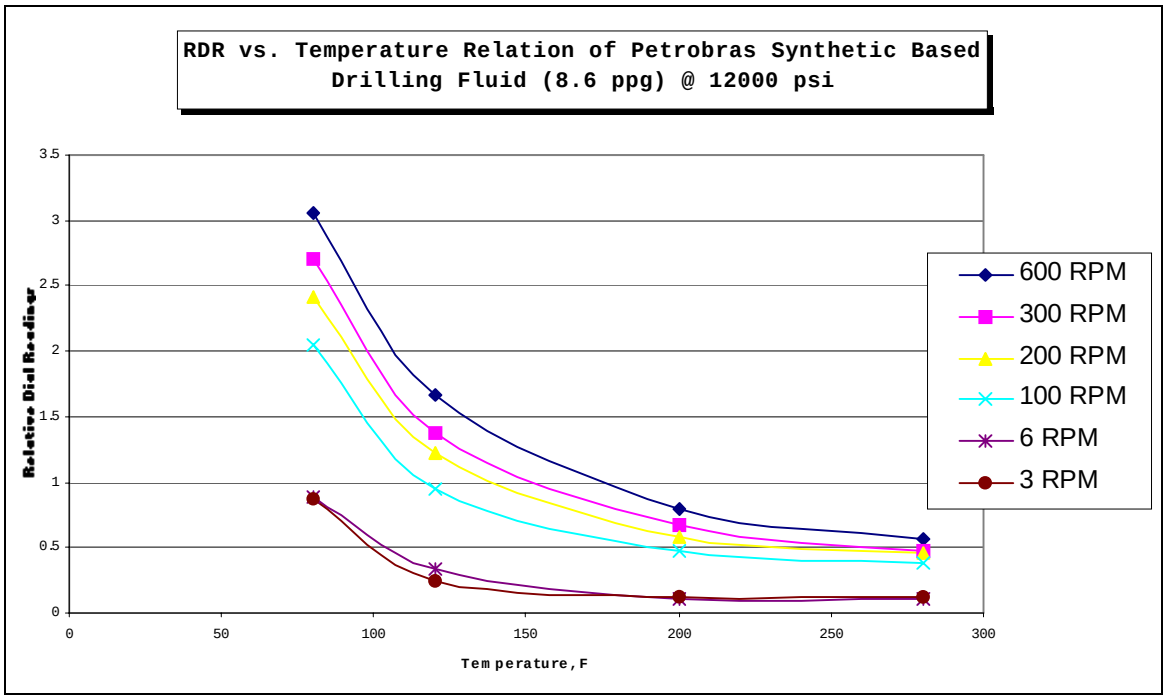

Figure 4.11 Effect of Temperature on Synthetic Based Drilling Fluid RDR Readings @ Different Shear Rates (Pressure = 12000 psig)

Rheological Characterization Process Based on Arrhenius Relationship;

TABLE 4.3.Coefficient Analysis of RDR vs. Temperature for Arrhenius Relation:

Press.	Shear Rate	R^2	C1	C2
Psi	Rpm			
500	600	0.983	0.320826	80.6122
	300	0.988	0.272093	85.2653
	200	0.987	0.250496	87.6856
	100	0.994	0.225315	92.8595
	6	0.998	0.080229	128.702
	3	0.998	0.056531	145.082
2000	600	0.986	0.352176	81.9132
	300	0.987	0.304635	85.3109
	200	0.988	0.281941	86.292
	100	0.996	0.254262	89.6297
	6	0.995	0.091201	123.519
	3	0.993	0.083536	129.377
4000	600	0.959	0.458345	78.0105
	300	0.965	0.391593	82.0268
	200	0.966	0.35925	83.2525
	100	0.981	0.32246	84.9091
	6	0.997	0.082948	125.097
	3	0.997	0.093316	125.097
8000	600	0.996	0.298135	164.262
	300	0.996	0.241878	169.561
	200	0.999	0.22308	169.003
	100	0.997	0.185524	172.998
	6	0.901	0.053721	199.601
	3	0.901	0.060436	199.601
12000	600	0.990	0.361526	171.845
	300	0.995	0.285691	180.328
	200	0.995	0.254668	180.683
	100	0.999	0.193276	188.972
	6	0.991	0.04809	246.669
	3	0.991	0.030311	268.491

TABLE 4.4. Modeling of Coefficient 'C_1' with respect to Pressure

Press.	C1 (3 RPM)	C1 (3cal)	Error, %	C1 (6RPM)	C1(6cal)	Error, %
500	0.056531	0.056797675	0.47	0.080229	0.0806435	0.51
2000	0.083536	0.0840232	0.58	0.091201	0.08882	2.07
4000	0.093316	0.0935216	0.22	0.082948	0.084168	1.47
8000	0.060436	0.0608368	0.66	0.053721	0.052856	1.61
12000	0.030311	0.0307312	1.38	0.04809	0.04788	0.43
Press.	C1 (100 RPM)	C1 (100cal)	Error, %	C1 (200 RPM)	C1 (200cal)	Error, %
500	0.225315	0.213327938	5.32	0.250496	0.23754982	5.16
2000	0.254262	0.285288	12.20	0.281941	0.3161088	12.11
4000	0.32246	0.298024	7.57	0.35925	0.3325904	7.42
8000	0.185524	0.193632	4.37	0.22308	0.2318832	3.94
12000	0.193276	0.192408	0.44	0.254668	0.2533008	0.53

Press.	C1 (300 RPM)	C1 (300cal)	Error, %	C1 (600 RPM)	C1 (600cal)	Error, %
500	0.272093	0.25676075	5.63	0.320826	0.3028365	5.60
2000	0.304635	0.342848	12.54	0.352176	0.399096	13.3
4000	0.391593	0.360464	7.94	0.458345	0.421448	8.05
8000	0.241878	0.250832	3.70	0.298135	0.310104	4.01
12000	0.285691	0.282768	1.02	0.361526	0.359336	0.60

TABLE 4.5 Modeling of Coefficient 'C_2' with respect to Pressure

Press	C2 (3 RPM)	C2 (3cal)	Error, %	C2 (6RPM)	C2 (6cal)	Error, %
500	145.0821	146.6956125	1.11	128.7026	130.7346625	1.57
2000	129.3772	124.8162	3.52	123.5191	118.2454	4.26
4000	125.0977	127.8986	2.23	125.0977	129.0502	3.15
8000	199.6012	197.2938	1.15	199.6012	197.8726	0.86
12000	268.4918	266.8042	0.62	246.6694	246.2214	0.18
Press	C2 (100 RPM)	C2 (100cal)	Error, %	C2 (200 RPM)	C2 (200cal)	Error, %
500	92.85959	96.5737875	3.99	87.6856	91.650125	4.52
2000	89.6297	78.8544	12.02	86.292	77.27	10.45
4000	84.9091	91.1032	7.29	83.2525	92.134	10.66
8000	172.9984	167.0136	3.45	169.0032	168.902	0.05
12000	188.9726	184.2104	2.52	180.6837	184.55	2.13
Press	C2 (300 RPM)	C2 (300cal)	Error, %	C2 (600 RPM)	C2 (600cal)	Error, %
500	85.26536	89.2961625	4.72	80.61222	84.9181625	5.34
2000	85.3109	74.9994	12.08	81.9132	71.6354	12.54
4000	82.0268	90.0162	9.73	78.0105	87.2202	11.80
8000	169.5616	166.5666	1.76	164.2622	162.9386	0.80
12000	180.3289	180.1154	0.11	171.8458	174.3114	1.43

Relation Between Coefficient C_1(P) and Shear Rate:

$$C_3(\gamma) = 0.0371Ln(\gamma) + 0.0039 \quad \text{.....(A-2.1)}$$

$$C_4(\gamma) = 4.289\times10^{-5} * \log10(\gamma) - 3.476\times10^{-6} \quad \text{.....(A-2.2)}$$

$$C_5(\gamma) = -5.926\times10^{-10} + 8.499\times10^{-09} * \log10(\gamma) \quad \text{.....(A-2.3)}$$

$$C_6(\gamma) = -6.636\times10^{-14} + 4.436\times10^{-13} * \log10(\gamma) \text{.....(A-2.4)}$$

Among these equations, equation that has been used to define the relation between C_3 and γ (equation A-2.1) approximates the actual C_3 coefficients with high accuracies (lower than 6% absolute error). However, the other relations used to relate shear rate to coefficients are not that accurate, especially at low shear rates (Table 4.6 – 4.9). This might be because of the fact that low shear rate and high shear rate behavior of the fluid is not the same. If this is the case then low shear rate and high shear rate analysis of the fluid should be done separately and two functions should be used instead of one to show the behavior of dial readings with pressure, temperature and shear rate.

TABLE 4.6 Relation Between Coefficient 'C3' and Shear Rate

Shear Rate	C3	C3-calculated	Error, %
600	0.251	0.24122609	3.89
300	0.21	0.21551033	2.62
200	0.195	0.200467574	2.80
100	0.174	0.174751814	0.43
6	0.075	0.070374276	6.16
3	0.043	0.044658516	3.85

TABLE 4.7 Relation Between Coefficient 'C4' and Shear Rate

Shear Rate	C4	C4-calculated	Error, %
600	1.15E-04	0.000115679	8.53E-01
300	1.04E-04	0.000102768	8.03E-01
200	9.42E-05	9.52152E-05	1.06E+00
100	8.72E-05	0.000082304	5.60E+00
6	1.29E-05	2.98989E-05	**1.31E+02**
3	3.02E-05	1.69877E-05	**4.37E+01**

TABLE 4.8 Relation Between Coefficient 'C5' and Shear Rate

Shear Rate	C5	C5-calculated	Error, %
600	2.26E-08	2.30189E-08	1.72E+00
300	2.07E-08	2.04605E-08	1.06E+00
200	1.87E-08	1.89639E-08	1.36E+00
100	1.75E-08	1.64054E-08	6.25E+00
6	3.53E-09	6.02091E-09	**7.06E+01**
3	5.28E-09	3.46245E-09	**3.44E+01**

TABLE 4.9.Relation Between Coefficient 'C6' and Shear Rate

Shear Rate	C6	C6-calculated	Error, %
600	1.15E-12	1.17E-12	1.22E+00
300	1.05E-12	1.03E-12	1.29E+00
200	9.39E-13	9.54E-13	1.68E+00
100	8.64E-13	8.21E-13	4.94E+00
6	1.74E-13	2.79E-13	**6.02E+01**
3	2.23E-13	1.45E-13	**3.50E+01**

Relation Between Coefficient C_2(P) and Shear Rate:

Similar analysis has been conducted to determine the effect of shear rate on coefficient C_2 using the coefficients C_7, C_8, C_9 and C_{10}. The relations between these coefficients and shear rate are determined as follows as a result of extensive non-linear regression analysis process.

$$C_7(\gamma) = 177.307 * (1+\gamma)^{(-0.1009353)} \quad \text{.....(A-2.5)}$$

$$C_8 = 0.025 \quad \text{.....(A-2.6)}$$

$$C_9(\gamma) = 5.674\times10^{-6} + 7.083\times10^{-7} * \log10(\gamma) \quad \text{.....(A-2.7)}$$

$$C_{10}(\gamma) = 2.284\times10^{-10} + 6.616\times10^{-11} * \log10(\gamma) \quad \text{.....(A-2.8)}$$

It has been found out that, the above relations approximated the relation between shear rate and coefficient C_2 with high accuracy. Absolute errors associated with the above relations are always smaller than 10 % even at low shear rates (Table 4.10 – 4.13). The reason for this might be the fact that, third degree polynomial in equation (4.45) approximates behavior of coefficient of C_2 much better than it does for coefficient C_1. It should be also noted that, among these coefficients, C_8 is almost constant for various shear rates so it can be taken as constant as shown in equation (A-2.6).

TABLE 4.10.Relation Between Coefficient 'C7' and Shear Rate

Shear Rate	C7	C7-calculated	Error, %
600	95.649	92.94785102	2.824
300	100.493	99.66691802	0.822
200	102.854	103.8130849	0.932
100	109.196	111.2805088	1.908
6	139.863	145.6886294	4.165
3	159.649	154.1547019	3.441

TABLE 4.11.Relation Between Coefficient 'C8' and Shear Rate

Shear Rate	C8	C8-calculated	Error, %
600	2.50E-02	0.025	0.00E+00
300	2.60E-02	0.025	3.85E+00
200	2.60E-02	0.025	3.85E+00
100	2.90E-02	0.025	1.38E+01
6	2.10E-02	0.025	**1.90E+01**
3	2.90E-02	0.025	1.38E+01

TABLE 4.12. Relation Between Coefficient 'C9' and Shear Rate

Shear Rate	C9	C9-calculated	Error
600	7.27E-06	7.64176E-06	5.11E+00
300	7.41E-06	7.42854E-06	2.77E-01
200	7.38E-06	7.30382E-06	1.01E+00
100	7.71E-06	7.0906E-06	8.03E+00
6	5.62E-06	6.22516E-06	1.08E+01
3	6.32E-06	6.01194E-06	4.84E+00

TABLE 4.13 Relation Between Coefficient 'C10' and Shear Rate

Shear Rate	C10	C10-calculated	Error, %
600	3.87E-10	4.12202E-10	6.59E+00
300	3.91E-10	3.92286E-10	4.06E-01
200	3.87E-10	3.80636E-10	1.64E+00
100	3.98E-10	3.6072E-10	9.30E+00
6	2.61E-10	2.79882E-10	7.36E+00
3	2.63E-10	2.59966E-10	1.19E+00

Comparison of Proposed Model and Experimental Dial Readings:

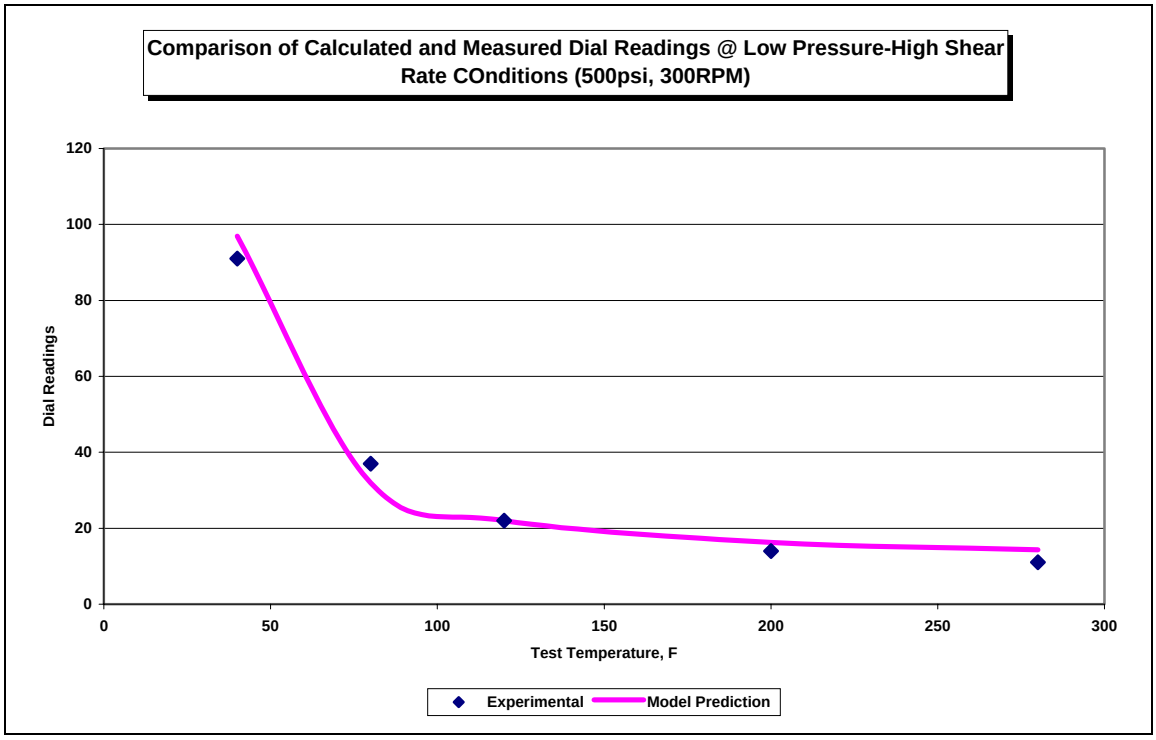

Figure 4.12 Comparison of Model and Experimental Data for Low Pressure-High Shear Rate Section of the Data

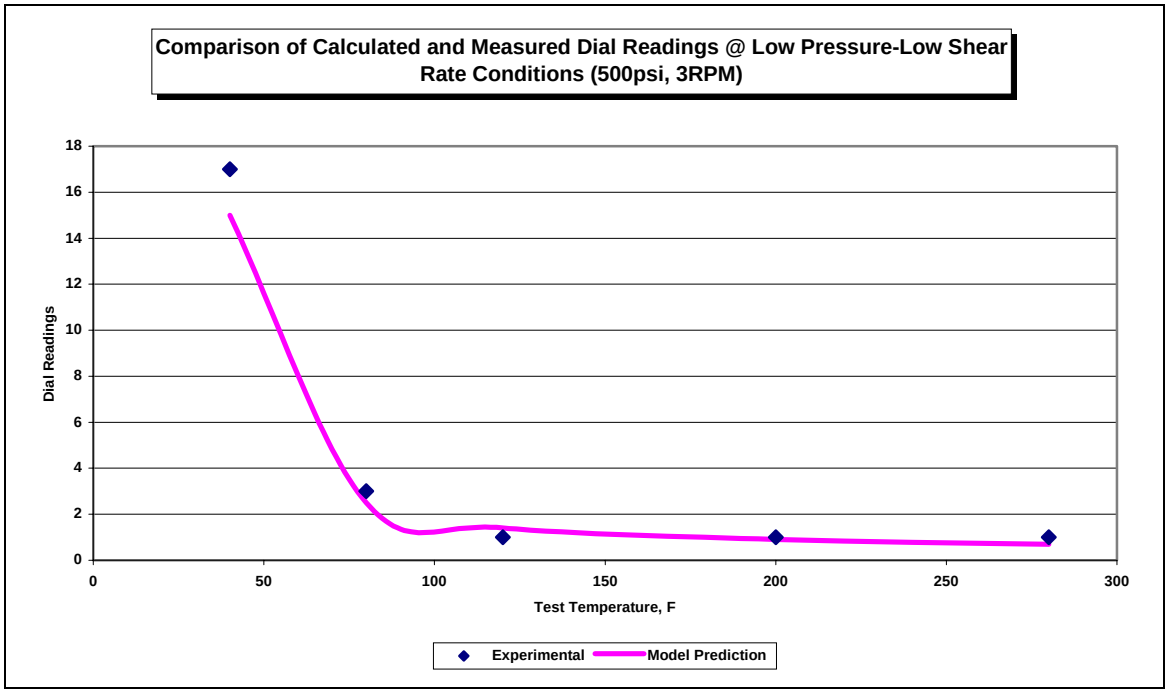

Figure 4.13 Comparison of Model and Experimental Data for Low Pressure-High Shear Rate Section of the Data

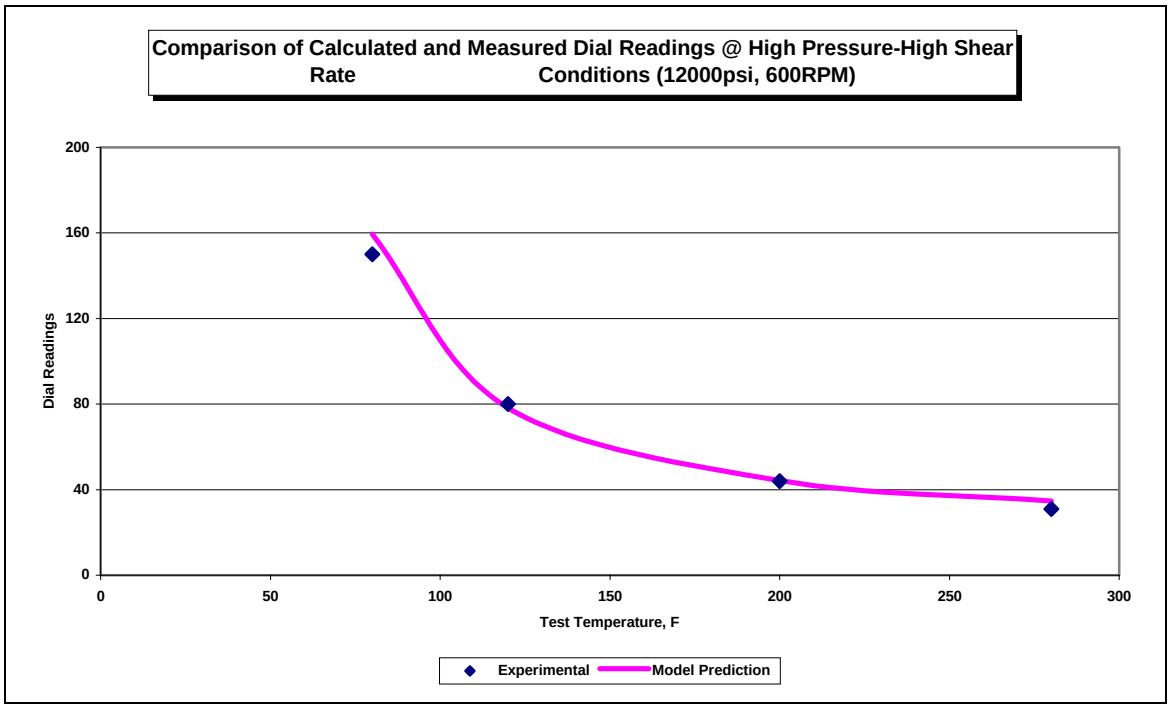

Figure 4.14 Comparison of Model and Experimental Data for High Pressure-High Shear Rate Section of the Data

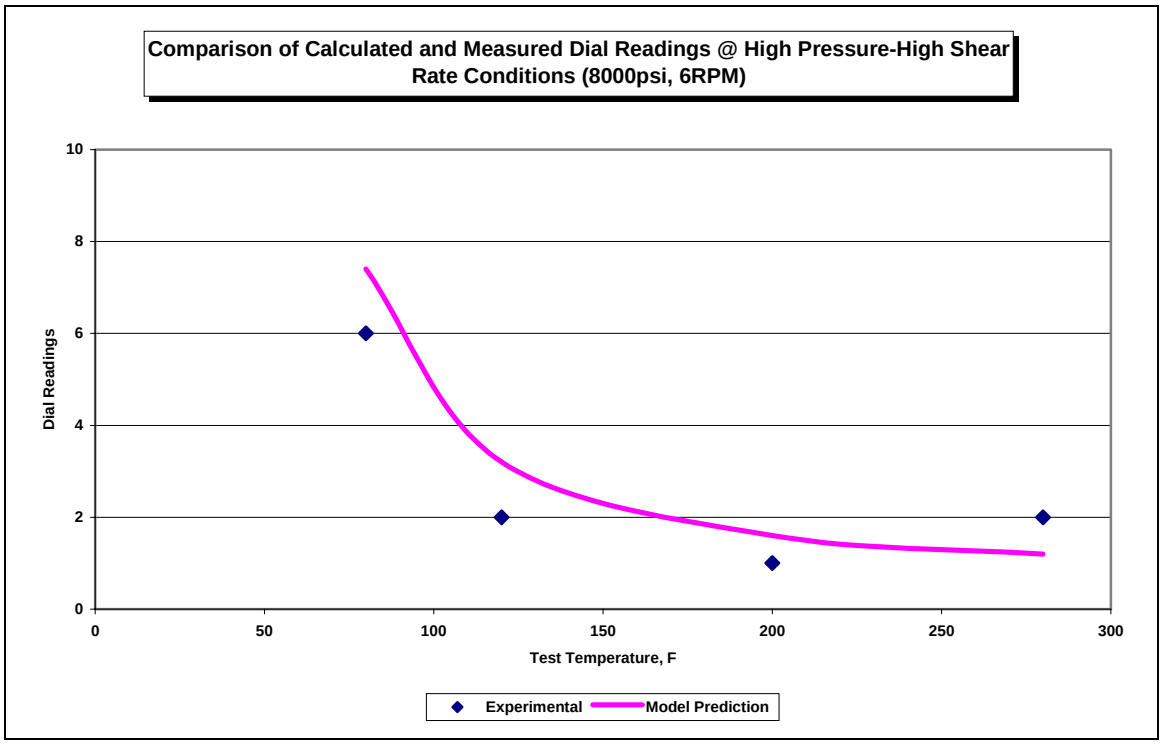

Figure 4.15 Comparison of Model and Experimental Data for High Pressure-Low Shear Rate Section of the Data

APPENDIX-B

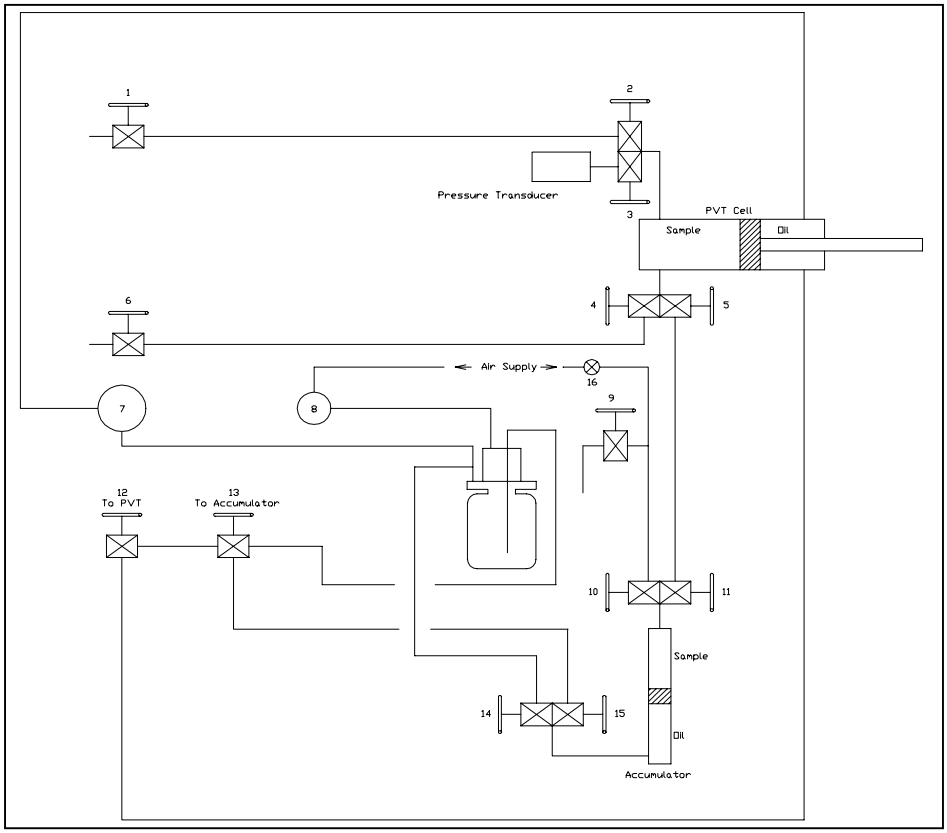

Figure 4-16. Schematic View of PVT Cell and Sampling System

TABLE 4.14. Test Matrix for PVT Calibration Tests with Distilled Water

	Temperature				
Pressure	70F	80F	120F	160F	200F
500	C_o & ρ	C_o & ρ	C_o & ρ	C_o & ρ	C_o & ρ
1000	C_o & ρ	C_o & ρ	C_o & ρ	C_o & ρ	C_o & ρ
1500	C_o & ρ	C_o & ρ	C_o & ρ	C_o & ρ	C_o & ρ
2000	C_o & ρ	C_o & ρ	C_o & ρ	C_o & ρ	C_o & ρ
2500	C_o & ρ	C_o & ρ	C_o & ρ	C_o & ρ	C_o & ρ
3000	C_o & ρ	C_o & ρ	C_o & ρ	C_o & ρ	C_o & ρ
3500	C_o & ρ	C_o & ρ	C_o & ρ	C_o & ρ	C_o & ρ
4000	C_o & ρ	C_o & ρ	C_o & ρ	C_o & ρ	C_o & ρ
4500	C_o & ρ	C_o & ρ	C_o & ρ	C_o & ρ	C_o & ρ
5000	C_o & ρ	C_o & ρ	C_o & ρ	C_o & ρ	C_o & ρ

TABLE 4.15. Test Matrix for PVT Experiments of Synthetic Base Oil and Synthetic Based Drilling Fluid

	TEMPERATURE					
Pressure	80F	120F	160F	200F	240F	280F
0	C_o & ρ	C_o & ρ	C_o & ρ	C_o & ρ	C_o & ρ	C_o & ρ
250	C_o & ρ	C_o & ρ	C_o & ρ	C_o & ρ	C_o & ρ	C_o & ρ
500	C_o & ρ	C_o & ρ	C_o & ρ	C_o & ρ	C_o & ρ	C_o & ρ
1000	C_o & ρ	C_o & ρ	C_o & ρ	C_o & ρ	C_o & ρ	C_o & ρ
1500	C_o & ρ	C_o & ρ	C_o & ρ	C_o & ρ	C_o & ρ	C_o & ρ
2000	C_o & ρ	C_o & ρ	C_o & ρ	C_o & ρ	C_o & ρ	C_o & ρ
2500	C_o & ρ	C_o & ρ	C_o & ρ	C_o & ρ	C_o & ρ	C_o & ρ
3000	C_o & ρ	C_o & ρ	C_o & ρ	C_o & ρ	C_o & ρ	C_o & ρ
3500	C_o & ρ	C_o & ρ	C_o & ρ	C_o & ρ	C_o & ρ	C_o & ρ
4000	C_o & ρ	C_o & ρ	C_o & ρ	C_o & ρ	C_o & ρ	C_o & ρ
4500	C_o & ρ	C_o & ρ	C_o & ρ	C_o & ρ	C_o & ρ	C_o & ρ
5000	C_o & ρ	C_o & ρ	C_o & ρ	C_o & ρ	C_o & ρ	C_o & ρ

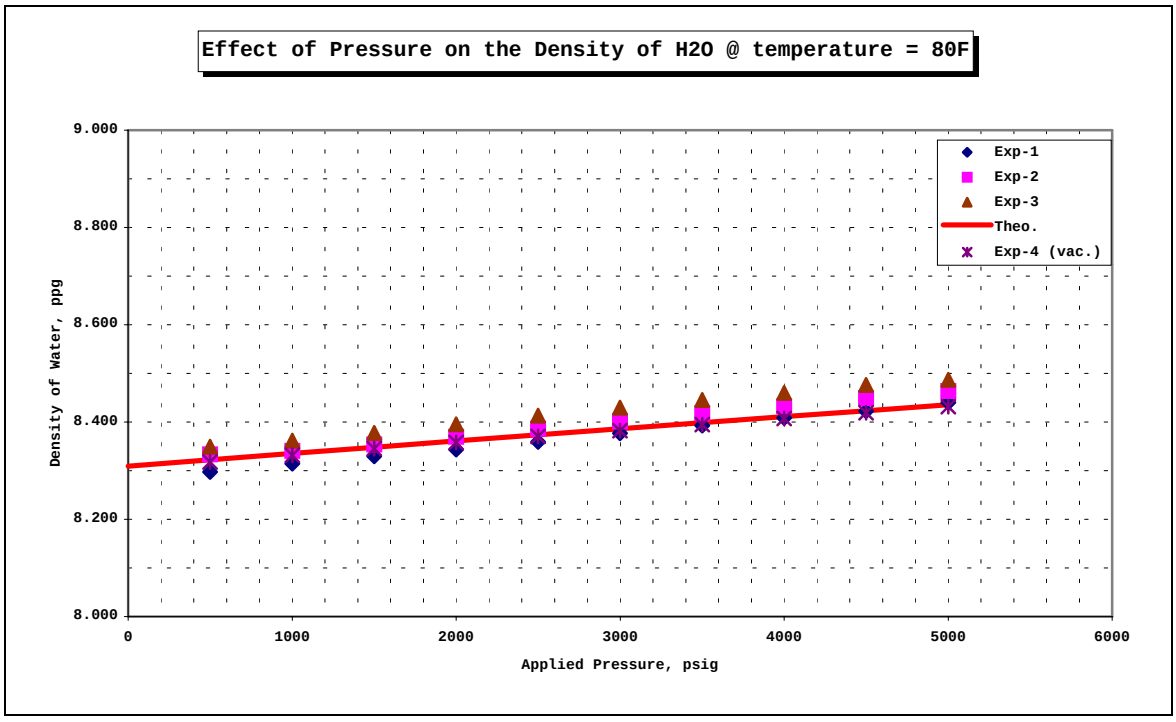

Figure 4.17. Comparison of Experimental Water Densities with Theoretical Water Densities for Calibration Experiments @ 80 F

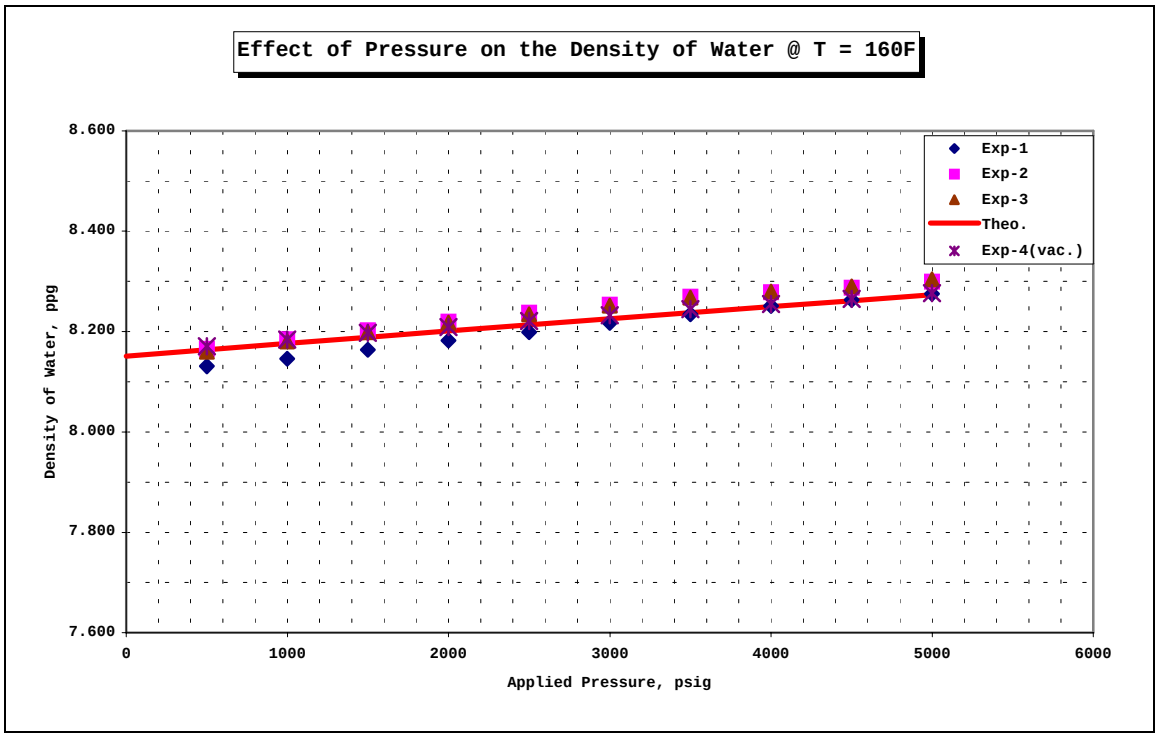

Figure 4.18 Comparison of Experimental Water Densities with Theoretical Water Densities for Calibration Experiments @ 160 F

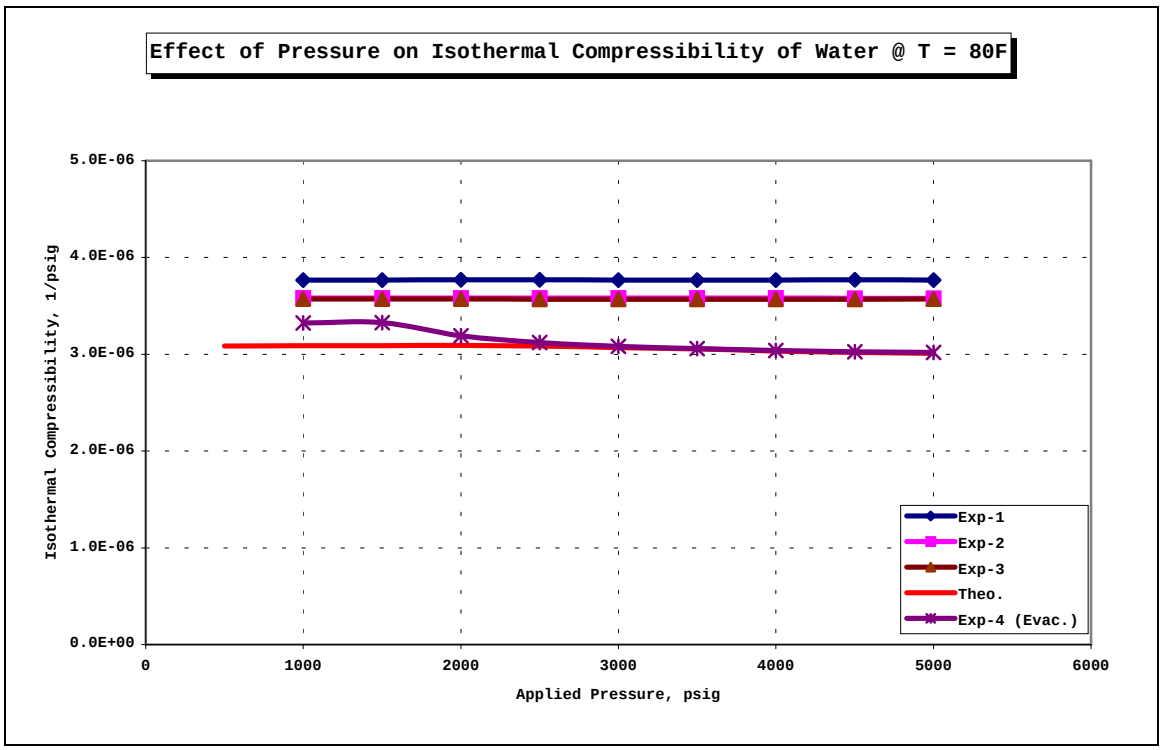

Figure 4.19. Comparison of Experimental Water Compressibility with Theoretical Water Compressibility for Calibration Experiments @ 80 F

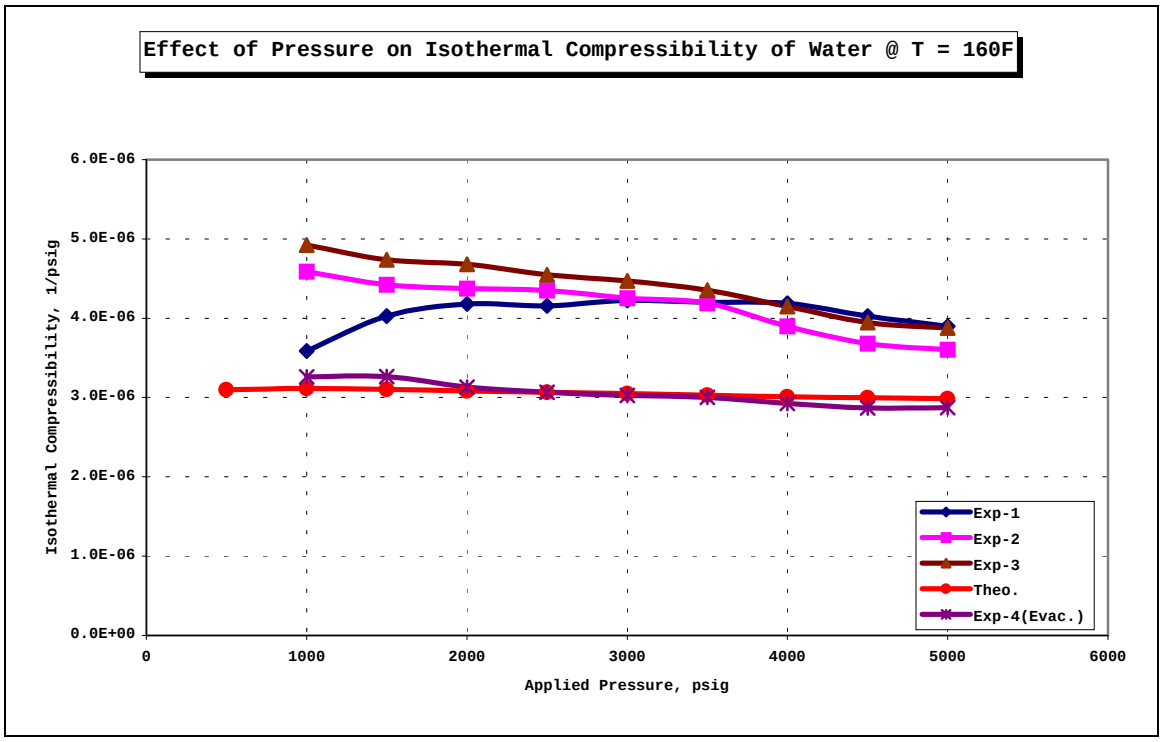

Figure 4.20 Comparison of Experimental Water Compressibility with Theoretical Water Compressibility for Calibration Experiments @ 160 F

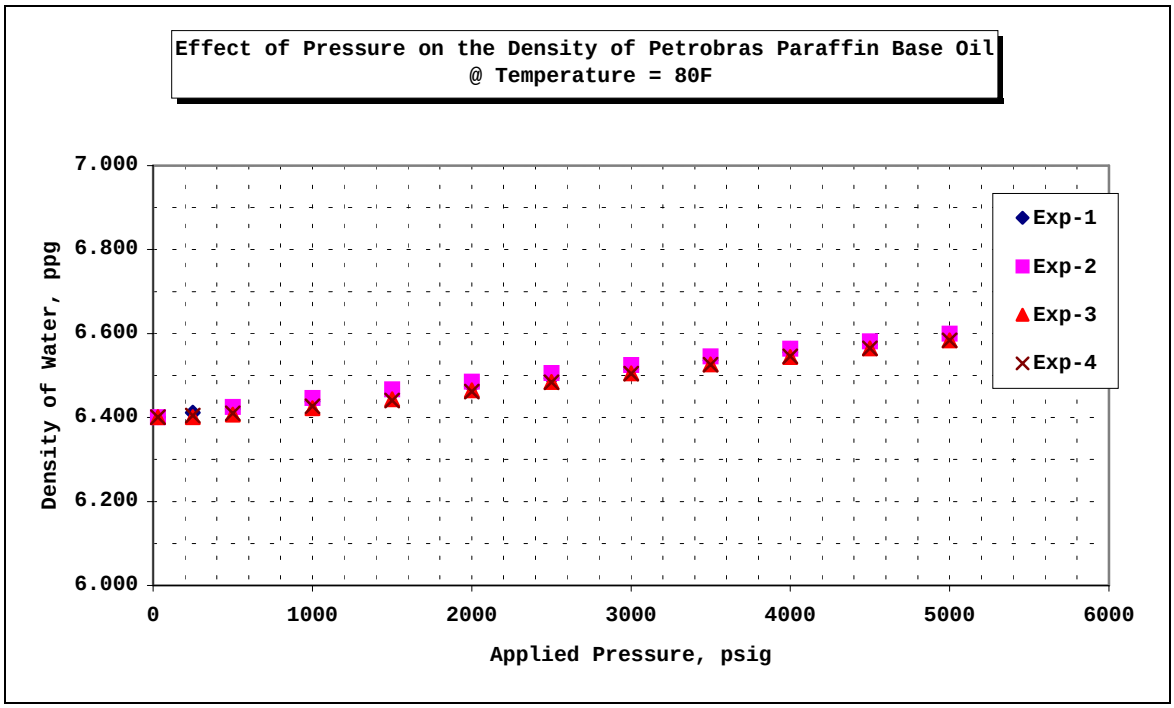

Figure 4.21. Effect of Pressure on Petrobras Synthetic Based Oil @ 80 F

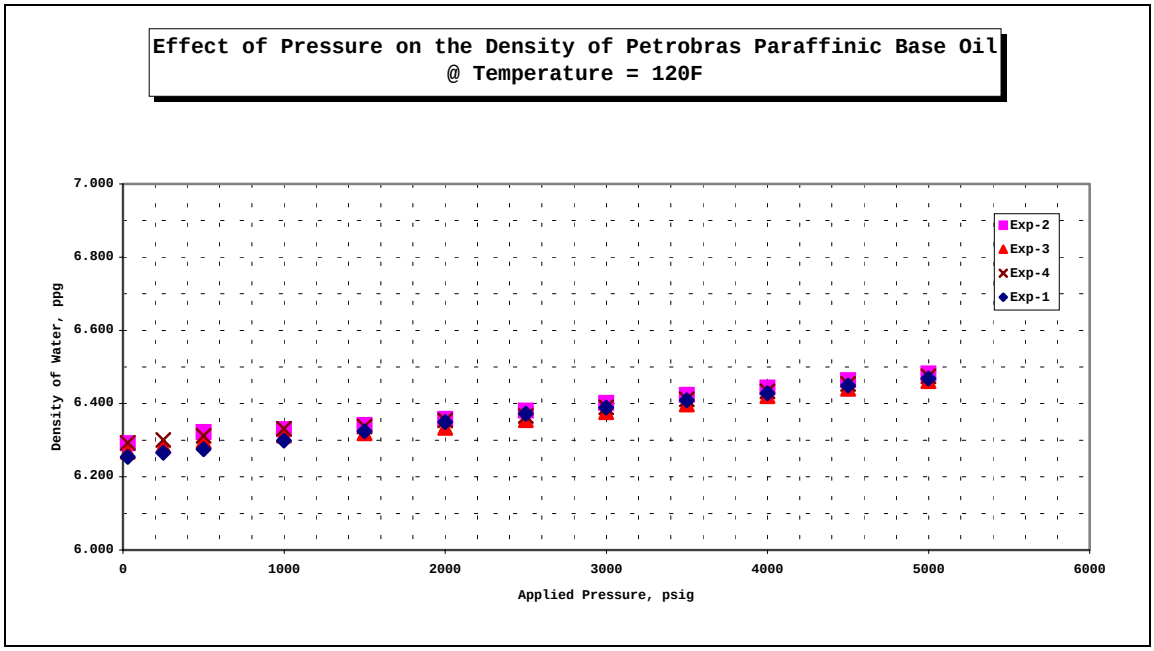

Figure 4.22 Effect of Pressure on Petrobras Synthetic Based Oil @ 120 F

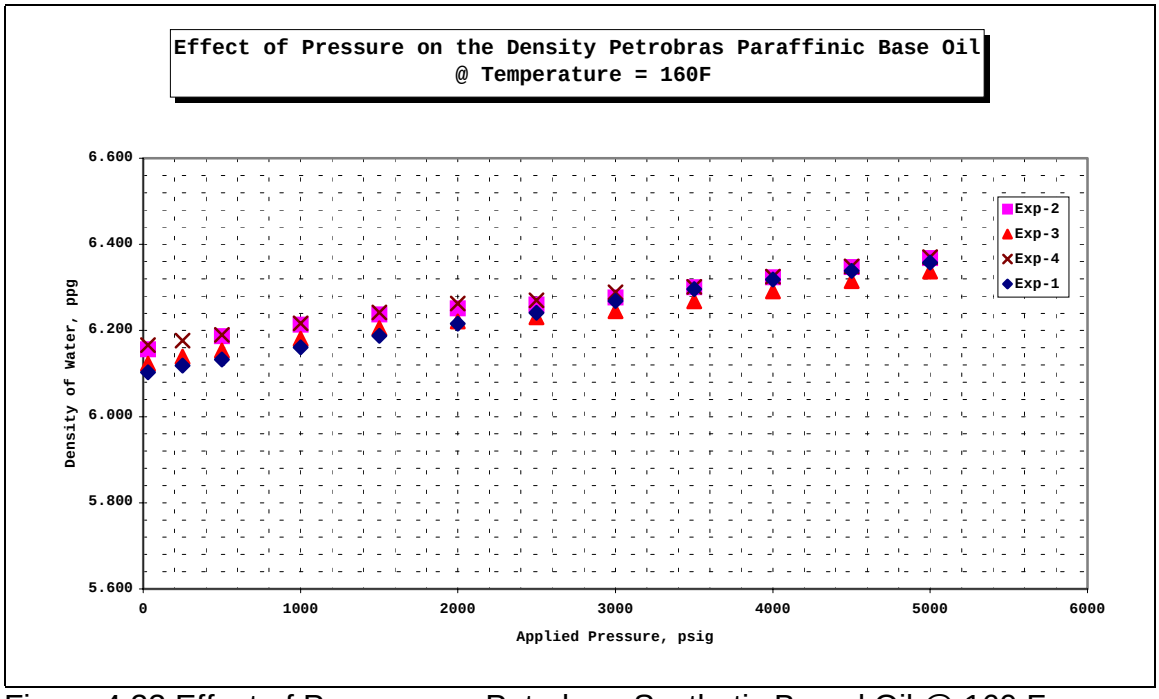

Figure 4.23 Effect of Pressure on Petrobras Synthetic Based Oil @ 160 F

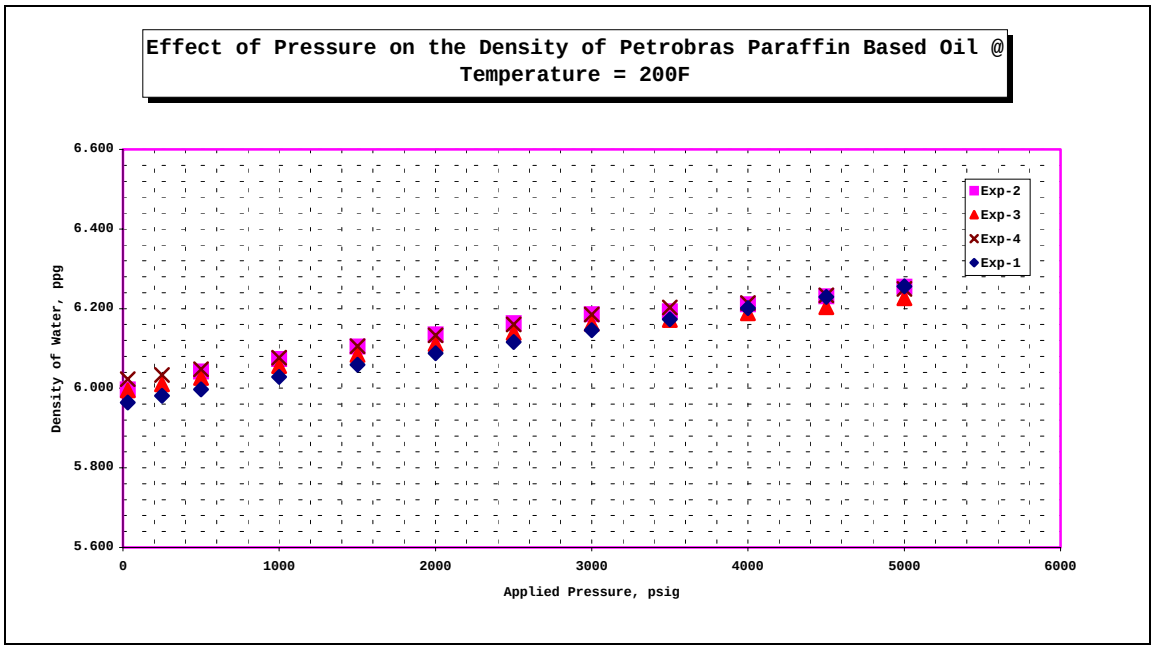

Figure 4.24 Effect of Pressure on Petrobras Synthetic Based Oil @ 200

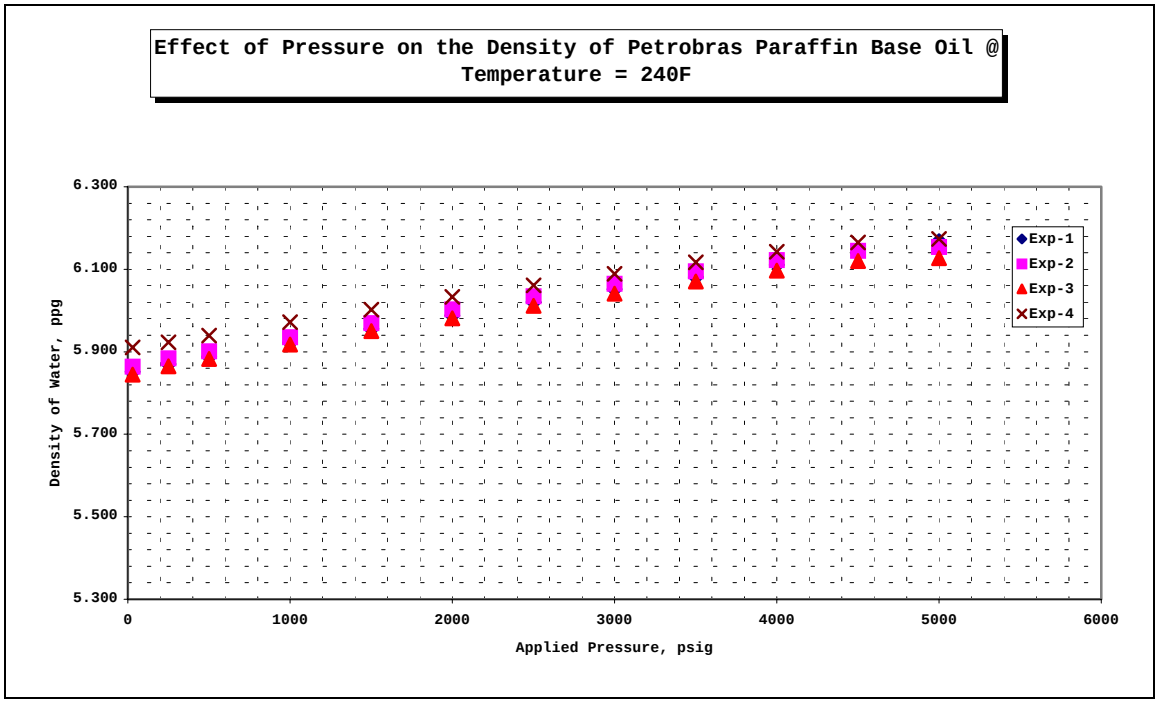

Figure 4.25 Effect of Pressure on Petrobras Synthetic Based Oil @ 240F

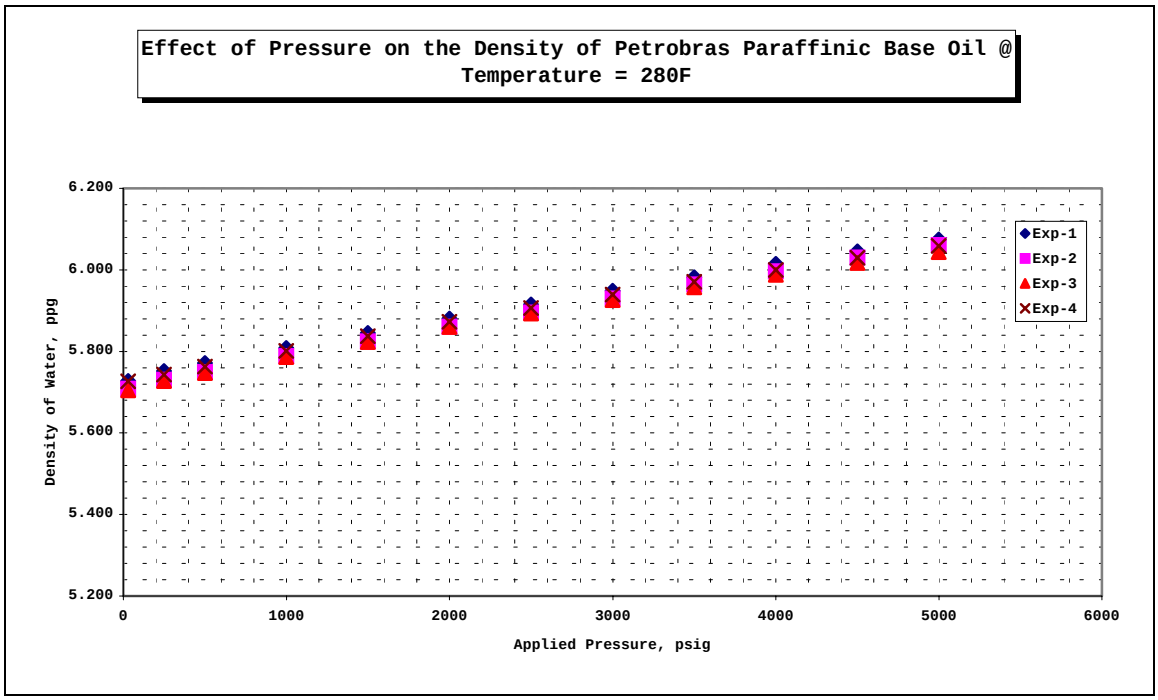

Figure 4.26 Effect of Pressure on Petrobras Synthetic Based Oil @ 280F

TABLE 4.16.R^2 Values for Eqn (5.1) to fit to the Experimental Data of Paraffin Base Oil @ Different Temperature Conditions

TEMPERATURE, F	R^2 VALUE
80	0.9993-0.9957
120	0.9926-0.9906
160	0.9902-0.9887
200	0.9845-0.9684
240	0.9979-0.9891
280	0.9981-0.9951

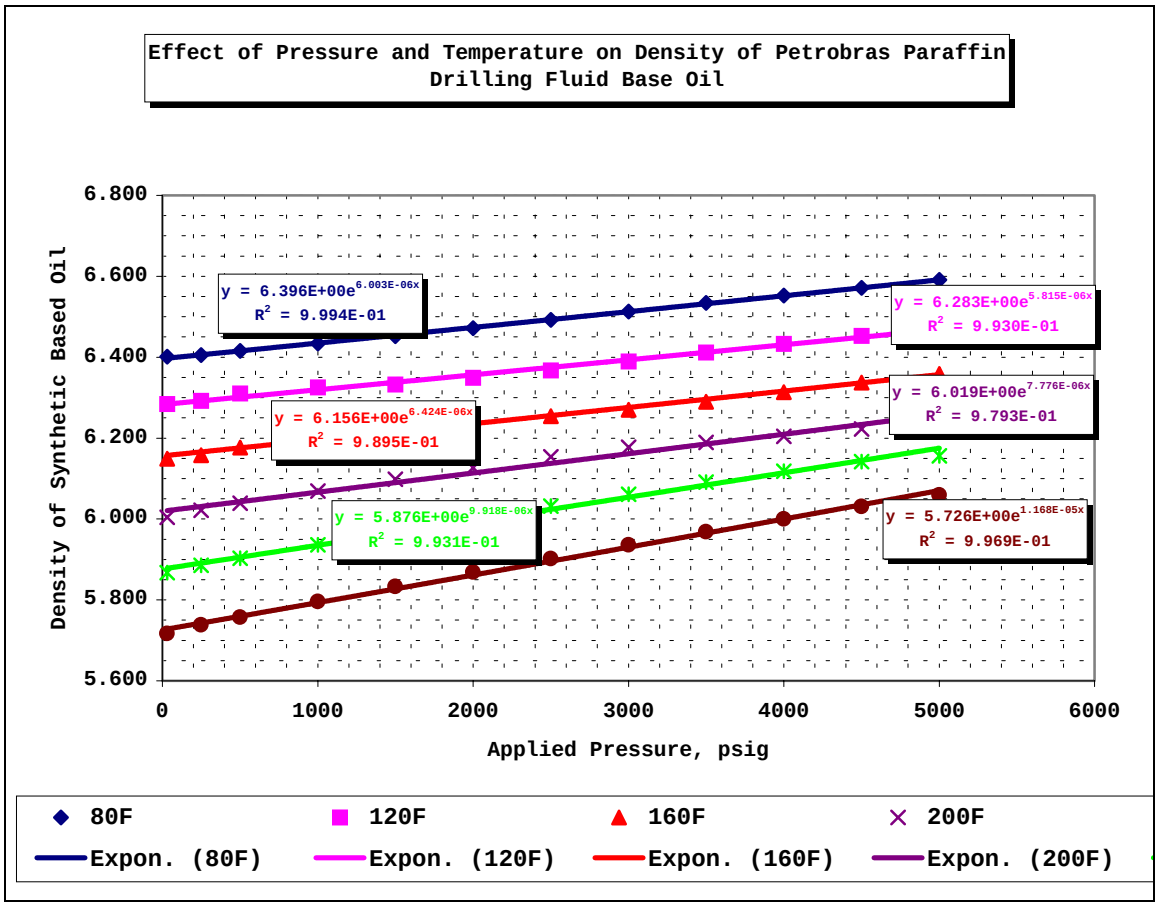

Figure 4.27 Effect of Pressure and Temperature on Petrobras Based Oil and Applicability of Incompressible Relation to Base Oil

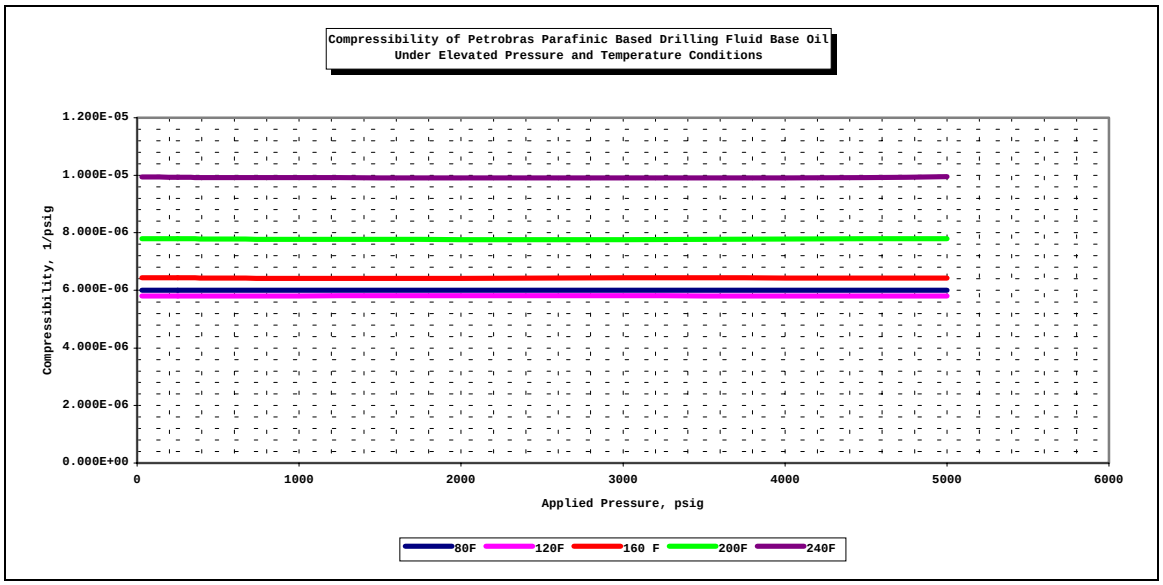

Figure 4.28 Change in Compressibility of Petrobras Synthetic Based Oil with Pressure and Temperature

TABLE 4.17 Effect of P and T on Density of Petrobras Base Oil

T= 80F

Pressure	Rho-exp	Difference	% Diff
30	6.39		
250	6.39	0	0.00
500	6.404	0.014	0.22
1000	6.422	0.032	0.50
1500	6.44	0.05	0.78
2000	6.46	0.07	1.10
2500	6.481	0.091	1.42
3000	6.501	0.111	1.74
3500	6.522	0.132	2.07
4000	6.541	0.151	2.36
4500	6.56	0.17	2.66
5000	6.58	0.19	2.97

T= 120F

Pressure	Rho-exp	Difference	% Diff
30	6.278	-0.112	1.75
250	6.282	-0.108	1.69
500	6.304	-0.086	1.35
1000	6.318	-0.072	1.13
1500	6.326	-0.064	1.00
2000	6.342	-0.048	0.75
2500	6.36	-0.03	0.47
3000	6.383	-0.007	0.11
3500	6.404	0.014	0.22
4000	6.425	0.035	0.55
4500	6.446	0.056	0.88
5000	6.466	0.076	1.19

T= 160F

Pressure	Rho-exp	Difference	% Diff
30	6.142	-0.248	3.88
250	6.147	-0.243	3.80
500	6.17	-0.22	3.44
1000	6.197	-0.193	3.02
1500	6.222	-0.168	2.63
2000	6.238	-0.152	2.38
2500	6.247	-0.143	2.24
3000	6.264	-0.126	1.97
3500	6.283	-0.107	1.67
4000	6.306	-0.084	1.31
4500	6.33	-0.06	0.94
5000	6.352	-0.038	0.59

T= 200F

Pressure	Rho-exp	Difference	% Diff
30	5.998	-0.392	6.13
250	6.011	-0.379	5.93
500	6.032	-0.358	5.60
1000	6.062	-0.328	5.13
1500	6.092	-0.298	4.66
2000	6.12	-0.27	4.23
2500	6.148	-0.242	3.79
3000	6.171	-0.219	3.43
3500	6.182	-0.208	3.26
4000	6.198	-0.192	3.00
4500	6.216	-0.174	2.72
5000	6.237	-0.153	2.39

T= 240F

Pressure	Rho-exp	Difference	% Diff
30	5.857	-0.533	8.34
250	5.875	-0.515	8.06
500	5.892	-0.498	7.79
1000	5.926	-0.464	7.26
1500	5.959	-0.431	6.74
2000	5.991	-0.399	6.24
2500	6.021	-0.369	5.77
3000	6.051	-0.339	5.31
3500	6.081	-0.309	4.84
4000	6.107	-0.283	4.43
4500	6.131	-0.259	4.05
5000	6.145	-0.245	3.83

T= 280F

Pressure	Rho-exp	Difference	% Diff
30	5.707	-0.683	10.69
250	5.728	-0.662	10.36
500	5.748	-0.642	10.05
1000	5.786	-0.604	9.45
1500	5.822	-0.568	8.89
2000	5.858	-0.532	8.33
2500	5.892	-0.498	7.79
3000	5.926	-0.464	7.26
3500	5.958	-0.432	6.76
4000	5.989	-0.401	6.28
4500	6.02	-0.37	5.79
5000	6.049	-0.341	5.34

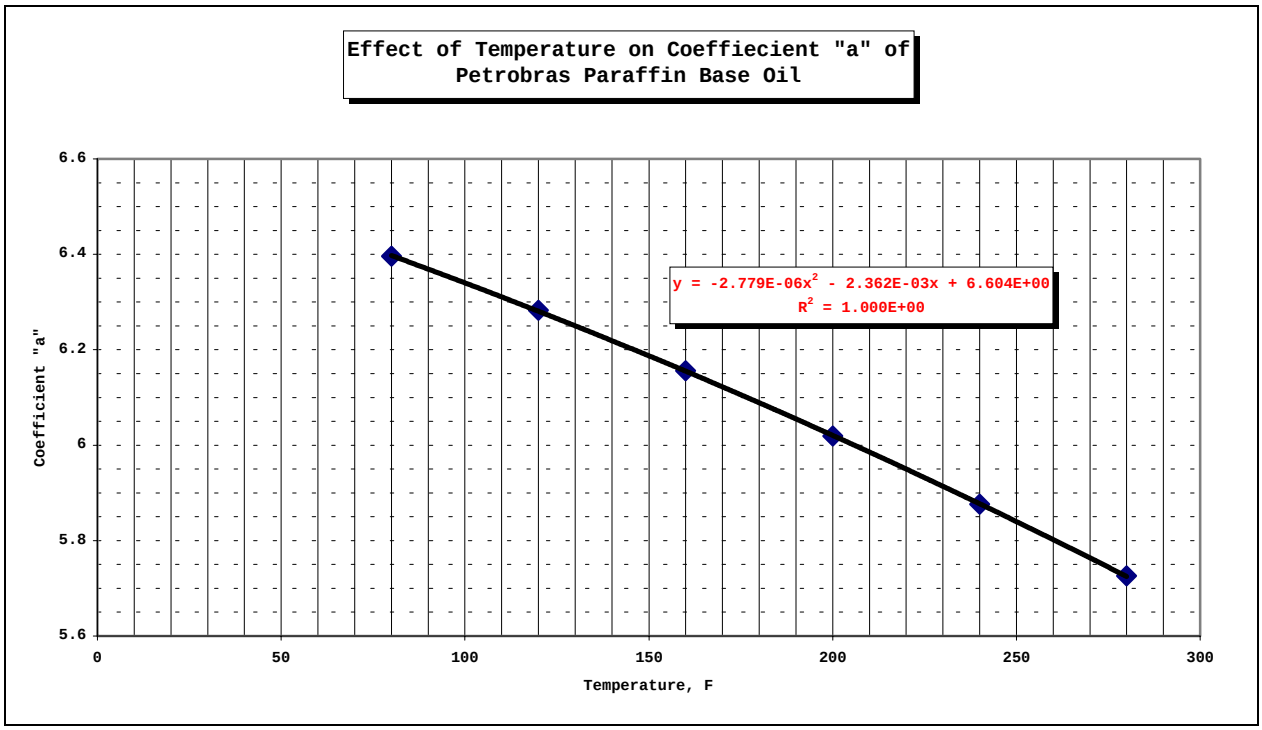

Figure 4.29 Effect of Temperature on Coefficient "a" of Petrobras Synthetic Base Oil

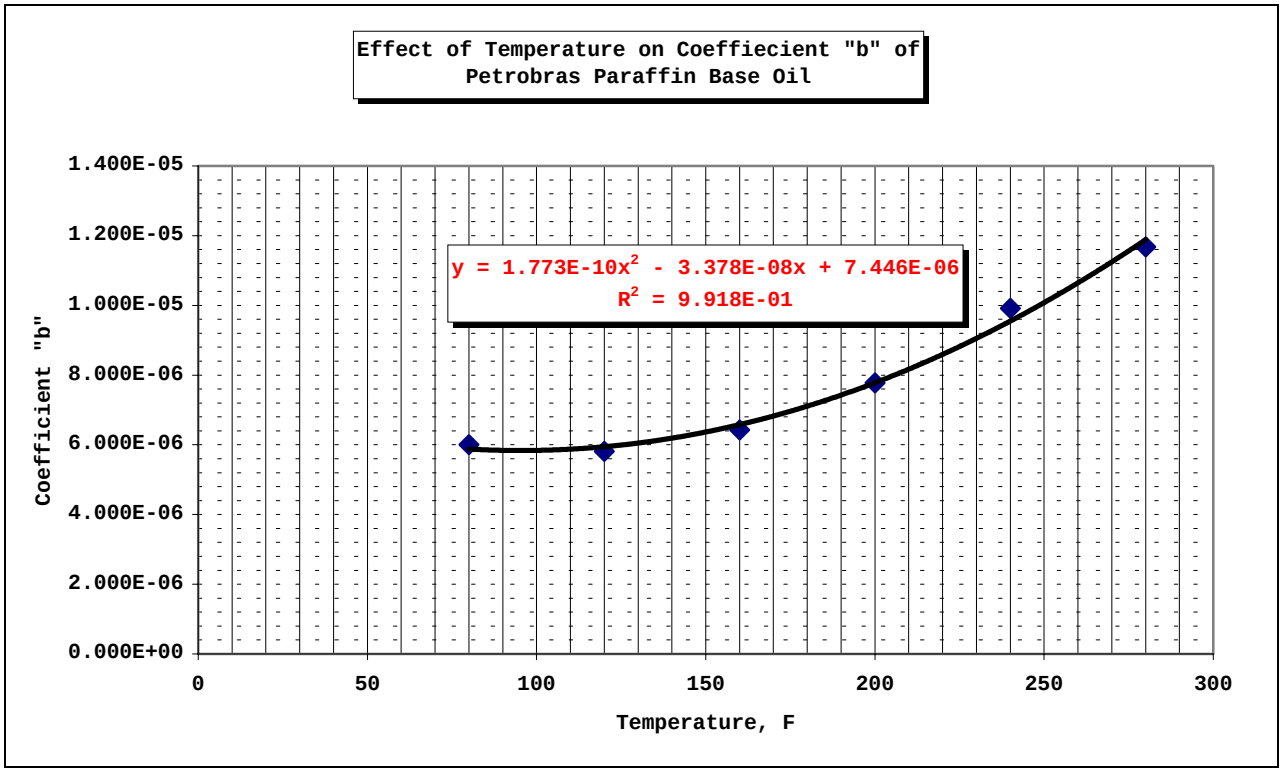

Figure 4.30 Effect of Temperature on Coefficient "b" of Petrobras Synthetic Base Oil

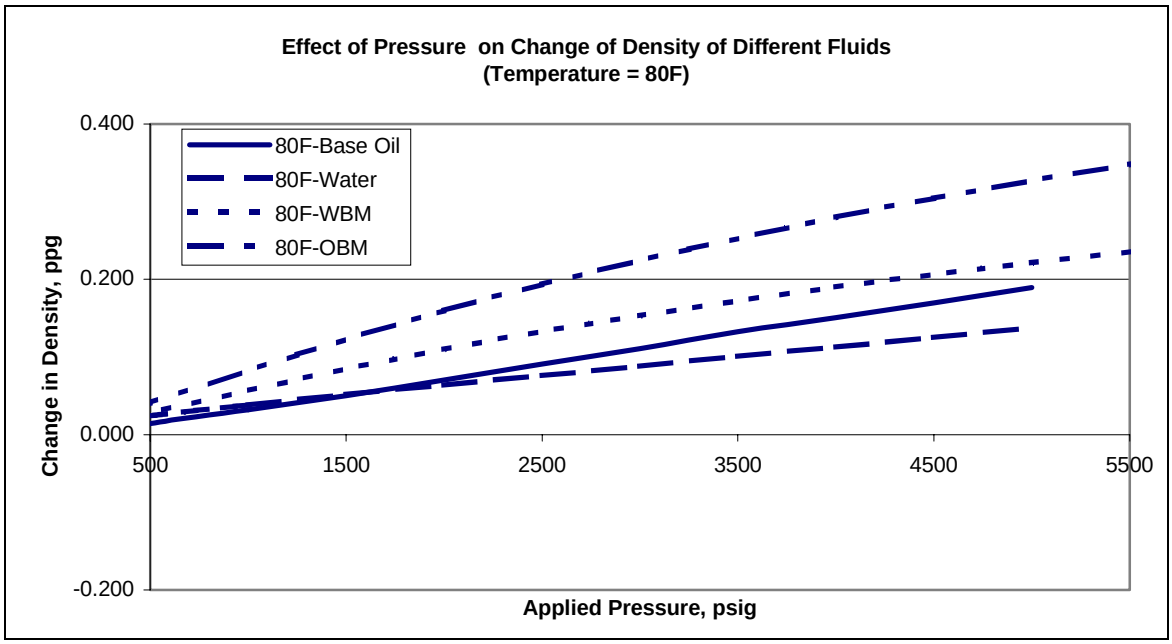

Figure 4.31- Change in Density of Different Based Drilling Fluids with Pressure @ Temperature = 80F

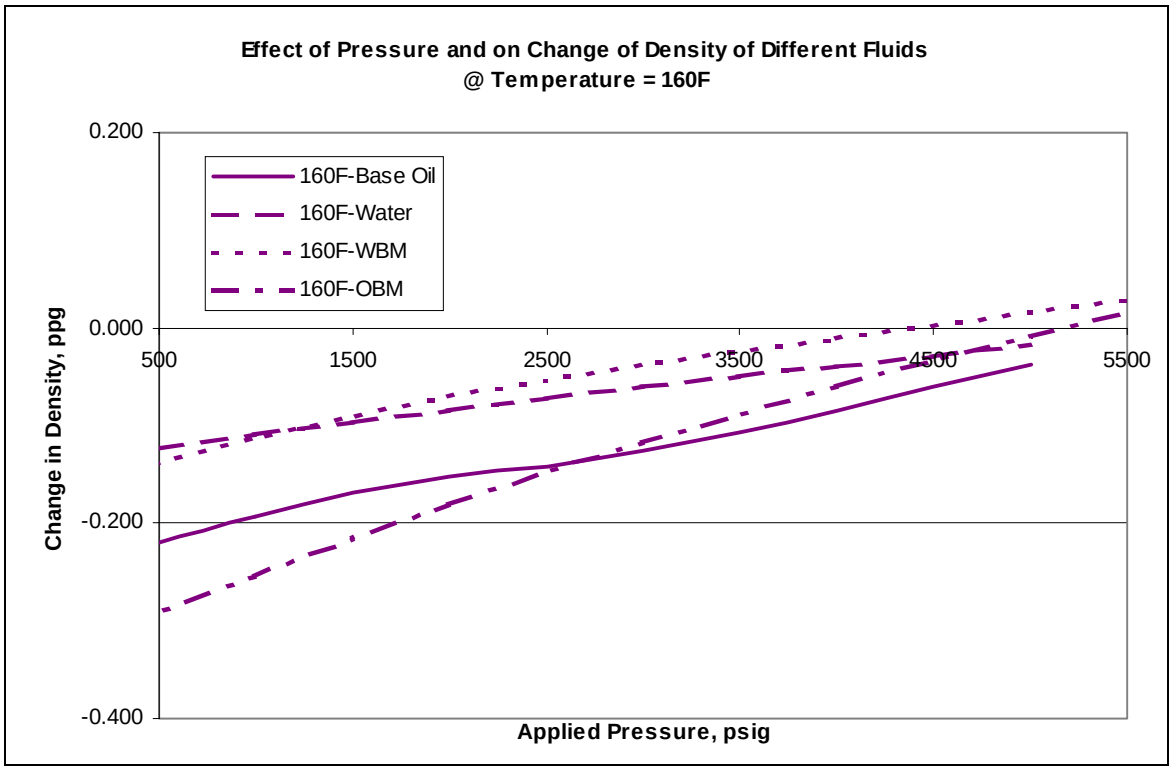

Figure 4.32- Change in Density of Different Based Drilling Fluids with Pressure @ Temperature = 160F

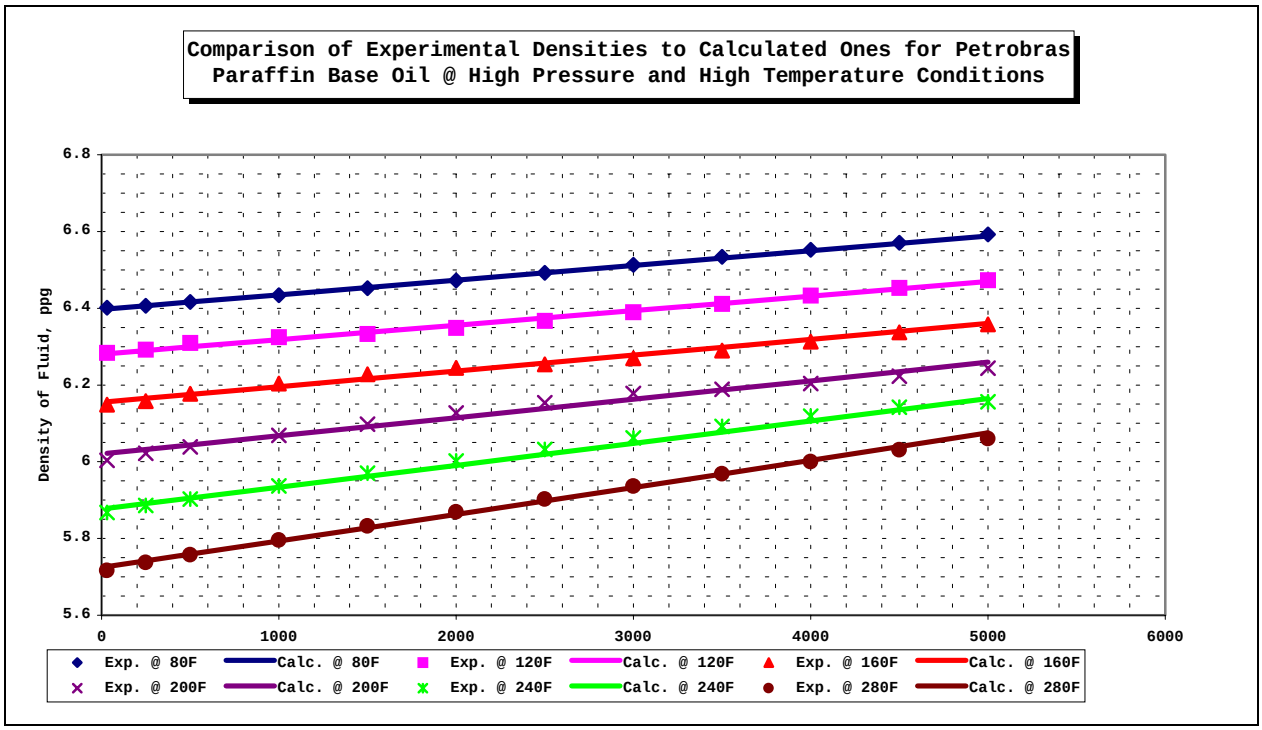

Figure 4.33 Comparison of Experimental and Calculated Petrobras Synthetic Based Oil Densities @ HPHT Conditions

APPENDIX C
ADVANCED CUTTING TRANSPORT FACILITY (ACTS) FLOW LOOP STUDIES

TABLE 4.18 Dimensions Related to the Geometry and Length of Test Section

EXP. SECTION	NOMINAL DIAMETERS	Real Geometries (inches)	LENGTH OF TEST SECTION
PIPE RHEO. #1	2"	1.918	52' 9"
PIPE RHEO. #2	3"	2.900	52' 9"
PIPE RHEO. # 3	4"	3.826	66' 6"
ANNULAR GEO.	6 × 3.5"	OD: 5.761 ID: 3.500	57' 4"

TABLE 4.19 Experimental Test Matrix for Calibration Tests with H_2O

	TEMPERATURES		
PRESSURE, psig	**65 ^oF**	**100 ^oF**	**140 ^oF**
0	50 gpm, 100 gpm 150 gpm, 200 gpm	50 gpm, 100 gpm 150 gpm, 200 gpm	50 gpm, 100 gpm 150 gpm, 200 gpm
400	50 gpm, 100 gpm 150 gpm, 200 gpm	50 gpm, 100 gpm 150 gpm, 200 gpm	50 gpm, 100 gpm 150 gpm, 200 gpm
800	50 gpm, 100 gpm 150 gpm, 200 gpm	50 gpm, 100 gpm 150 gpm, 200 gpm	50 gpm, 100 gpm 150 gpm, 200 gpm
1200	50 gpm, 100 gpm 150 gpm, 200 gpm	50 gpm, 100 gpm 150 gpm, 200 gpm	50 gpm, 100 gpm 150 gpm, 200 gpm

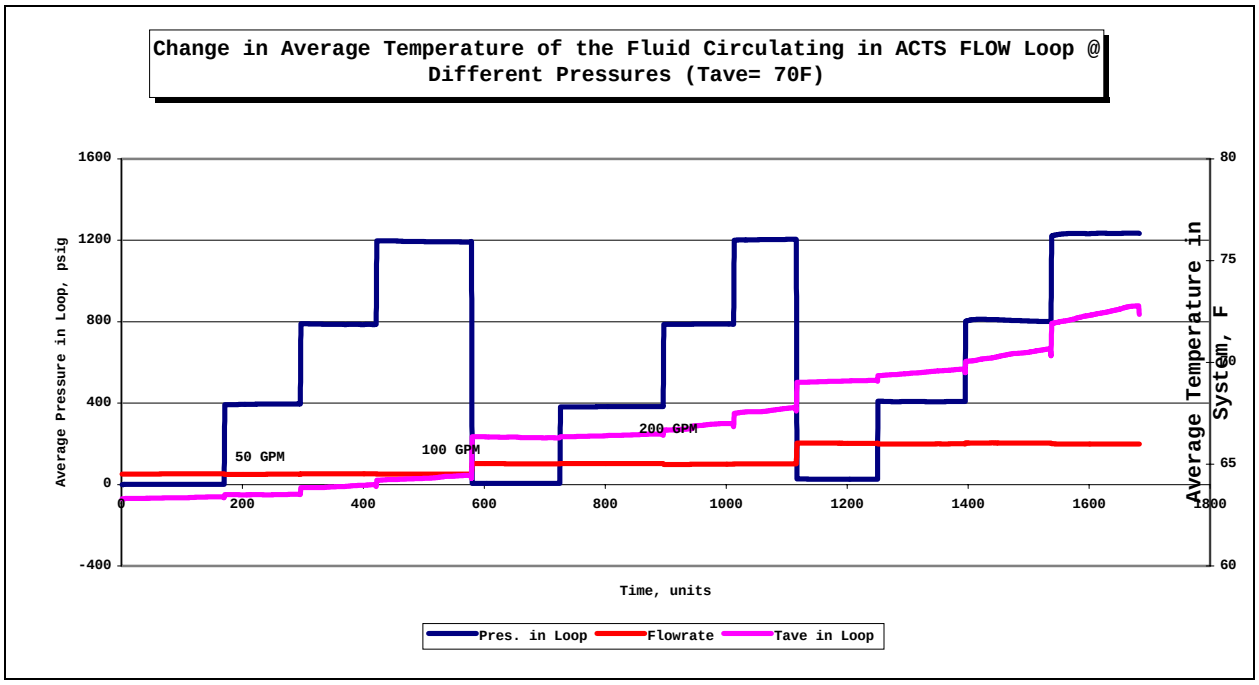

Figure 4.34 Experimental Data Taken During Circulation of Water at average Temperature of 65 ^{o}F

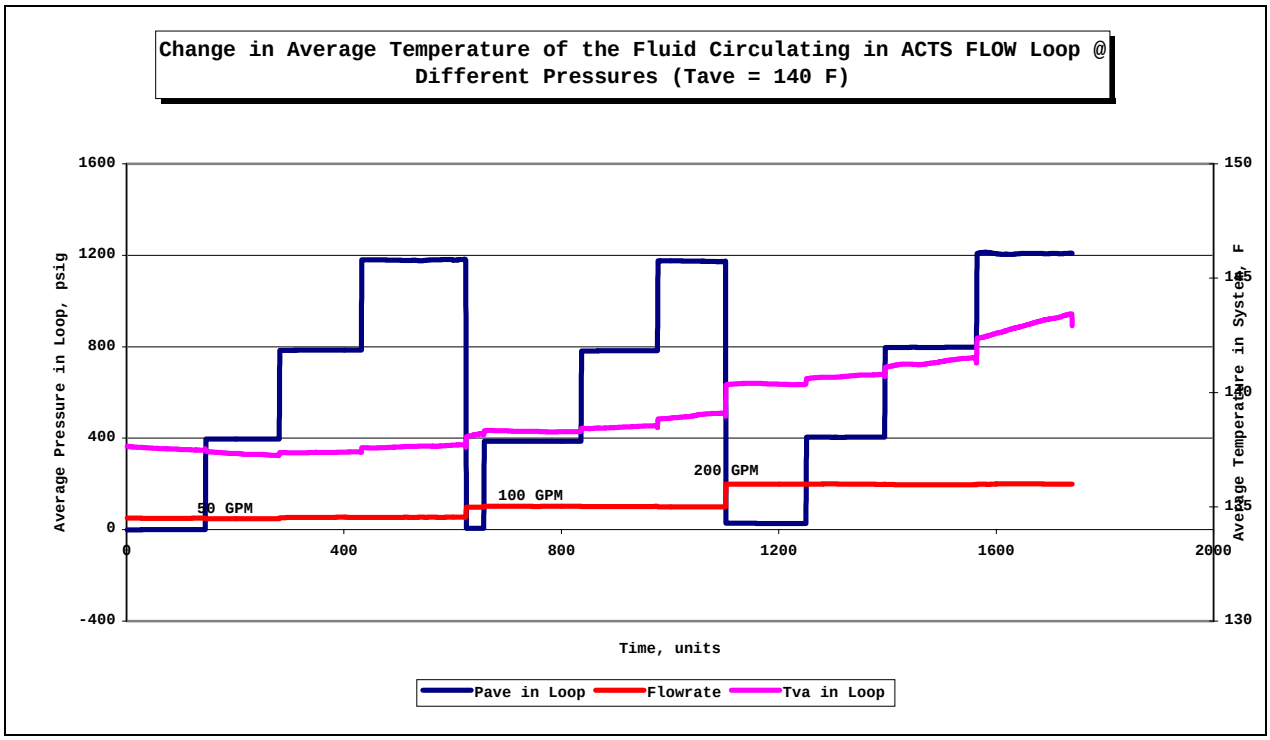

Figure 4.35 Experimental Data Taken During Circulation of Water at average Temperature of 140 ^{o}F

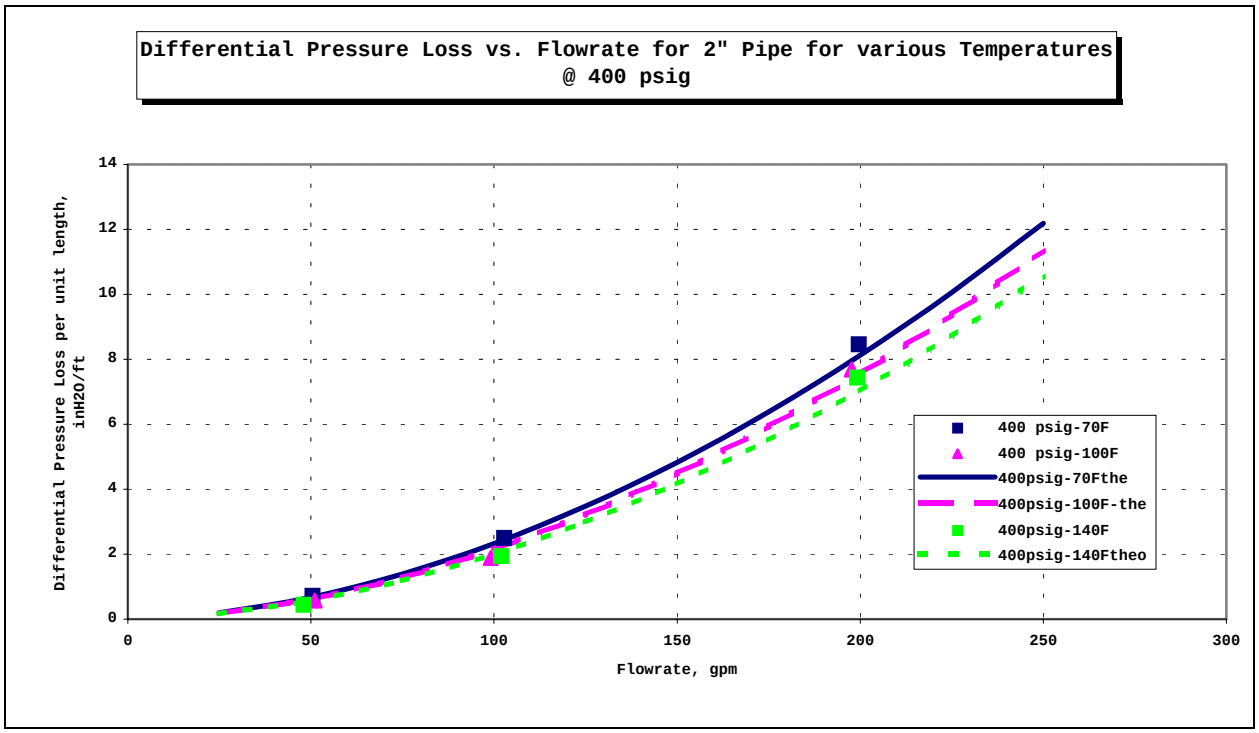

Figure 4.36 Flow rate vs. Differential Pressure Drop per unit length of 2" pipe for various Temperatures when System Pressure is 400 psig

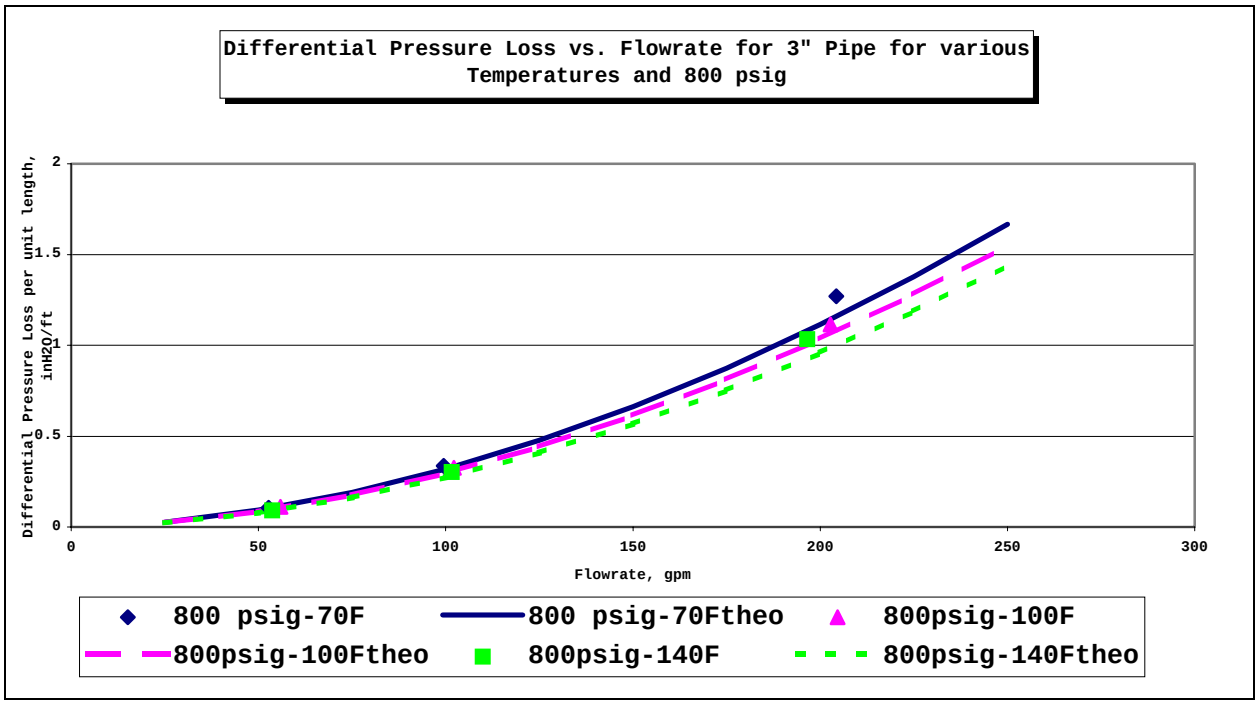

Figure 4.37 Flow rate vs. Differential Pressure Drop per unit length of 3" pipe for various Temperatures when System Pressure is 800 psig

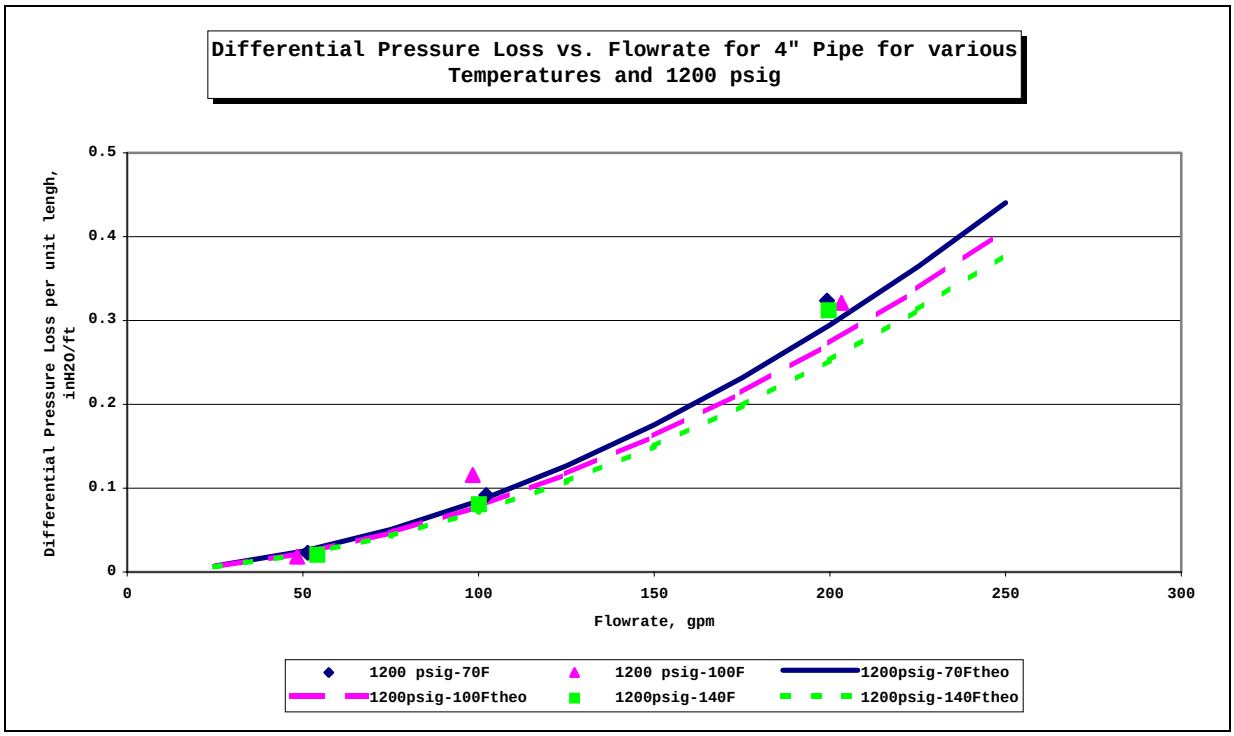

Figure 4.38 Flow rate vs. Differential Pressure Drop per unit length of 4" pipe for various Temperatures when System Pressure is 1200 psig

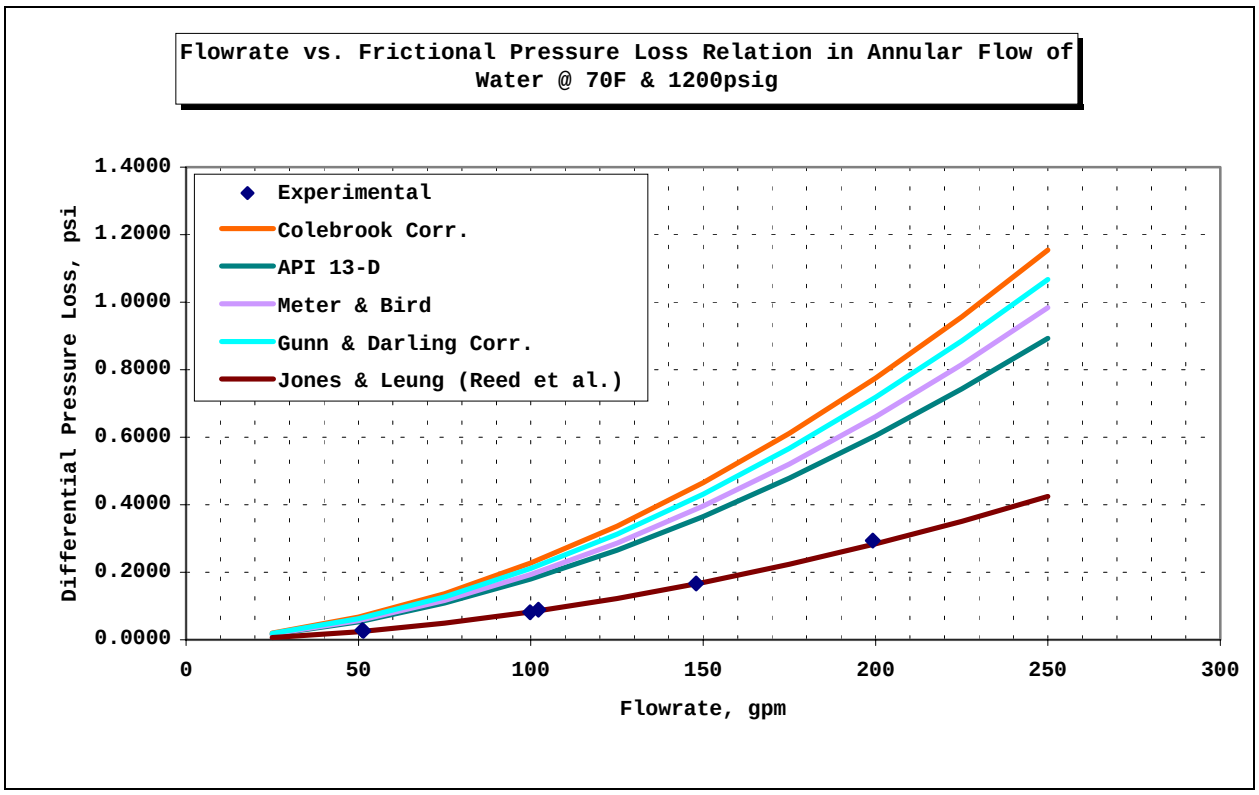

Figure 4.39 Comparison of Calculated and Experimental Frictional Pressure Losses for Water @ 70 F and 1200 psig

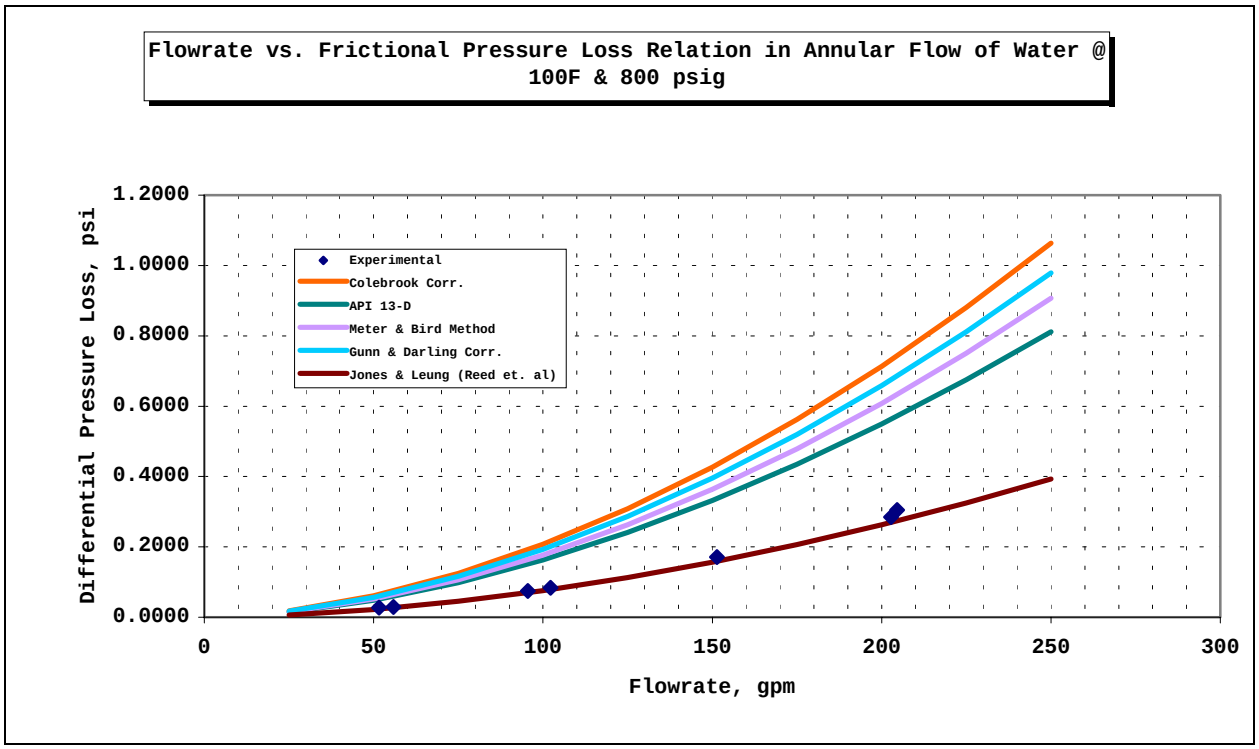

Figure 4.40 Comparison of Calculated and Experimental Frictional Pressure Losses for Water @ 100 F and 800 psig

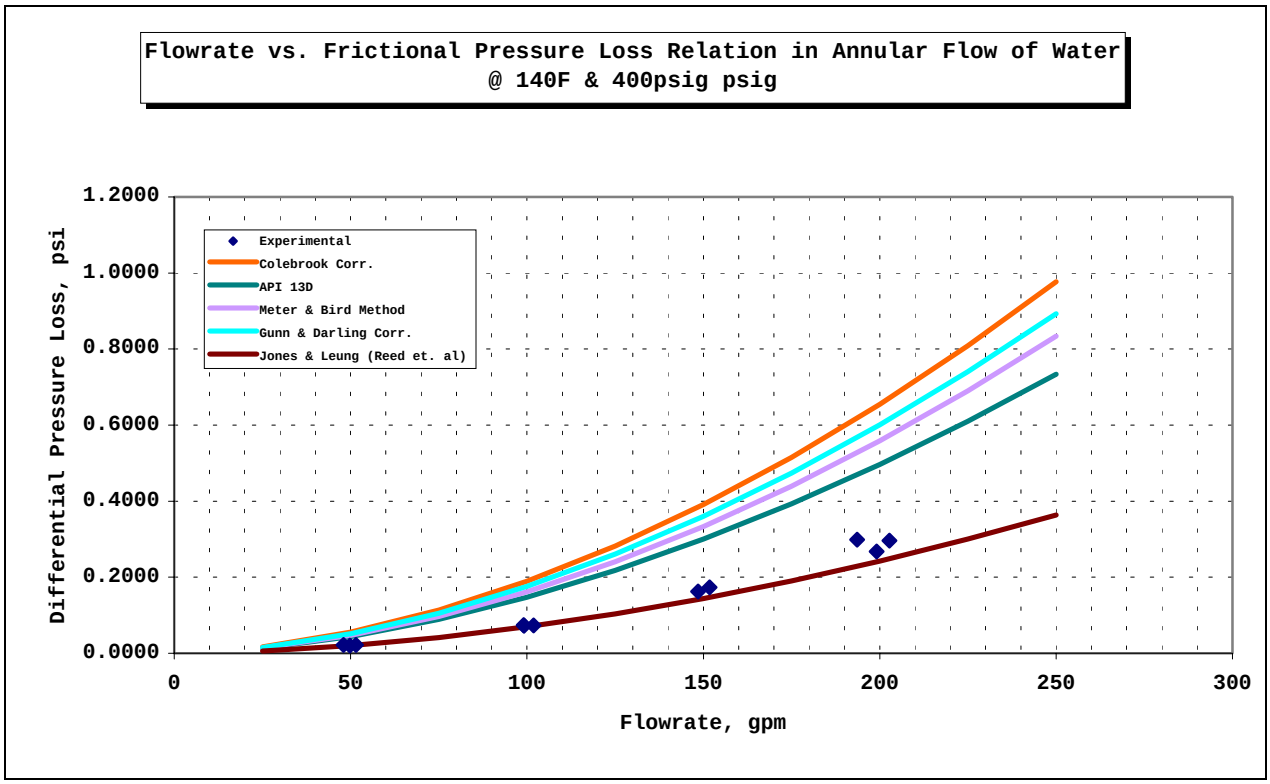

Figure 4.41 Comparison of Calculated and Experimental Frictional Pressure Losses for Water @ 140 F and 400 psig

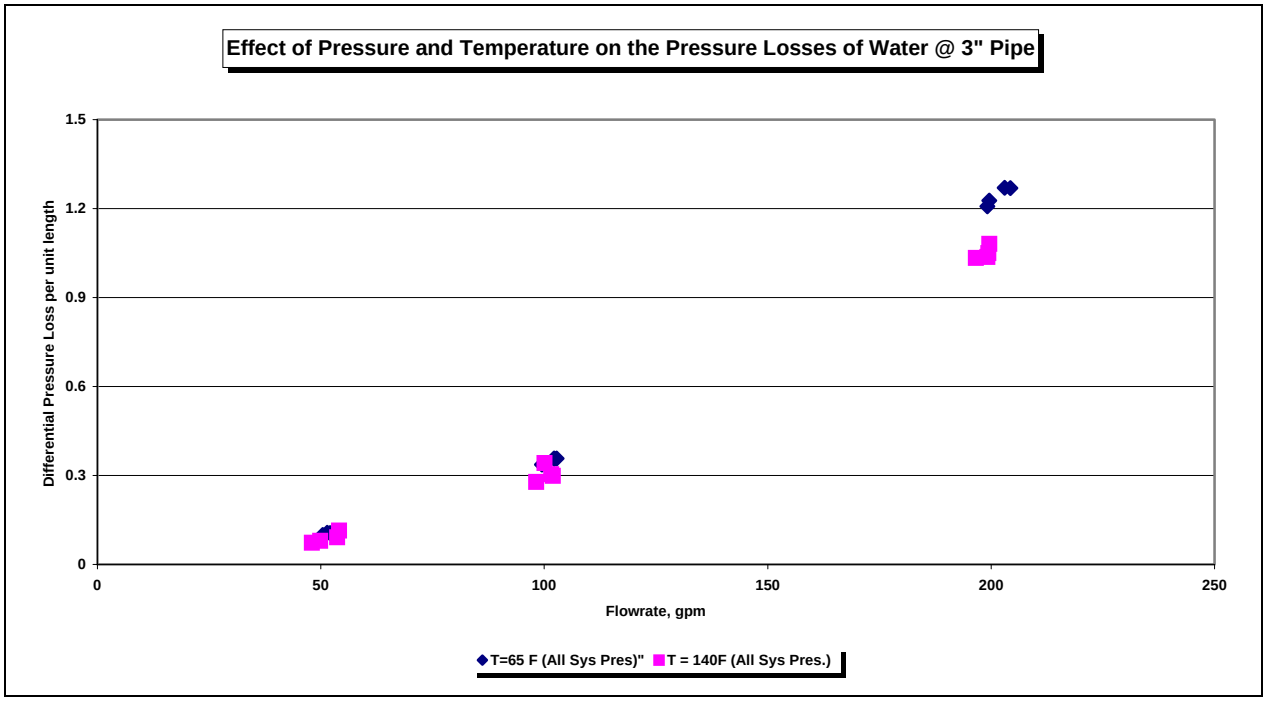

Figure 4.42 Effect of Pressure and Temperature on Differential Pressure Losses of Water @ 3" Pipe

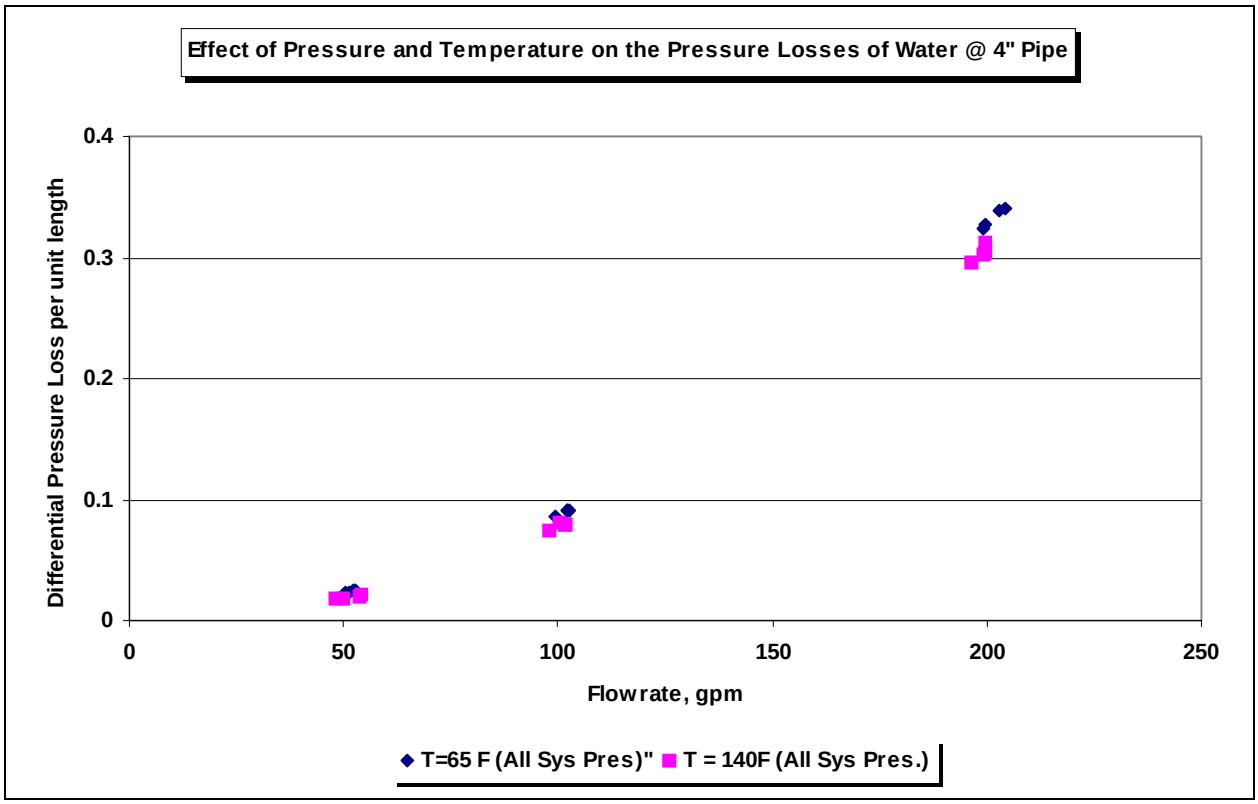

Figure 4.43 Effect of Pressure and Temperature on Differential Pressure Losses of Water @ 4" Pipe

5. STUDY OF CUTTINGS TRANSPORT WITH FOAM UNDER LPAT CONDITIONS

Investigator: Evren Ozbayoglu

5.1 Objectives

-To investigate foam rheology and flow behavior in pipe and annulus.
-To determine (experimentally) and to predict (numerically) frictional pressure losses (with and without cuttings) and volumetric requirements (injection rate, injection pressure and backpressure) for effective cuttings transport with foam flow in inclined and horizontal wellbores.

5.2 Literature Review

Extensive studies have been conducted on foam behavior and rheology. Capillary tubes, rotational viscometers, parallel plate viscometers, cone-and-plate viscometers and flow loops with circular pipes were used for determination of rheological parameters of foams. Most research has shown that foams behave like yield-pseudoplastic fluids. Some researchers have explained foam behavior by pseudoplastic and Bingham Plastic models. Other observations include:

- The liquid fraction of foams has significant effects on foam behavior due to slippage;
- Increase in quality causes increase in apparent viscosity of foam;
- Bubble size, texture and shear rate affects foam viscosity;
- The yield point of the foam increases with increasing quality and decreasing pipe diameter;
- Temperature has minor effects on flow behavior, but does affect rheological parameters;
- Slippage has a significant influence on rheological parameters and flow behavior;
- In order to discard the effect of slippage, viscoelastic measurements have been conducted.

5.3 Foam Flow Experiments

The foam rheology experiments have been conducted on TUDRP's low pressure-ambient temperature flow loop. A schematic view of the loop is given in Fig. 5.1. Experiments have been conducted for 70%, 80 % and 90% foam with flow rates varying from 50 gpm to 250 gpm.

The following procedure has been followed for data analysis:
For pipe flow, the relation between pressure drop and shear stress is derived as

$$\tau_w = \frac{\Delta P}{L}\frac{D}{4} \tag{5.1}$$

and for annulus

$$\tau_w = \frac{\Delta P}{L}\frac{D_2 - D_1}{4} \tag{5.2}$$

For pipe flow, Newtonian shear rate is defined as

$$\gamma = \frac{8v}{D} \tag{5.3}$$

and for annulus, by using the slot flow approach

$$\gamma = \frac{12v}{D_2 - D_1} \tag{5.4}$$

where D_2 is the inner diameter of the larger cylinder, and D_1 is the outer diameter of the smaller cylinder.
Since the pipe section consists of three different pipe sizes (2", 3" and 4"), it is possible to conduct a wall slip analysis. In order to check whether there is slip or not; for a constant foam quality, shear rate vs. shear stress graph is plotted for each pipe diameter as shown in Figs. 5.2-5.4. If there is no slip, all data for different pipe diameter should fall onto a single curve. If a set of curves are obtained, this means that there is slip.

As shown from the Figs. 5.2-5.4 slip effect is present and therefore, a slip correction is required. The well known method for investigating slip effect is using Rabinowitch-Mooney[1] method. In this method, the slip velocity is defined as

$$v_{slip} = \beta\tau_w \tag{5.5}$$

Here, β is called "slip factor", and is a function of wall shear stress. The effect of slip is defined as

$$q_{observed} = q_{actual} + q_{slip} \tag{5.6}$$

If the cross-sectional area of flow is constant, the equation can be written as

$$\left(\frac{8v}{D}\right)_{observed} = \left(\frac{8v}{D}\right)_{actual} + \frac{8v_{slip}}{D} \tag{5.7}$$

So, if the definition of slip velocity is inserted into the equation

$$\left(\frac{8v}{D}\right)_{observed} = \left(\frac{8v}{D}\right)_{actual} + \frac{8\beta\tau_w}{D} \tag{5.8}$$

This equation tells that, if a graph of $\frac{8v}{D}$ vs. $\frac{1}{D}$ is plotted, the result should be a straight line with a slope of $8\beta\tau_w$. Enzendorfer[3] et al studied the slip effect for nitrogen and carbon-dioxide foams, and showed that, when $\frac{8v}{D}$ vs. $\frac{1}{D}$ is plotted for various shear stresses, the intercept values of y-axis, true shear rate value, is negative, which is showing that the slip model is not applicable. They suggested to use Oldroyd-Jastrzebski[2]'s slip model instead for analyzing slip effects in foam. The difference between this model and the previous one is that, the slip factor, β, is not only a function of shear stress, but also a function of diameter. The slip velocity defined by Oldroyd-Jastrzebski[2] is

$$v_{slip} = \frac{\beta}{D}\tau_w \tag{5.9}$$

In the same manner as mentioned in the previous slip model, the effect of slip can be written as

$$\left(\frac{8v}{D}\right)_{observed} = \left(\frac{8v}{D}\right)_{actual} + \frac{8\beta\tau_w}{D^2} \tag{5.10}$$

This time, if a graph of $\frac{8v}{D}$ vs. $\frac{1}{D^2}$ is plotted, the result should be a straight line with a slope of $8\beta\tau_w$. The y-intercept of this line is observed to be positive (Figs. 5.5-5.7), so it is concluded that, the application of Oldroyd-Jastrzebski[2]'s slip model should be used for foam flow instead of Rabinowitch-Mooney[1] model. A graph of slip coefficient, β, vs. shear stress is plotted for different foam qualities to define the relationship between β and τ_w for each quality as shown in Fig. 5.8. By using these relations, the slip corrected shear rates are calculated, and the graph of $log\frac{8v_{actual}}{D}$ vs. $log\,\tau_w$ is plotted as shown in Fig. 5.9.

According to Rabinowitch-Mooney[1]'s work, a generalized shear stress-shear rate relation can be derived as

$$\gamma_w = \frac{8v}{D}\frac{3n'+1}{4n'} \tag{5.11}$$

$$\tau_w = \frac{\Delta P}{L}\frac{D}{4} \tag{5.12}$$

where

$$n' = \frac{d\ln(\tau_w)}{d\ln\left(\frac{8v}{D}\right)} \tag{5.13}$$

If *n'* is equal to unity, the fluid is a Newtonian fluid. The statistical analysis of the logarithmic $\frac{8v_{actual}}{D}$ vs. logarithmic τ_w plot showed that, for each quality value, the best possible description of the behavior of points were a straight line representation, meaning that *n'* is constant for different shear rate values. Corrected shear rate vs. shear stress graph is plotted for determination of rheological parameters for different rheological models as shown in Fig. 5.10. Rheological models are determined by using a commercial software, Statistica, which allows to make nonlinear analysis. The model parameters are determined for Power Law, Bingham Plastic and Yield-Power Law models.
The model parameters obtained from experimental data are used in the computer simulator for comparing the existing rheological models.

5.4 Comparison of Foam Hydraulic Models

Sanghani[4], Blauer[5] et al, Beyer[6] et al, Valko[7], and Gardiner[8] et al rheological models proposed for foam flow are compared. The computer simulator is used for comparing the experimental results with existing models. Input data for the simulator , i.e., pressure, temperature, flow rates, pipe diameter and length, are set same as the experimental conditions. The effects of change in volume of foam due to the pressure change in the pipe is also calculated by

$$V_2 = V_1\left[(1-\Gamma_1)+\frac{P_1T_2}{P_2T_1}(\Gamma_1)\right] \tag{5.14}$$

where subscript “1” addresses the present position, and subscript “2” addresses the next position of foam in the pipe. The change in volume of foam leads to a change in quality of foam, so a change in rheological properties of foam and a change in velocity of foam. The comparison of rheological models with experimental data is plotted in a manner of comparing the behavior of each model by plotting pressure drop for a constant length vs. flow rate for constant quality and constant pipe diameter as well as comparing the results point-wise those obtained from each model by plotting pressure drop for a constant flow rate, constant quality and constant pipe diameter. Figs. 5.11-5.13 show the comparison of rheological models and their behavior for different pipe diameters for 80% quality foam. Also, Figs. 5.14 and 5.15 show a point-wise comparison of models and the experimental data.

5.5 Rheological Model Parameters

The slip corrected shear rate and shear stress data are used for obtaining rheological model parameters for Power Law ($\tau = K(\gamma)^n$), Bingham Plastic ($\tau = \tau_y + \mu_p \gamma$) and Yield-Power Law ($\tau = \tau_y + K(\gamma)^n$) by using Statistica. The data is analyzed by using Quasi-Newton, a non-linear curve fitting technique, including standard deviation. The rheological parameters obtained from statistical analysis are as follows:

	Power Law		Bingham Plastic		Yield Power Law		
	n	K	μ_p	τ_y	τ_y	*n*	K
70%	0.782461	0.005186	0.001292	0.060989	-0.19127	0.735755	0.007064
80%	0.737645	0.010491	0.002111	0.09225	-0.33353	0.399837	0.104177
90%	0.562189	0.02681	0.001744	0.156834	-145.098	0.001575	144.4365

where *K* is in $\frac{lb.\sec^n}{ft^2}$, μ_p is in $\frac{lb.\sec}{ft^2}$ and τ_y is in $\frac{lb}{ft^2}$

An error analysis is also performed for each model. The error is calculated as

$$error(\%) = \left| \frac{A_{actual} - A_{\mathrm{mod}\,el}}{A_{actual}} \right| 100 \qquad (5.15)$$

where *A* is any data point. For each data point, the error is calculated, and average of the error is determined. The results are plotted in Fig. 5.16.

5.6 Discussions

For each foam quality value, $\frac{8v}{D}$ vs. τ_w is plotted as shown in Figs. 5.2-5.4. From the graphs, it can be seen that different curves are obtained for different pipe diameters, which indicates the presence of slip.

When $\frac{8v}{D}$ vs. $\frac{1}{D^2}$ plots (Figs.5.5-5.7) are analyzed, similar behavior is observed with Enzendorfer[3]'s work. When pipe diameter goes to infinity, theoretically, the effect of slip is negligible, so y-intercept of the plot for a constant τ_w gives the true shear rate value. For all τ_w values, the straight lines intercept y-axis in positive region, so this indicates that the slip model is applicable. It is suggested to determine the true shear rate values not from the y-intercept of the $\frac{8v}{D}$ vs. $\frac{1}{D^2}$ plot, but using the slip coefficient determined from the slope of the line for a

constant τ_w (figure 5.8), and using this coefficient in $\left(\frac{8v}{D}\right)_{observed} = \left(\frac{8v}{D}\right)_{actual} + \frac{8\beta\tau_w}{D^2}$ and solving for actual shear rate.

After shear rate values are corrected for slip, $log\frac{8v_{actual}}{D}$ vs. $log\,\tau_w$ is plotted. The graph is analyzed by using Statistica, and it is observed that, describing the plots as straight lines gave the best fit for each quality value. This showed that *n'*, defined by Rabinowitch-Mooney, is same for all shear rate values for a constant quality.

Statistically, rheological parameters are determined for Power Law model, Bingham Plastic model and Yield-Power Law model. Analysis showed that the Yield-Power Law model is not applicable for the foam used in the experiments since the yield point values, τ_y, are determined to be negative for all quality values, which is physically impossible.

The statistical analysis also showed that, Power Law model was more successfully described the foam behavior for foam qualities of 70% and 80%, however, Bingham Plastic model was better for 90% foam quality.

Comparison of the existing rheological models with experimental results showed that, there is no "best" model for describing the foam flow behavior. From Figs. 5.11-5.15, it is observed that Gardiner[8] et al's model overestimated the pressure drop. It is also observed that, different models predicted the pressure drop better for different conditions.

5.7 Conclusions

After the analysis of the experimental data and the results of the comparative study, the following conclusions are offered:

1. Foam flow experiments have verified the presence of wall slip effect. The true shear rates need to be determined by correcting for the slip effect.
2. Statistical analysis showed that, Yield-Power Law model is not applicable for the foam used in this research. For foam qualities of 70% and 80%, foam rheology can be characterized by Power Law model, and for foam quality of 90%, Bingham Plastic model can be used.
3. It is concluded that, there is no "best" model present for describing foam rheology. Model predictions differed from experimental results by about 5 to 250% depending on the pipe geometry, foam quality and flow rate.

Nomenclature

D = Pipe Diameter
K = Consistency index
L = Pipe length
n = Flow behavior index

P = Pressure
T = Temperature
v = Velocity
V = Volumetric flow rate
β = Slip factor
γ = Shear rate
τ_w = Wall shear stress
τ_y = Yield point
μ_p = Plastic viscosity
Γ = Quality

References

1. Mooney, M., “Explicit Formulas for Slip and Fluidity,” Journal of Rheology, 2, 210-222, 1931
2. Jastrzebski, Z.D., “Entrance Effects and Wall Effects in an Extrusion Rheometer During the Flow of Concentrated Suspensions,” Ind.Eng.Chem.Fund. 6, 445-453, 1967
3. Enzendorfer, C., “Pipe viscometry of foams,” Journal of Rheology, 2, 345-358, 1995
4. Sanghani, V., “Rheology of Foam and Its Implications in Drilling and Cleanout Operations,” M.S. Thesis, University of Tulsa, Tulsa, 1982
5. Blauer R.E., Mitchell B.J., Kohlhaas C.A., “Determination of Laminar, Turbulent and Transitional Foam Flow Losses in Pipes,” SPE Paper 4885, San Francisco, April 4-5, 1974
6. Beyer A.H., Millhone R.S., Foote R.W., “Flow Behavior of Foam as a Well Circulating Fluid,” SPE Paper 3986, San Antonio, October 8-11, 1972
7. Valko P., Economides M.J., “Volume Equalized Constitutive Equations for Foamed Polymer Solutions,” Journal of Rheology, August 1992
8. Gardiner B.S., Dlugogorski B.Z., “Rheology of Fire Fighting Foams,” Fire Safety Journal, 1998

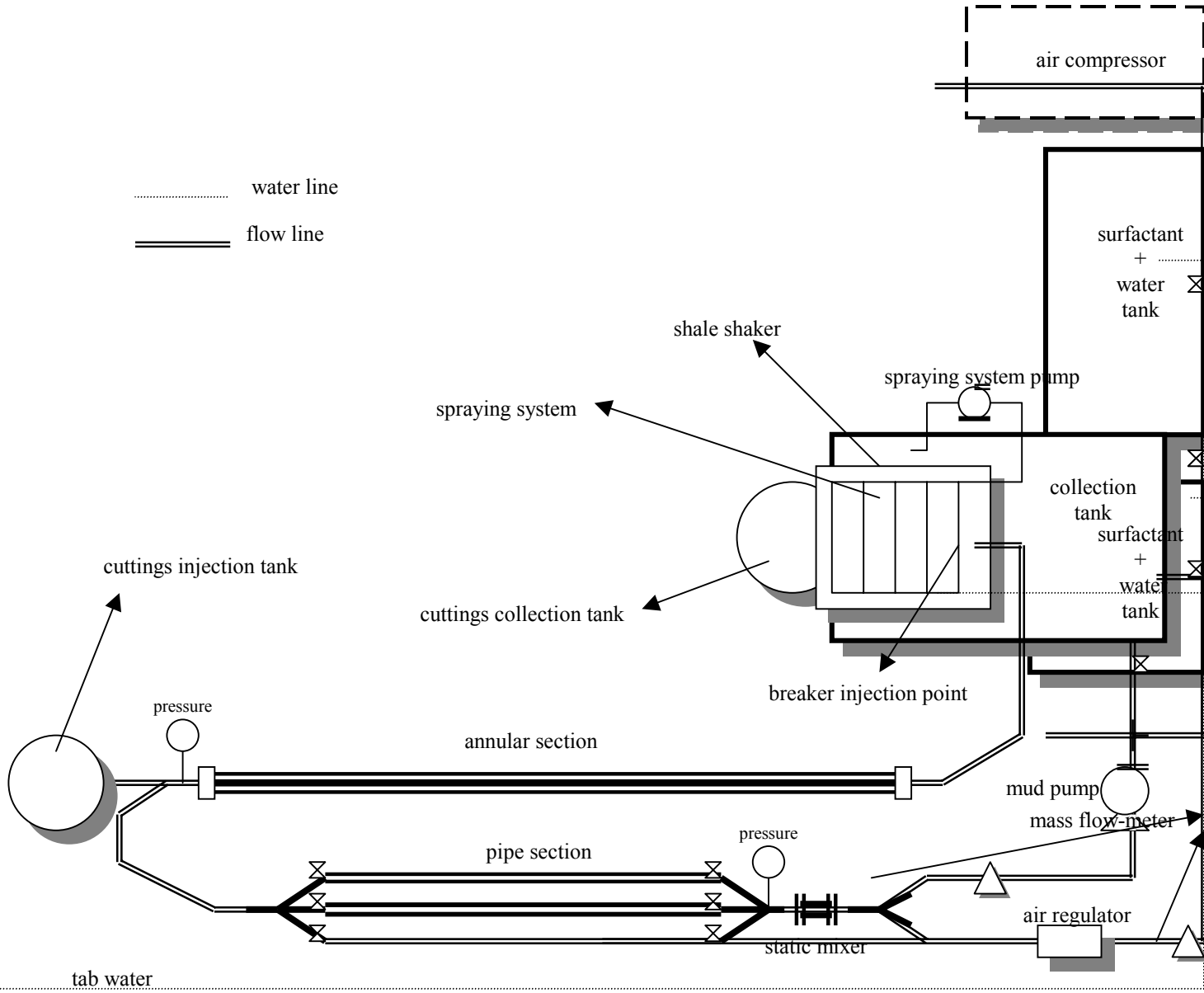

Figure – 5.1 Schematic View of LPAT Flow Loop Modified for Fo

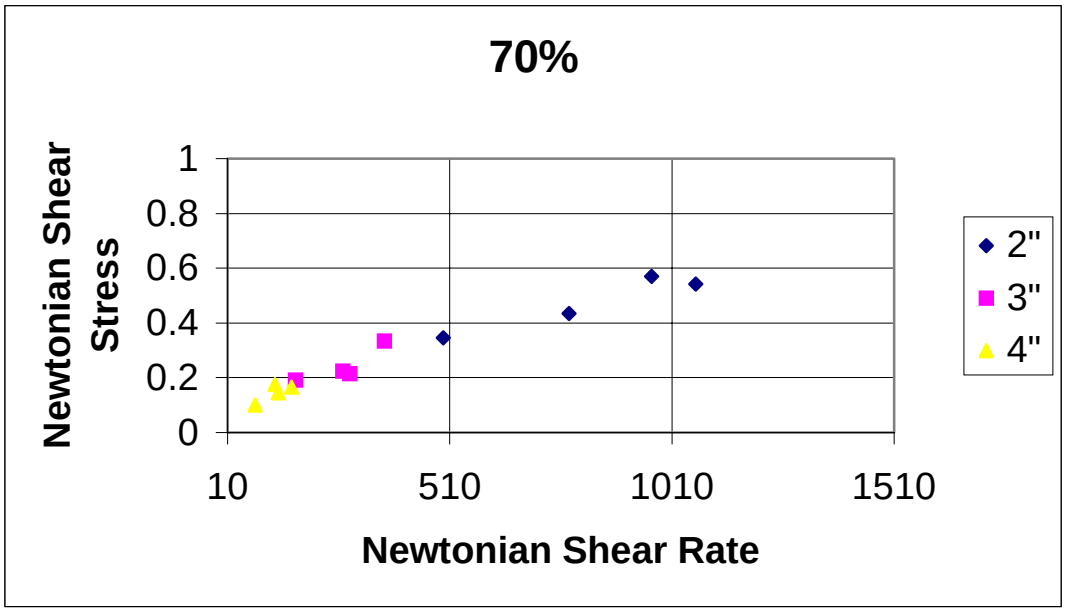

Figure 5.2 – Experimental Data Showing the Presence of Wall Slip Effect for 70% Quality Foam

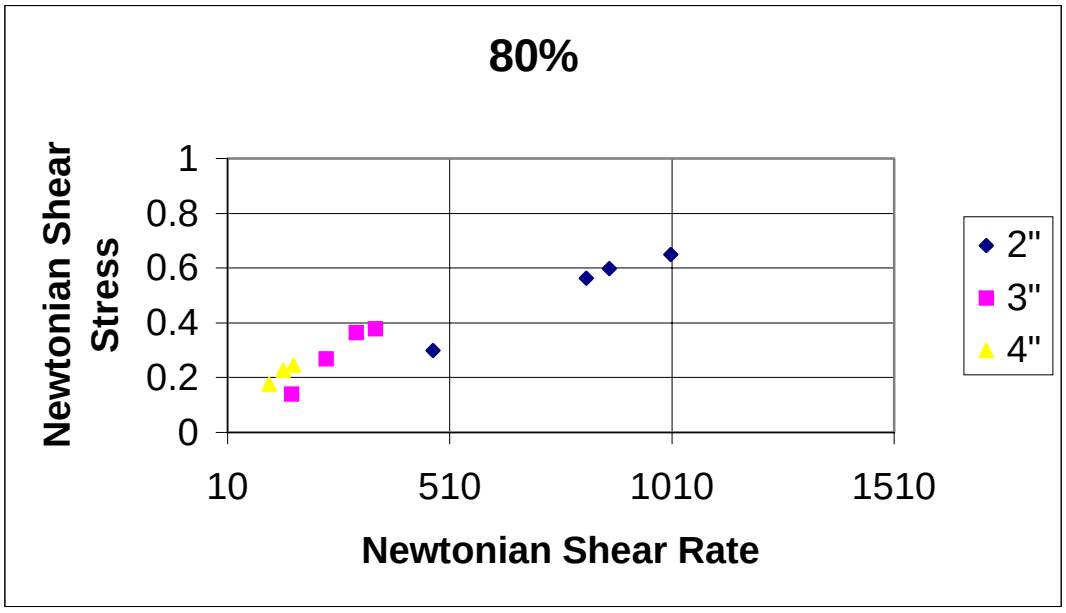

Figure 5.3 – Experimental Data Showing the Presence of Wall Slip Effect for 80% Quality Foam

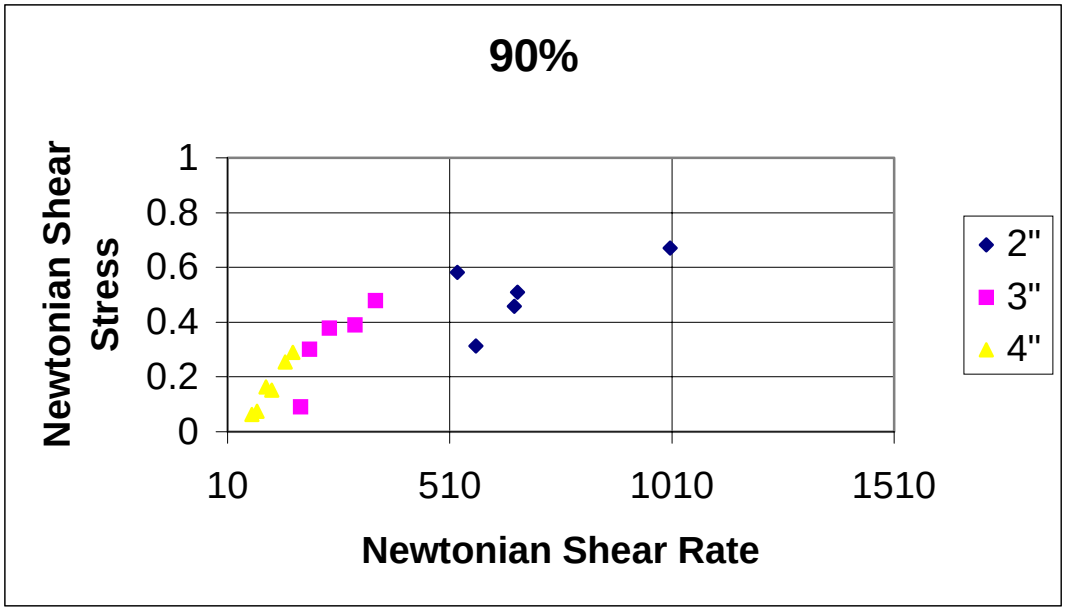

Figure 5.4 – Experimental Data Showing the Presence of Wall Slip Effect for 90% Quality Foam

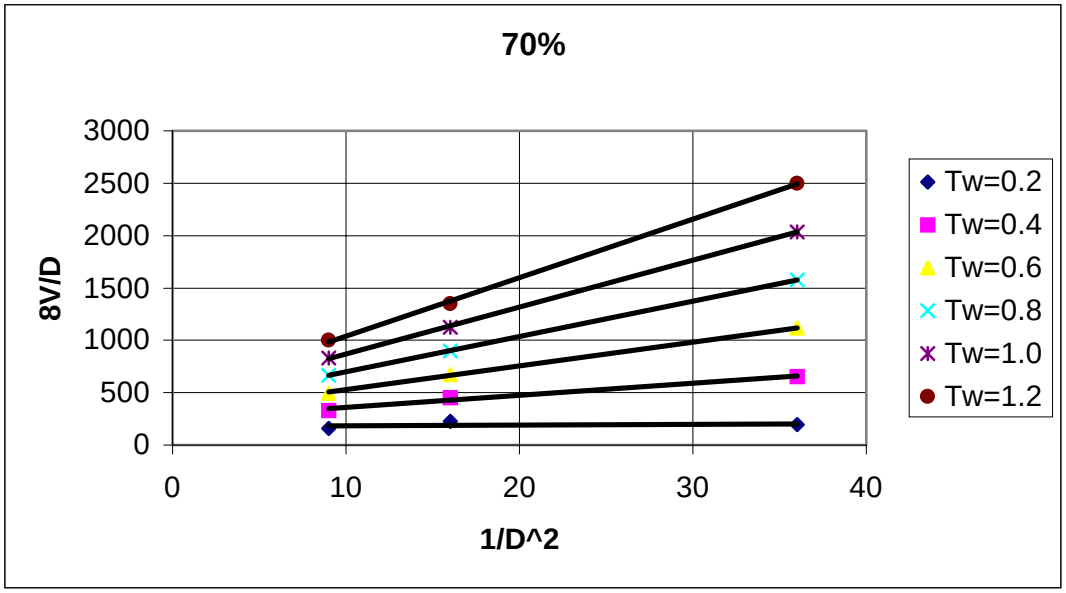

Figure 5.5 – Shear rate vs. $1/D^2$ for 70% quality foam

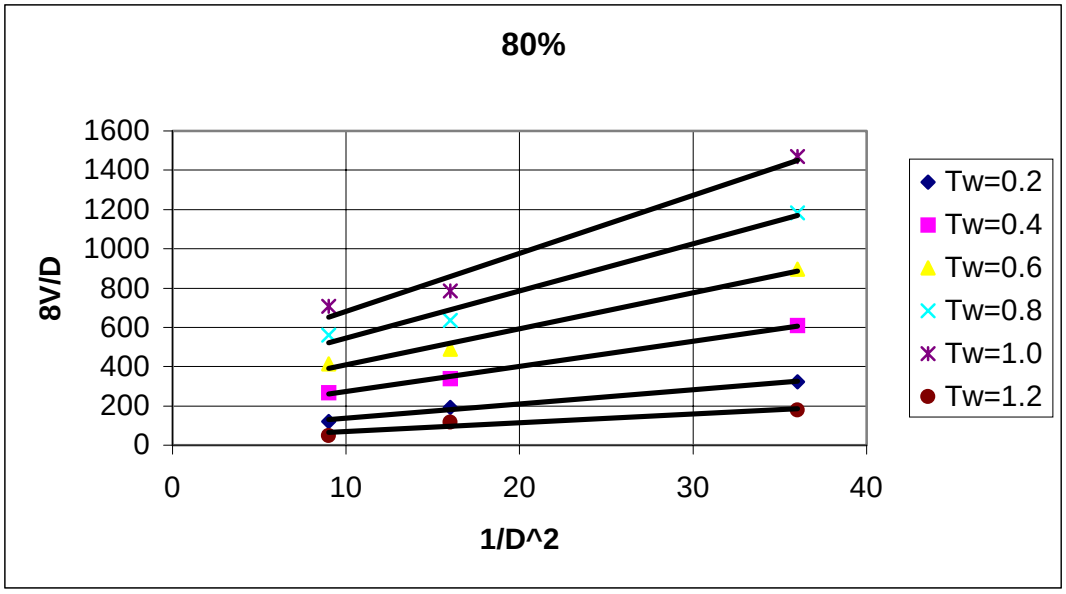

Figure 5.6 – Shear rate vs. $1/D^2$ for 80% quality foam

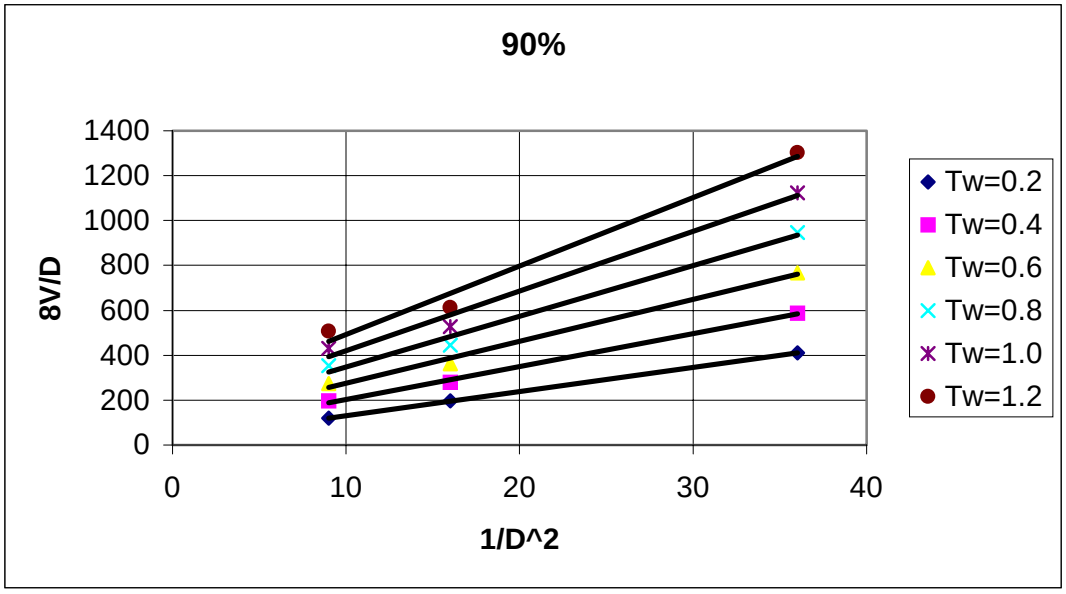

Figure 5.7 – Shear rate vs. $1/D^2$ for 90% quality foam

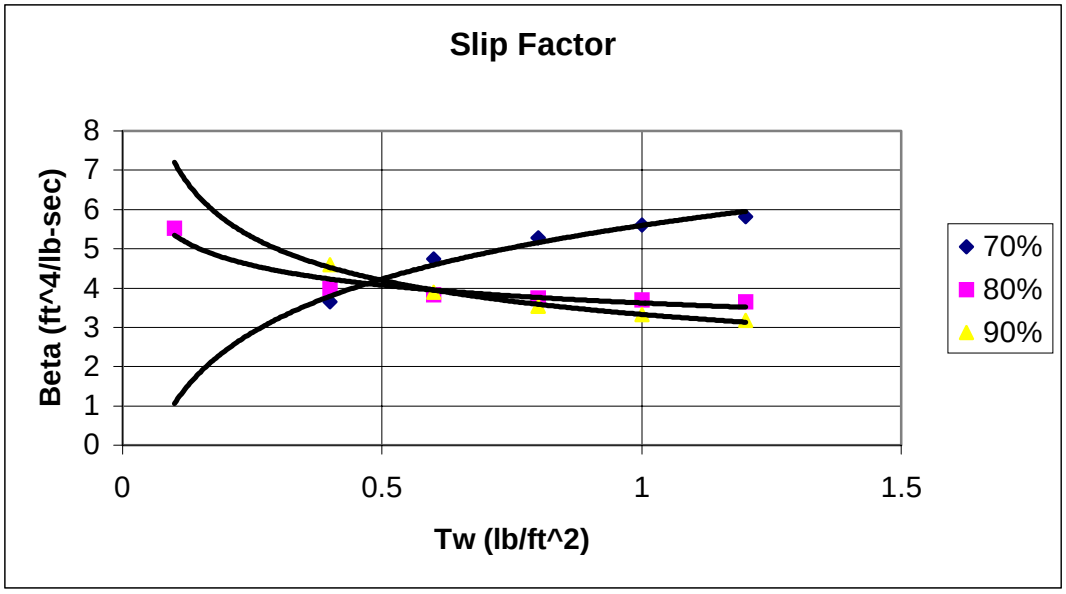

Figure 5.8 – Slip coefficient

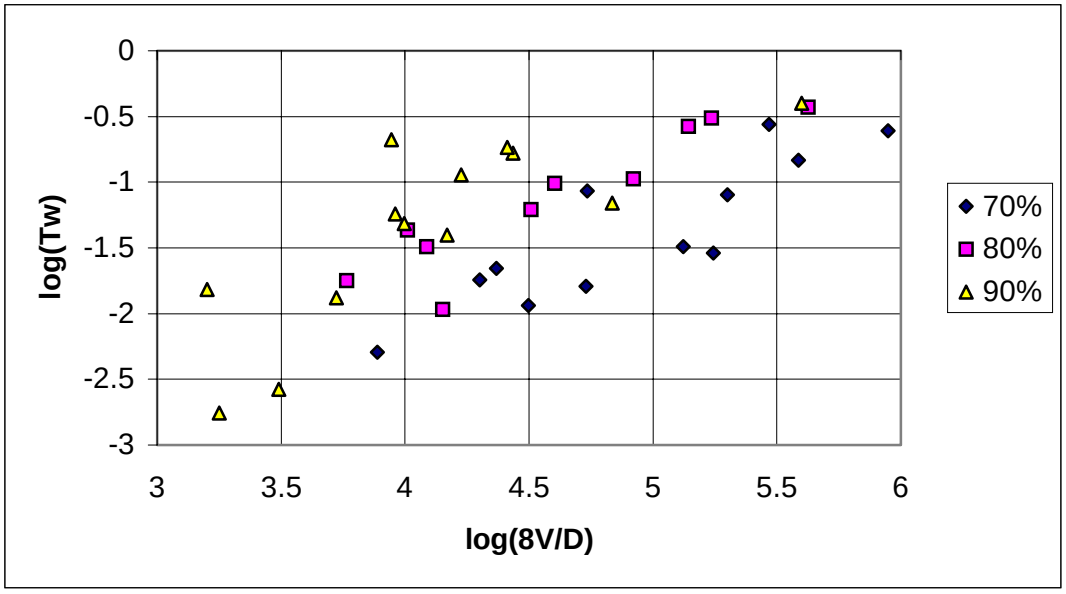

Figure 5.9 – Generalized Flow Curve Data for Foam (Log-Log Plot)

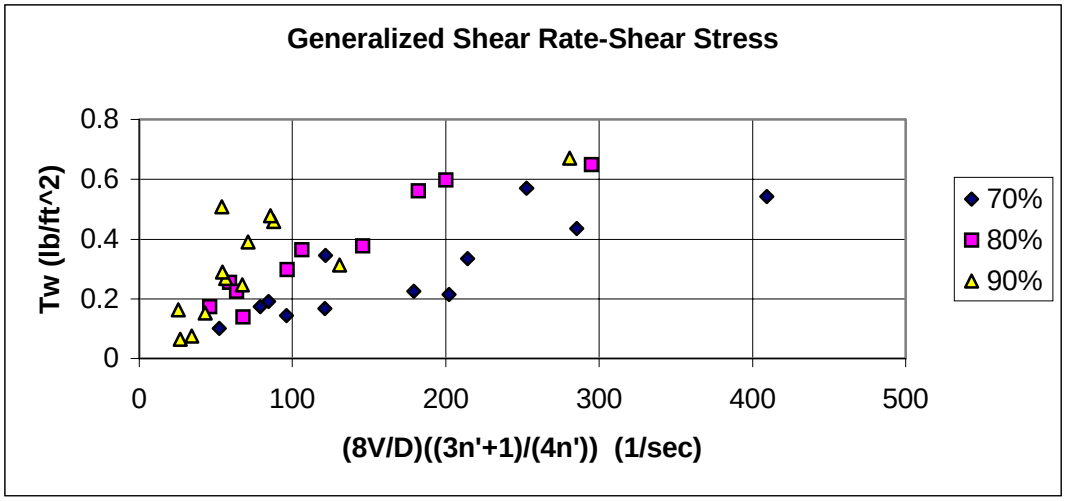

Figure 5.10 – Generalized Flow Curve Data for Foam (Linear Plot)

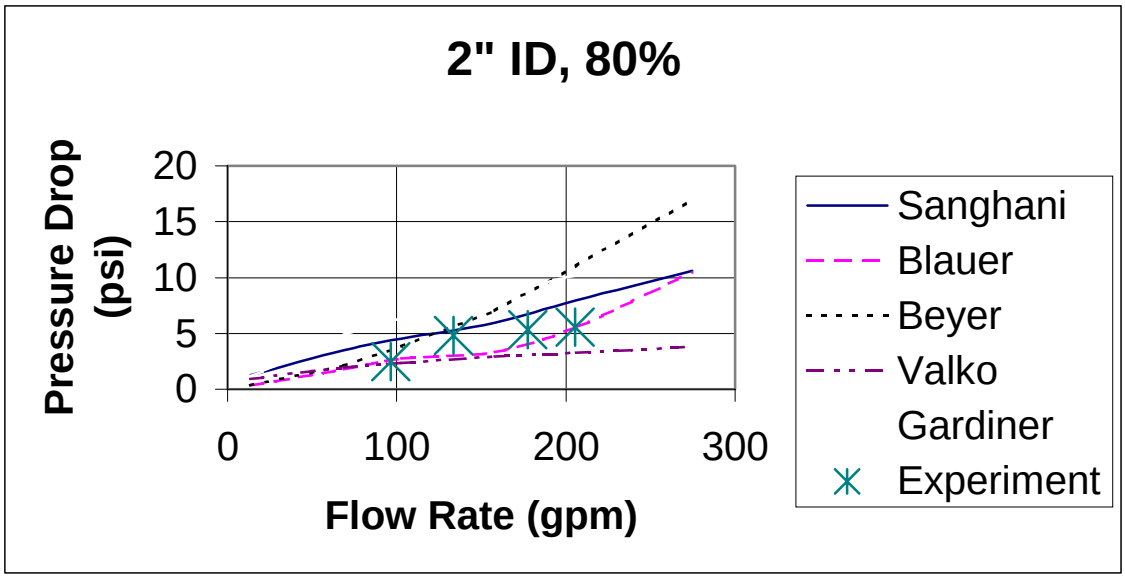

Figure 5.11 – Comparison of Foam Hydraulic Model Results with Experimental Results for 2" ID pipe

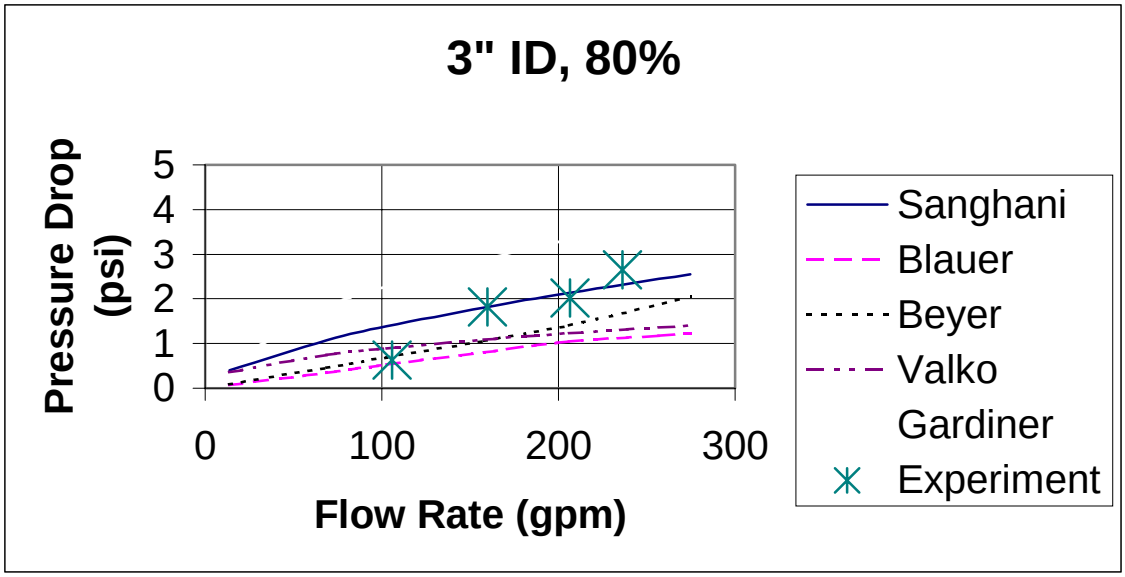

Figure 5.12 – Comparison of Foam Hydraulic Model Results with Experimental Results for 3" ID pipe

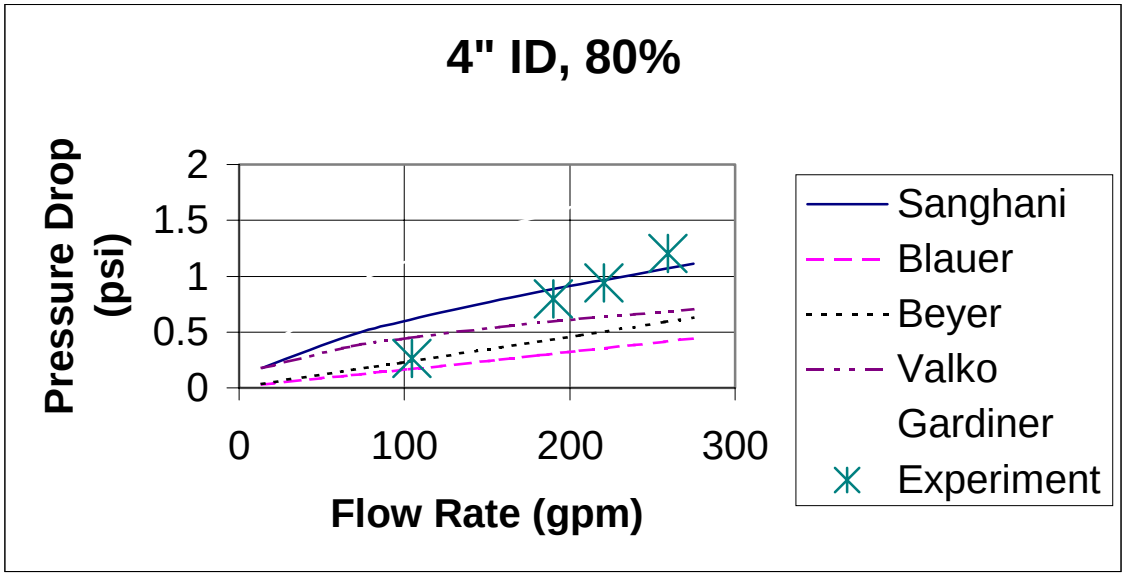

Figure 5.13 – Comparison of Foam Hydraulic Model Results with Experimental Results for 4" ID pipe

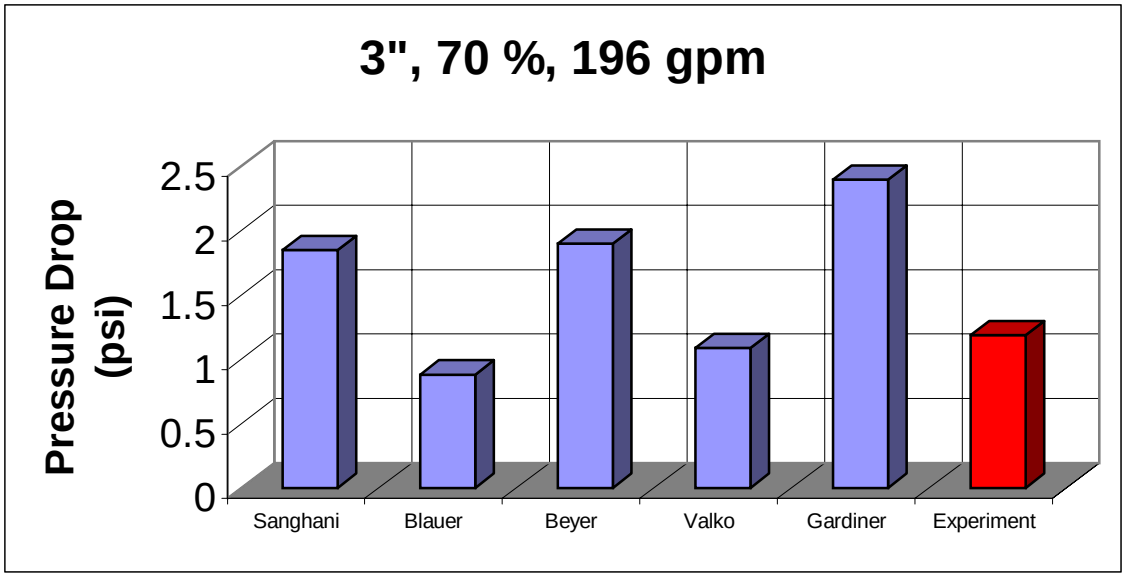

Figure 5.14 – Point-wise comparison for 3” ID pipe

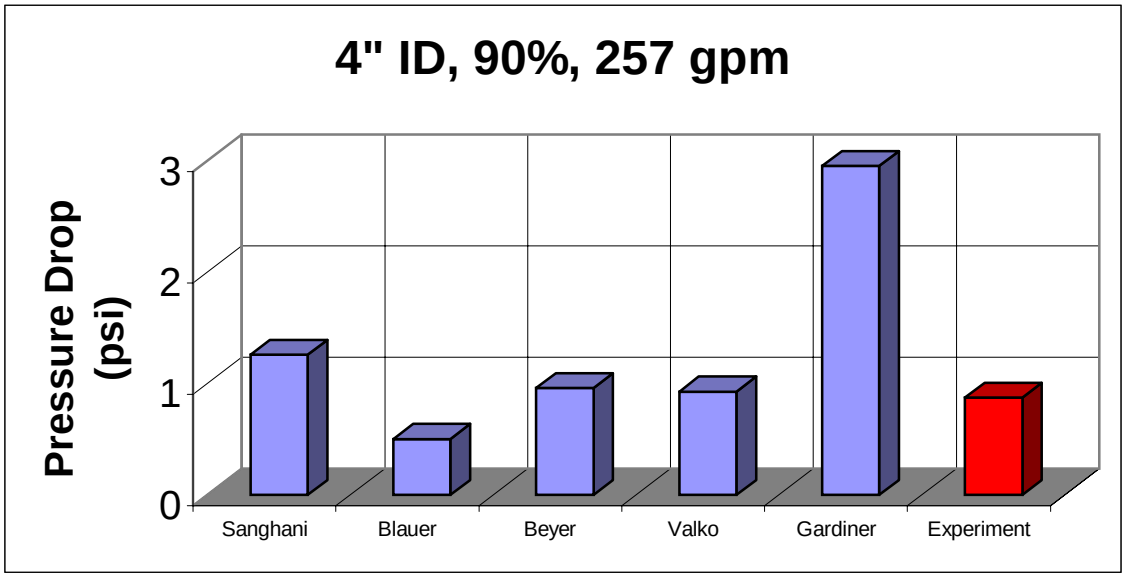

Figure 5.15 – Point-wise comparison for 4” ID pipe

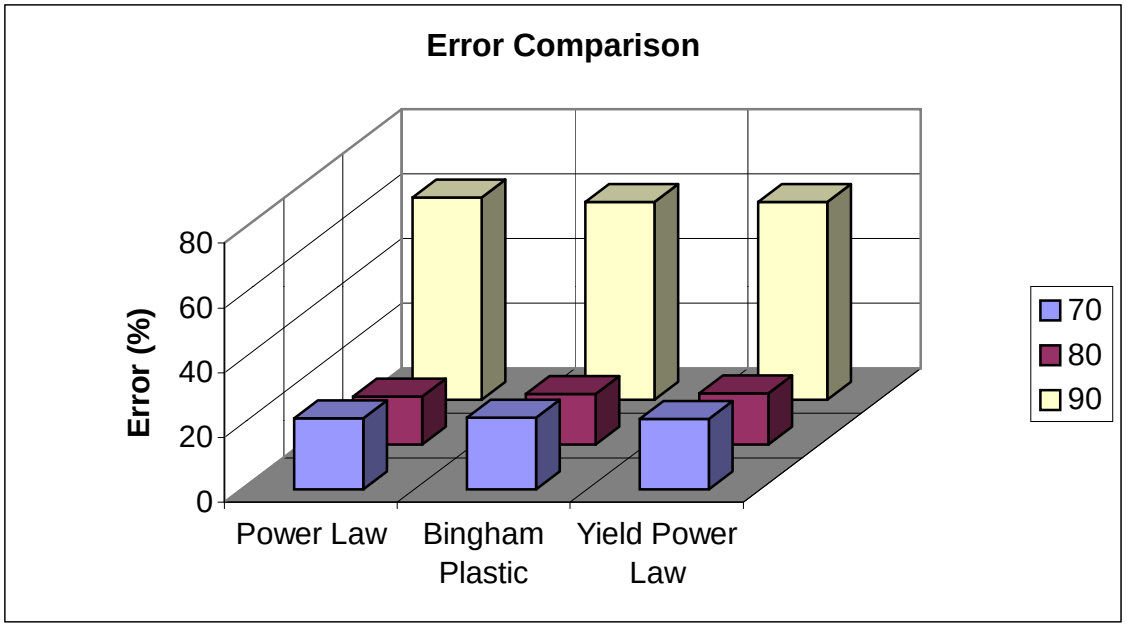

Figure 16 – Error Analysis for Curve Fitting of Experimental Data with Rheology Models

6. STUDY OF CUTTINGS TRANSPORT WITH AERATED MUDS UNDER LPAT CONDITIONS

Investigator: Paco Vieira.

6.1 Objectives

1. Determine experimentally the minimum flow rates for water and air that guarantee the hole cleaning while drilling horizontal and near horizontal sections.
2. Develop charts that help to establish minimum requirements of air and water injection rates to plan drilling of high angle and horizontal sections, using air-water system as drilling fluid.

6.2 Introduction

One of the primary functions of a drilling fluid is to transport efficiently the drilled particles (cuttings) to the surface through the wellbore annulus. This property is called the “carrying capacity “ of drilling mud. During the past 2 decades, especially in recent years, many studies have been conducted to obtain a better understanding of the cuttings transport phenomena. Several mechanistic models and empirical correlations have been developed in order to give the drilling engineer better tools that help him to design efficient hydraulic programs and assure the economical success of drilling a hole. As is well known, improper hole cleaning could create problems such as stuck pipe and increased torque and drag that cost the oil industry millions of dollars in losses.

Applications of horizontal and deviated well drilling have been combined in recent years with the non-conventional drilling techniques; underbalanced and nearbalanced drilling. In underbalanced / nearbalanced drilling, mixture of liquid and gas is commonly used as a drilling fluid to reach the desired bottomhole pressure condition. Examples of these fluids are aerated mud, foam and mist. The increased use of non-conventional fluids in horizontal and deviated well drilling created a need for better understanding of cuttings transport under these conditions. As part of these recent efforts, this research is dedicated to investigate cuttings transport in horizontal and near-horizontal wellbores by using an aerated mud system.

6.3 Statement of Problem

Cutting transport has been studied for horizontal and vertical wellbore configuration using conventional drilling fluid systems (single phase). Experiments have been conducted by many investigators to determine the minimum flow rates needed to avoid problems that are created by insufficient cleaning. However, there is a lack of information when two-phase fluids are used for drilling purpose. The increasing use of aerated drilling fluids, foam and mist, in high angle wellbore, has created the need of understanding cuttings transport in those conditions. Also for production purposes (after drilling) two phase flow is

commonly used in the oil industry to clean sand production that is accumulated in the well and affecting the production rate. It is a normal procedure in this case to run a Coiled-tubing unit and circulate the sand with gasified liquid at high rates but there is no knowledge about the optimum flow rates that could be used in order to reduce operations costs.

In order to understand the mechanism of cutting transport using multiphase fluids experiment will be conducted using the TUDRP- Low Pressure ambient temperature flow loop.

In order to obtain a complete operational domain of the low-pressure ambient temperature flow loop, previous experiments a three step experimental program have been adopted. As a first step, experiments using single phase (Water) were conducted. In the second step, experiments using two-phase flow (Water/Air) were conducted. Finally, three phase (Air/Water/Cutting) flow experiments have been scheduled and some preliminary tests have been conducted.

6.4 Literature Review

Gillies et al (1997)[1] presented the results of experiments conducted in order to investigate the ability of gas liquid mixtures to transport sand in a horizontal pipe or well at low velocities. Using a 30 meters in length flow loop they investigate the effect of gas addition in laminar and turbulent liquid flow regimes on the sand transport. One of the main conclusions of the study is that the gas injection has a little influence on the ability of a laminar flow to transport sand at low superficial velocities. This is due to the fact that the gas and the solids travel in different regions of the pipe. They also observed that the gas injection increases the solid transport rate and the axial pressure gradient if the liquid flow is turbulent.

Kamp and Mayela (1999)[2], presented a paper where they reviewed the state of the art of mechanistic modeling of cuttings transport. They developed a two-layer model simulating a moving bed of packed cutting below a heterogeneous layer of drilling fluid and cuttings. The model has been used to perform numerical simulation, predicting bed heights, pressure drops and transport velocities at different rates of penetration and mud flow rates. Results have been compared with other empirical models. The differences are discussed and improvements on the current model are proposed

Xiao et. al (1990)[3], presented a paper where a mechanistic model for flow pattern and pressure drop prediction for pipe flow is developed. This model is applicable for the flow of gas and liquid in horizontal and near horizontal pipe pipes. They used Barnea's[4] liquid holdup criteria of 35% for determination of transition from stratified wavy flow to slug flow. They also used Blasius type relationship for wall and interfacial shear stresses. The model was validated against a comprehensive database and shown to be particularly strong for predicting intermittent flow regime pressure drops.

Doron et. al (1986)[5], investigated the hydraulic transport of coarse particles in horizontal pipes. A physical model for the prediction of the pressure drop and flow patterns is presented. The process of analyzed the pressure drop during slurry flow and various flow patterns using a two-layer model. It is assumed that for each layer the flow is represented by means of the average properties and there is no slip between the two phases. The proposed model was compared with new experimental data showing good agreement. The model was also compared with others correlations.

Barnea et. al (1986)[6], presented a paper where he investigated the effect of gas injection on the flow of liquid-solid mixtures. They observed that the gas injection has two different effects on the pressure drop. The first effect is a reduction on the pressure drop due to formation of gas voids for a constant total flow rate. The second effect is a pressure drop increased due to the acceleration losses associated with the slug flow. It was concluded that the addition of gas, combined with an increased of pipe diameter may be a practical way to reduce the pressure drop for a given slurry flow rate.

Tippetts et. al (1997)[7], presented the results of experiments conducted by using on a horizontal flow loop with a transparent pipe flowing water, air and sand. Based on the experimental results they presented the results of the experiments on a flow pattern map using superficial velocities of water and air.

Matthew et. al (2000)[8]. Presented a paper showing the results from some experiments preformed on the BP Amoco 6” multiphase flow facility located at Sunbury. They investigated at the transport sand through a pipeline with dip angle. Several fluids were selected for these experiments to examine the influence of liquid viscosity on the results. Water, oil and two different Carboxy Tethy and Cellulose solution (150 and 300 cP) were used for the experiments. Experiments showed that, in slug flow, water and low viscosity oil was able to transport the solids. They also showed a model for solid transport used by BP Amoco based on the concept of minimum transport velocity, the velocity, which is sufficient to removes particles from a settled bed. The model was based on the criteria for solid transport with single phase (liquid) (Thomas 1962)[9] he established a minimum pressure gradient is required for solid transport.

Larsen (1990)[9], conducted several experiments using a low pressure, low temperature, flow loop at TUDRP to study the effect of inclination, annular flow, mud rheology, drill pipe eccentricity, cutting size, mud weight, drilling rate, and drill pipe rotation on the critical fluid velocity needed to avoid cutting bed formation. He developed empirical correlations to predict bed height and critical cuttings transport velocity. In the experiments Larsen could observe that in angles between 40° and 90° the flow requirements were strongly dependent of the angle of inclination, whereas for high angles the eccentricity has no significant effects on the critical velocity for cuttings transport. Also he could determine that smaller cutting particles are more difficult to clean and the annular critical transport velocity increases with the rate of penetration.

Jalurkar (1993)[10)]studied the effect of hole size on the critical and sub-critical velocities. The objective of this study was to develop empirical correlations to introduce hole geometry into the Larsen's model. The most important conclusion was that for subcritical flow, the effect of hole size on cuttings bed was insignificant.

Sanchez (1997)[11] presented his results on the effect of pipe rotation has a significant effect on the hole cleaning during directional well drilling. The study show that the cuttings concentration is a function of rotary speed, hole inclination and flow rates.

Azar et al (1997)[12], presented a paper for a SPE drilling conference where they defined the factors that influence hole cleaning as annular fluid velocity, drill string rotation, mud properties, drilled cuttings, annular eccentricity and drilling rate. They also discuss their limitation in actual field practices.

J. Li (1999)[13] presented the result of his study on experimental analysis of cuttings transport in a multi-phase system (gas-liquid-cuttings). He investigated effects of the liquid/gas volume flow rate, in-situ liquid velocity, ROP, inclination angle and fluid properties on the cuttings bed height. He observed that the fraction of the circulation liquid has a significant impact on the cuttings transport. He also observed that the changing of liquid flow rate has more effect on the cuttings transport than the gas volume flow rate.

Pilehvari et al(1996)[14] presented the State-of-Art in Cuttings transport in Horizontal Wells. He summarized the results from pioneering experimental work done in cuttings transport the remarking of the pioneer experimental works done in cuttings transport using TUDRP test facility at the University of Tulsa. These works has been done in a flow loop that is capable to vary and control inclination angle, mud pumping rate, drilling rate, drill pipe rotation and eccentricity. Test conducted in this facilities show that is a significant difference between the cutting transport in inclined wellbores and that of vertical. It was seen that the mud rheology and flow regimes have a considerable impact on cuttings transport. However, the effects were different for horizontal and vertical wellbores. The paper also discusses the models that have been developed in recent years for cuttings transport and the future research and technology needs.

Peden, et al (1990)[15] presented results of an experimental study of the influence of hole inclination angle, cuttings size, drill-pipe eccentricity, flow rate, annular geometry and pipe rotation on the minimum cuttings transport velocity. They observed that the hole inclination angle has a strong effect on cuttings transport. They found that the worst situation occurs in angles between 40 and 60 degrees. They also observed that smaller cuttings are transported more efficiently at all inclination angles using low viscosity fluids while in angles between 0 and 50º largest cuttings are transported efficiently. The cuttings transport for this case is strongly influence on flow pattern. Eccentric annuli is easier to clean than

concentric one. In large annuli, pipe rotation has no significant effect on hole cleaning.

Martins et al (1996)[16], presented an experimental study of the erosion of a cuttings bed deposited at the bottom of a horizontal section using Newtonian fluids. In his study the evaluated the effect of hole and drill pipe diameter, eccentricity, inclination, cuttings diameter and drill pipe rotation on the cutting bed removal. Based on the result empirical correlation were develop.

Fang (1992)[17], presented results of an experimental study of the free settling of cuttings in Newtonian and non-Newtonian fluids. Two settling patterns of cuttings were observed as stable and swinging. New predictive expressions for the drag coefficient of cuttings and for the settling velocity of cuttings were also developed for the two settling patterns.

Guo et al (1993)[18] presented a theoretical model to predict the required air and mud flow rates in aerated mud drilling operation, based on the carrying cutting capacity and the maximum rate of penetration for vertical holes. In this approach the treated they multiphase fluid as a homogeneous mixture of liquid, gas and solid flowing in a bubbly flow regimen. They defined the carrying capacity of the aerated mud as the maximum cuttings that can be lifted by it. They consider the maximum cuttings concentration (Cc) admissible as 4% by volume.

Campos (1995)[19] presented two mechanistic models for predicting, cuttings transport in highly incline wellbore. The first model, one dimensional mechanistic model, takes into account only the area average, fluid velocity and cuttings concentration across an annular section. The second, a solid liquid model, take into account the fluid velocity and cuttings concentration profiles. Model prediction are compared to experimental data obtained from different flow loops. The results show that the first model is sufficiently accurate for practical application. Improvements however, would be archive by including the effect of liquid and solid velocity profiles and cuttings concentration distribution in the annulus across the section. The results of the second model indicated that prediction of flow rate and rate of penetration, that are required for maintaining the solids suspended, show good agreement with the experimental data.

Iyoho et al (1993)[20] presented a new mathematical models for solid-liquid flow at low throughput velocities for different configurations of horizontal and eccentric annuli. At velocities below the deposition velocity, flow characteristics include the formation of dunes, coupled with velocity and pressure fluctuations. This quasi-steady flow occurs frequently in highly deviated well bores. Slurry dunes observed from laboratory experiments are modeled as continuous triangular waves. The Bernoulli and the continuity equations are used to develop mathematical relations linking the annulus conduit dimensions, velocity, pressure, and concentrations. Preliminary model tests with laboratory pipe data from previous studies show reasonable agreement. They also presented an

extensive review on the basic relationship and differences between pipeline and annular slurry flow in vertical and horizontal flow

Bassal (1995)[21], investigated the effect of drill pipe rotation on hole cleaning during directional well drilling. A 8-in. diameter well-bore simulator, 100 ft long, with a 4-in. drill pipe is used for the study. Variables considered in this experimental work are drill pipe rotary speed, hole inclination, mud rheology, cuttings size, and mud flow rate. A total of 576 tests were conducted. Results have shown that drill pipe rotation has a significant effect on hole cleaning in directional well drilling. The level of enhancement in cuttings removal as a result of drill pipe rotary speed is a function of the combination of mud rheology, cuttings size, mud flow rate and the manner the drill string dynamically behaves. Generally, smaller cuttings are more difficult to transport. However, using high rotary speed with high viscosity mud, small cuttings become easier to transport. Low viscosity mud in the hole cleans better than high viscosity mud with no drill pipe rotation.

6.5 Two Phase Flow - Flow Patterns Identification

The two phase flow is characterized by a large number of flow variables. The two phase flow (Gas-Liquid) the liquid and the gas can be distributed in the pipe in a variety of flow configurations. The flow configuration differs from each other in the special distribution of the interface. The distribution of the interface it is mainly governed by gas and liquid volumetric fractions. The flow patterns depends mainly on the liquid and gas volumetric fraction. In 1982 Shoham defined an acceptable set of flow patterns based in experimental data acquired from vertical and horizontal well flow experiments [22].

6.5.1 Flow Patterns in Horizontal Flow

Stratified Flow:

Occurs at relative low gas and liquid flow rates. This configuration can be also classified in two "Stratified Smooth" and Stratified Wavy" (Fig. 6.1).

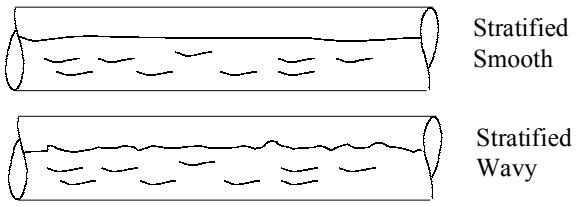

Fig 6.1- Flow Pattern for Horizontal Flow- Stratified Flow

Intermittent Flow:

Alternate of liquid and gas flow characterizes intermittent flow. Can be also classified in two groups as "Elongated Bubble" and "Slug" (Fig. 6.2).

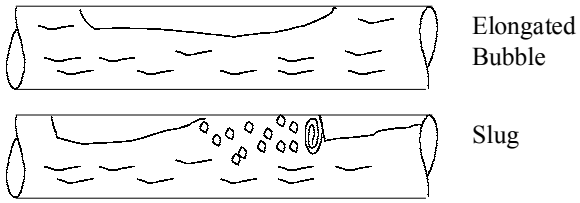

Fig 6.2- Flow Pattern for Horizontal flow - Intermittent

Annular Flow:

Annular flow occurs at very high gas flow rates. This configuration can be also classified in two groups as "Annular" and "Wavy Annular" (Fig. 6. 3).

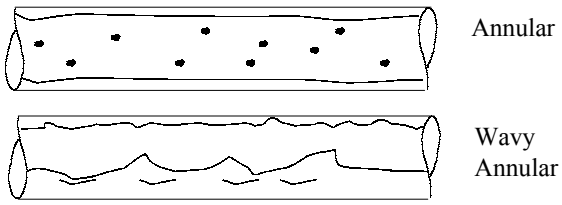

Fig 6.3- Flow Pattern for Horizontal Flow - Annular

Dispersed Bubble Flow:

Dispersed Bubble flow occurs a very high liquid flow rate (Fig.6.4).

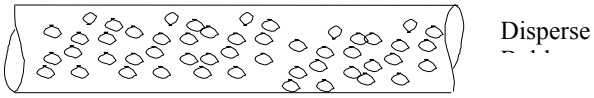

Fig. 6.4- Flow Pattern for Horizontal Flow- Dispersed Bubble.

6.5.2 Flow Patterns in Vertical Flow

Bubble Flow:

Bubble flow occurs for low gas flow rates. (Fig. 6.5)

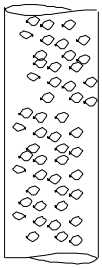

Fig. 6.5- Flow Pattern for Vertical Flow - Bubble Flow

Slug Flow:

In this flow pattern most of the gas phase is located in a large bubble call " Taylor Bubble" with diameter almost equal to the pipe diameter. The flow consists in successive Taylor bubbles. (Fig. 6.6).

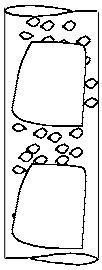

Fig. 6.6- Flow Pattern for Vertical Flow - Slug Flow

Churn Flow:

An oscillation motion characterizes this flow pattern. Churn flow is similar to slug flow but looks more chaotic. (Fig. 6.7)

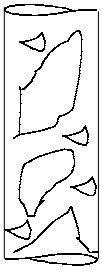

Fig. 6.7- Flow Pattern for Vertical Flow - Churn Flow

Annular Flow:

In the annular vertical flow the liquid phase moves slower as a film around the pipe wall. (Fig. 6.8).

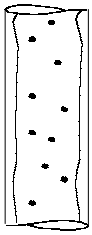

Annular

Fig. 6.8- Flow Pattern for Vertical Flow - Annular Flow

6.6 Experimental Test Matrix

Based on the PDVSA experience using aerated muds for drillings operation the following test matrix was decided to be followed in the experiments using air/water/cuttings. (See Table 6.1)

. Table 6.1- Test Matrix

ROP (ft/h)	30		50		70							
Inclination	90		80		70							
Total Flow Rate (GPM)	200		300		400		500		600		700	
	Water (GPM)	Air (GPM)	Water (GPM)	Air (GPM)	Water (GPM)	Air (GPM)	Water (GPM)	Air (GPM)	Water (GPM)	Air (GPM)	Water (GPM)	Air (GPM)
	200	0	300	0	400	0	500	0	500	100	500	200
	100	100	200	100	300	100	400	100	400	200	400	300
			100	200	200	200	300	200	300	300	300	400
					100	300	200	300	200	400	200	500
							100	400				

Table 6.2 - Experimental Conditions

Cutting Size	Cutting Density	Cutting Bed Porosity	Drill Pipe Eccentricity	Drill Pipe Rotation
3.29 mm	22.28 Lb/gal	38%	Positive	NO

6.7 Three Phase Flow Experiments

Tests were conducted using different combinations of gas and liquid flow rates for the horizontal position (90 degrees from vertical) and simulating a constant rates of penetration of 30, 50 and 70 ft/h. The amount of cutting in the test section and the pressure drop were recorded. The bed height was measured directly in the test section at 10 different locations. The flow pattern was also observed for each combination of liquid and gas flow rate. Due to problems in the programming of the Data Acquisition system, the gas flow rates were lower than expected and was not possible maintain the total flow rate constant in each experiment. However, the data was analyzed and the results for each experiment are shown in the Appendix A.

In order to estimate the superficial gas and liquid velocities above the cutting bed, the open area above the cutting bed have to be determine after a steady state condition is reached. A computer program was generated to estimate the open area above the cutting bed. The idea is to calculate the superficial liquid and gas velocities in which cuttings are efficiently transported and identify the flow pattern that are observed in the experiments.

For the calculation of the open areas in annular geometries with variable eccentricities different cases have been studied as are shown in Fig. 6.9, 6.10 and 6.11.

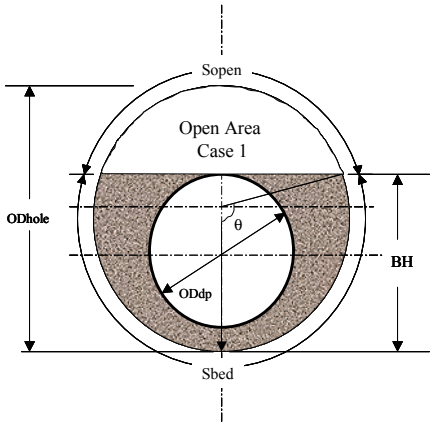

Fig.6.9- Case 1- Drill Pipe Totally Covered With Cuttings

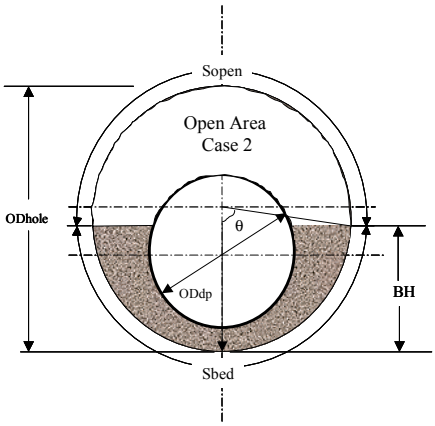

Fig.6.10- Case 2- Drill Pipe Partially Covered With Cuttings

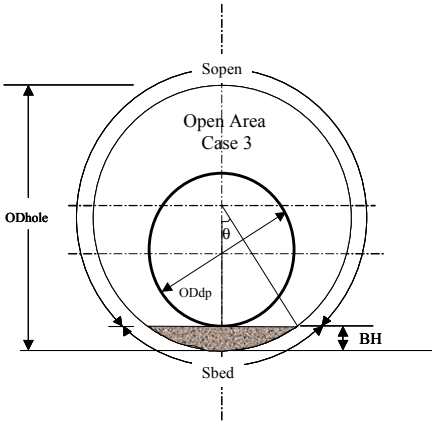

Fig. 6.11- Case 3- Drill Pipe Uncovered

For each test the open area above the cutting bed and the superficial liquid and gas velocities were calculated and the results are presented in Table 3 to 5.

Table 6.3- Calculation of Superficial Liquid and Gas Velocities Above the Cutting Bed Horizontal Position - 30 ft/h ROP

Ql (GPM)	Qg (GPM)	Qt (GPM)	BH (in)	Open Area (in^2)	Vsl (ft/s)	Vsg (ft/s)
200	0	200	5.26006	14.89455614	4.308062	0
100	80	180	5.47911	13.56687471	2.364829	1.891863
300	0	300	4.580269	18.17122834	5.296835	0
200	75	275	4.873492	16.85832761	3.80623	1.427336
100	150	250	5.156671	15.45426635	2.076018	3.114027
400	0	400	3.040786	23.84007773	5.383092	0
300	80	380	3.839416	21.08674475	4.564479	1.217194
200	160	360	4.456597	18.69268397	3.432716	2.746172
400	80	480	2.872229	24.38988613	5.261744	1.052349
300	166	466	3.839416	21.88199443	4.398594	2.433888
200	240	440	4.132191	19.988968	3.210104	3.852125
300	225	525	3.38949	22.67305566	4.245127	3.183845
200	300	500	4.034601	20.36162263	3.151353	4.72703

Table 6.4- Calculation of Superficial Liquid and Gas Velocities Above the Cutting Bed Horizontal Position - 50 ft/h ROP

Ql (GPM)	Qg (GPM)	Qt (GPM)	BH (in)	Open Area (in^2)	Vsl (ft/s)	Vsg (ft/s)
200	0	200	5.30116	14.66269033	4.376186	0
100	75	175	5.7273	11.68536505	2.7456	2.0592
300	0	300	4.69804	17.65797637	5.450794	0
200	80	280	5.02625	16.12118811	3.980269	1.592108
100	160	260	5.28576	14.75026918	2.175102	3.480162
400	0	400	4.211351	19.6812133	6.520601	0
300	75	375	4.537311	18.35428422	5.244007	1.311002
200	150	350	4.772664	17.32336679	3.704053	2.77804
100	225	325	5.156671	15.45426635	2.076018	4.67104
500	0	500	2.972497	24.06378239	6.666311	0
400	75	475	3.844834	21.0669561	6.091688	1.142192
300	150	450	4.143031	19.94712317	4.825257	2.412629
200	225	425	4.569535	18.21716815	3.522318	3.962608
500	75	575	1.965286	27.27667633	5.881093	0.882164
400	150	550	3.24031	23.17784345	5.536897	2.076336
300	225	525	3.74735	21.42027103	4.493407	3.370055
200	300	500	4.088824	20.15545818	3.183588	4.775381
500	150	650	2.261605	26.33643951	6.091054	1.827316
400	225	625	2.862867	24.42020196	5.255212	2.956057
300	300	600	3.493663	22.31489095	4.313263	4.313263
200	375	575	3.769003	21.34228444	3.006551	5.637283

Table 6.5- Calculation of Superficial Liquid and Gas Velocities Above the Cutting Bed

Ql (GPM)	Qg (GPM)	Qt (GPM)	BH (in)	Open Area (in^2)	Vsl (ft/s)	Vsg (ft/s)
500	150	650	2.626067	25.18071549	6.370616	1.911185
400	225	625	3.247357	23.15419533	5.542552	3.117686
600	0	600	2.059402	26.97695038	7.135721	0
500	80	580	3.019742	23.90916225	6.709422	1.073508
400	160	560	3.590633	21.9768853	5.839469	2.335787

Horizontal Position - 70 ft/h ROP

The superficial liquid and gas velocities presented in Tables- 6.3, 6.4, and 6.5, for the combinations of liquid and gas used in each experiment (gas/liquid ratios), can be assumed as the minimum superficial liquid and gas velocities required for avoiding cutting bed formation in a horizontal for the corresponding rate of penetration.

In order to verify the flow pattern observed during each experiment when the steady state condition is reached, the boundaries for each flow patter transition were estimated using the computer program FLOMAP. The estimated values for the transition boundaries for the different flow patterns are presents in Fig. 6.12.

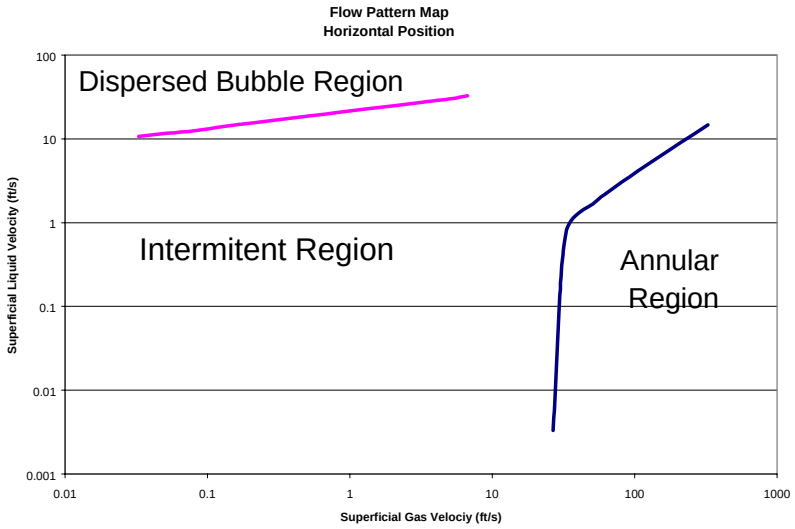

Fig. 6.12- Flow Pattern Map - Horizontal Position

The results from Table 6.3, 6.4 and 6.5 are plotted in a Horizontal Flow pattern map. (See Figs. 6.13, 6.14 and 6.15)

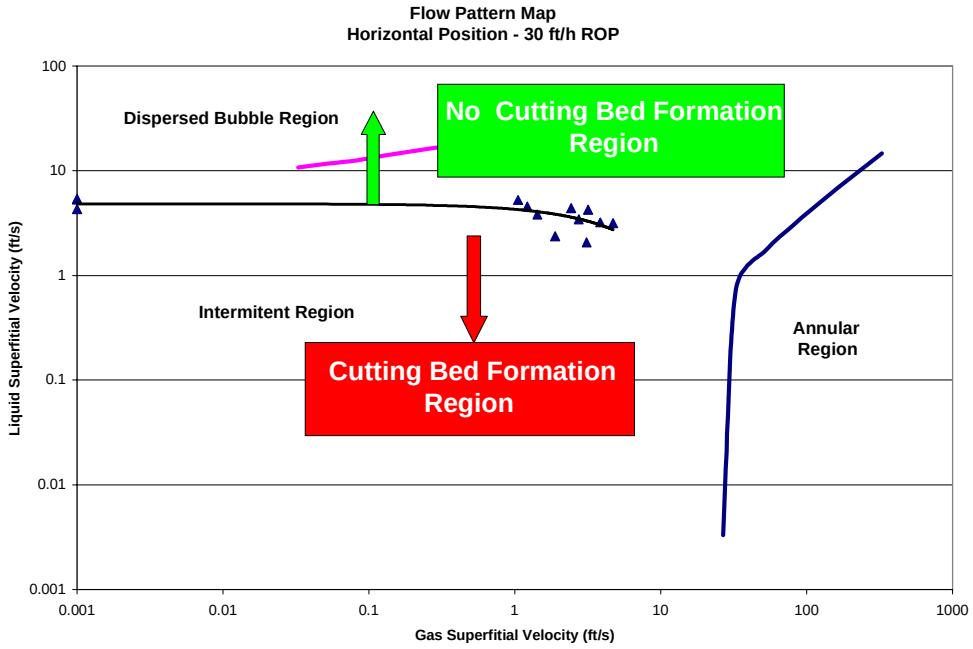

Fig.6.13- Experimental Results - Horizontal Position - 30 ft/h ROP

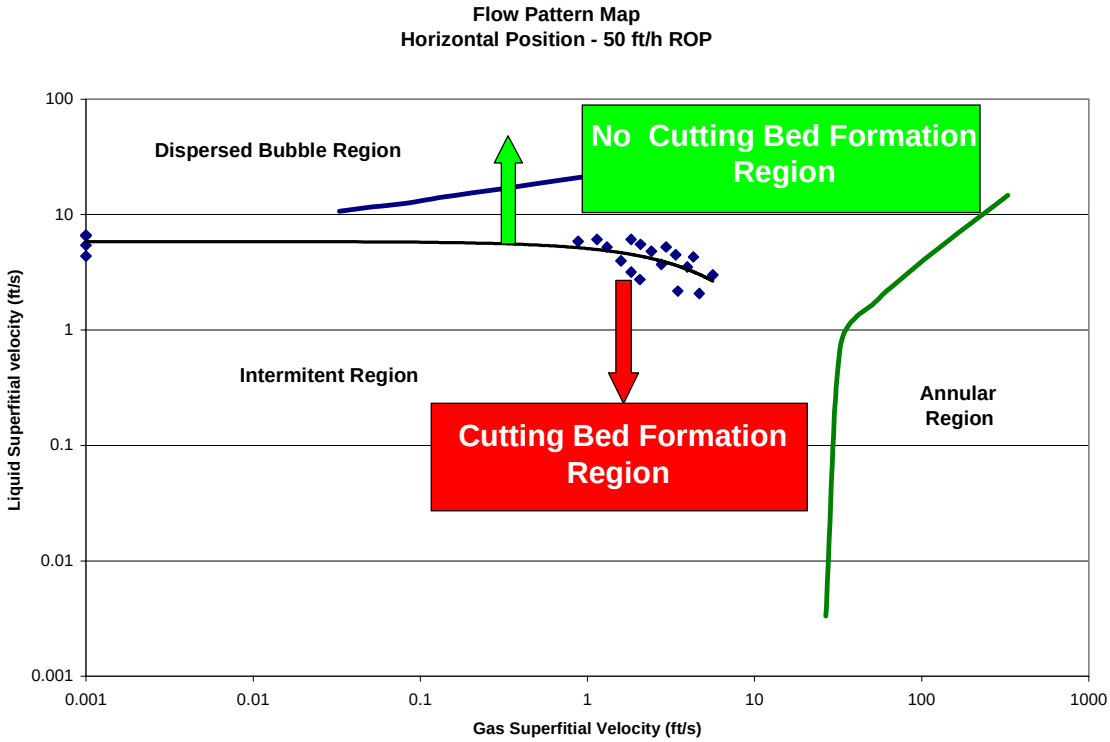

Fig.6.14- Experimental Results - Horizontal Position - 50 ft/h ROP

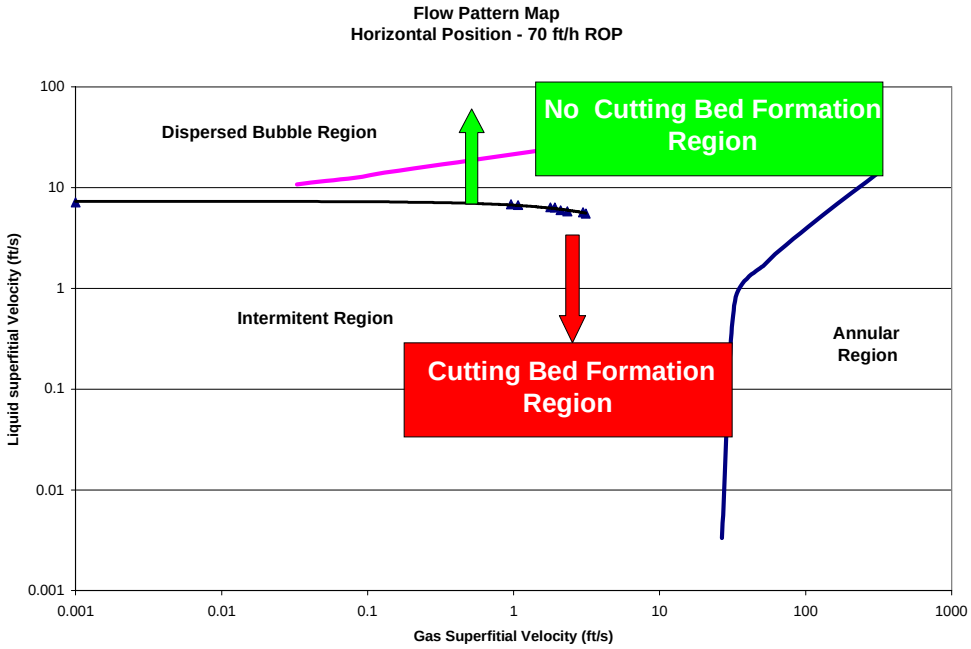

Fig. 6.15- Experimental Results - Horizontal Position - 70 ft/h ROP

As we can observe in Figs. 6.13, 6.14 and 6.15, the flow pattern estimates for each experiment, when the steady condition is reached are located in the intermittent region. This has agreement with the observation reported for each experiment where the flow patterns are always in the intermittent region vary from elongated bubbles, transition between elongated bubbles and slug flow and slug flow.

It can be observed in Fig. 6.13, 6.14 and 6.15 that it is possible to establish an approximate boundary that separate the region where the gas and liquid superficial velocities allows the cutting bed formation and another region where the cutting are transport efficiently.

6.8 Conclusions

Based on the results obtained in the experiments the following conclusions are offered:

- It is possible to establish an approximate boundary for the minimum air and water requirements in order to avoid the cutting bed formation. This boundary is estimated from the calculated values of superficial gas and liquid velocities above the formed cutting bed when the steady state condition is reached in each experiment.

- As the rate of penetration increased the accumulation of cuttings in the horizontal section also increased.

- As the Gas/Liquid ratio increases the average the frictional pressure drop decreases.

- The minimum requirements for gas and liquid injection for a horizontal wellbore configuration are always in the intermittent region for flow patterns.

References

1. R.G. Gillies, M.J.McKibben, C.A. Shook, “Pipeline Flow of Gas, Liquid and Sand Mixture at Low Velocities” The Journal of Canadian Petroleum Technology, 39 (9), 36-42

2. A.M. Kamp, M. Rivero "Layer Modeling for Cutting Transport in Highly Inclined Wellbores" SPE 53942 presented at the 1999 SPE Latin and Caribbean Petroleum Engineering Conference held in Caracas, Venezuela 21-23 April 1999

3. Xiao, J. J., et al.: “A Comprehensive Mechanistic Model for Two-Phase Flow in Pipelines,” paper SPE 20631, presented at SPE Annual Fall Meeting, New Orleans, Louisiana, (September 23-26, 1990).

4. Barnea, D., Shoham, O. and Taitel, Y. “Flow Pattern Transition for Vertical Downward Inclined Two Phase Flow; Horizontal to Vertical” Chem. Eng. Sci. 37, No. 5, 735-740 (1982a)

5. P. Doron, D. Granica and D. Barnea "Slurry Flow in Horizontal pipes - experimental and Modeling" Int. J. Multiphase Flow, Vol. 13, No. 4 p 535-547, 1987

6. D. Barnea, D. Granica, P. Doron and Y. Taitel " Hydraulic Transport Of Course Particles With Gas Injection" 10 th. International Conference on the Hydraulic Transport of Solid in Pipes, Innsbruck, Austria: 29-31 October 1986

7. Tippetts, J. R. and Priestman, G. H., “Mobility of Solids in Multiphase undulating pipe flow” Paper presented at the 7 International Conference of Multiphase Production, Cannes, France 18-20 June 1997

8. Matthew J. S. King, C. Paul Fairhust and Trevol J. Hill, “Solids Transport in Multiphase Flows Application to High Viscosity System”. Paper submitted to the Energy Sources Technology Conference and Exhibition, New Orleans, Feb 14-17, 2000

9. Larsen “ A Study of the Critical Fluid Velocity in Cutting Transport for Inclines Wellbores” M.S. thesis, University of Tulsa, 1990.

10. Jalukar, L. S. "A Study of Hole Size Effect on the Critical and Subcritical Drilling Fluid Velocity in Cuttings Transport for Inclined Wellbores" M.S. thesis, University of Tulsa, 1993.

11. Sanchez, R. A., Azar, J. J., Bassal, A. A., and Martins, A. L.: “The Effect of Drillpipe Rotation on Hole Cleaning During Directional Well Drilling,” paper SPE 37626 presented at the 1997 Drilling Conference, Amsterdam (Mar. 4-6, 1997).

12. Azar, J.J; Sanchez, R. Alfredo. “Important Issues in Cuttings Transport for Drilling Directional Wells”. paper SPE 39020 presented at the 1997 at the Fifth Latin American and Caribbean Petroleum Engineering conference, Brazil.

13. J. Li and S. Walker “Sensitivity Analysis of Hole Cleaning Parameters in Directional Wells” SPE paper number 54498.

14. Pilehvari,A., Azar,J.J.,. “State-Of-Art Cutting Transport in Horizontal Wellbores”. paper SPE 37079 presented at the 1996 at the conference on Horizontal Well Technology held in Calgary.

15. J.M. Peden, J.T. Ford, M.B. OyeneyIn, “Comprehensive Experimental Investigation of Drilled Cuttings Transport In Inclined Wells Including The effects of Rotation and Eccentricity”. paper SPE 20925 presented at the Europec 90, The Hague, Netherlands, 22-24 October 1990.

16. A.L. Martins, C. H. M. Sa, A. M. F. Lourenco, “Optimizing Cuttings Transport In Horizontal Well Drilling”. Paper SPE 35341 presented at the Petroleum Conference & Exhibition of Mexico, 5-7 March 1996

17. Guoqiu Fang. " An Experimental Study of Free Settling of Cuttings in Newtonian and No Newtonian Drilling Fluids: Drag Coefficient and Settling Velocity" Paper SPE 26125, 1992.

18. Buyon Guo, Geir Hareland, Jerzy Rajtar. " Computer Simulator Predicts Unfavorable Mud Rate and Optimum Air Injection Rate for Aerated Mud Drilling". Paper SPE 26892 presented at the Eastern Regional Conference & Exhibition held in Pittsburgh, PA. U.S.A., 2-4 November 1993.

19. Campos W., "Mechanistic Modeling Of Cuttings Transport In Directional Well" PhD Thesis, Tulsa Univ., Tulsa, Oklahoma, 1995

20. Iyoho A W; Takahashi H, “Modeling Unstable Cuttings Transport In Horizontal, Eccentric Wellbores”. : SPE-27416 (Dec 1993)

21. Bassal A A, 1995, "Study Of The Effect Of Drill Pipe Rotation On Cuttings Transport In Inclined Wellbores", Ms Thesis, Tulsa Univ., Tulsa, Oklahoma, 1995

22. Shoham, O. “ Two Phase Flow Modeling” Aug. 1997

Appendix A

Experimental Results

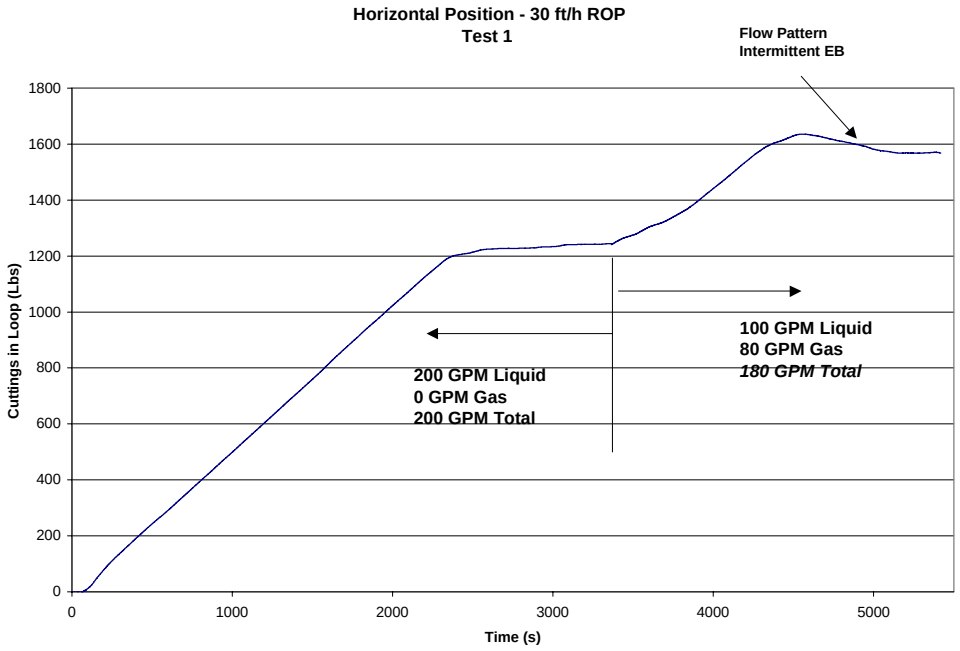

Fig. 6.16- Cutting accumulation - Horizontal Position - 30 ft/h ROP
Experimental Results - Test 1

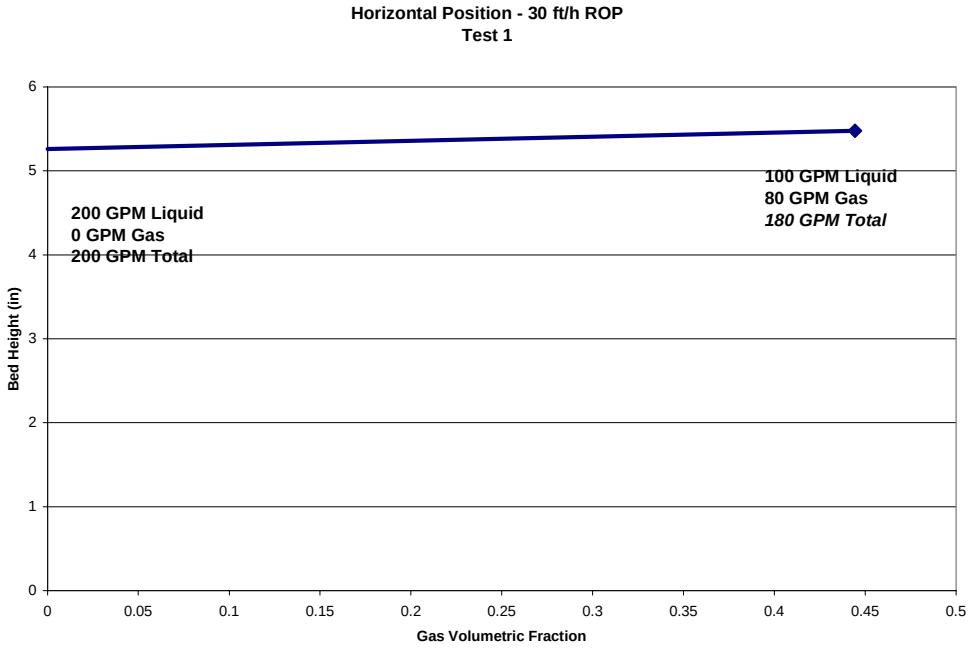

Fig. 6.17- Bed Height - Horizontal Position - 30 ft/h ROP
Experimental Results - Test 1

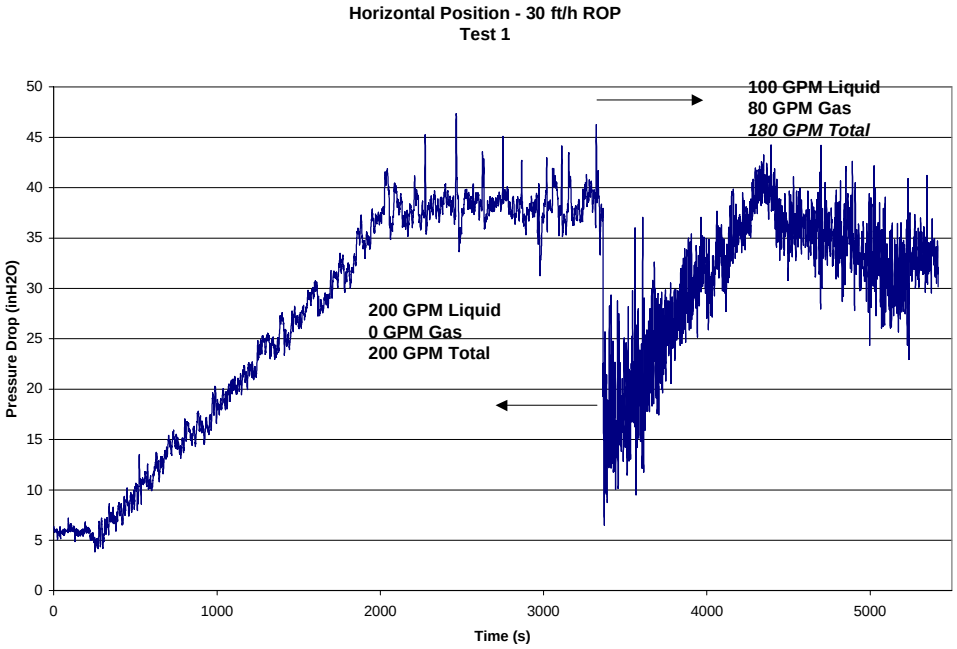

Fig. 6.18- Pressure Drop - Horizontal Position - 30 ft/h ROP
Experimental Results - Test 1

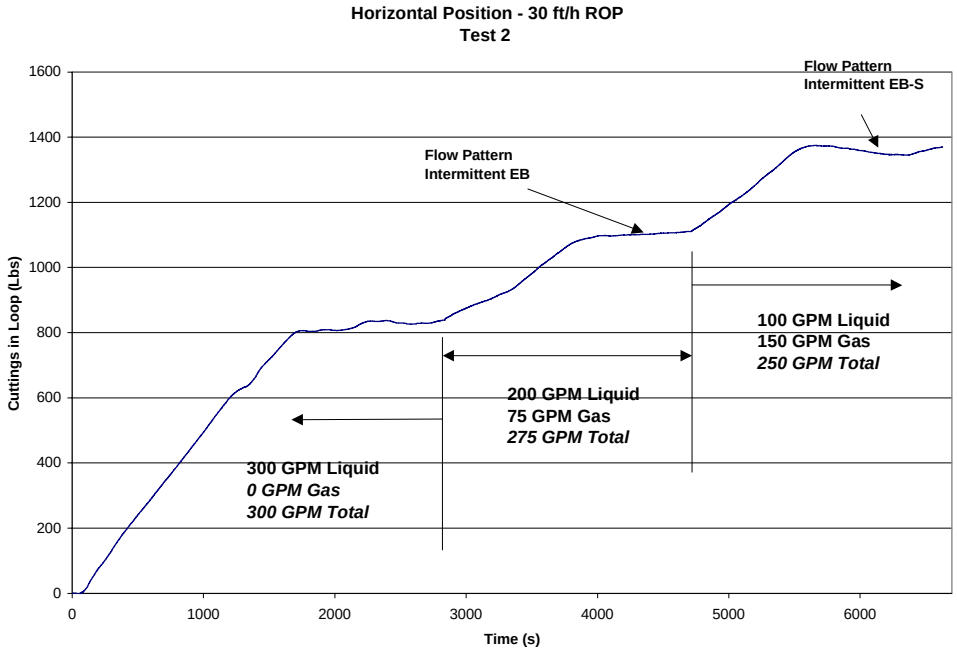

Fig. 6.19- Cutting accumulation - Horizontal Position - 30 ft/h ROP
Experimental Results - Test 2

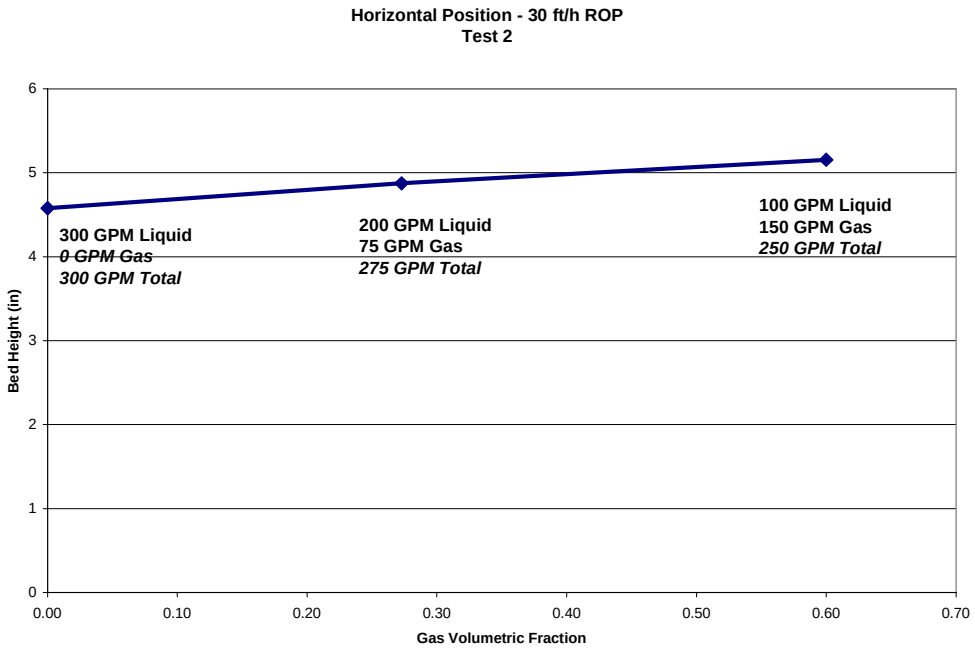

Fig 6.20- Bed Height - Horizontal Position - 30 ft/h ROP
Experimental Results - Test 2

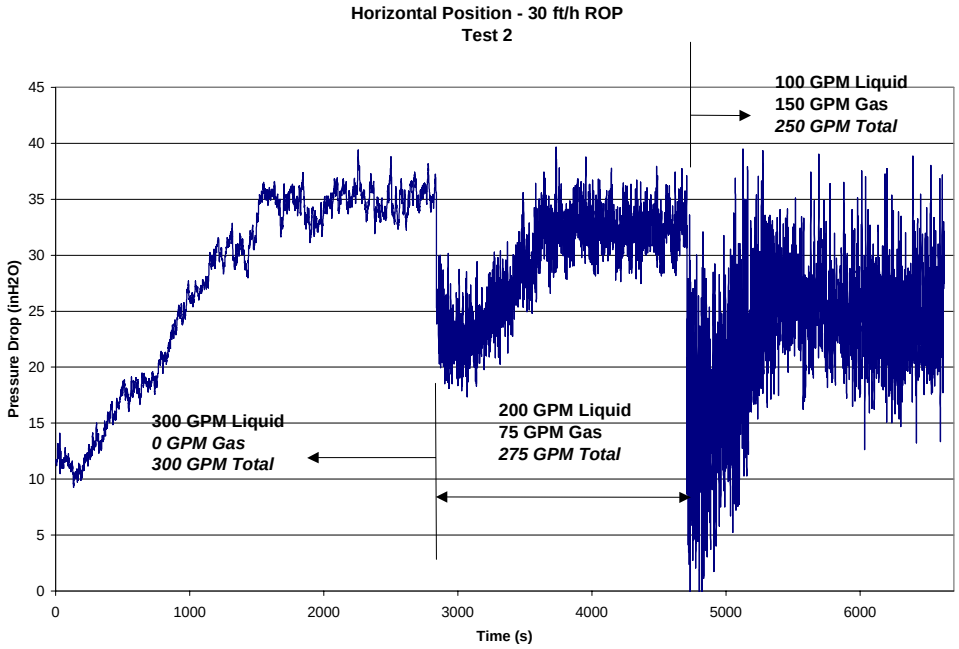

Fig. 6.21- Pressure Drop - Horizontal Position - 30 ft/h ROP
Experimental Results - Test 2

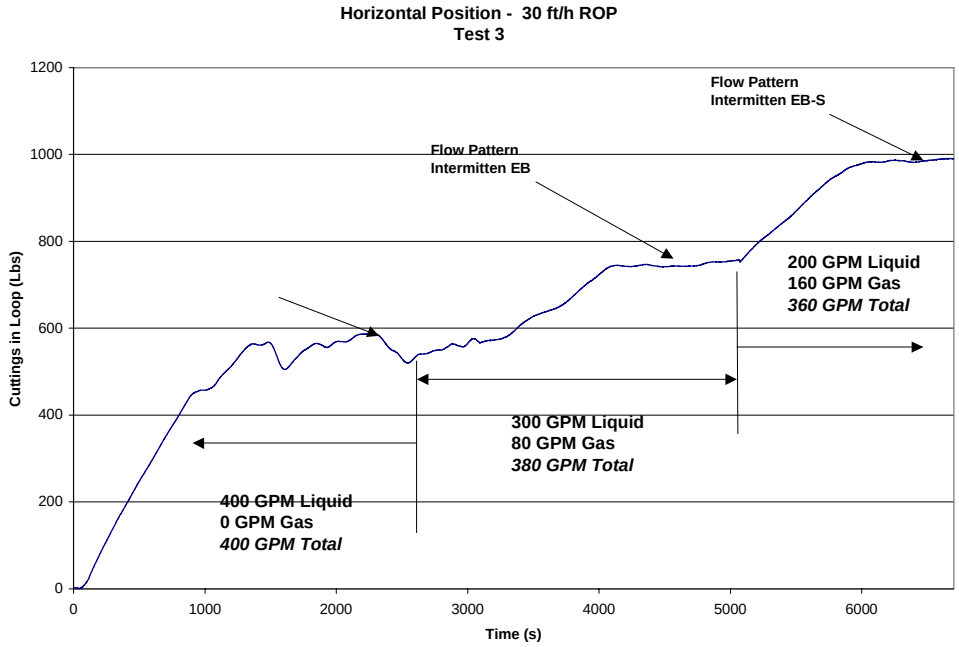

Fig. 6.22- Cutting accumulation - Horizontal Position - 30 ft/h ROP
Experimental Results - Test 3

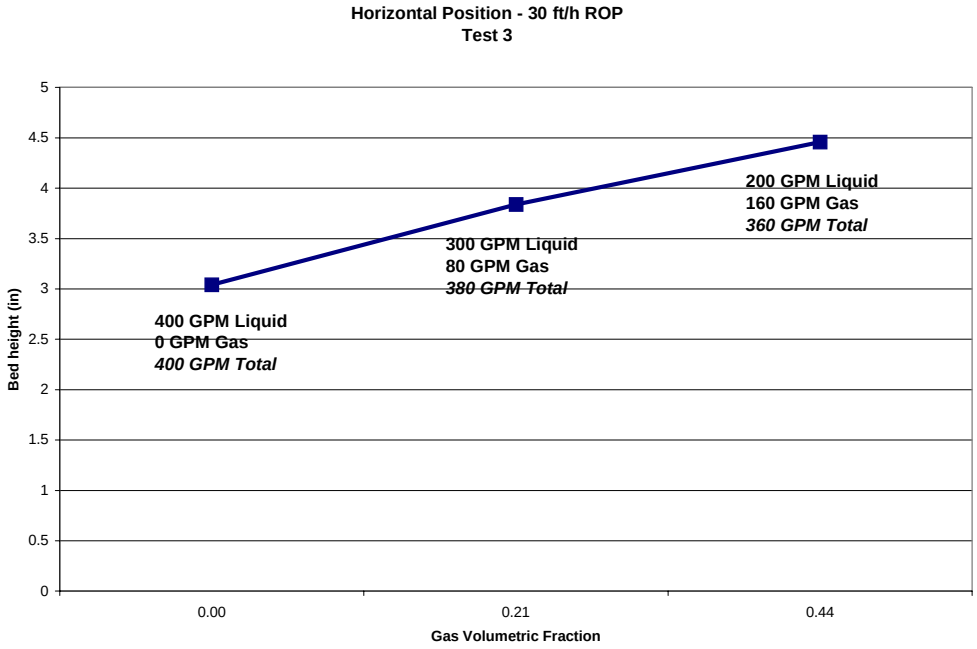

Fig. 6.23- Bed Height - Horizontal Position - 30 ft/h ROP
Experimental Results - Test 3

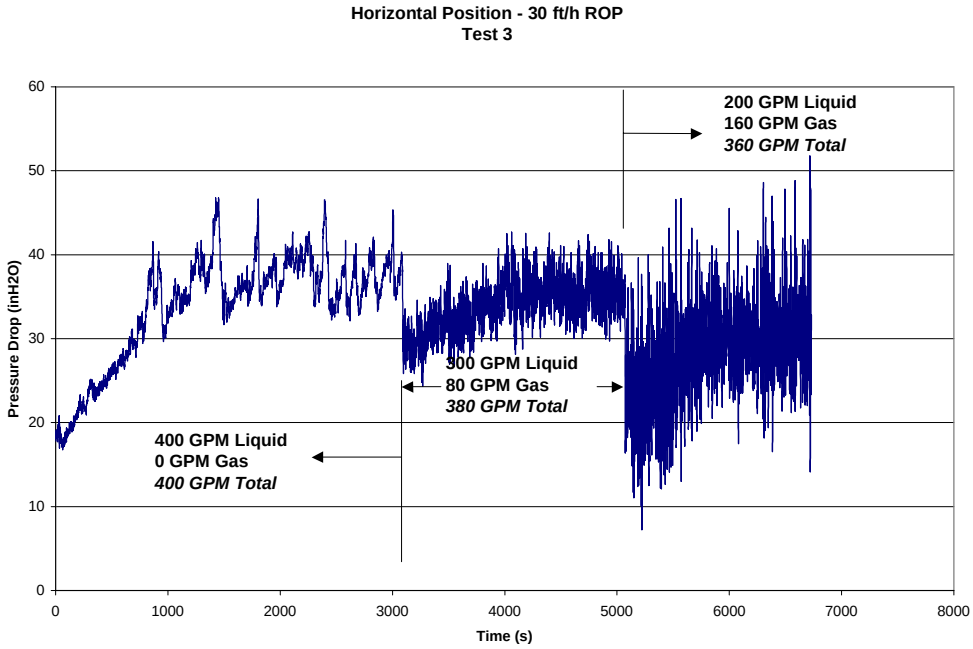

Fig. 6.24- Pressure Drop - Horizontal Position - 30 ft/h ROP
Experimental Results - Test 3

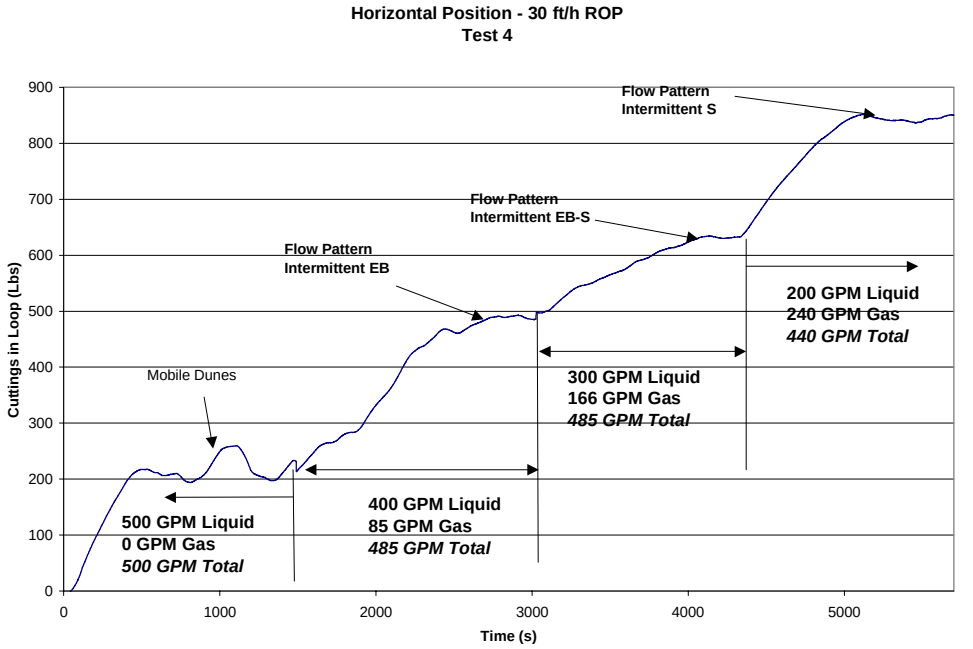

Fig. 6.25- Cutting accumulation - Horizontal Position - 30 ft/h ROP
Experimental Results - Test 4

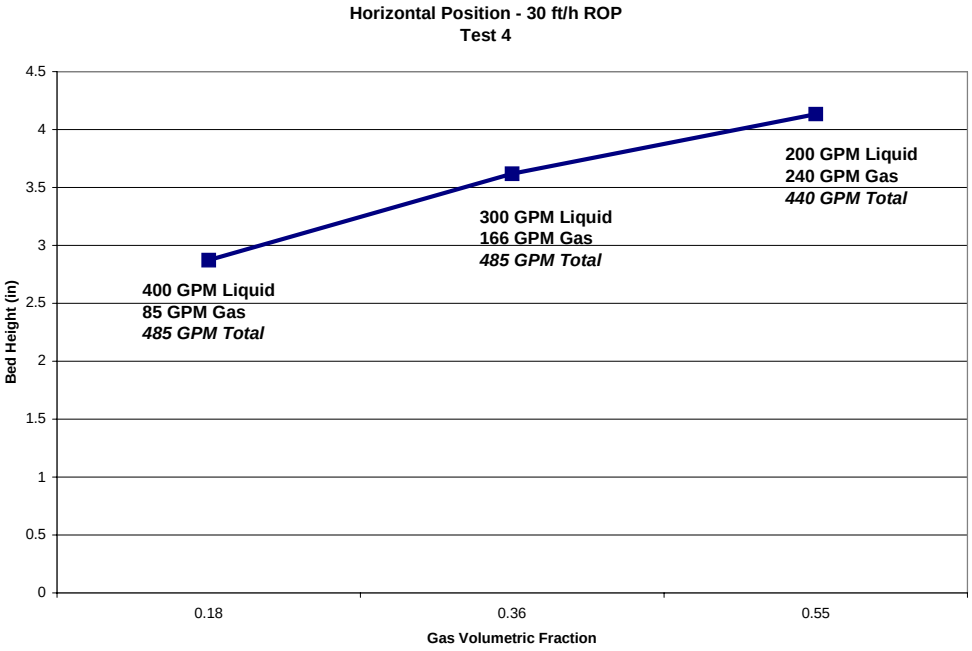

Fig. 6.26- Bed Height - Horizontal Position - 30 ft/h ROP
Experimental Results - Test 4

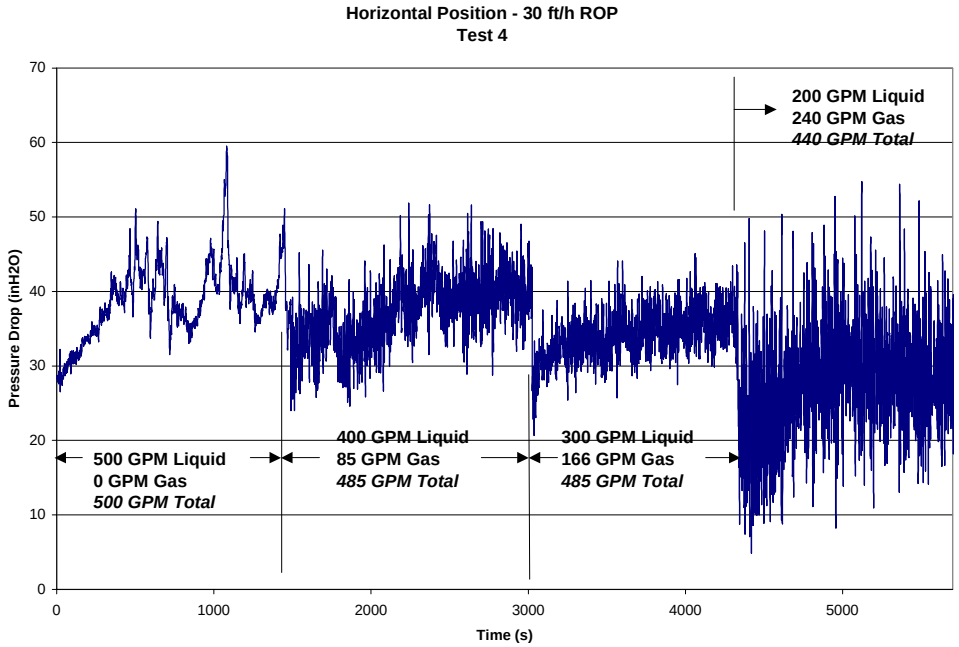

Fig. 6.27- Pressure Drop - Horizontal Position - 30 ft/h ROP
Experimental Results - Test 4

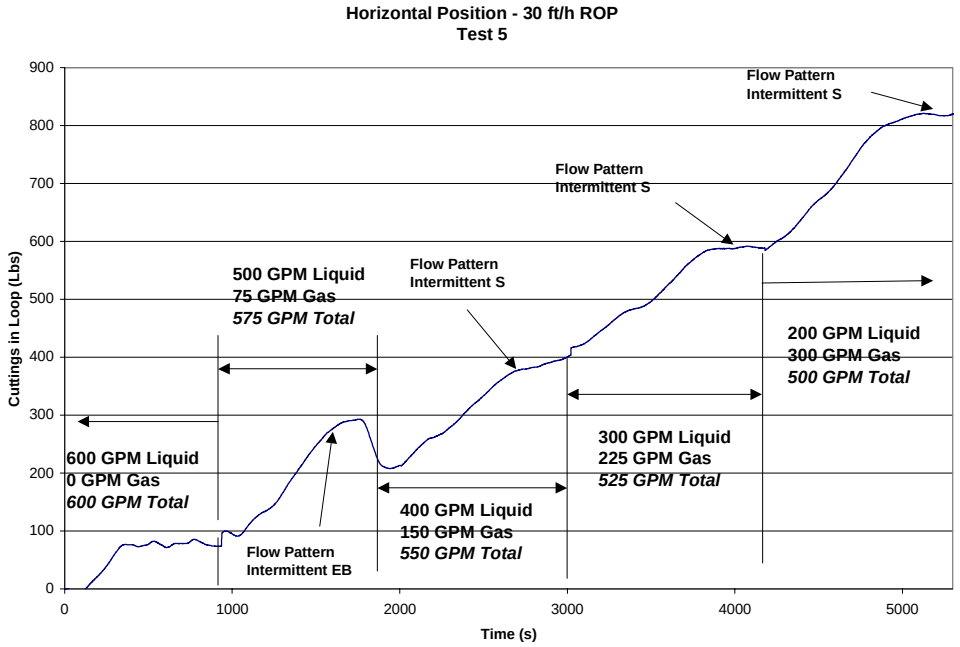

Fig. 6.28- Cutting accumulation - Horizontal Position - 30 ft/h ROP
Experimental Results - Test 5

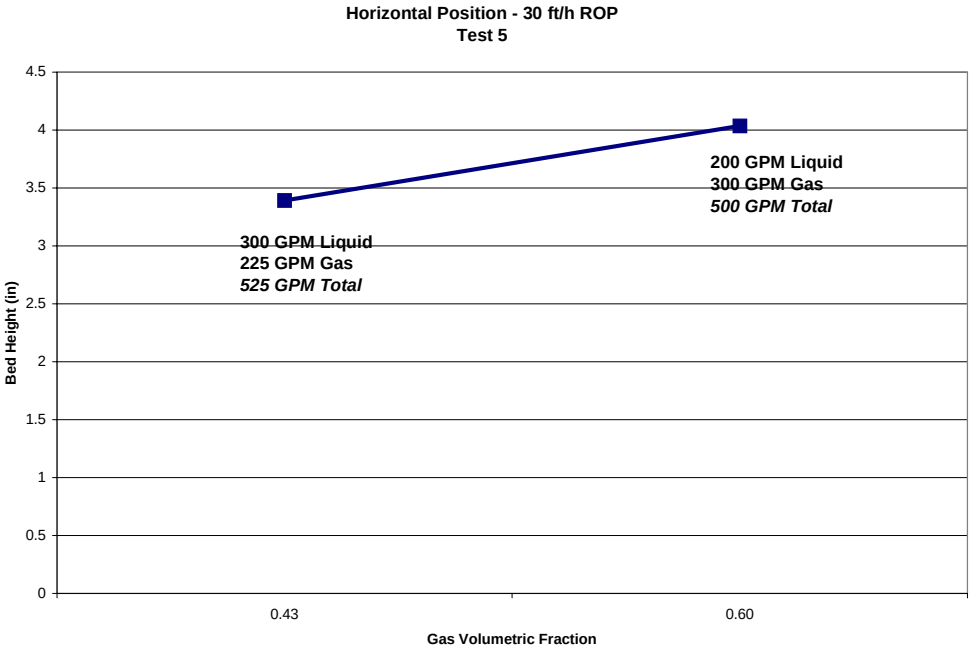

Fig. 6.29- Bed Height - Horizontal Position - 30 ft/h ROP
Experimental Results - Test 5

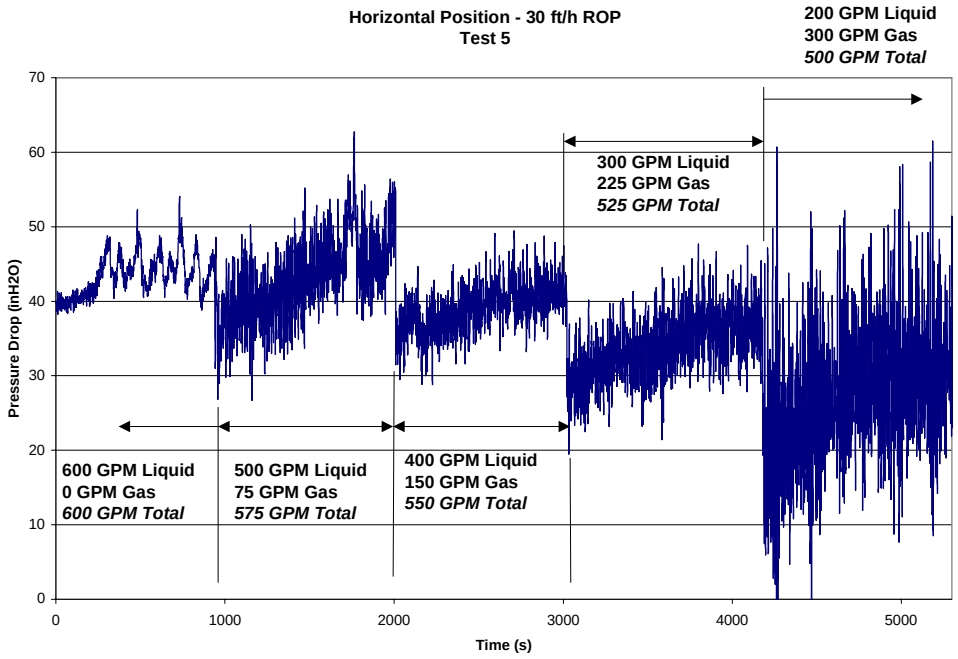

Fig. 6.30- Pressure Drop - Horizontal Position - 30 ft/h ROP
Experimental Results - Test 5

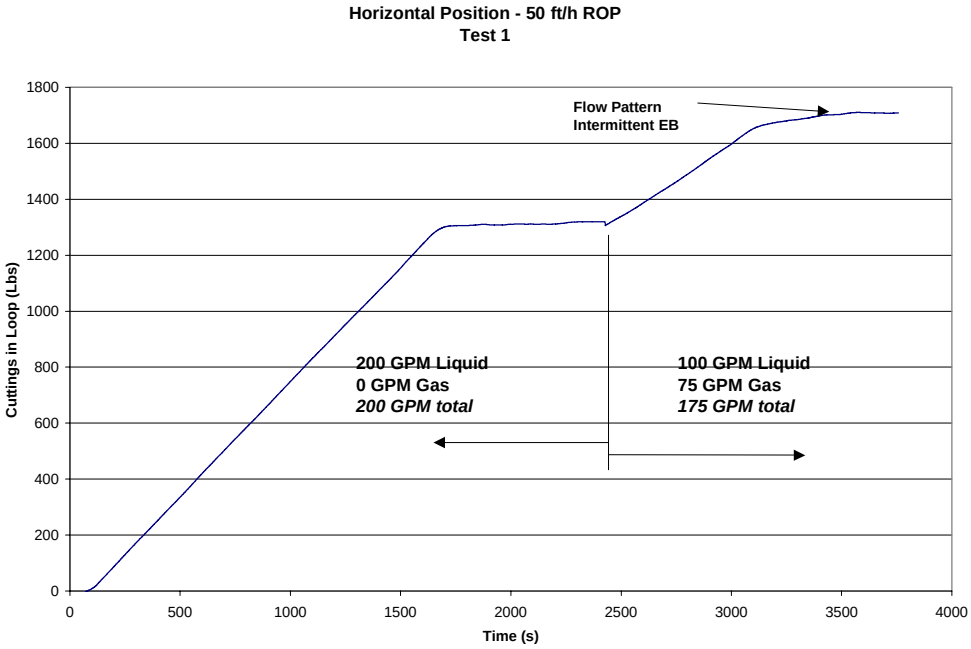

Fig. 6.31- Cutting accumulation - Horizontal Position - 50 ft/h ROP
Experimental Results - Test 1

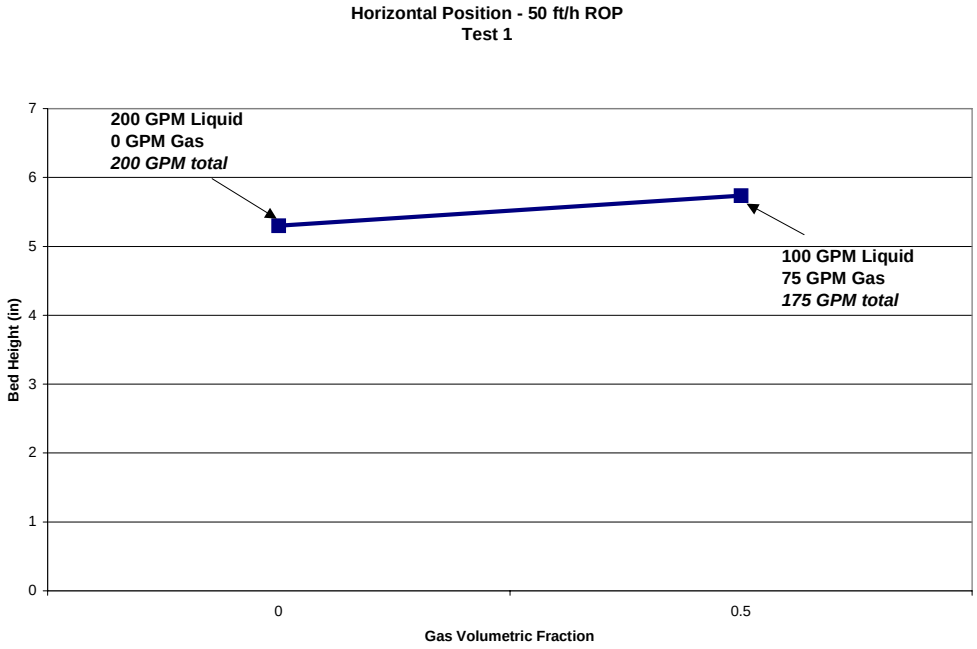

Fig. 6.32- Bed Height - Horizontal Position - 50 ft/h ROP
Experimental Results - Test 1

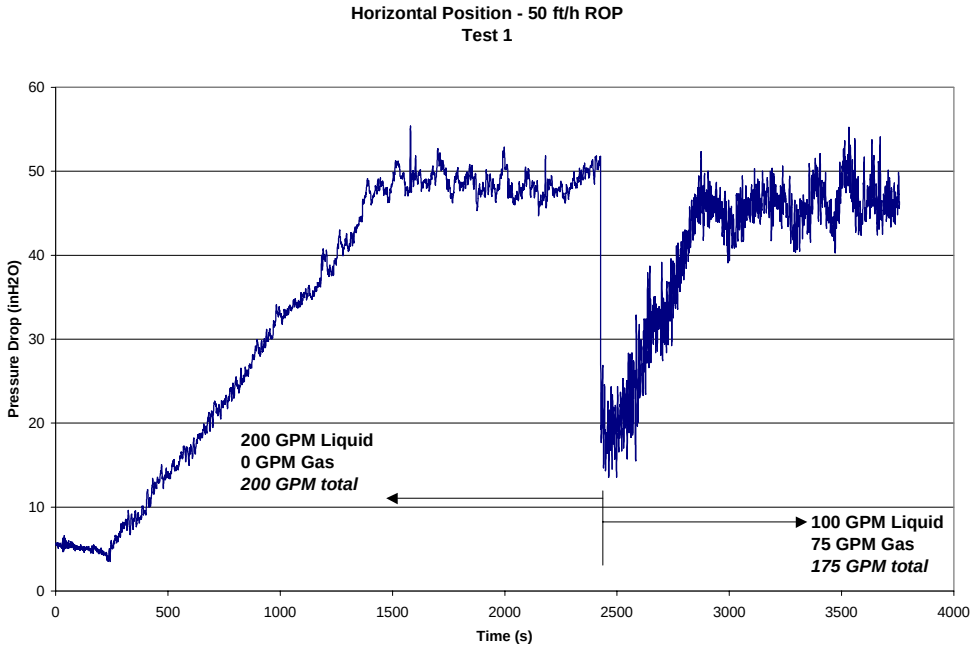

Fig. 6.33- Pressure Drop - Horizontal Position - 50 ft/h ROP
Experimental Results - Test 1

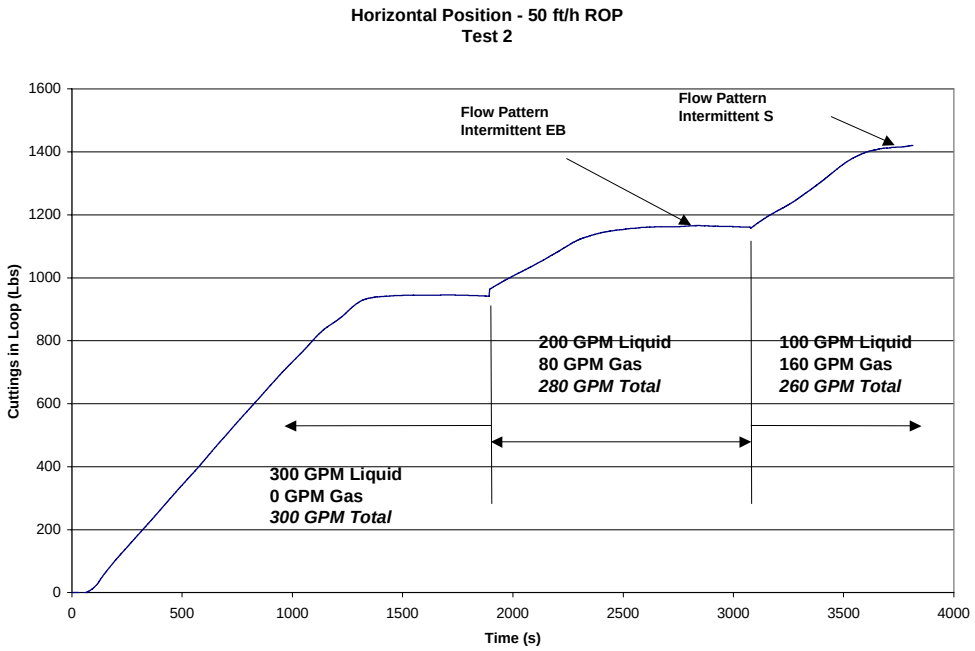

Fig. 6.34- Cutting accumulation - Horizontal Position - 50 ft/h ROP
Experimental Results - Test 2

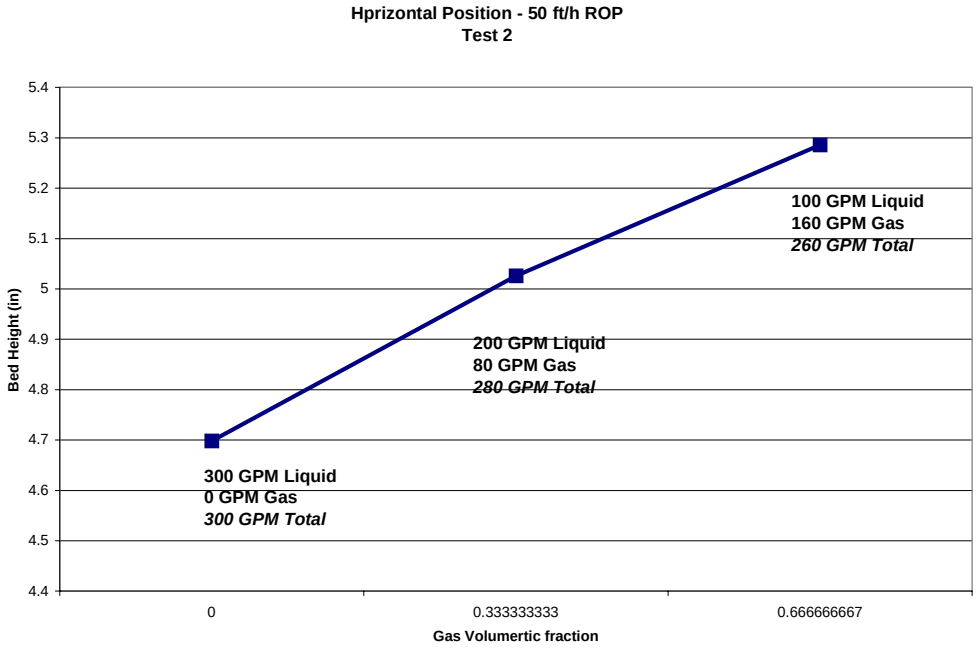

Fig. 6.35- Bed Height - Horizontal Position - 50 ft/h ROP
Experimental Results - Test 2

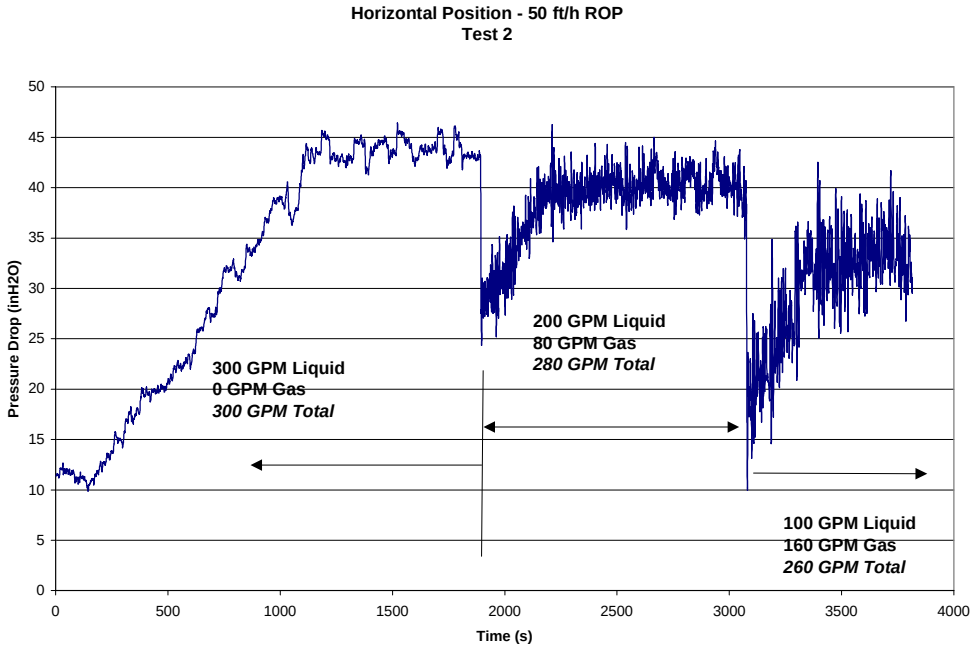

Fig. 6.36- Pressure Drop - Horizontal Position - 50 ft/h ROP
Experimental Results - Test 2

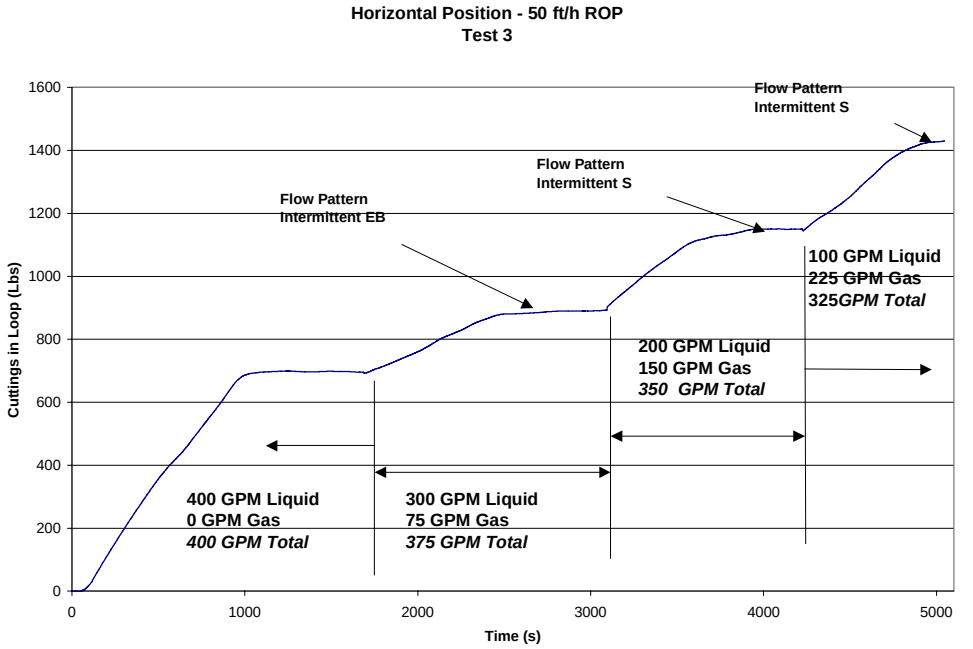

Fig. 6.37- Cutting accumulation - Horizontal Position - 50 ft/h ROP
Experimental Results - Test 3

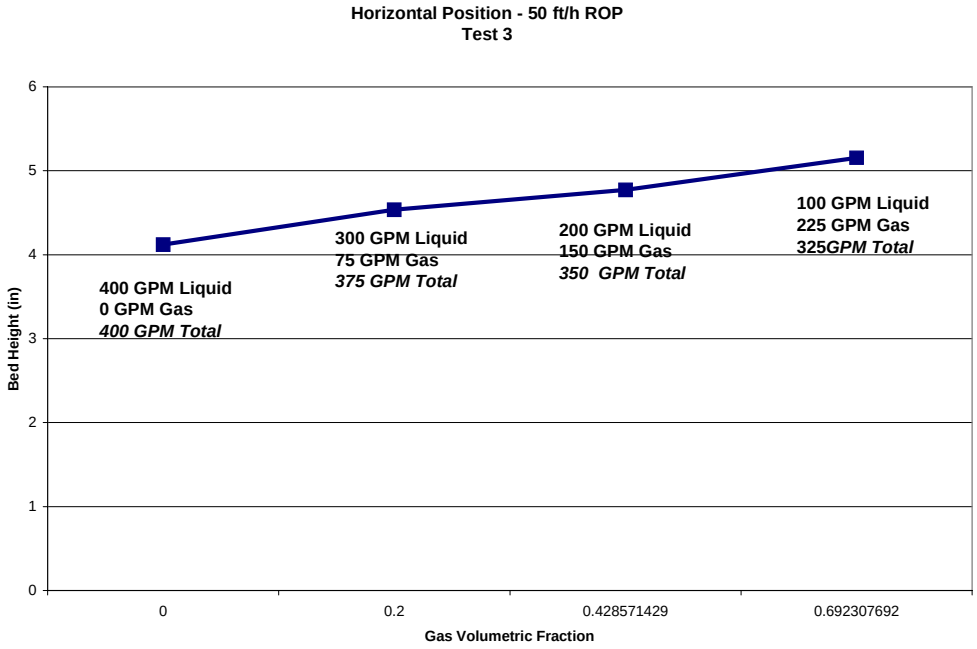

Fig. 6.38- Bed Height - Horizontal Position - 50 ft/h ROP
Experimental Results - Test 3

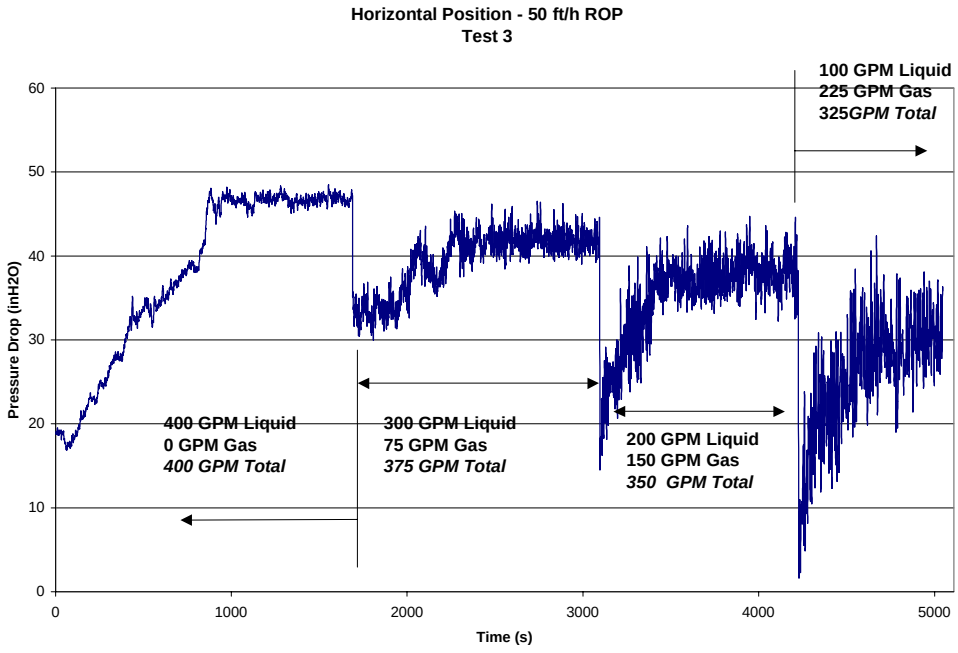

Fig. 6.39- Pressure Drop - Horizontal Position - 50 ft/h ROP
Experimental Results - Test 3

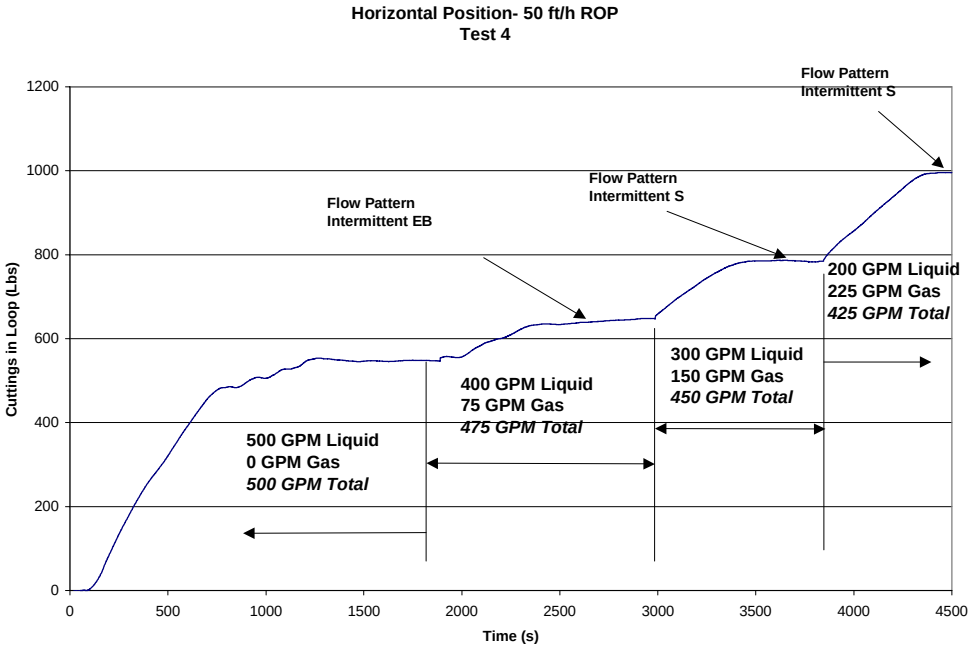

Fig. 6.40- Cutting accumulation - Horizontal Position - 50 ft/h ROP
Experimental Results - Test 4

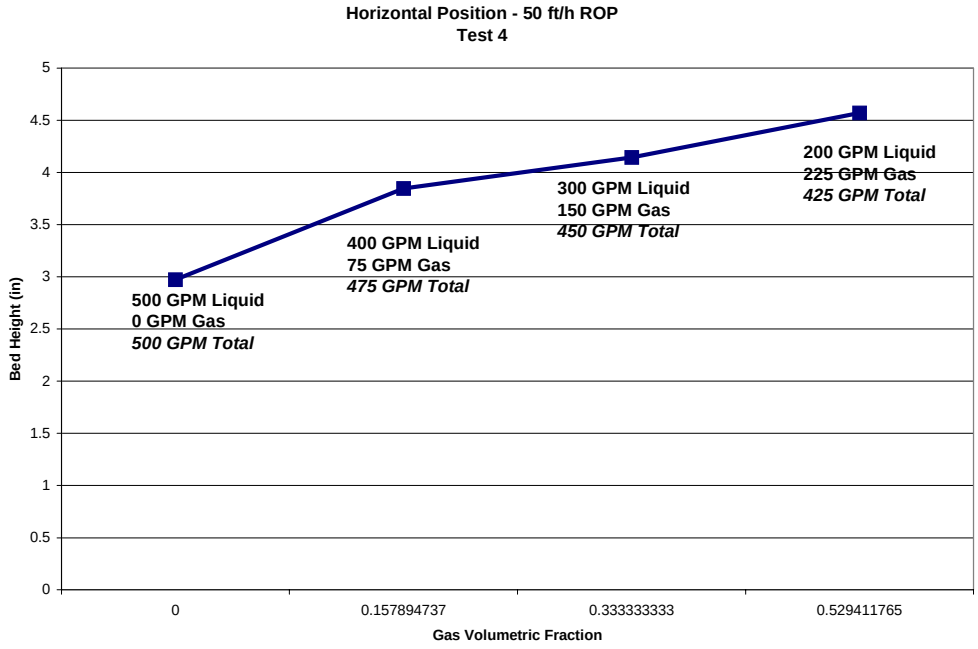

Fig. 6.41- Bed Height - Horizontal Position - 50 ft/h ROP
Experimental Results - Test 4

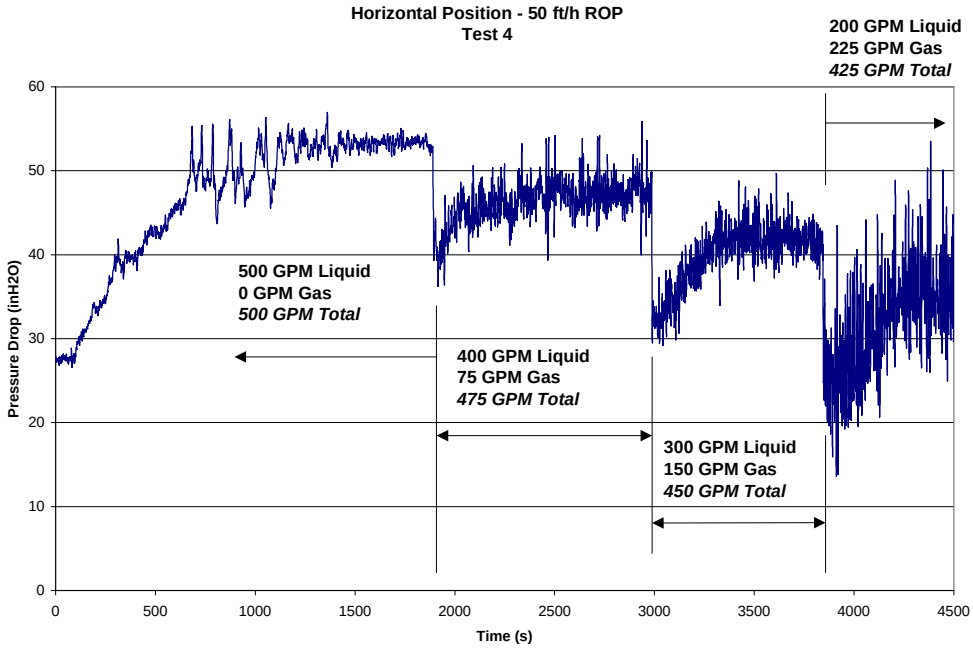

Fig. 6.42- Pressure Drop - Horizontal Position - 50 ft/h ROP
Experimental Results - Test 4

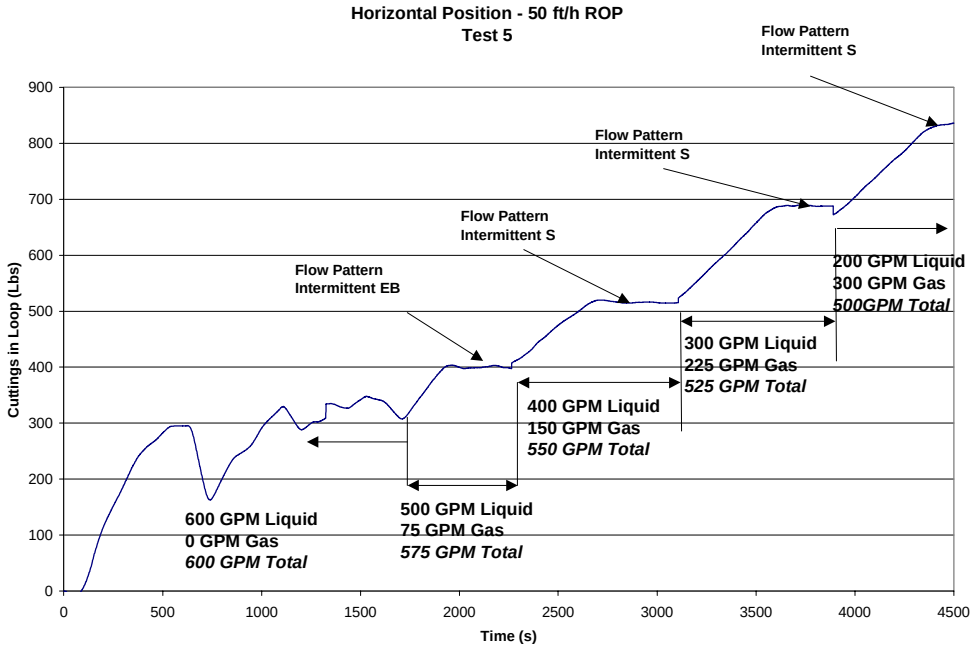

Fig. 6.43- Cutting accumulation - Horizontal Position - 50 ft/h ROP
Experimental Results - Test 5

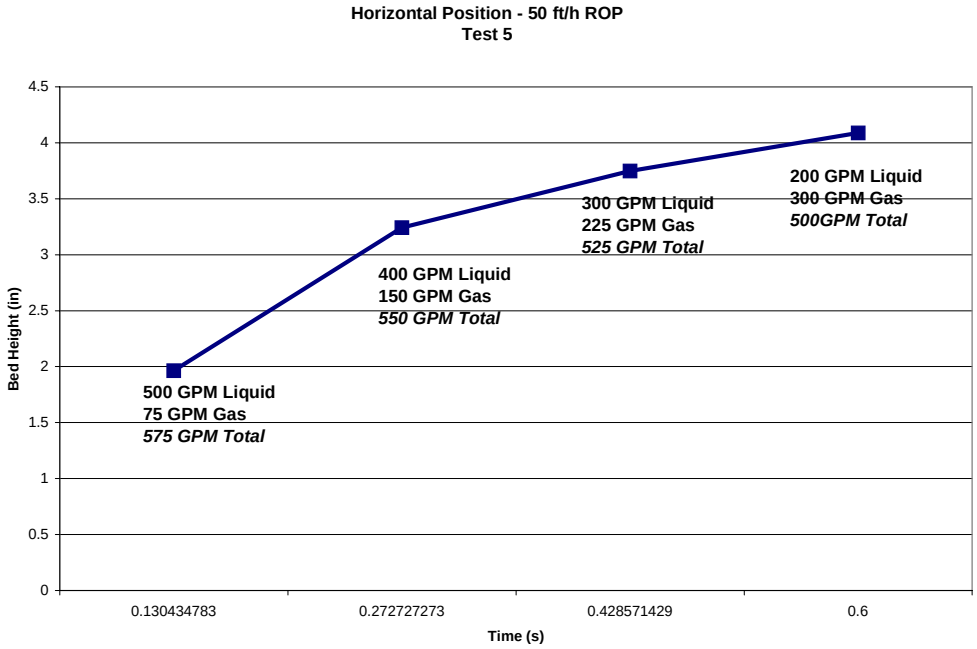

Fig. 6.44- Bed Height - Horizontal Position - 50 ft/h ROP
Experimental Results - Test 5

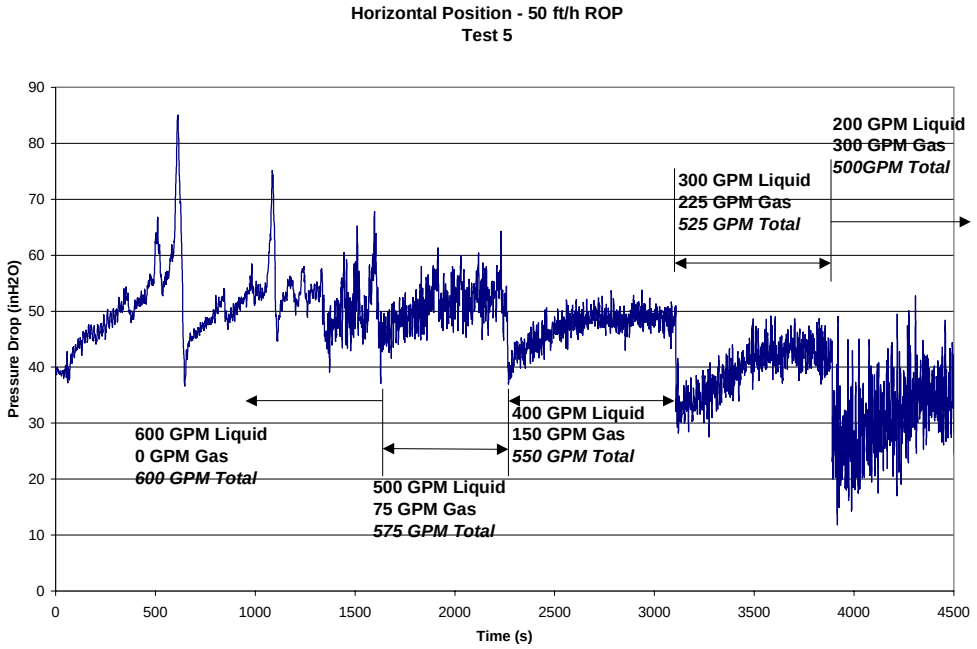

Fig. 6.45- Pressure Drop - Horizontal Position - 50 ft/h ROP
Experimental Results - Test 5

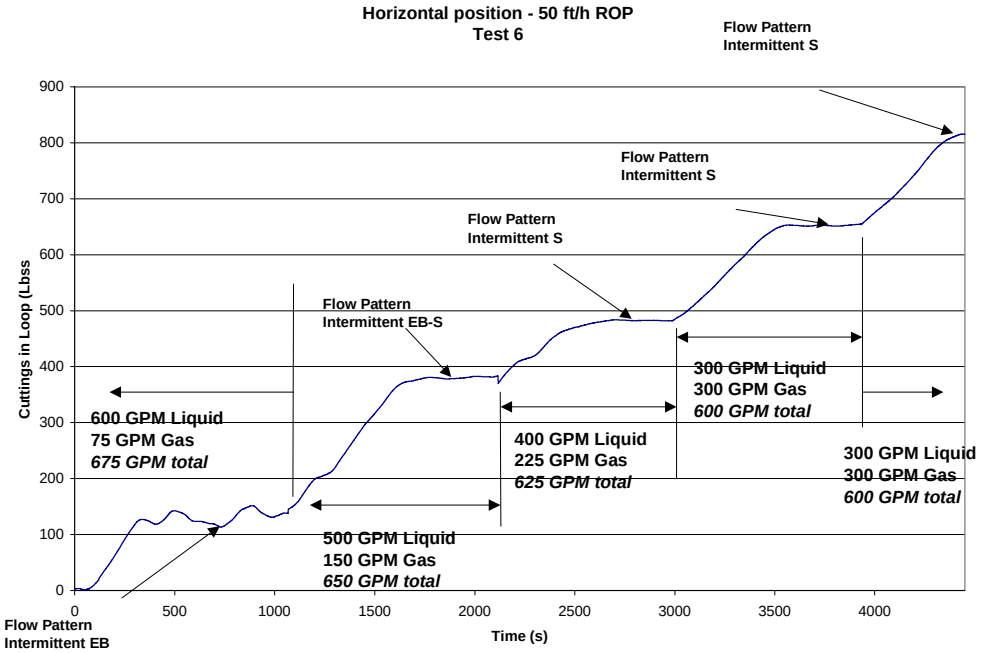

Fig. 6.46- Cutting accumulation - Horizontal Position - 50 ft/h ROP
Experimental Results - Test 6

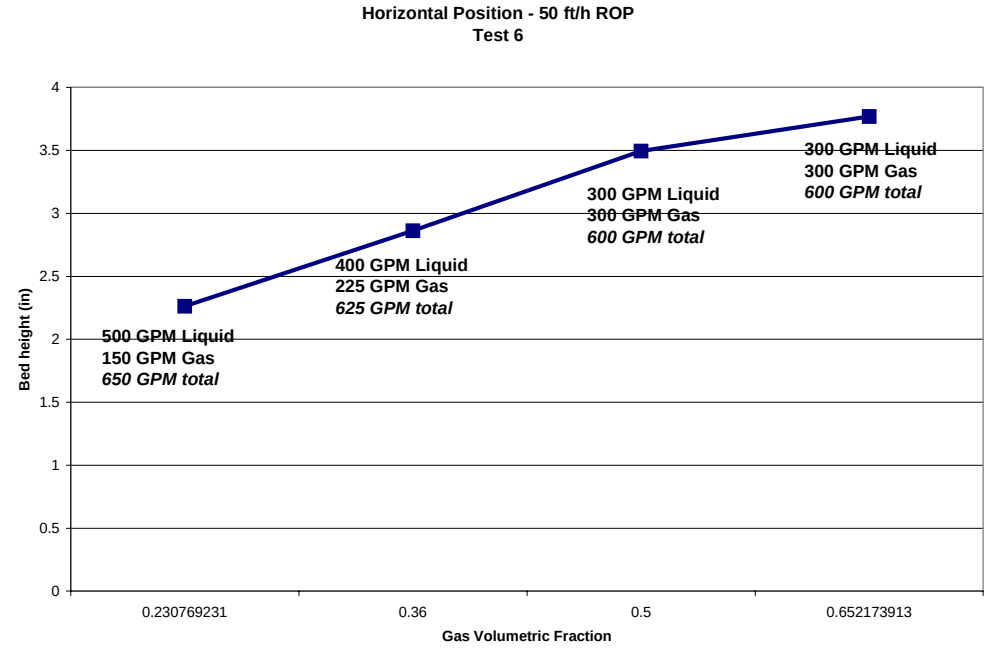

Fig. 6.47- Bed Height - Horizontal Position - 50 ft/h ROP
Experimental Results - Test 6

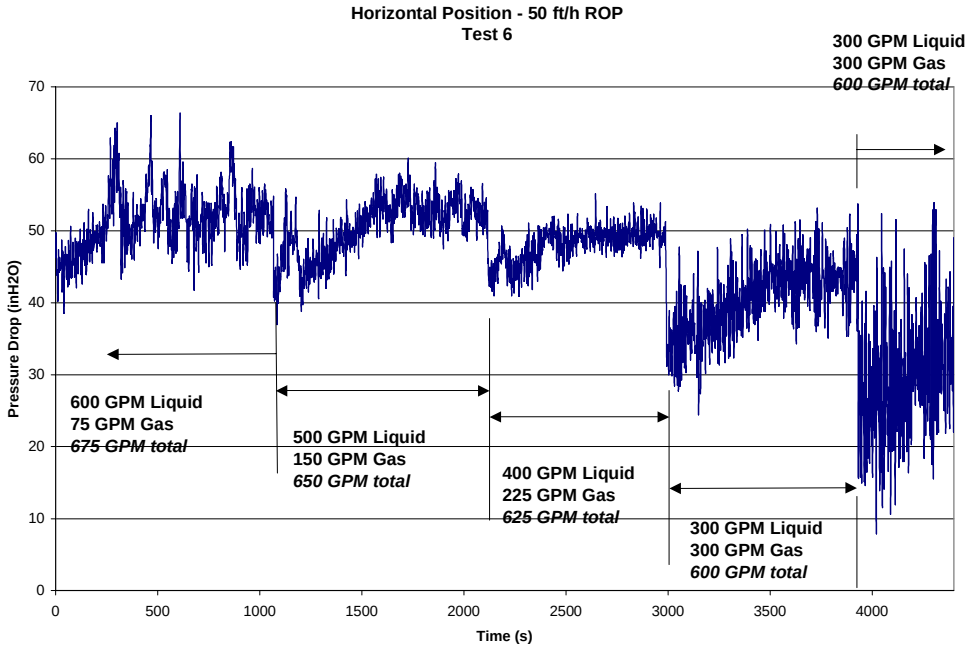

Fig. 6.48- Pressure Drop - Horizontal Position - 50 ft/h ROP
Experimental Results - Test 6

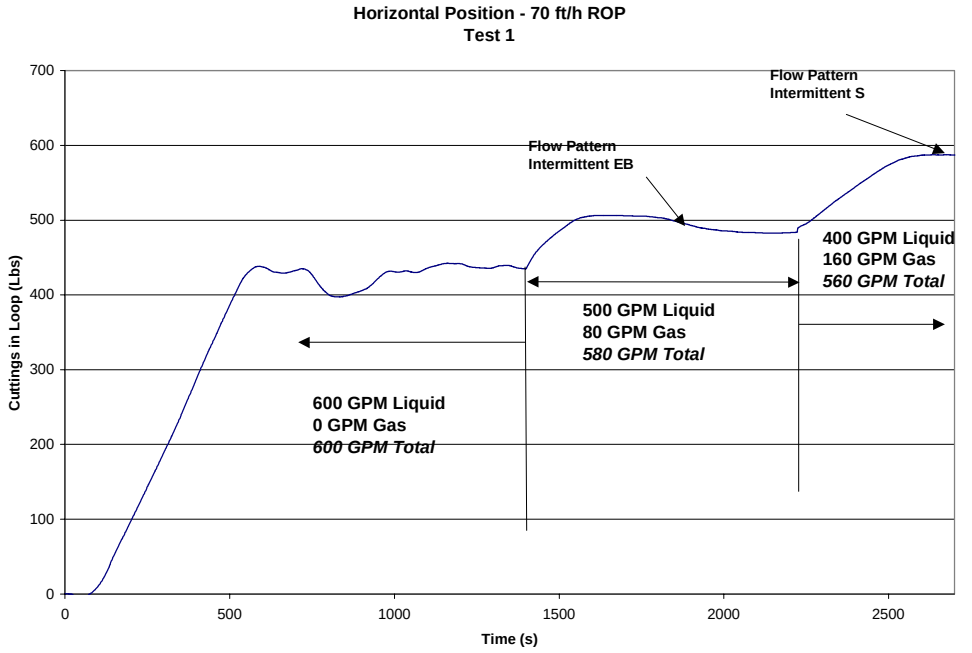

Fig. 6.49- Cutting accumulation - Horizontal Position - 70 ft/h ROP
Experimental Results - Test 1

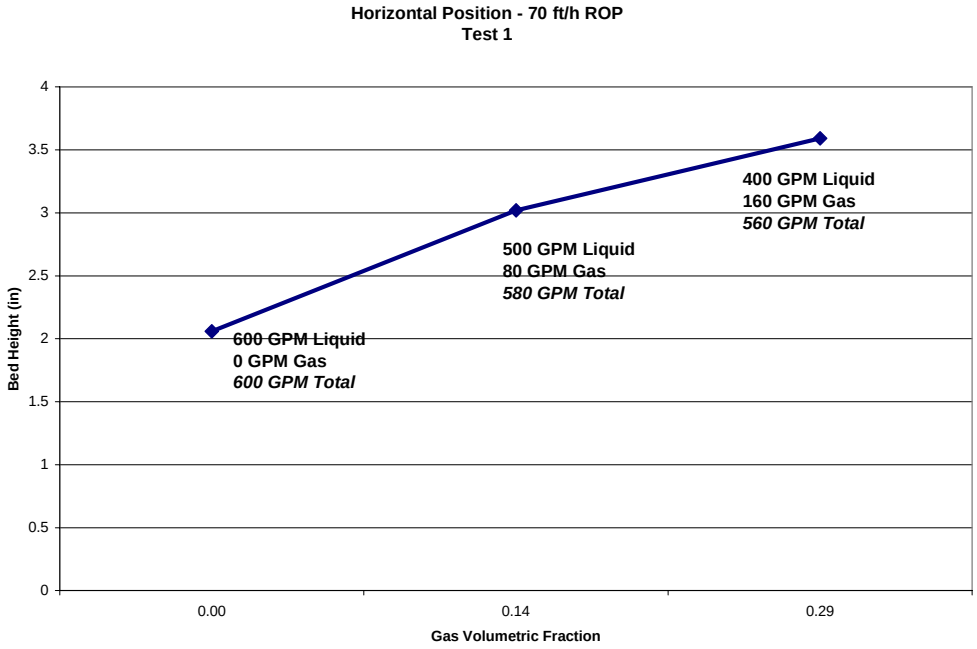

Fig. 6.50- Bed Height - Horizontal Position - 70 ft/h ROP
Experimental Results - Test 1

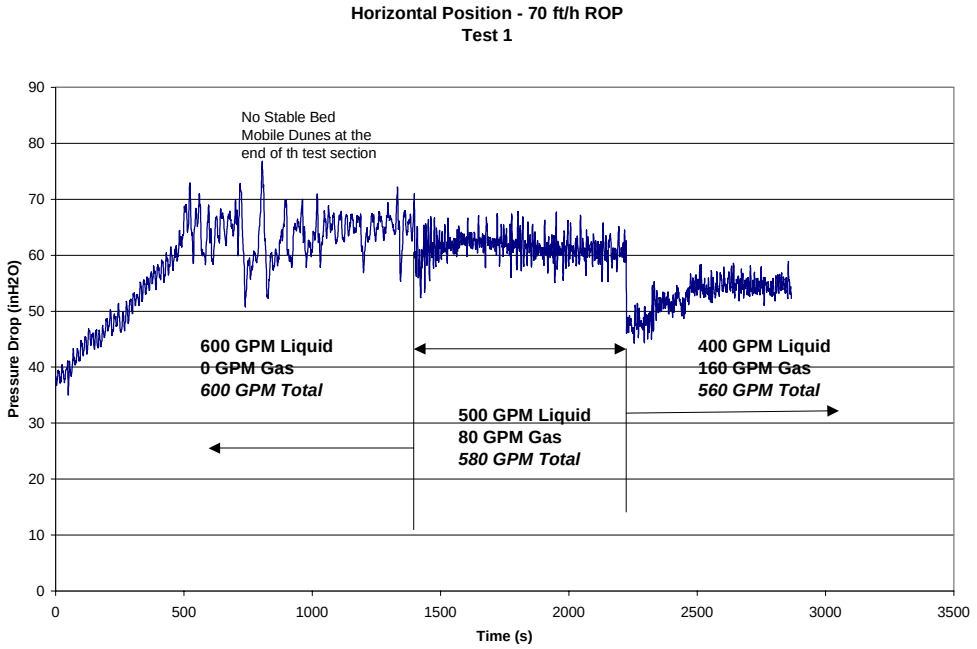

Fig. 6.51- Pressure Drop - Horizontal Position - 70 ft/h ROP
Experimental Results - Test 1

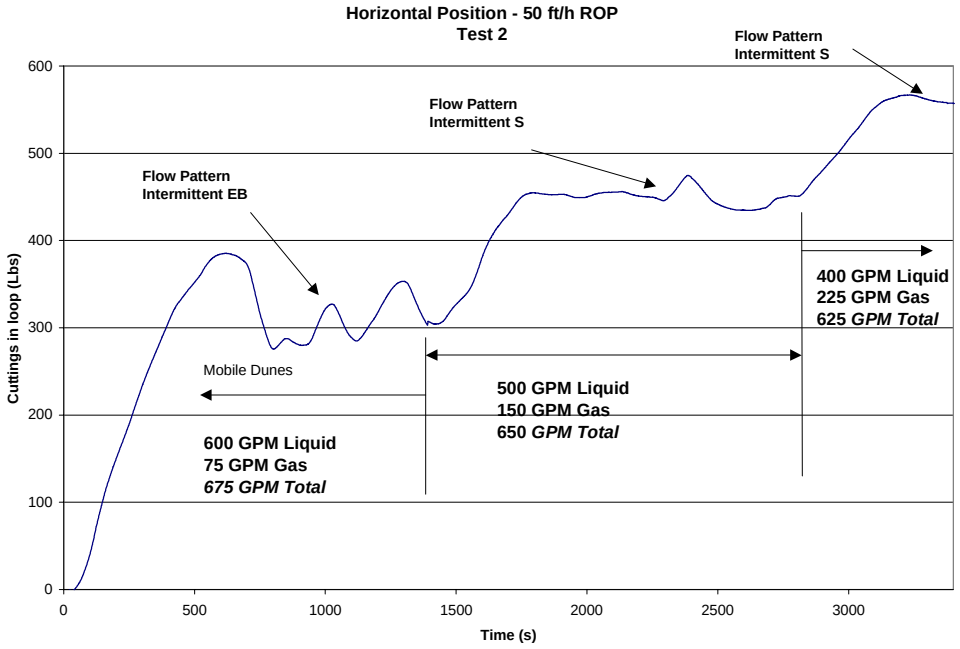

Fig. 6.52- Cutting accumulation - Horizontal Position - 70 ft/h ROP
Experimental Results - Test 2

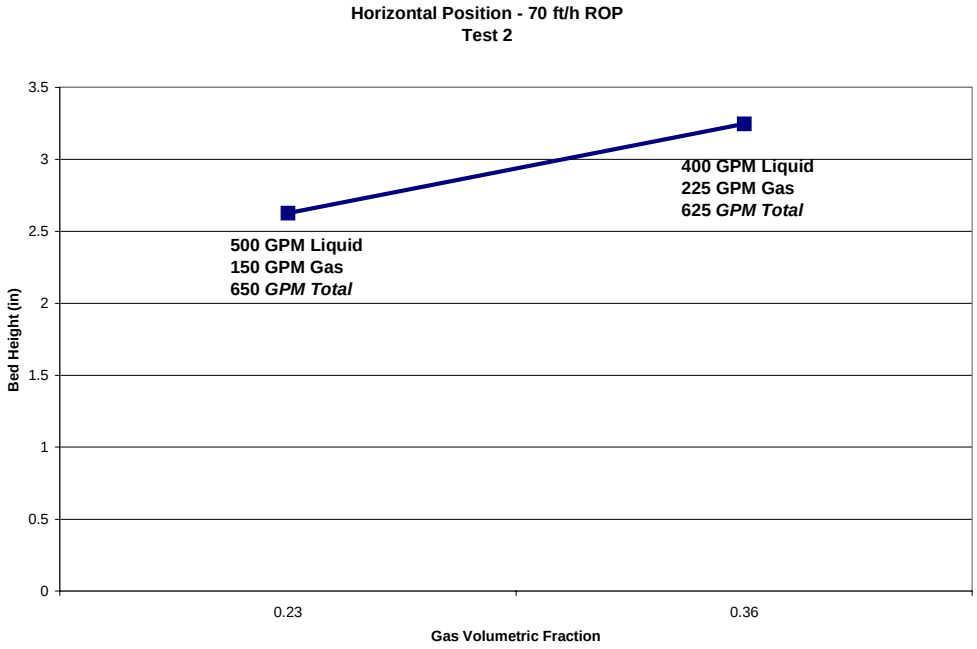

Fig. 6.53- Bed Height - Horizontal Position - 70 ft/h ROP
Experimental Results - Test 2

7. STUDY OF FOAM FLOW BEHAVIOR UNDER ELEVATED PRESSURE AND ELEVATED TEMPERATURE CONDITIONS

Investigator: Affonso Marcelo Fernandes Lourenço

7.1 Objectives

- Perform experimental study of foam flow behavior inside pipes and annuli in a large-scale loop (ACTS) under elevated pressure and temperature.
- Develop empirical correlations to estimate pressure losses during foam flow under a given gas-liquid ratio, temperature and pressure conditions.

7.2 Introduction

The use of lightweight fluids in drilling operations is becoming a common practice all over the world. Among the various types of available lightweight fluids, foams are one of the most commonly used in drilling operations. High cuttings transport capacity, minimum formation damage and better control of gas and liquid phases flow are examples of advantages of using foam as a drilling fluid.

Many difficulties arise when trying to model the flow behavior of foams: compressibility, shear thinning effects, slippage effects, bubble shape and size distribution, type of liquid phase, viscoelastic behavior, etc. In order to properly calculate flow properties, and friction pressure losses while drilling with foam, effects of elevated pressures and temperatures must be understood.

7.3 Summary of Year 1 Activities

The following major tasks have been undertaken since September 1999:

- Literature review
- ACTS flow loop improvement
- Development of procedure for foam tests
- Foam stability tests
- PVT analysis for foams

7.4 Literature Review

Literature survey about the static and dynamic behavior of foam systems has been conducted since the beginning of the project. Heller and Kuntamukkula[1] presented a critical literature review about foam rheology, and stated the difficulties associated with these measurements and the different results found in many experimental works.

Rheology and foam hydraulic were experimentally studied by Mitchell[2], David and Mardsen[3], Beyer, Millhone and Foote[4], Reidenbach and Harris[5] (1983), Okpobiri and Ikoku[6], Saintpere, Herzhaft and Toure[7]. Methodologies to predict friction pressure losses were proposed based on rheological parameters and quality. Pseudo-plastic behavior of foam flow, slip effects and yielding point presence were reported. Reidenbach and Harris[8] (1987),Cawiezel and Niles[9], Phillips et al.[10], Bonilla et al.[11], also covered the same subject and studied the effect of elevated temperatures and pressures on foam rheological parameters. Harris[12] studied the effect of texture on rheology of foams. One important conclusion was that high pressure produces finer texture foams and viscosity measurements at low pressure may not adequately simulate field usage at high pressure.
Valko and Economides[13] introduced an interesting approach to model the foam flow. This is called volume equalization method and it is based on the definition of specific expansion ratio (density of liquid per density of foam). Rheological parameters and friction pressure losses were correlated as a function of the expansion ratio. Gardiner, Dlugogorski and Jameson[14] and Winkler[15] used the same approach and extended Valko's work. Lourenco et al.[16] and Argillier et al[17] studied the stability of static foams using bench scale tests. In addition rheological study was also performed based on pipe flow rheometer data. Lourenco et al. correlated Power Law rheological parameters as function of quality.

7.5 Design of ACTS Flow Loop Modification for Foam Flow

This section presents the actual stage of development of ACTS flow loop and future steps to be included in order to run experiments with foam at elevated pressures and temperatures. In addition, a more detailed test procedure is presented and issues considered important to the future success of experiments are commented. Two different configurations for the flow loop modification for foam flow were discussed. Volumetric and pressure capacity of the compressor were calculated.

Heating and Cooling System

The boiler is operating and water can be circulated with temperatures up to 200°F. The chiller is also installed and can cool test fluids down to slightly less than an ambient temperature. Although the equipments are working properly, the heating system can be improved by changing the boiler's heating fluid type. This modification will reduce heating time. The insulation proved to be efficient keeping the water temperature constant for hours after heating.

Pumping System
The flow loop counts with a HT-400 high pressure piston pump. Tests with liquid flow rates around 250 GPM, pressure of 1500 psi and temperature of 200 F can be performed in the loop.

Multiphase Pumping

A tri-phase Moyno pump was purchased and will provide multiphase pumping capability after installation. According to observation of similar pumps in other research institutions and companies, the equipment presented good performance in pumping multiphase fluids.

In spite of this, the idea of generating foam before the pumping system was introduced. Such a configuration would help to avoid possible difficulties of the pumping system consisting of two-phases (water + air).

According to experiments performed at Halliburton Research Center, a Moyno pump shows good performance in pumping foam with small pressure drop between suction and discharge. Considering the high differential pressure drop expected for foam flow, concerns remain regarding the ability of the Moyno pump to circulate foam and aerated fluids with cuttings.

The piston pump was considered inadequate for pumping and pressurizing foams.

Foam Generation

According to the experiments performed at Halliburton using a small scale facility, the foam properties change during a transient period that depends on the shear rate induced during the foam's generation. This effect will be investigated and considered to avoid measurements during a possible transient period.

Another observation concerned the configuration used in the reduced scale facility, where the liquid is injected into the gas one, and not vice-versa.

Foam Breaking System

A quick depressurization operation after the test section was suggested. The abrupt expansion of foam would break bubbles and release considerable amount of gas at this point. In addition, this procedure would allow the foam breaking device, where defoaming agents are injected, to operate at lower pressure conditions. The liquid part coming from the second defoam operation may contain small gas bubbles dissolved in it, and this could regenerate foam after the final decompression step. The lower pressure conditions would minimize this possible problem.

An investigation of available foaming and defoaming agents and their optimum concentrations was suggested. The foaming and defoaming agents do not produce disposal problems if diluted at right proportions with water.

Compressor Selection

With the objective of simulating as close as possible bottomhole conditions for foam drilling operations, a study was conducted to identify average field operational parameters (ref. 22 to 25); i.e., liquid and air flow rates for the experiments.

Table 7.1 summarizes the preliminary data collected from literature and member companies.

Table 7.1 – Field Cases

ANNULAR GEOMETRY (IN)	BOTTOMHOLE PRESSURE (PSI)	GAS FLOW RATE (SCFM)	LIQUID FLOW RATE (GPM)	BOTTOMHOLE VELOCITIES (FT/S)
7 x 3.5	753	1000	50	3.05
	751	400	50	1.65
	166	1000	20	10.83
12 ¼ x 5	800	700	200	1.00
6 ¼ x 3.5	490	900	80	4.61
8 ½ x 4.5	590	900	80	2.08
8 ½ x 5	800	1000	12	1.41
12 ¼ x 4.5	350	500	35	0.65
7 x 3.5	1000	1400	40	3.27
	700	1400	40	4.40
	400	1400	40	7.24
	1000	700	40	1.95
	700	700	40	2.51
	400	700	40	3.93

Bottomhole velocities were calculated for different field cases based on reported data of bottomhole pressure, temperature, wellbore geometry and liquid and gas rates.

Table7.1 shows average bottomhole pressures of 635 psi and average bottomhole foam velocities around 3.4 ft/s. Comparing the bottomhole parameters with available compressors in the market, a maximum test pressure around 600 psi, and velocities of 2 ft/s were considered reasonable values to be simulated. Also a maximum bottomhole foam quality of 0.6 was established. Thus, a simple compressor capacity analysis could be carried out for these conditions.

Considering that the Moyno pump can achieve around 480 psi discharge pressure, the compressor should be capable of delivering 265 SCFM at 120 psi and maximum temperature of 200 ºF. The computed liquid flow rate considering these maximum conditions is 41 GPM. A variable liquid flow rate injection pump, a PD pump, can be used for this purpose.

Numerical simulations have been made by using foam drilling simulators developed at the University of Tulsa. Preliminary results indicate that for the conditions stated above, the ACTS flow loop would simulate bottom hole pressure and velocity of a 3000 ft to 4000 ft vertical well.

At this point two major possible configurations can be identified depending upon the compressor location. Figure 7.1 shows a schematic drawing of the flow loop configuration for each case.

Plan 1 - This shows the compressor injecting air before the cuttings injection system and Moyno pump. This configuration calls for a medium pressure and medium air flow rate type of compressor to obtain the required tests conditions. The total pressure required for the test section is provided partially by using the three-phase Moyno pump. The injected air can help to carry the cuttings into the loop test section. This system provides good test pressure control, but poor temperature control due to injection of a significant amount of gas at ambient temperature.

Plan 2 - The second configuration shows the injection of air after the Moyno pump and cuttings injection system. It is clear that this scenario requires a compressor delivering low air flow rates at high pressure, and air could not be used for cuttings injection if necessary.

A price survey was done for several air compressor types. Table 7.2 shows the result.

Table 2 – Market Price for Different Air Compressor Types

CASE	AIR FLOW RATE CAPABILITY (SCFM)	MAXIMUM PRESSURE (PSI)	APPROXIMATE PRICE (1000 US $)
1	400	100	20
2	175	200	25
3	400	200	30
4	900	350	100
5	1070	350	116
6	1250	350	165
7	750	1200	245

According to Table 7.2, we note a considerable compressor price difference between case 3 and 4. The plan 1 in Fig. 7.1. was selected for the modification of the flow loop.

7.6 TEST PROCEDURE FOR FOAM FLOW EXPERIMENTS UNDER SIMULATED DOWNHOLE CONDITIONS

This section presents an operation manual regarding the flow loop operation to conduct foam flow tests under elevated pressure and temperature conditions.

The procedure was developed considering the design of piping system shown in Fig. 3.7 (in Chapter 3).

1. SET AND CALCULATE DESIRED TEST CONDITIONS
    a. Set pressure
    b. Set temperature
    c. Set annular velocity
    d. Set quality
    e. Calculate necessary liquid and gas flow rates at test conditions

Table 7.3 - Pipe data:

PIPE NOMINAL DIAMETER (in)	PIPE ID (in)	LENGTH
2	1.918	52'9''
3	2.9	52'9''
4	3.826	66'6''
Annular (6 x 3.5)	5.761x 3.5	57'4''

Cross Sectional Area for Annular and Pipe Flow:

$$A_{flow} = \frac{\pi(OD^2 - ID^2)}{4} \tag{7.1}$$

$$A_{flow} = \frac{\pi(ID^2)}{4} \tag{7.2}$$

Total Foam Flow Rate:

$$Q_T = vA_{flow} \tag{7.3}$$

Liquid and Gas Flow Rates at Test Condition:

$$Q_G = Q_T\Gamma \tag{7.4}$$

$$Q_L = Q_T - Q_g \tag{7.5}$$

    f. Calculate standard gas flow rate using an equation of state for foam:

$$V_{F2} = V_{F1}\left[(1-\Gamma_1) + \frac{P_1 z_1}{P_2 z_2}\frac{T_1}{T_2}(\Gamma_1)\right] \tag{7.6}$$

V_1 – Volumetric flow rate of foam at inlet condition.
V_2 – Volumetric flow rate of foam at test section condition.

T_1- Temperature at inlet condition
T_2 - Temperature at test section condition
P_1- Pressure at inlet condition
P_2 - Pressure at test section condition
z_1 – Gas compressibility factor at inlet condition
z_2 - Gas compressibility factor at test section condition
Γ_1- Foam Quality at inlet condition (volume of gas per volume of foam)

2. Calculate compressor's output pressure:
    a. use the compressor capability up to its limit to compress air. If the test requires more than its capability, use the Moyno pump for additional compression.
3. Read the correct rotor RPM for the Moyno pump at the pump curve (vendor/or experimental pump curve):
    a. calculate Moyno pump differential pressure: Total test pressure – control valve set pressure.
    b. with differential pressure across the pump and total flow rate read the adequate RPM.
    c. The maximum motor power is 75 HP for the Moyno pump.

At this point all necessary parameters to run the tests are defined.

4. Turn on the data acquisition system.
5. Fill mud tank 1 with water to initiate heating loop process (if necessary)
    a. 500 gal minimum volume required.
    b. The final volume will be defined depending upon the amount of tests and available time for the tests.
6. Fill the surfactant tank and breaker tank.
7. Valves must be arranged to allow circulation through the heating loop. Follow the check valve Table 7.4 for heating operation. Fig 3.7 shows the details.
8. Set up the Boiler and heating operation:
    a. Check the level of heat transfer fluid tank.
    b. Turn on the main control panel.
    c. The boiler is primarily programmed to:
        i. 200°F
        ii. *normal* fire level
    d. Turn on the water pump (heat loop centrifugal pump).
    e. Turn on the heat transfer fluid pump.
    f. Turn on the burner.
    g. Check all pressure and temperature gauges/transmitters and flow meters.
    h. Heat the loop until reach desired temperature.
    i. Turn off the boiler after desired temperature has been reached:
        i. Turn off the burner
        ii. Turn off the heat transfer fluid
        iii. Turn off the water centrifugal pump

9. If cooling operation is required, the chiller should be used. See check valve Table 7.4 and Fig 3.7
    a. Turn on the main control panel.
    b. Turn on the chiller's heat transfer fluid pump and then check if its line pressure is around 40 psi.
    c. Turn on the water pump (heating/cooling loop centrifugal pump).
    d. Turn on the chiller
    e. Check all pressure and temperature gauges/transmitters and flow meters.
    f. Cool the loop until reach desired temperature.
    g. Turn off the chiller after desired temperature has been reached:
        i. Turn off the chiller
        ii. Turn off the heat transfer fluid pump
        iii. Turn off the water centrifugal pump
10. Set valves to run the test. The heating loop is by-passed. Follow run operation at the check valve table.
11. With primary information about the test parameters the controllers will be feed with the required information to proceed with the test. Details at process control section.

The following steps can be changed with further experience while running primary tests with the equipments.

12. Start air compressor.
13. Fill accumulator tank.
14. Set control valve 29 (Fig. 3.7) to the pressure calculated at step 2.
15. Turn on metering pumps: liquid pump, surfactant and breaker.
16. Start liquid metering pump.
17. Turn on Moyno Pump and set RPM.
18. Start Moyno pump.
19. Set backpressure valve 19 (Fig. 3.7) to the desired test section pressure.
20. Check all pressure and temperatures transducers and flow meters at the control room and simulator. Wait for steady state conditions of pressure and flow rates.
21. Record temperature, pressure drop and flow rates at the rheology and annular test sections.
22. The foam will be generated at the static mixer installed before the test section and broken at the foam breaking system. The gas will be vent for atmosphere and water will be stored at mud tank 2.

These previous steps summarized the actions to be taken by the operator to run foam tests at the ACTS facility. The following section talks about complementary topics that is related directly or indirectly with the tests. They will provide information about the process control loops and issues to be considered in order to conduct the tests under optimized and safe way. The following subjects were covered:

- Safety procedure
- Process Control
- Moyno Pump Cooling Solutions

- Effluents disposal (clean the loop)
- Possible future configurations and standby solutions
- Test Optimization
- Data Acquisition System

Safety Procedure

Because the tests will be performed under high temperature and high pressure conditions, the safety procedure must be followed carefully. Some recommendations are described in this section and a more detailed and complete safety procedure will be further developed.

- Use hat, boots, goggles and gloves whenever staying in the simulator.
- Use mask if necessary.
- No fire close to the boiler.
- Identify and isolate the hot pipe and hot equipment area.
- Work with caution in the hot area.
- Check all valves, nozzles and instrumentation before running any test.
- Check temperature and pressure limits of all equipment, pipes, valves and instruments.
- Check pressure gauges, fluid temperature, fluid level and flow rate before any direct action in the loop.
- Document and report any damage and/or modification in the loop.
- Avoid work alone and out of normal time schedule of the university.
- Keep first aid box in the loop area.

Process Control

Description of the Main Control Loop (Fig 7.12)

The called main loop consists in a group of sensors, transmitters, controllers and final elements (usually a control valve or variable speed pumps), responsible for the pressure and flow rates (air and liquids) control during the foam tests. Based on a feedback type of control it can be summarized as follows:

- Recalling step 11 in the test procedure the controllers will be fed with desired test foam quality, liquid and gas flow rates, surfactant concentration, foam breaker concentration.
- Variable speed liquid pump 8 starts pumping water at desired flow rate.
- Moyno pump starts.
- Controllers 5 read the liquid flow rate signal from flow meter 9 and send information (electrical sign) to Surfactant metering pump 10 start injecting surfactant at the desired percentage of liquid flow rate.
- Air compressor starts compressing air. Control valve 2 controls the air inlet pressure at the Moyno pump based on pressure information supplied by PI/PT at the Moyno pump suction.

- Flow meter 7 registers air flow rate, density and temperature. Flow meters' transmitter feed the controllers with this information.
- Controllers 5 also receive information from pressure and temperature transmitters 6 and liquid flow meter 9.
- Controllers 5 calculate foam volumetric flow rate inside the test section using equation 6. With foam quality information the controllers send information back to liquid metering pumps 8 and 10 to keep quality at desired value.

Important comments:

Possibly an extra micromotion flow meter or a densitometer will be installed in the test section to provide direct measurement of foam density and/or flow rates. This would provide experimental data about foam volumetric flow rate and density, instead of theoretical calculations. In addition, it would permit a more simple and accurate flow rate control.

Foam Breaking System Control Loop

Another closed control loop is the one that controls the foam breaking system. It will be made by using level and pressure control. The following topics summarize the foam breaking process control:

- Foam breaker injection can be controlled by the main loop. The controllers can set beaker pump to inject the desired percentage value of total local foam volumetric flow rate.
- A quick depressurization will occur after the first backpressure valve helping to break foam bubbles.
- The foam stream reaches the breaking vessel at low pressure (around 50 psi maximum pressure) after receiving the chemical injection at nozzle N1.
- Level controller LC keeps liquid level under certain limit sending a sign to control valve at downstream of the breaker tower to open or close as required. The liquid is directed to mud tank 2.
- A pressure controller PC maintain pressure under desired range by receiving information from pressure transmitter PT, and sending information to control valve at the air venting system to open or remain closed as required.
- Any remaining foam will be broken by demister pads installed at the top of breaking vessel.

Back Pressure Valves

Backpressure valve 19 will be set when tests starts and a self control system will keep the test section at the desired pressure. This control loop will be composed

basically of a pressure transmitter attached to a control valve controlling the necessary amount of nitrogen to release or squeeze the bladder.

Details about the process control system will be implemented in the future. Information like which actions will be possible to be taken from the control room (ex: change parameters' set points) and type of control valves will be further defined.

Moyno Pump Cooling System

The heat generate during compression may represent a problem especially at high quality tests If necessary, water sprinklers can be used direct on the pump for cooling purposes. More sophisticate systems as cooling jackets are also available for purchase.

Effluent Disposal

The hot water containing surfactant and foam breaker will be storage at mud tank 2. According to the foaming and defoaming agent data sheet, they can be dumped when diluted at 2% in volume concentration or below. The fluid can rest in the tank for cooling or if necessary the chiller can be used to cool the water for further disposal.
Possible Design Modifications and Standby Options
Static mixer location

One possible change is in the static mixer location. It could be installed before the Moyno pump and then foam would be generated at upstream of it. This would be an option if problems concerning multiphase pumping occur. Nothing changes under the process control point of view. Few changes like the surfactant injection point and position of some valves may occur. The static mixer in this situation would be installed at upstream of cuttings injection vessel

Manual Control

If the process control system fail for any chance, all reported action can be taken manually, by-passing automatic controls and setting instruments manually. Increase in test time may occur, but all operation can be performed.

Spare Compressor

TUALP have two compressors that could be use occasionally to run the tests. The capabilities of the compressors are:

- 600 psi and 694 SCFM
- 1000 psi and 69,9 SCFM

A Problem associated to this option is the construction of a high pressure air line from the compressors into the loop. This problem could be solved by using the mobile unit with 30 nitrogen high pressure bottles (2400 psi pressure and 260 gal of water volumetric capacity). This would avoid the high pressure line construction, but offers limited operation time and logistic problems.

Viewing Window

A viewing window or possibly smaller view ports will be installed in the annular section. This window will allow visualization of the test and further details such as the material that will be used to construct this device is still under discussion. It will be used for bubble size and bubble shape characterization. The technique to capture bubbles motion by using cameras and microscopes and analyze the data is still under development.

Test Optimization

This topic is highly dependent on future experience with the tests and can be changed based on it. Some suggestions about how to organize the sequence of tests of the test matrix are given in this section.

- Heat the loop as much as possible.
  - Fill the tank only with the necessary amount of water to run the desired tests. This choice should be based on time available and number of tests for one day.
  - The attached charts show experimental result about the transient time to heat and cool the loop. An average value around 0.5°F/min was found for the particular test. The heating time can be reduced using optimum amount of water and the tank mixer.
- For a specific temperature vary quality, pressure and annular velocity.
  - Start with high pressure and low quality foams.
  - Finish with low pressure and high quality foams.
  - Repeat the same procedure as temperature decreases.

Data Acquisition System

A Lab View data acquisition system provides real time information about pressure, temperature, differential pressure and flow rates in different points of the loop. All information can be storage at the same time. Further improvements will be implemented and actualized in the test procedure. The actual available information is listed below:

Differential Pressure Codes:

DT-RL-01: Differential Frictional Pressure Loss @ 4’’Pipe

DT-RL-02: Differential Frictional Pressure Loss @ 3’’Pipe
DC-CT-03: Differential Frictional Pressure Loss @ 6X3.5 ’’ Annular Section
DP4: Differential Friction Pressure Loss @ 2’’ Pipe

Static Pressure Codes:

PT-RL-01: Static pressure at the middle of 4’’ Pipe
PT-RL-02: Static pressure at the middle of 3’’ Pipe
PT-CT-03: Static pressure at the middle of 6’’x 3.5 Annular Section
PT-S-04: Pressure at the Discharge side of Halliburton Pump (Supply Pump Pressure)
PT-05: Static pressure at the middle of 2’’ Pipe

Flow Rate Codes:

FT-IN-01: Doppler Flow Meter @ inlet of test section
FT-RL-02: Doppler Flow Meter @ inlet of test section
FT-3: Micromotion Flow meter (Total liquid Flow Rate entering to the system)

Temperature Codes:

TS1: Inlet Temperature of the Fluid (has LCD monitor)
TS2: Temperature of the Fluid while entering 2” line
TS3: Temperature of the Fluid while leaving 2” line
TS4: Temperature of the Fluid while entering 3” line (has LCD monitor)
TS5: Temperature of the Fluid while leaving 3” line
TS6: Temperature of the Fluid while entering 6x3.5” annular section
TS7: Temperature of the Fluid while leaving 6x3.5” annular section
TS8: Temperature of the Fluid while entering 4” line
TS9: Temperature of the Fluid while leaving 4” line
TS10: Temperature of the Fluid while leaving the ACTS loop (has LCD Monitor)

Table 7.4 - Check Valve Table:

2	3	4	5	6	7	8	9	10	11	12	13	14	15	16	17	18	19	20	21	22	23	24	25	26	27	28	29	30	31
c	c	c	o	o	o	c	o	o	c	o	c	o	c	o	o	c	o	o	c	c	c	c	o	c	c	c	c	c	c
o	c	c	c	o	c	c	o	o	c	o	c	o	c	o	o	c	o	o	c	o	c	c	c	c	c	c	c	c	c
c	c	c	o	c	o	c	o	o	c	o	c	o	c	o	o	c	o	o	c	c	c	c	c	o	o	o	c	c	c

Operation	36	37	38	39
Heat the loop	c	c	c	o
Run the test	o	o	o	o
Cool the loop	c	c	c	o

7.7 FOAM STABILITY EXPERIMENTS

Tests to evaluate the stability of foam generated by using Bachman's anionic foaming agent in the presence of salt and oil were performed. Mineral salt (99% Complex Chlorides) concentrations in a range of 5 to 30% w/v (weight of salt (g) to volume of surfactant solution (ml)) were used. The influence of 5% v/v and 10% v/v of mineral oil was also tested. Most of test matrix was repeated and additional tests will be performed. The test matrix is given in Table 5.

Table5 – Test Matrix for Foam stability Experiments

Case Studied	Number of Tests
99 ml Water + 1ml Bachman foamer (1% v/v)	2
Water + Bachman foamer 1% v/v + 5% w/v mineral salt	3
Water + Bachman foamer 1% v/v + 10% w/v mineral salt	2
Water + Bachman foamer 1% v/v + 20% w/v mineral salt	2
Water + Bachman foamer 1% v/v + 30% w/v mineral salt	1
Water + Bachman foamer 1% v/v + 5% v/v mineral oil	3
Water + Bachman foamer 1% v/v + 10% v/v mineral oil	2

7.7.1 Test Procedure

The test procedure consisted of mixing 100 ml of foamer solution 1% v/v in a kitchen blender for 30 s. For the tests containing oil or salt, the desired amount of each contaminant was added to the foamer solution and then foam was created. Typically 600 to 750 ml of foam was created, corresponding to initial qualities of 84 to 87%. The foam was transferred to a graduated cylinder and recording of time was started counting. The drained volume was recorded after 1 and 2 minutes. After that, the time was recorded when each 5 ml of liquid was drained.

7.7.2 Results

The foam stability was measured by using two different parameters: half-life time and drainage rate. The half-life time is the time when half of the foamer solution volume is drained. High half-life time values indicate a more stable system. Another technique to compare stability of foam systems is to measure the drainage rate. Once the graph showing the drained liquid volume versus time is developed, the drainage rate when half of the liquid volume is drained is defined as follows:

$$DR = \frac{kVo}{2} \quad \text{.....(7.7)}$$

where Vo is the initial foamer solution volume and the time constant *k* can be calculated by approximating the liquid drainage curve using a first order kinetic equation:

$$V = Vo\left(1 - \exp(-kt)\right) \quad \text{.....(7.8)}$$

A graph of Ln ((Vo-V)/Vo) versus time is used to compute *k* for a specific foam system. Figure 7.2 shows the drained volume curve for foam without salt and oil. Figure 7.3 shows the drained liquid volume versus time for foam with salt. The half-life time and drainage rate are shown in Figure 7.4 for the same system. Results indicate that stability of the foam is enhanced by the addition of salt up to 20% w/v. Half-life time value indicates a clear decrease in foam stability for 30% w/v of salt. Figure 7.5 shows that salt concentrations greater than 5% w/v seem to affect the foamability of the foaming agent.

Figure7.6 shows half-life time and drainage rate for foam with 5% v/v and 10% v/v oil concentration. The oil presence also enhanced foam stability in these particular tests.

It is important to mention that the results obtained from these tests should not be extrapolated to any type of foam systems. Because of the variety of surfactant types, salts compositions and hydrocarbon encountered, is hard to drawn general conclusions about the foam stability behavior for all possible systems. For example, oils are frequently used as antifoaming agents, but the results showed that for this particular case the foam stability was increased. It was observed before in other experiments[18] and explained by the appearance of a pseudo emulsion film (water film between emulsified oil droplets inside the Gibbs-Plateau borders and gas phase). If this is stable, the oil presence will enhance foam stability, otherwise the oil will work as an antifoaming agent. Besides that, the increase in liquid phase viscosity can also contribute to the increase of foam stability. Then these tests were performed to test foam stability under different situations for foaming agent that will be used in the future experiments in the ACTS flow loop. The possibility to expand the test matrix and perform additional tests is being studied.

7.8 PVT ANALYSIS of FOAM

The compressibility of foam was evaluated by using the PVT cell. A test procedure was developed. The actual test procedure and results are given in this section. Figure 7.7 shows the schematic drawing of PVT cell test operation. Test matrix for this part is given in Table 7.6.

Table 7.6 – Test Matrix for PVT Tests

Case Studied	Test
Water + Bachman foamer 2% v/v; 66°F	1
Water + Bachman foamer 2% v/v; 65°F	2
Water + Bachman foamer 2% v/v; 66°F	3

7.8.1 Test Procedure

1. Inject water into the PVT cell chamber performing operation number 1 in the schematic drawing. The piston should move all the way back to its maximum position (3 inches in the displacement reading).
2. Release the remaining pressure from the PVT cell chamber by opening valve 4.
3. Move the PVT cell to the downward position using the electrical drive system. The oven doors must be closed for this operation.
4. Open the main front cap and remove all remaining water from the chamber.
5. Connect a flexible hose to valve 6 (open) and inject air into the line up to valve 4 (open) to remove any trapped water from the pressure release operation.
6. Close valves 6 and 4 and dry the PVT cell chamber.
7. Move the PVT cell position upward.
8. Prepare 150 ml of foamer solution with concentration of 2% v/v.
9. Blend the solution for 30 s.
10. Transfer manually, as much as possible, the volume of foam to the PVT cell chamber.
11. Keep any remaining foam volume for further volumetric calculation.
12. Close, as soon as possible, the PVT chamber with the main cap.
13. Move the PVT cell to the downward position.
14. Inject air at 80 psi using the flexible hose into valve 6 and valve 4 for 2 min. The air supply valve, valve 6 and valve 4 must be opened respectively.
15. Move PVT cell to the horizontal position.
16. Compress the foam sample by performing operation 3 in schematic drawing.
17. Measure pressure and displacement of the piston (indirect volume measurement) at desired intervals.
18. Relieve the PVT cell pressure by opening valve 4 and 6 respectively.
19. Open the main cap and dry the cell.

One test was performed and repeated. The data were analyzed and compared with the results from different equations of state for foam.

Several equations of state were found in the literature, David and Mardsen (1969)[3] proposed a simple equation for the compressibility of foam:

$$C_F = C_G \Gamma \quad \text{.....(7.9)}$$

where C_F is the compressibility of foam, C_G is gas compressibility and Γ is foam quality. This equation can be used as an equation of state when pressure/volume dependence of both quality and C_G is established.

Huey and Bryant (1967) [19] proposed the following equation of state:

$$P = \left(\frac{1}{\rho_f} - \frac{1}{1+\beta} \cdot \frac{1}{\rho_l l} \right) = S \cdot T \quad \text{.....(7.10)}$$

where;

$$S = \frac{\beta}{\text{Mol}} \left(\frac{\text{R}}{1+\beta} \right) \text{.....} \quad (7.11)$$

R – Universal gas constant
Mol – molecular weight of gas
ρ_f – foam density
ρ_l – liquid density
T – absolute temperature

$$\beta = \frac{m_g}{m_l} \quad \text{.....(7.12)}$$

where;

m_g - mass of gas phase
m_l – mass of liquid phase
This equation of state was developed considering an ideal gas-phase behavior.

Lord et al. (1981) [20] also proposed an equation of state using the definition of quality and the engineering gas law:

$$\text{PV}_\text{F} = \text{bP} + \text{a} \text{.....(7.13)}$$

where;

$$\text{a} = \frac{\text{WgZRT}}{\text{Mol}} \text{.....(7.14)}$$

Z – compressibility factor
Wg – foam quality
Mol – gas molecular weight

$$\text{b} = (1 - \text{Wg})\hat{\text{V}}_\text{F} \text{.....(7.15)}$$

V_F – foam volume per unit mass

Ross (1969) [21] proposed a foam equation of state as follows:

$$(P_s - P_{gf})V_F + \frac{2}{3}\sigma\alpha = nRT_{gf} \quad \text{.....(7.16)}$$

where

Ps –surrounding's pressure
P_{gf} – gas phase pressure
α -interfacial area per unit volume
σ - liquid surface tension

The volumetric properties of foam were also studied using the following EOS:

$$V_{F_2} = V_{F_1}\left[(1-\Gamma_1) + \frac{P_1 z_1}{P_2 z_2}(\Gamma_1)\right] \quad \text{.....(7.17)}$$

This equation of state was derived using the real gas law and quality definition and will be called modified real gas law equation of state in this section.

The comparison of theoretical equations of state with experimental data was done for foam density. Foam compressibility model proposed by David and Mardsen[1] was also studied. Figures 7.8 and 7.9 show the results.

7.8.2 Conclusions:

The following conclusions can be derived from the experiments:

- The modified real gas law, Lord's[20] and Huey's[19] equation of state showed good results when compared with experimental data. In spite of this, the equations of state for foam tend to under predict density values for low quality foams.
- David and Mardsen's[3] model tends to under predict foam compressibility.

Further experiments will be performed to confirm the observed behavior.

7.9 Future Work

- Complete tests in the PVT cell in different temperatures and compare the results with theoretical predictions from available equations of state for foams.
- Modify the ACTS loop for foam flow and conduct preliminary foam flow tests.
- Perform theoretical study about interface properties of foams.
- Define a test matrix and run the experiments

➢ Develop correlations for friction pressure loss prediction while flowing foam under elevated pressure and temperature.

References

1. Heller, J.P. ; Kuntamukkula M.S. , “Critical Review of the Foam Rheology Literature”, Ind. Eng.Chem.Res. 26, 318 - 325, 1987.
2. Mitchell B.J., “Test Data Fill Theory Gap on Using Foam as a Drilling Fluid”, Oil and Gas Journal, 96 – 100, September 1971.
3. David A., Marsden S.S. Jr., “The Rheology of Foam”, Society of Petroleum Engineers of AIME, SPE 2544, 1969.
4. Beyer A. H., Millhone R.S., R.W. Foote , “Flow Behavior of Foam as a Well Circulating Fluid”, SPE 3986 , 1972.
5. Reidenbach V.G., Harris P.C., Lee Y.N., Lord D.L., “Rheological Study of Foam Fracturing Fluid Using Nitrogen and Carbon Dioxide”, SPE 12026, 1983.
6. Okpobiri G.A, Ikoku G.A., “Volumetric Requirements for Foam and Mist Drilling Operations”, SPE 11723,1986.
7. Saintpere S., Herzhaft B., A. Toure, Jollet S., “Rheological Properties of Aqueous Foam for Underbalanced Drilling”, SPE 56663,1999.
8. Harris P.C., Reidenbach V.G, “High-Temperature Rheological Study of Foam Fracturing Fluid”, SPE 13177, 1987.
9. Cawiezel K.E., Niles T.D., “Rheological Properties of Foam Fracturing Fluids Under Downhole Conditions”, SPE 16191, 1987.
10. A.M. Phillips, D.D. Couchman, J.G. Wilke, “Successful Field Application of High –Temperature Rheology of CO_2 Foam Fracturing Fluids”,SPE 16416, 1987
11. L.F. Bonilla, Subhash N. Shah, “ Experimental Investigation on the Rheology of Foams”, SPE 59752, 2000.
12. Harris P.C., “Effect of Texture on Rheology of Foam Fracturing Fluids”, SPE 14257, 1985.
13. Valko P., Economides M.J., “Volume Equalized Constitutive Equations for Foamed Polymer Solutions”, Journal of Rheology, August 1992.
14. Gardiner B.S., Dlugogorski B.Z., Jameson G.J., “Rheology of Fire-Fighting Foams”, Fire Safety Journal, 1998.
15. Winkler W., “Polymer Foam Rheology in Circular Pipes”, PhD. Dissertation, University of Leoben,
16. Affonso M.F. Lourenço, Andre L. Martins, Carlos H.M. Sa, Edimir M. Brandao, Sara Shayegi, “ Drilling With Foam: Stability and Rheology Aspects”, ETCE200O/DRILL-10033,2000.
17. J.F. Argillier, S. Saintpere, B. Herzhaft, A.Toure, “Stability and Flowing Properties of Aqueous Foams for Underbalanced Drilling”, SPE 48982,1998.
18. D.T. Wasan, K. Koczo, and A.D. Nikolov, “Mechanisms of Aqueous Foams Stability and Antifoaming Action with and without oil”, Foams: fundamentals and applications in the petroleum industry, Edited by Laurier L. Schramm,1994.

19. Huey, C.T and Bryant, R.A.A: “Isothermal Homogeneous Two-Phase Flow in Horizontal Pipes”, AIChe J., 1967, v.13, 70.
20. Lord, D.L.: “Analysis of Dynamic and Static Foam Behavior”, SPE 7927.
21. Ross, S: “Bubbles and Foams”, *Ind. Eng. Chem. ,* 1969, 61,48.
22. A.F. Negrao and A.C.V.M. Lage, “An Overview of Air/Gas/Foam Drilling in Brazil”, SPE/IADC 37678, 1997.
23. D.L. Hall, R.D. Roberts, “Offshore Drilling With Preformed Stable Foam”, SPE 12794, 1984.
24. T. Hanking, T.F. Rappuhn, “ Case History: Breitbrunn – Horizontal Foam Drilling Project in an Environmentally Sensitive Area in Bavaria, Germany”, SPE 35068,1996.
25. I.M. Fraser, R.H. Moore, “Guidelines for Stable Foam Drilling Through Permafrost”, SPE 16055,1987.

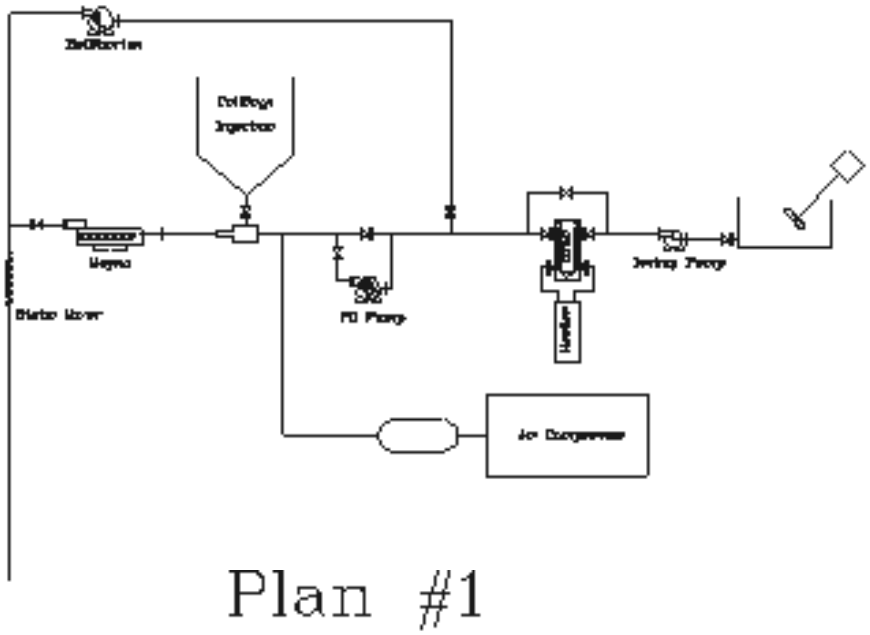

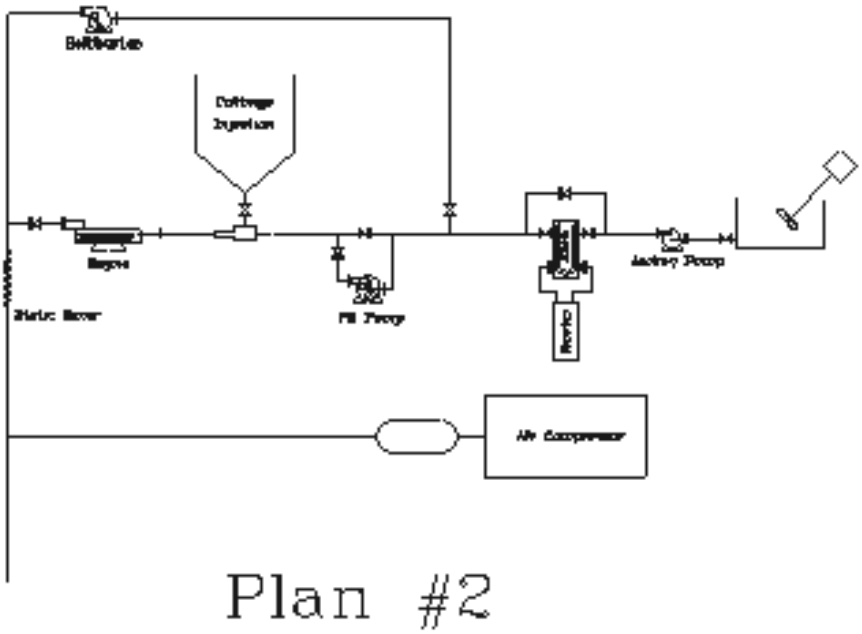

Figure 7.1 - Schematic Drawing of Flow Loop Configurations

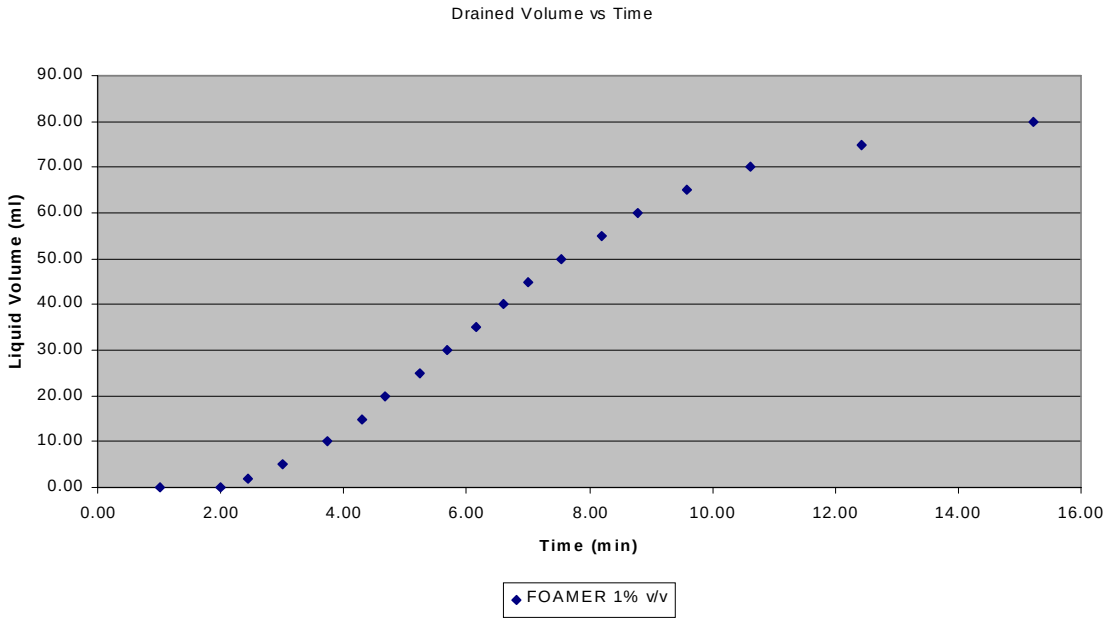

Figure 7.2 – Drained Liquid Volume – Foamer Solution 1% v/v with no salt or oil.

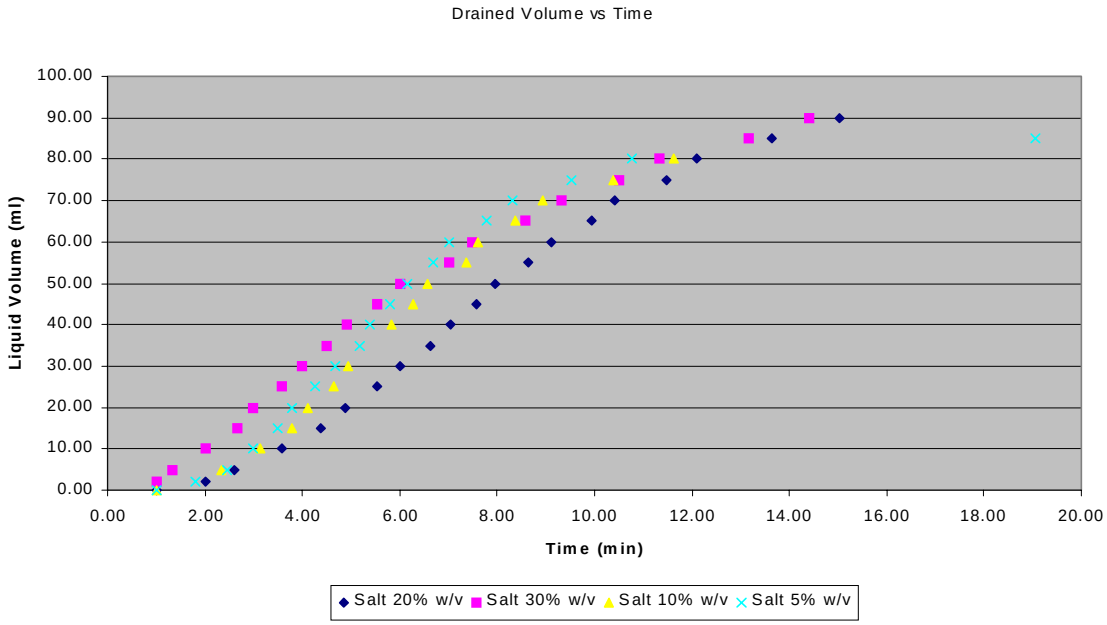

Figure 7.3 - Drained Liquid Volume – Salt Concentraton Effect.

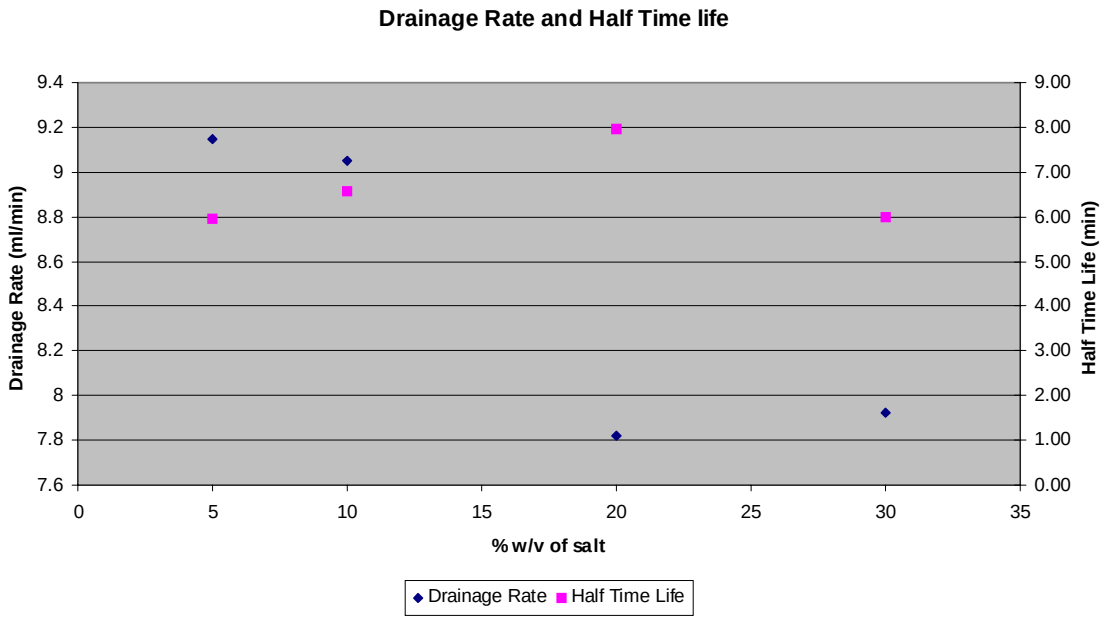

Figure 7.4 – Drainage Rate and Half-life time Measurements for Salty System

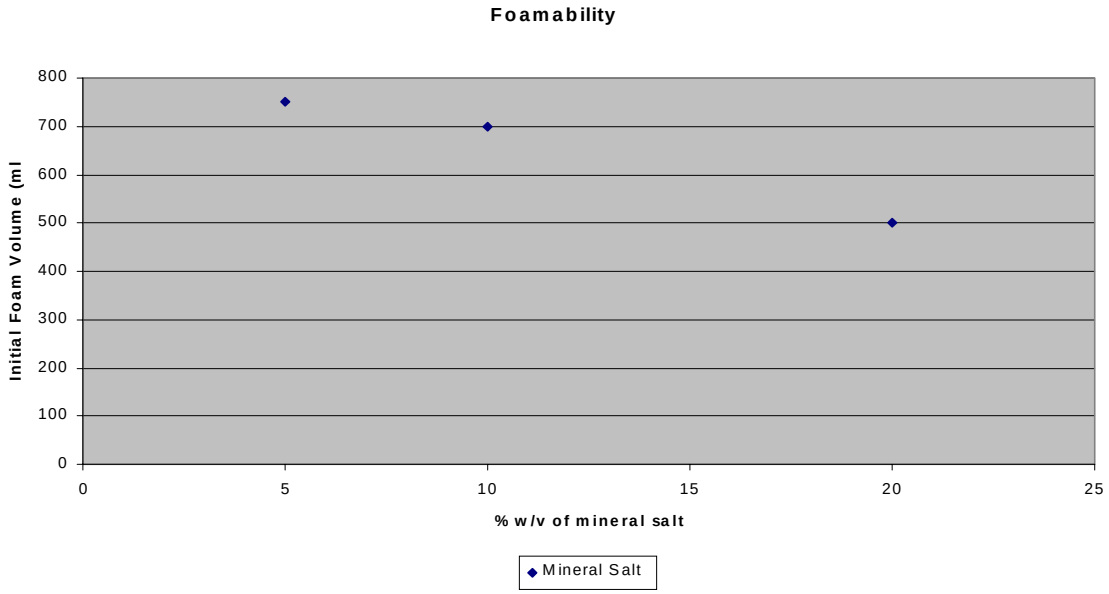

Figure 7.5- Foamability

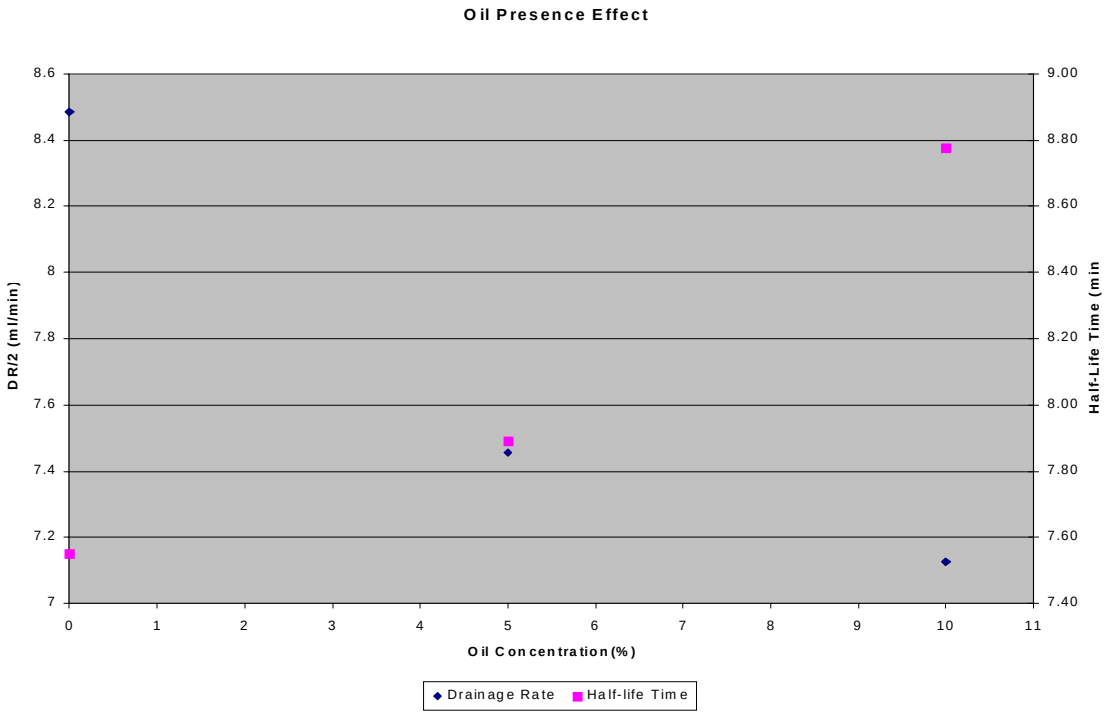

Figure7. 6 – Drainage Rate and Half-life time Measurements – Oil Presence

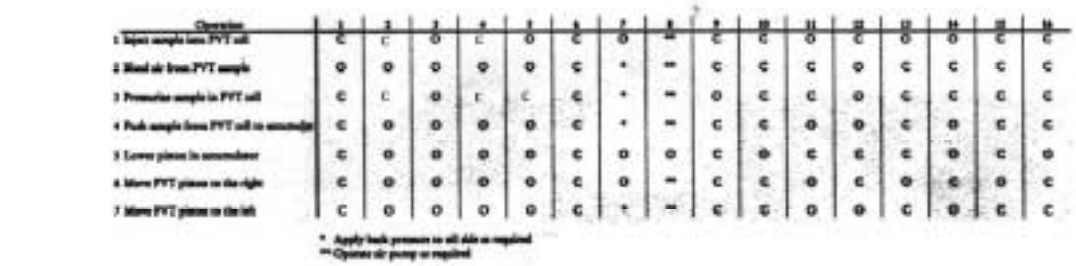

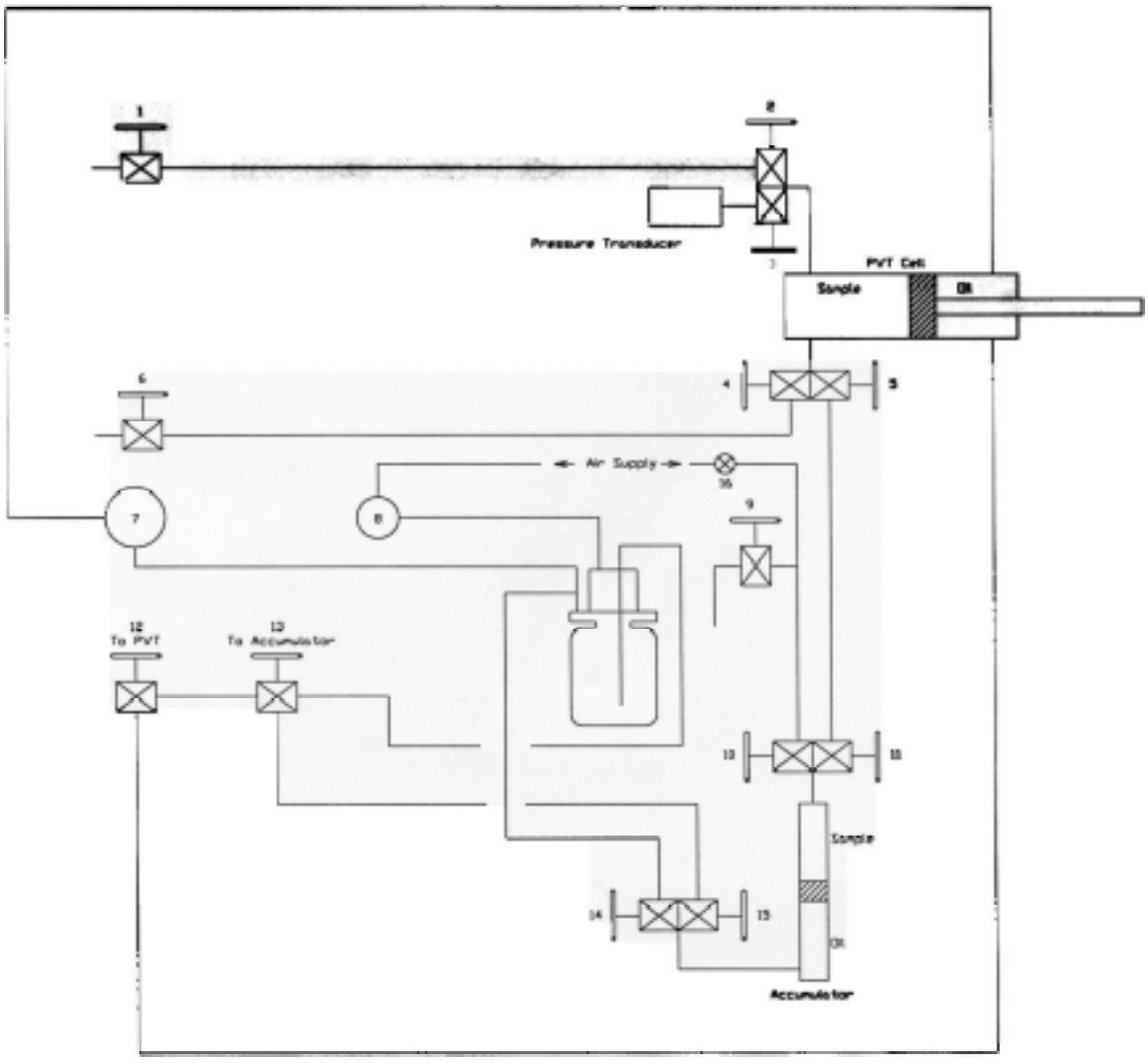

Figure 7.7 –PVT Schematic Drawing.

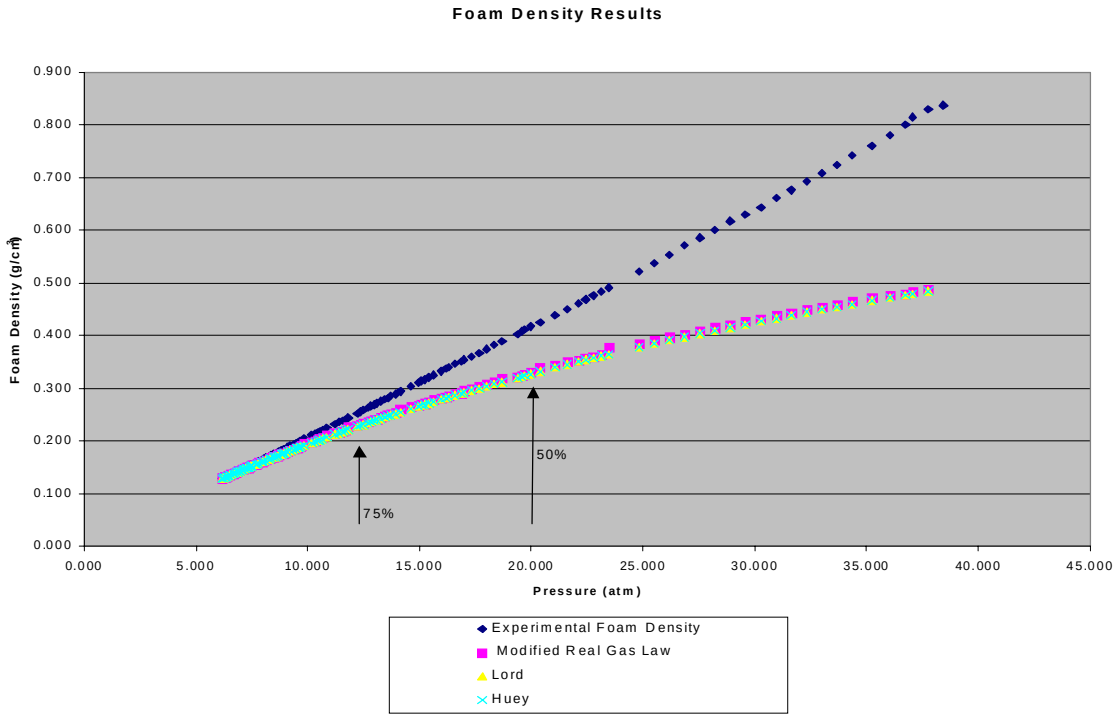

Figure 7.8 – Comparison of the Experimental and Theoretical Foam Foam Density Data.

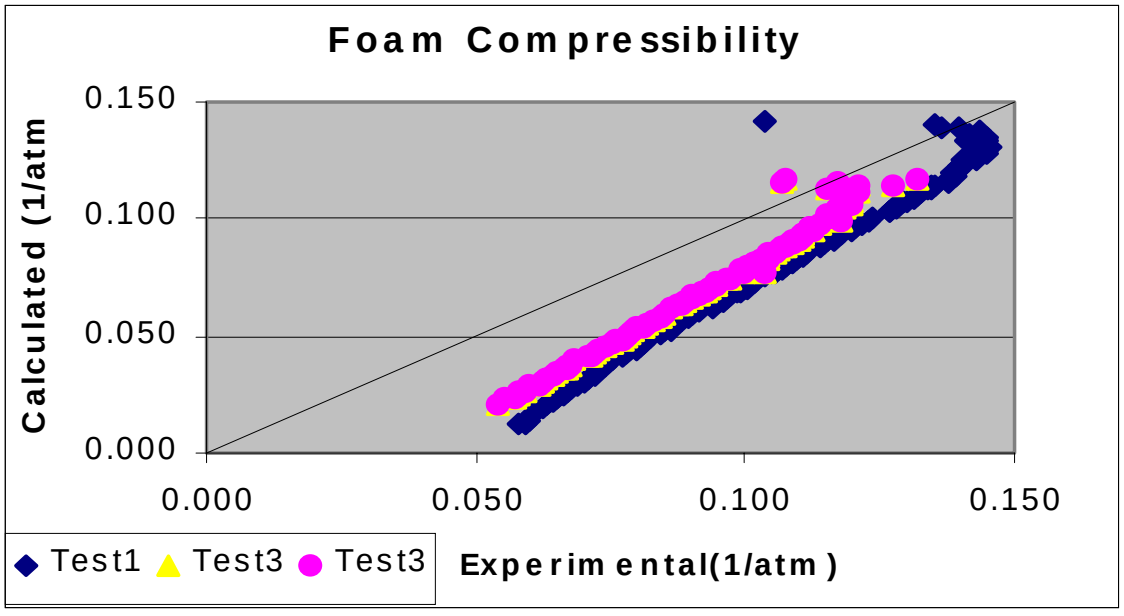

Figure 7.9 - Comparison of the Experimental and Theoretical Foam Foam Compressibility Data.

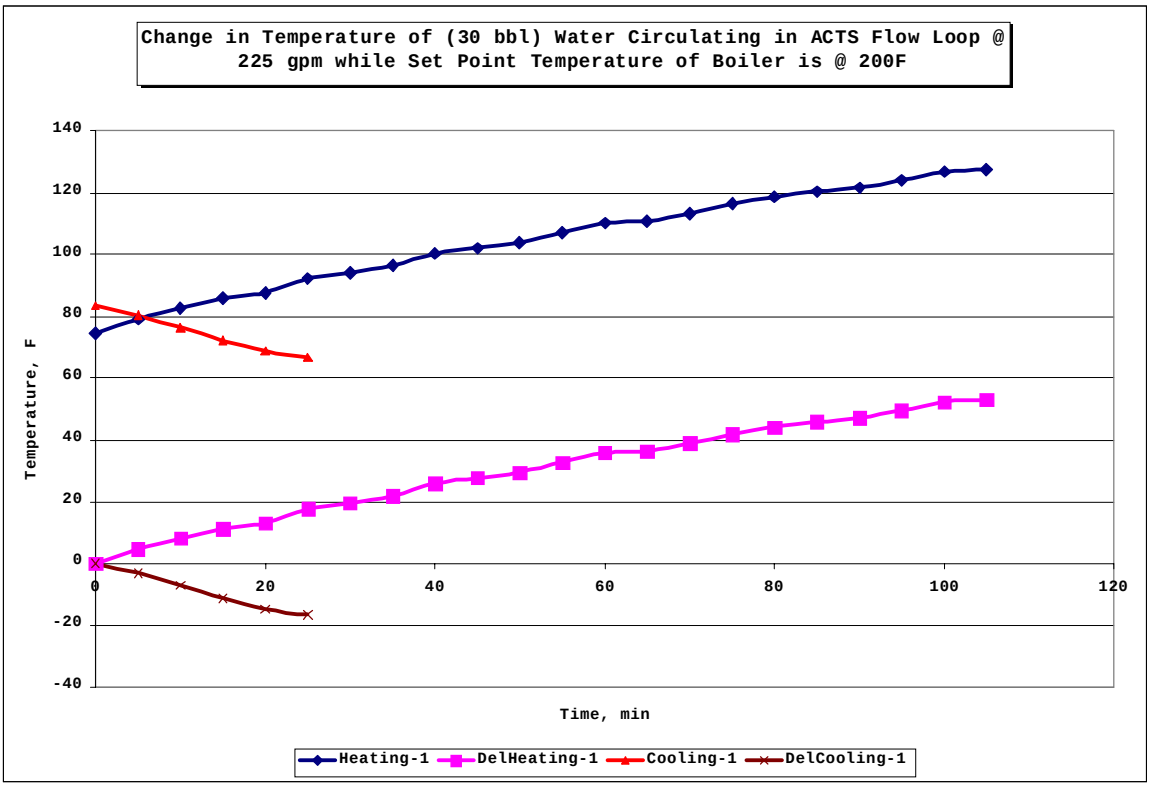

Figure 7.10 - Heating and Cooling Rate of Heating-Cooling System- with Water

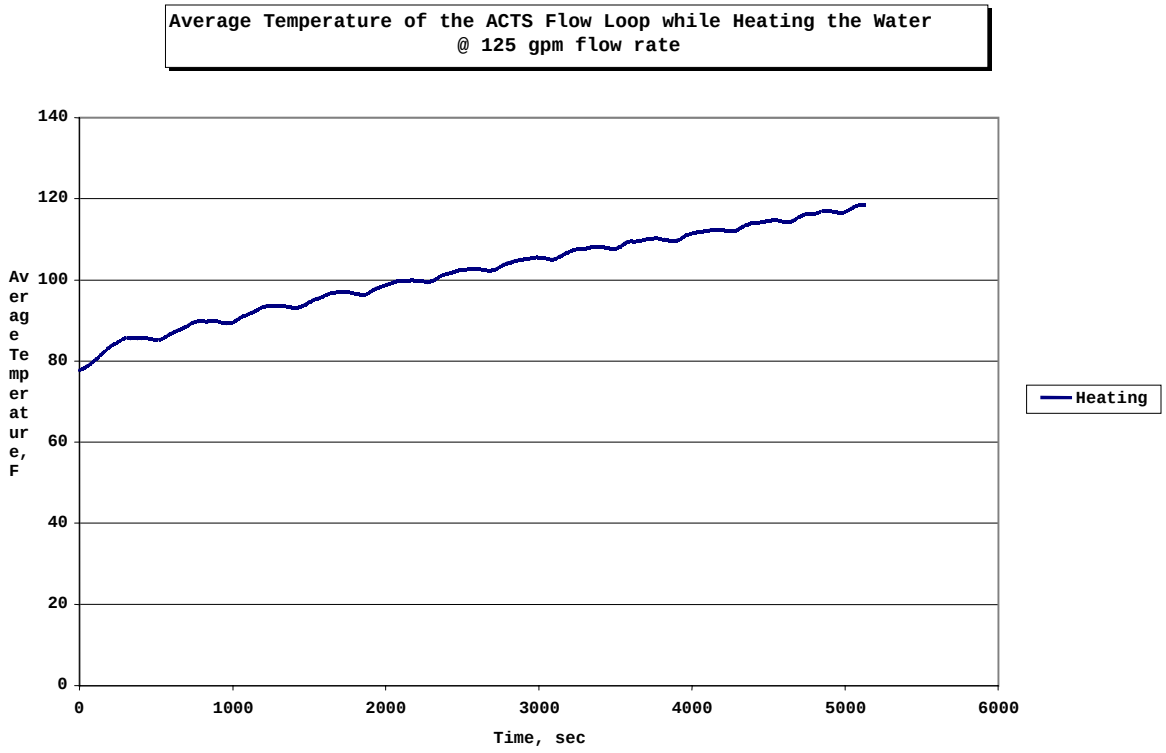

Figure 7.11 - Heating Rate of the Heating System- with Water

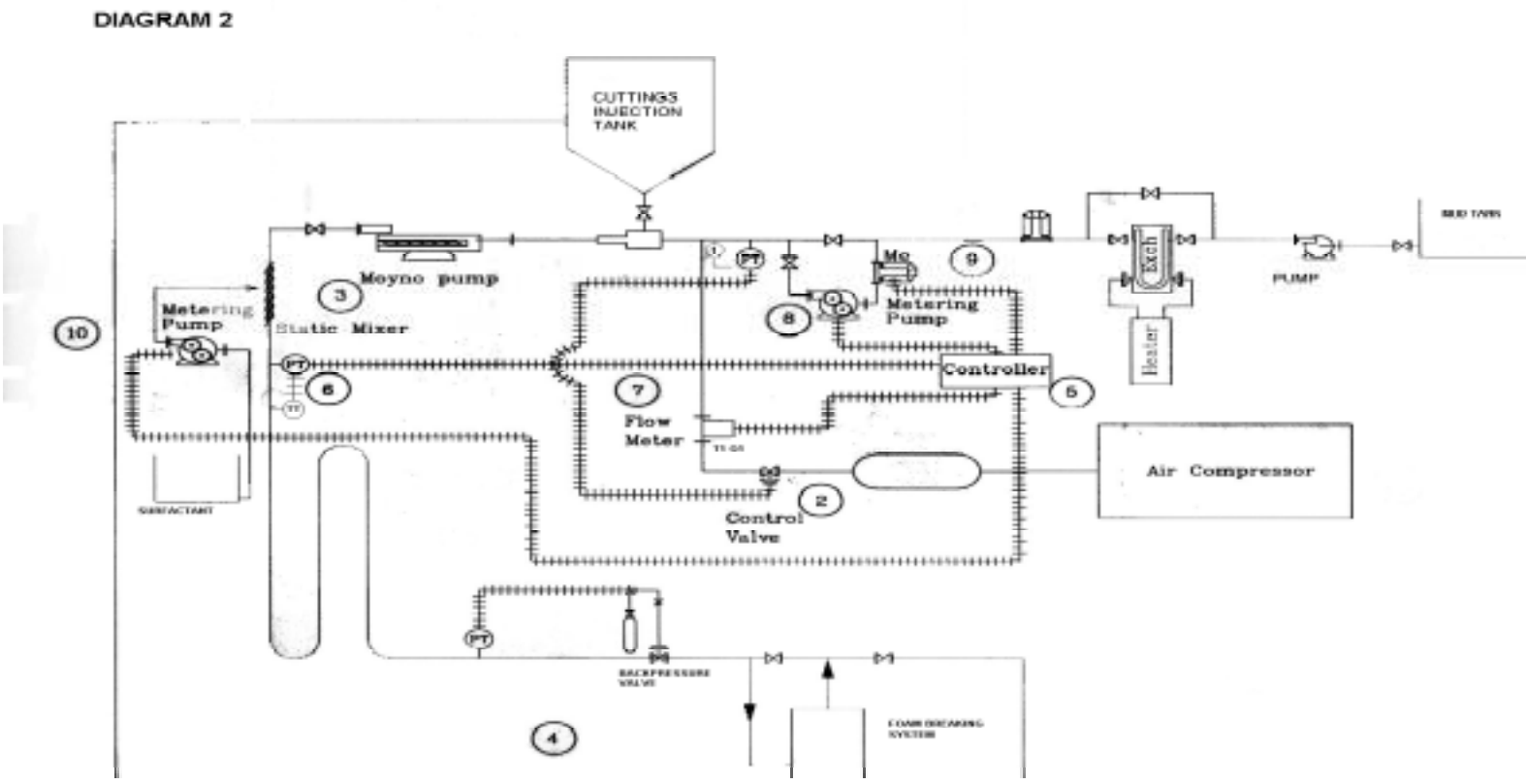

Figure 7.12 Diagram 1

8. DEVELOPMENT OF CUTTINGS MONITORING METHODOLOGY

INVESTIGATORS: Kaveh Ashenayi, Gerald Kane, Len Volk, Neelima Godugu

8.1 OBJECTIVES

The ultimate objective of this task (Task 11) is to develop a non-invasive technique for quantitatively determining the location of cuttings in the drill pipe. There are four different techniques that could be examined. However, as it was pointed out in the previous reports only three have good potential for success. These are:

1. Ultrasound
2. X-Ray/Gamma-Ray
3. Optical

8.2 Progress to Date:

The team started work on this project on August 15, 1999.

We have developed an MS-Access database. This database is used to store information about all sensors that we identify.

In addition, we completed the test plans for the first phase of task 11. And parts were ordered.

A PC (Pentium III – 450 MHz) based data collection system has been assembled. The system uses a DAC (PCL-818HG) designed by Advantech, Inc. The following are the card features:

- 16 single-ended or 8 differential analog inputs
- 100kHz 12-bit A/D conversion
- 1 K word FIFO
- Programmable gain for each input channel (up to 1000)
- Automatic channel/gain scanning with DMA
- 16 digital inputs and 16 digital outputs
- One 12-bit analog output channel
- Programmable pacer/counter
- Free DOS driver/Windows DLL driver included

- Software support from VisiDAQ 3.1, ActiveDAQ, LabVIEW, and Windows 3.1/95/NT High Speed DLL drivers.

The operating system used is the Windows/NT workstation.

We have developed and are in the process of the debugging the software needed for data collection. This is a MS-VB based application that controls the data sampling and data storage. Data is stored in a MS-Access database for analysis.

The DAC and the VB application are working correctly and we have the capability of displaying the data collected (either in a table or as a plot). In addition, the data recorded can be stored for future analysis.

We encountered a small problem with the accuracy of the temperature data read from temperature sensors. We have identified the problem and are in the process of correcting it. The problem is specific to VB. We are developing a "C" code to replace the problematic portion of the VB code.

The expansion card that would have allowed us to connect as many as 32 sensors to the same board is not functioning correctly. We are working with the DAC vendor's technical support to solve the problem.

This problem will not stop us from testing the static cell unit. We need this feature for the full system. Then we need to connect a large number of sensors. Without this expansion board we need to have a large number of DACs to handle all the sensors.

We have continued to update the sensor database. An ultrasound sensor has been identified and we are in the process of ordering it.

We have expanded our search for sensors to include gamma ray sensors as well.

Also, plans for a static cell have been completed. The manufacturing phase on the cell will start almost immediately.

8.3 *Approach:*

In subtask one of the Task 11 we are to develop a static radial test cell and to develop a preliminary set of instruments to detect presence of cuttings in this cell. There are four different methods that can be used. However, as it was pointed out in the previous report at present we will concentrate on the approaches with the greatest potential for success. These are:

- Ultrasound transmission
- X-ray/Ray-ray transmission

X-ray/Ray-ray approach has good potential for success. However, there may be health risks associated with these so we will utilize them in a limited capacity unless ultrasound approach proves to be uneconomical or not feasible. Additionally, the cost of the X-ray/Ray-ray sensors appears to be higher than ultrasound sensors.

Literature search revealed that Ultrasonic-transducers are more viable than X-ray transducers in the present context. However, we have come across an article that has opened up the potential of having reasonably priced X-ray/Ray-ray sensors. We will pursue this further and report on it at a later date.

The main approach to be investigated is the ultrasound transmission. We will setup a set of rings (see Figs.8.1 and 8.2) in the outer pipe and a corresponding ring in the inner pipe. The inner ring will act as source and the outer ring will act as receivers. We will measure the sound received and compare it against sound transmitted. After suitable data processing we believe it is possible to get an acceptable picture of what is inside the pipe. This is very similar to the ultrasound technique used by physicians.

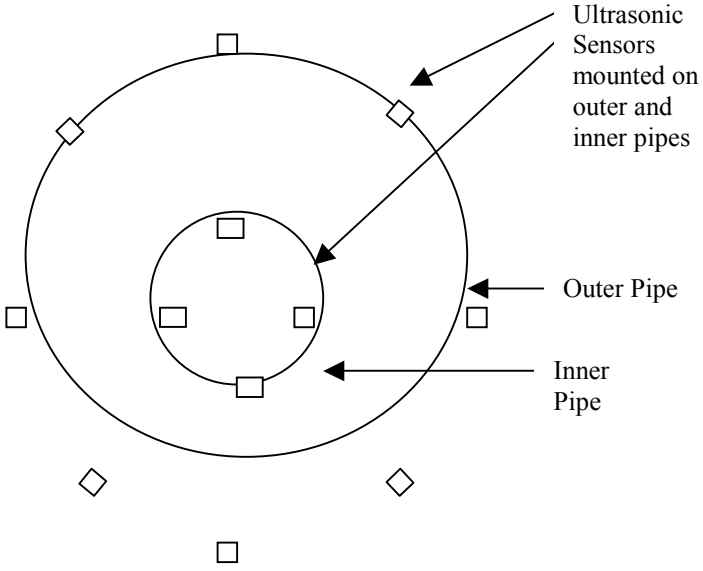

Figure 8.1 - Frontal View of the Experimental Setup

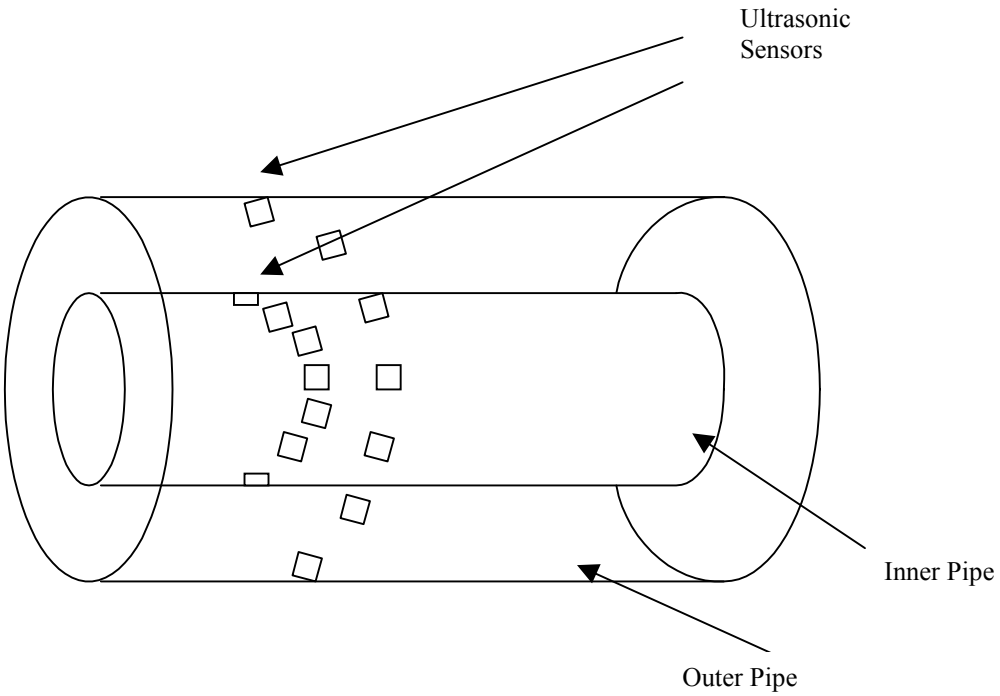

Figure 8.2 – Horizontal View of the Experimental Setup

8.4 Future Work:

To use the implemented test bed (a closed static system) to evaluate different designs of the ultrasonic sensing package. The sensors will be used to identify and monitor a known static concentration of cuttings in a simulated drill pipe.

In this stage we propose to use the cell consisting of two concentric pipes about 2 feet high. Cuttings of known size will be placed in a predetermined location in the cell (under a static environment). Using sensors we will try to locate these cuttings.

A PC based data acquisition system developed will be tested. This system software will be finished and then it will be used to store and process information received from sensors.

The cell for dynamic testing will be designed and implemented. Then the developed system will be used for modeling the dynamic cell behavior. In this case the fluid will be moving but no drilling action will be simulated.

9. DEVELOPMENT OF A METHOD FOR CHARACTERIZING BUBBLES IN ENERGIZED FLUIDS(TASK 12)

INVESTIGATOR: Len Volk

9.2 Objectives

The objective of this task is to develop the methodology and apparatus needed to measure the bubble size, size distribution and shape during cuttings transport experiments.

9.2 Introduction

Bubbles (as foam or aerated fluid) will be moving at a high rate (up to 6 ft/sec) in the drilling section of the ACTF, and may be very small (down to 0.01 mm). The bubble size and size distribution influence the fluid rheology and the ability of the fluid to transport cuttings. Bubbles in a shear field (flowing) may tend to be ellipsoidal which might alter both the rheology and transport characteristics.

This project is Task 12 (Develop a Method for Characterizing Bubbles in Energized Fluids in the ACTF During Flow) in the Statement of Work, and is divided into three subtasks:

- Subtask 12.1. Develop/test a microphotographic method for static conditions
- Subtask 12.2. Develop/test a method for dynamic conditions
- Subtask 12.3. Install the foam bubble size and distribution monitoring system on the ACTF

Subtask 12.1 includes (1) magnifying and capturing bubble images, (2) measuring bubble sizes and shapes, and (3) calculating the size distribution and various statistical parameters.

Subtask 12.2 develops the methods needed to apply the results of Subtask 12.1 to rapidly moving fluids, especially the method of “freezing” the motion of the bubbles. A dynamic testing facility will be developed in conjunction with Task 11 for development and verification.

Subtask 12.3 applies the techniques developed under Subtask 12.2 to the drilling section of the ACTF.

9.3 Project Status

9.3.1 Static Bubble Characterization

Microscopy. Bubble size in foams can vary over a wide range, depending on how the foam is prepared, the final system pressure and the chemical composition, but it is not uncommon to find bubbles with diameters down to 10μm (0.01 mm). The minimum magnification to be able to analyze the bubble images will be 250X, but more may be needed, possibly up to 400X. The microscope will need a minimum working distance (distance from the object being photographed to the bottom of the objective lens) of 4 to 5 cm to allow for the thickness of the high-pressure glass window (~3/4 inch) and the window-retaining ring (~1/2 inch). This is illustrated in figure 9.1.

Stereomicroscopes typically have large working distances to view the surface features of large objects and should be adequate for our needs. These microscopes can have maximum magnifications ranging from 225X to 450X. The microscope will require a boom stand to accommodate thick pressurized cells or the windowed, high-pressure pipe of the ACTF.

After evaluating several stereomicroscopes, we have purchased a Nikon SMZ-800. It offers excellent optics at an affordable price with the required magnification.

Illumination Method. An ambient pressure optical cell was constructed to evaluate various microscopes and examine different illumination methods. This cell is shown schematically in figure 9.2. In initial experiments, bubbles were easily seen using transmitted light. Figure 9.3 shows a schematic representation of this illumination method. The layer of bubbles beneath those next to the window could be seen, but not easily. Figure 9.4 is a photo of foamed drilling fluid taken through a microscope with a 35 mm camera. The biggest drawback with using transmitted light is the loss of light intensity as the light passes through the bubbles (absorption by the liquid phase and scattering at the gas-liquid interface). In the current sample the optical length through the foam was ½ inch.

If the illuminating light is directed directly onto the region being observed through the microscope (but illuminated from an angle), the bubbles are almost indistinguishable (no contrast). This is the most common illumination method for microscopic studies and is shown in figure 9.5.

If, however, the light is directed into the front surface of the bubbles somewhat remotely from the viewing region, the bubbles become visible, but appear very different from transmitted illumination. This is schematically shown in figure 9.6. Figure 9.7 shows shaving cream illuminated in this way. The appearance is similar to transmission electron micrographs where the object is gold sputtered.

Image Acquisition. There are basically three methods of recording the bubble images for further processing: video (CCD) cameras, digital cameras and film cameras. Available digital cameras have non-removable lenses and are therefore not useful. Those with removable lenses are just becoming available and are expensive (~$5000). For static samples, any imaging method can produce acceptable results.

Attaching a 35mm camera to the microscope via a phototube was only marginally successful. Determining the appropriate light level using the built-in light meter was difficult at best. Several of the prints were not in sharp focus, most likely due do to vibration of the camera's focal-plane shutter when operating at ½ to 1/16 second. Manufacturers of the better grade of microscopes have coped with this problem by developing their own exposure meter and shutter system. Our experience with a 35mm camera increases the attractiveness of a CCD camera.

Image Processing. If a digital CCD camera or an analog CCD with a frame grabber is used, the images will be ready for image processing. The bubble images may need to be enhanced using Adobe PhotoShop. The National

Institute of Health has developed software for processing images for Macintosh-based computers. Recently, Scion Corporation has rewritten this program for PC Windows-based application (www.scioncorp.com). At least one microscope manufacturer has developed and supports comparable software. This software is required to measure the bubble sizes and shapes for further analysis.

9.3.2 Dynamic Bubble Characterization

Light Source. Since fluids containing microscopic bubbles might be flowing at up to 6 ft/s, the motion of the bubbles must be "frozen" to image. In ordinary photography, the shutter serves this purpose. However, the speed of mechanical shutters is too slow. To freeze a 0.01mm diameter bubble moving at 6ft/s, the shutter speed must be ~0.3 μs. The simplest method is to use a pulsed light source. Figure 9.8 gives the relation between bubble size, fluid velocity and shutter speed or flash duration for 5% blur (5% blur means that the bubble can move 5% of its diameter while the shutter is open or the flash is on). Figure 9.9 shows the timing sequence using a pulsed light source. Commercially-available xenon strobes have flash durations longer than 7-10μs. Gas discharge lamps with flash durations down to 4 ns are known, but their light intensity is very low. Lasers operating in the visible or ultraviolet having pulse widths shorter than 0.1μs are common. If an ultraviolet laser is used, the light can be converted to visible light using a laser dye. One question that still needs to be answered is the required light intensity. Once we receive our microscope, we plan to "borrow" a CCD camera and verify that a pulsed laser can provide sufficient light intensity for photography. If not, we will pursue a xenon pulsed light source.

Image acquisition. Considerable advancements have been made in CCD cameras in recent years. Shutter speeds down to 1 millisecond are possible (still too slow for our purposes). Light sensitivities can be at least 10 times better than film. Manufacturers/suppliers of CCD cameras agree that a short flash or pulse of light is the best method of freezing the fluid motion, and that high energy pulsed light should not be a problem for these cameras. As with film, a CCD camera tends to "integrate" the light it receives. The cost of a high performance CCD could be in excess of $15,000. A CCD camera would offer some advantages over film photography for dynamic imaging:

- Almost unlimited imaging
- No digitization requirement
- Easy synchronization with pulsed light source
- Electronic aperture control
- Pseudo real-time imagining

Imaging is almost real time (delayed by a few minutes at most) will be of considerable advantage because if the imaging settings are not correct, changes can be made to correct the problem without "losing" the experimental run.

9.3.2.2 Dynamic Testing Facility

Figure 9.10 is a schematic of the Dynamic Testing Facility. Its purpose is to provide a means of checking tomographic systems and bubble characterization equipment under flowing conditions prior to installation on the cuttings transport loop. Anticipated operating pressure will be 100 psi although the system is designed to handle up to 150 psi if needed. The facility will be able to handle aqueous liquids, foams, with or without cuttings. It can also be used to check out new ideas before installation on the large loop (ACTF). It is centered around a two-stage stainless Moyno pump capable of pumping 0.7 to 14 gpm at ~ 150 psi. Once filled, the testing facility operates as a true closed loop. If non-energized fluids are to be used, the loop will be pressurized with a pulsation dampener. The pulsation dampener will also compensate for minor temperature fluctuations. Injected gas will pressurize the loop if energized fluids are to be used. The entire Dynamic Testing Facility is being constructed on a 16’ x 2-1/2’ skid.

The Screening Cell and Cuttings Separator in figure G are similar in construction but have different functions. The Screening Cell (see figure 9.11) is designed to remove fluid (primarily liquid) from the system without removing any cuttings thereby allowing the quality of foam to be increased. The Cuttings Separator (see figure 9.12) will remove (and store) the cuttings from the system while it is still pressurized. It therefore needs to be physically larger than the Screening Cell.

9.4 Planned Activities

- Evaluate and purchase a suitable CCD camera.
- Acquire software needed for bubble analysis.
- Identify and acquire suitable pulsed light source.
- Construct the Dynamic Testing Facility.

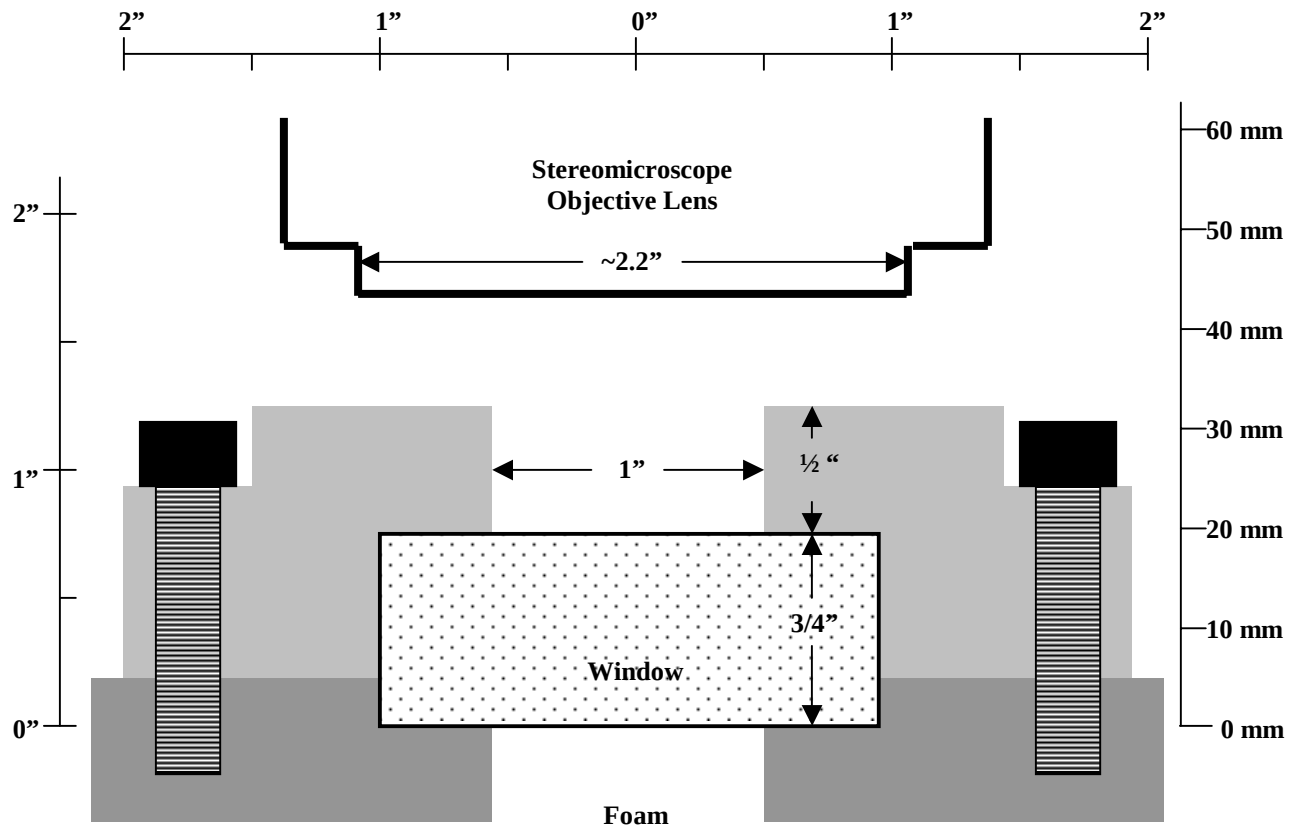

Figure 9.1. Minimum working distance requirement and typical windowed high-pressure cell geometry.

Figure 9.2. Ambient pressure optical cell for microscope evaluation and illumination studies.

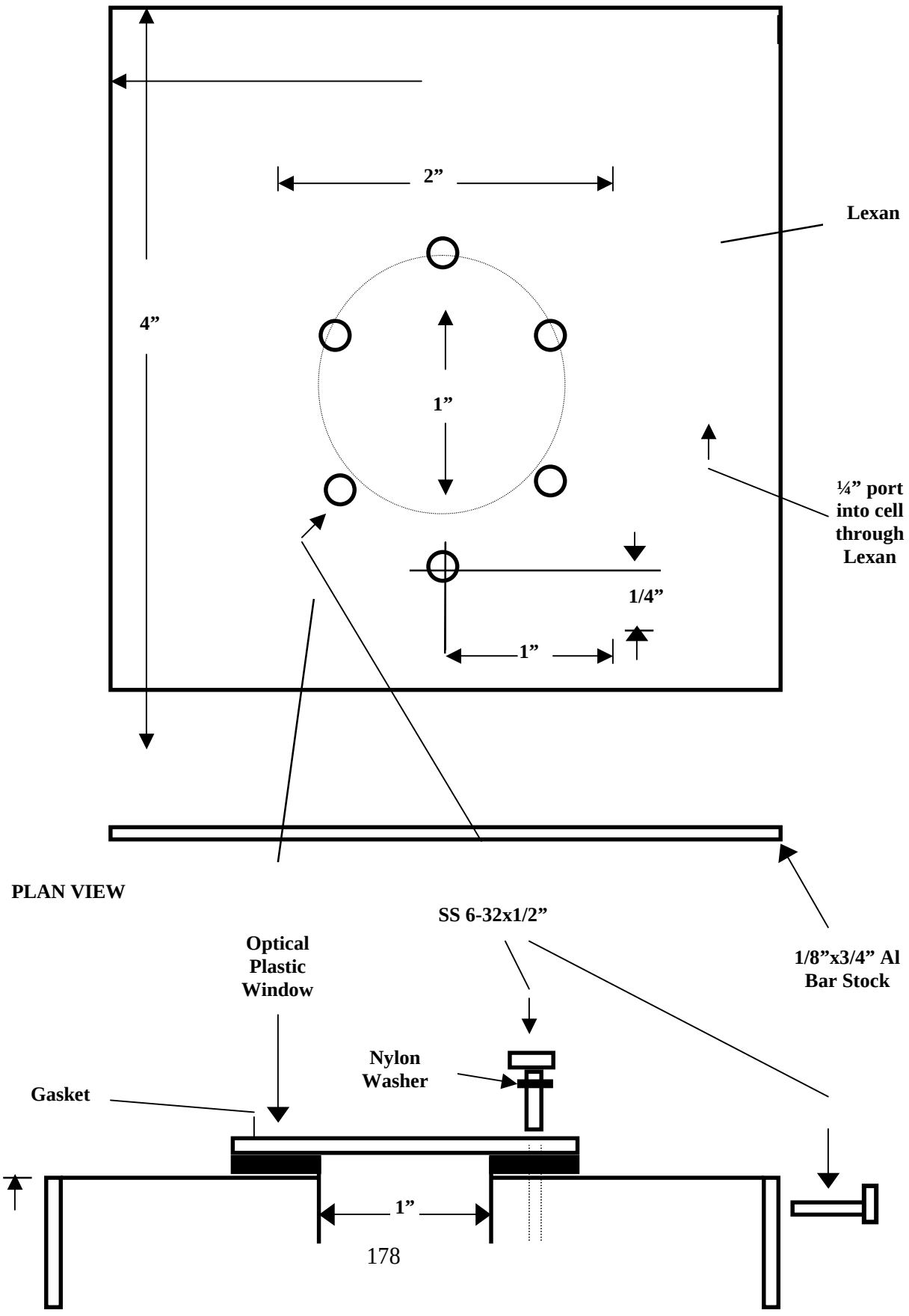

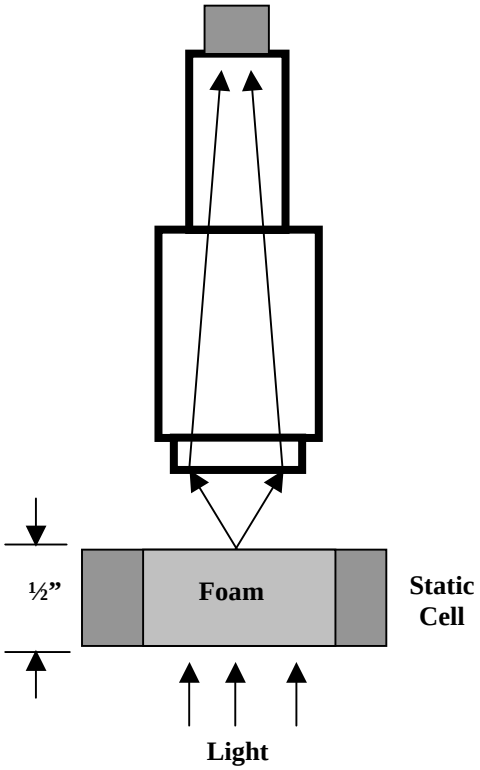

Figure 9.3. Foam illumination using transmitted light.

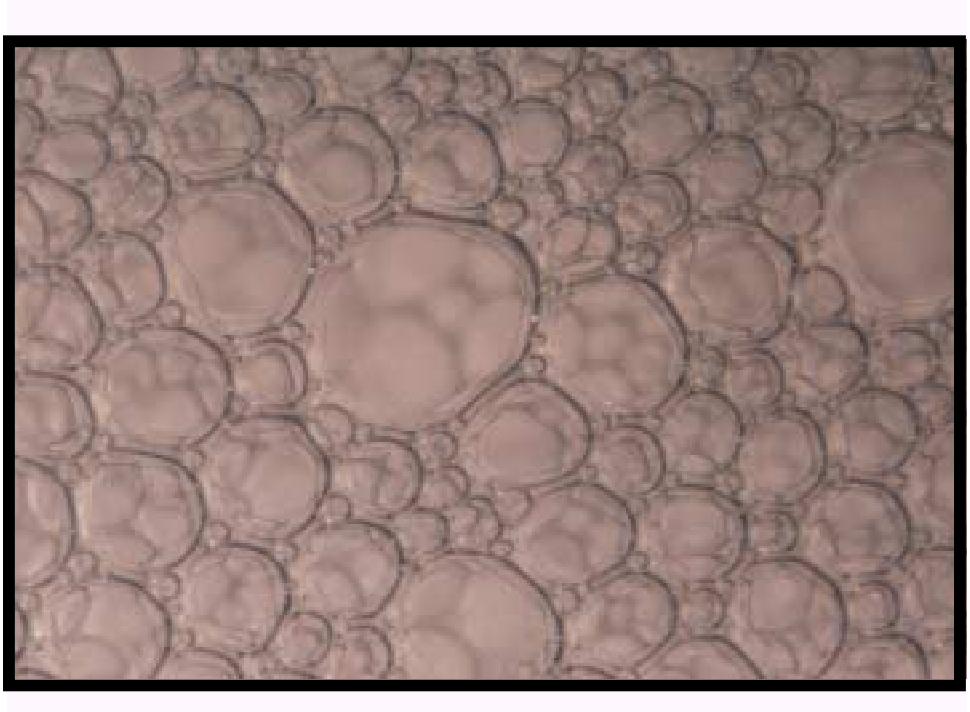

Figure 9.4. Microphotograph of foamed drilling fluid using transmitted light. Note the second level bubbles visible through the larger surface bubbles.

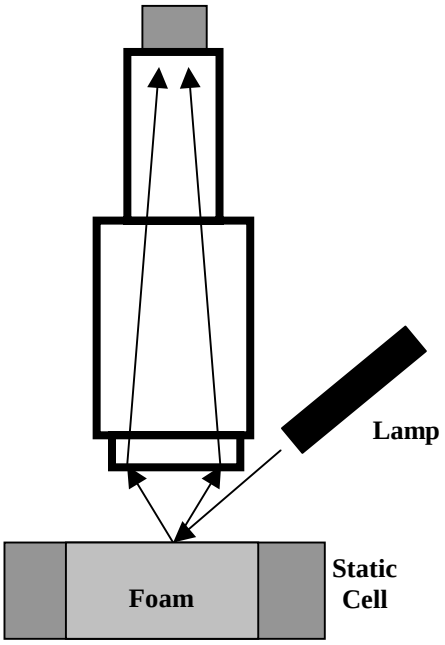

Figure 9.5. Direct method for surface sample illumination.

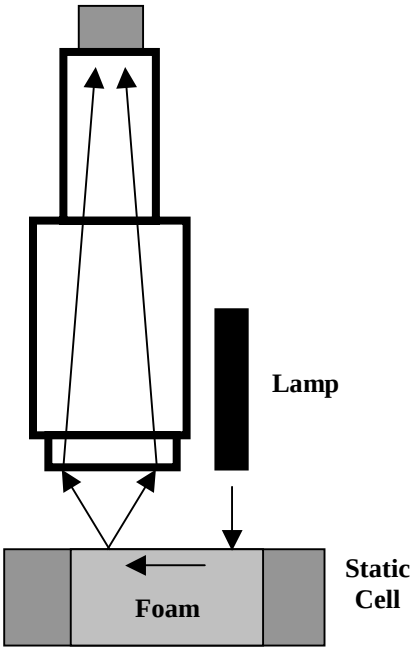

Figure 9.6. Indirect method for surface sample illumination.

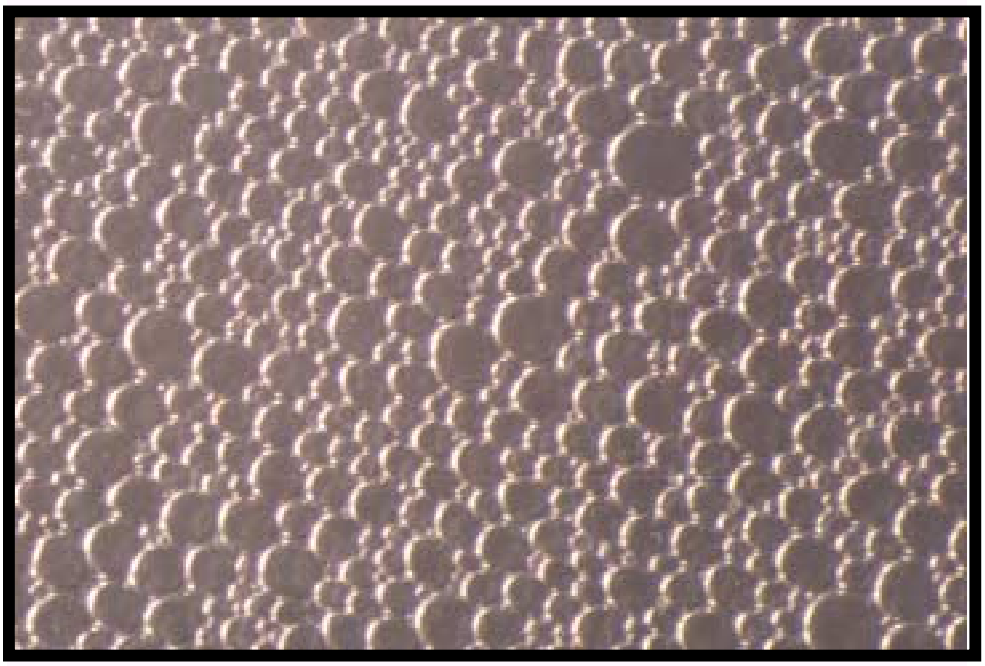

Figure 9.7. Shaving cream illuminated indirectly from the front surface.

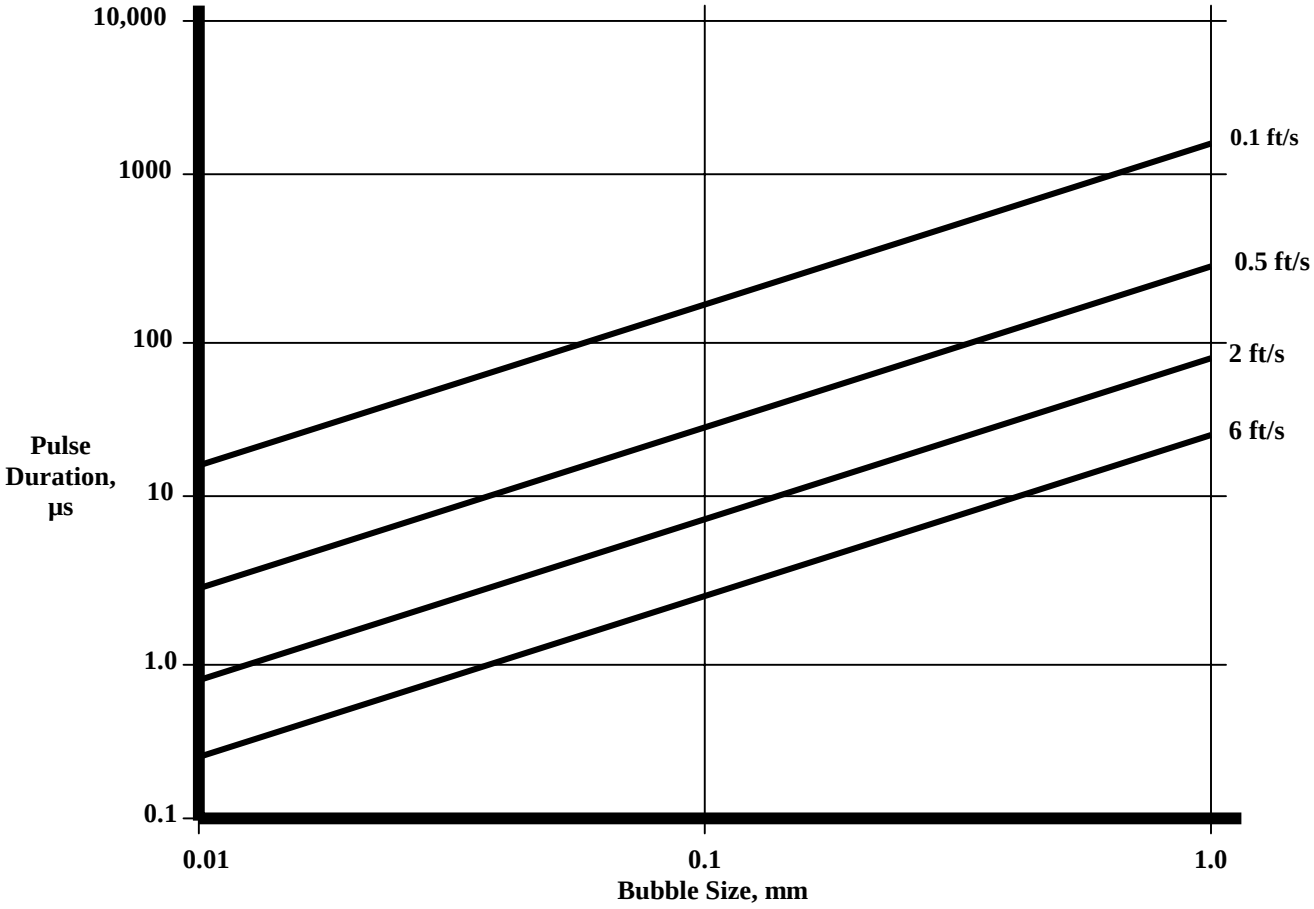

Figure 9.8. Bubble size versus light pulse duration (shutter) for various fluid velocities.

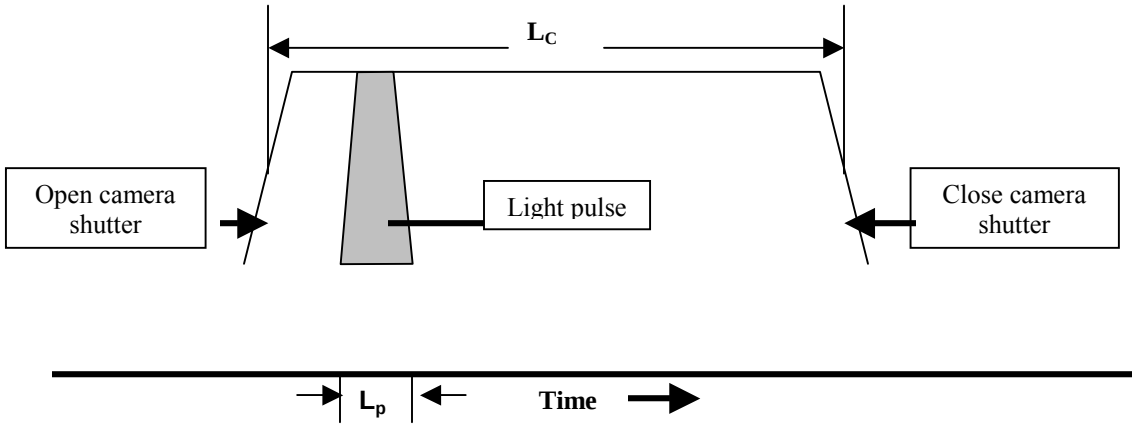

L_p = Width of light pulse

L_c = Duration camera ready to acquire a signal.

Figure 9.9. Relationship between camera signal acquisition and light pulse.

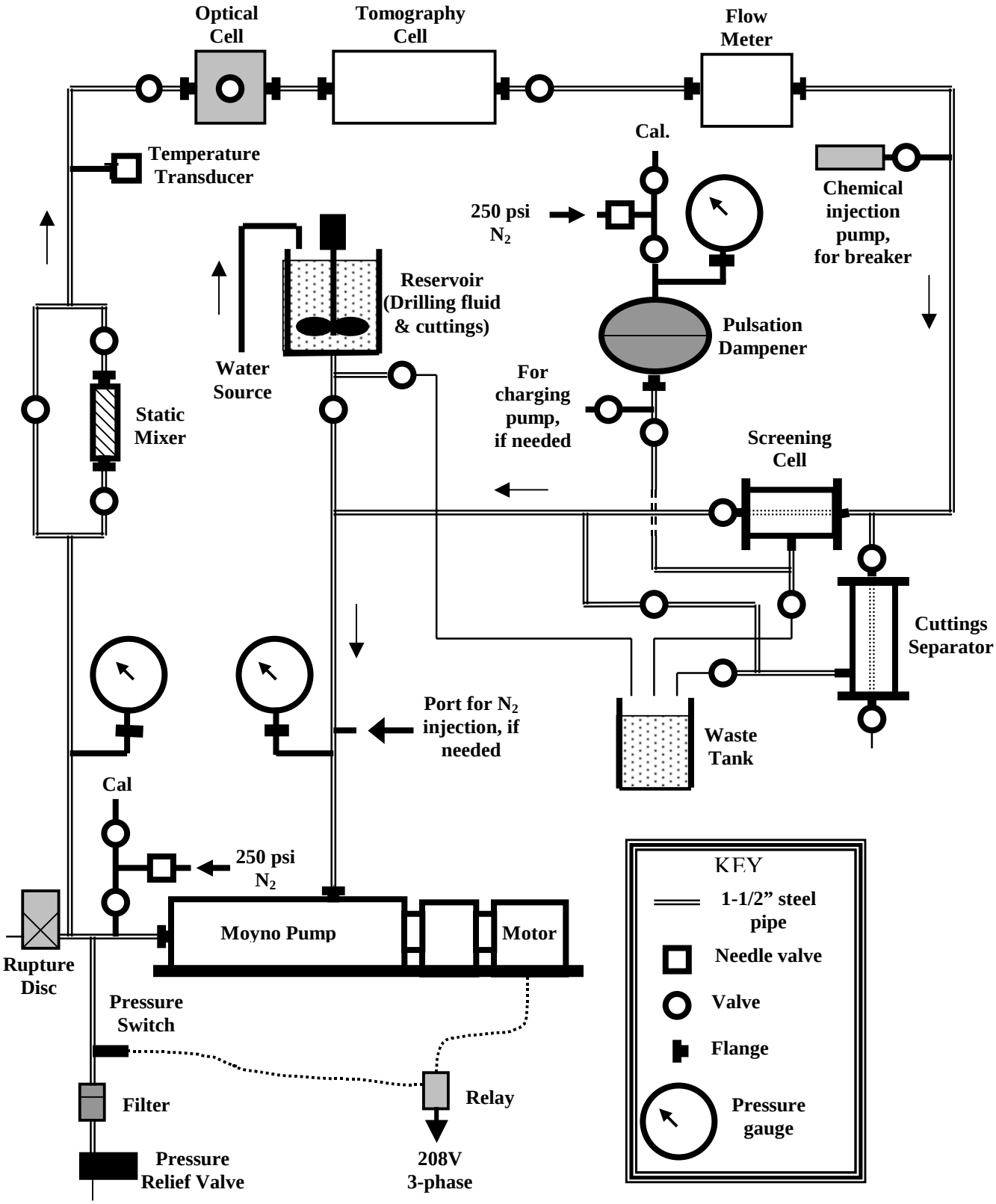

Figure 9.10. Schematic for the Dynamic Testing Apparatus

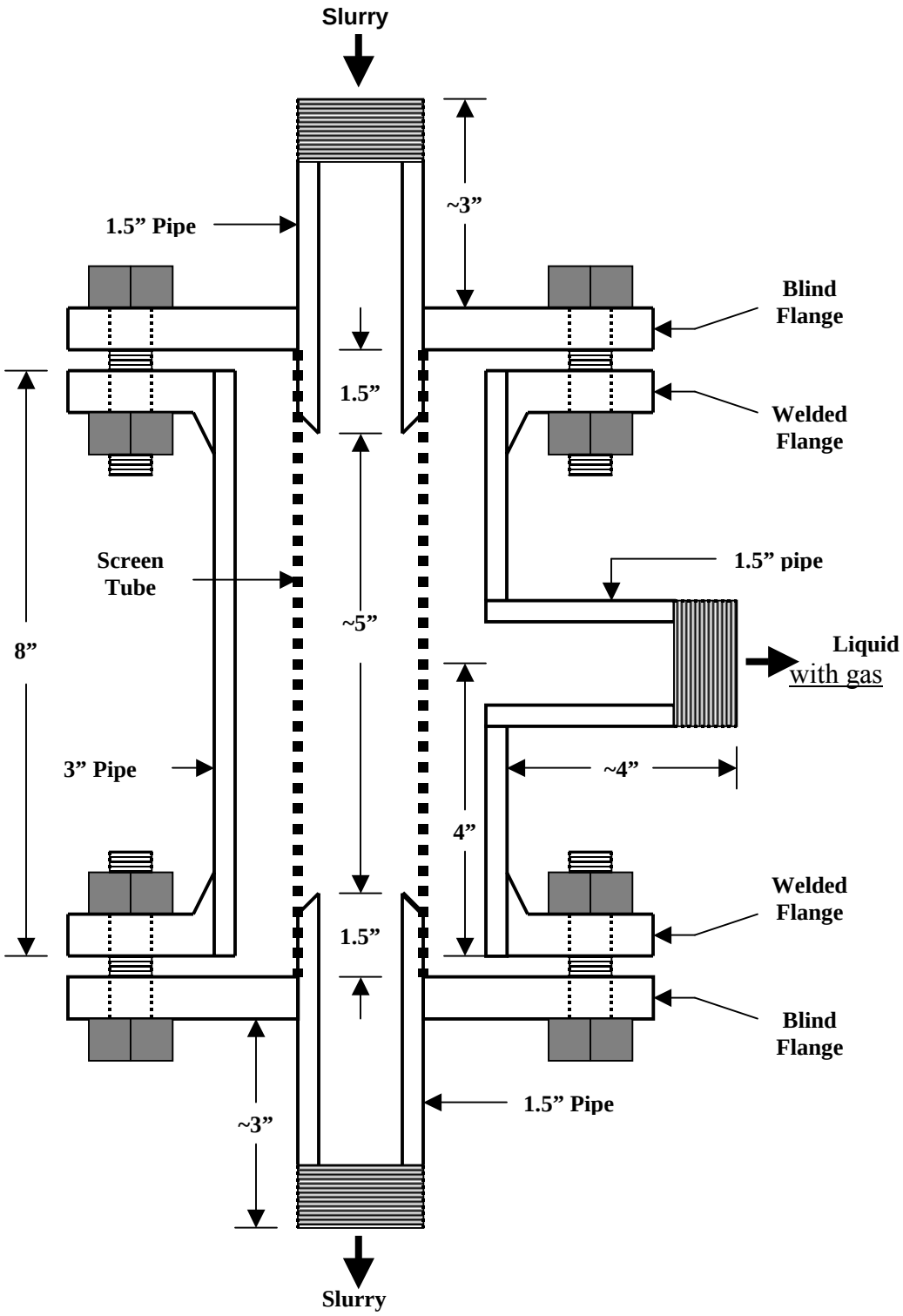

Figure 9.11. Schematic of Screening Cell (shown at right angle to operation orientation).

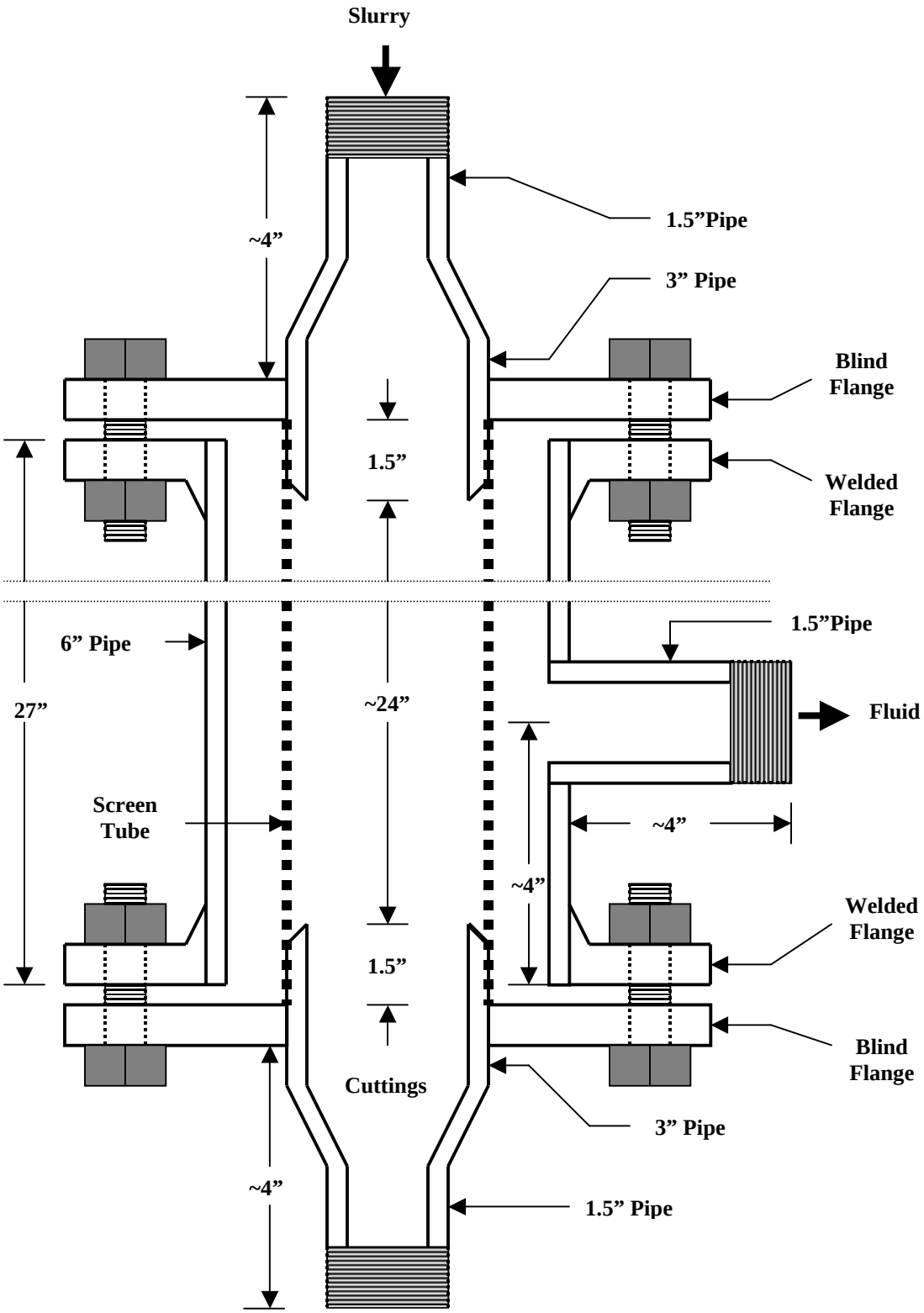

Figure 9.12. Schematic of Cuttings Separator (cuttings removed at bottom).

10. TECHNOLOGY TRANSFER

a- Meetings with Oil and Service Company Members

Efforts have been spent continuously to increase the number of industry members supporting the ACTS projects. As a result of our continuous efforts to develop more contact with oil and service companies, two new companies, namely, Intevep, Petrobras have decided to join ACTS-JIP in year 1. Currently, there are 9 members of the ACTS-JIP including, BP-Amoco, Chevron, Dowell Schlumberger, Halliburton, Intevep, JNOC, Petrobras, Statoil, and the U.S. D.O.E.

b-Technical Work Groups

As part of the activities of construction work group, we have visited Phil Harris at the Halliburton research center in Duncan, Oklahoma. Phil Harris is a well known expert on foam rheology and applications. In a meeting with Dr. Harris, we have discussed our plans for flow loop modification to accommodate foam flow.

We have also visited Ohio State University multi-phase flow technology center where they have been using tri-phase Moyno pump to circulate air-liquid and solid mixtures. We had discussions with the OSU people regarding the performance of Tri-phase Moyno pump when circulating air/liquid/solid mixtures.

c- ACTS-JIP Advisory Board Meeting

Two advisory board meetings with ACTS-JIP industry members have been organized (November 16, 1999 and May 23, 2000).